WT-1153 (EX)
EXTRACTED VERSION

OPERATION TEAPOT

Technical Summary of Military Effects, Programs 1-9

February-May 1955

Nevada Test Site

NOTICE

This is an extract of Operation TEAPOT, which remains classified SECRET/RESTRICTED DATA as of this date.

Extract version prepared for:

Director
DEFENSE NUCLEAR AGENCY
Washington, D.C. 20305

1 May 1981

~~UNCLASSIFIED~~

SECURITY CLASSIFICATION OF THIS PAGE (When Data Entered)

REPORT DOCUMENTATION PAGE		READ INSTRUCTIONS BEFORE COMPLETING FORM
1. REPORT NUMBER WT-1153 (EX)	2. GOVT ACCESSION NO. AD-A995120	3. RECIPIENT'S CATALOG NUMBER
4. TITLE (and Subtitle) Operation TEAPOT Technical Summary of Military Effects, Programs 1-9		5. TYPE OF REPORT & PERIOD COVERED 6. PERFORMING ORG. REPORT NUMBER WT-1153 (EX)
7. AUTHOR(s)		8. CONTRACT OR GRANT NUMBER(s)
9. PERFORMING ORGANIZATION NAME AND ADDRESS Office of the Deputy Chief of Staff for Weapons Effects Tests Headquarters Field Command, Defense Atomic Support Agency Sandia Base, Albuquerque, New Mexico		10. PROGRAM ELEMENT, PROJECT, TASK AREA & WORK UNIT NUMBERS
11. CONTROLLING OFFICE NAME AND ADDRESS Headquarters Field Command Defense Atomic Support Agency Sandia Base, Albuquerque, New Mexico		12. REPORT DATE February 23, 1960 13. NUMBER OF PAGES 231
14. MONITORING AGENCY NAME & ADDRESS(if different from Controlling Office)		15. SECURITY CLASS. (of this report) Unclassified 15a. DECLASSIFICATION/DOWNGRADING SCHEDULE

16. DISTRIBUTION STATEMENT (of this Report)

Approved for public release; unlimited distribution.

17. DISTRIBUTION STATEMENT (of the abstract entered in Block 20, if different from Report)

18. SUPPLEMENTARY NOTES

This report has had the classified information removed and has been republished in unclassified form for public release. This work was performed by Kaman Tempo under contract DNA001-79-C-0455 with the close cooperation of the Classification Management Division of the Defense Nuclear Agency.

19. KEY WORDS (Continue on reverse side if necessary and identify by block number)

Operation TEAPOT
Military Effects
Blast Measurements
Nuclear Radiation
Thermal Measurements

20. ABSTRACT (Continue on reverse side if necessary and identify by block number)

FOREWORD

This report has had classified material removed in order to make the information available on an unclassified, open publication basis, to any interested parties. This effort to declassify this report has been accomplished specifically to support the Department of Defense Nuclear Test Personnel Review (NTPR) Program. The objective is to facilitate studies of the low levels of radiation received by some individuals during the atmospheric nuclear test program by making as much information as possible available to all interested parties.

The material which has been deleted is all currently classified as Restricted Data or Formerly Restricted Data under the provision of the Atomic Energy Act of 1954, (as amended) or is National Security Information.

This report has been reproduced directly from available copies of the original material. The locations from which material has been deleted is generally obvious by the spacings and "holes" in the text. Thus the context of the material deleted is identified to assist the reader in the determination of whether the deleted information is germane to his study.

It is the belief of the individuals who have participated in preparing this report by deleting the classified material and of the Defense Nuclear Agency that the report accurately portrays the contents of the original and that the deleted material is of little or no significance to studies into the amounts or types of radiation received by any individuals during the atmospheric nuclear test program.

PREFACE

This summary report has been prepared from an evaluation of the military significance of the individual projects that made up the military effect test program of Operation Teapot. Short summaries of the individual projects are presented in the appendix.

This report has been prepared with the assistance of the program directors, representatives of Headquarters, AFSWP, AFSWP consultants, and personnel of the Directorate of Weapons Effects Tests (DWET), Field Command, AFSWP. A partial list of contributors includes: Col H.K. Gilbert, USAF; Lt Col P.S. Gwynn, USAF; Dr. F.H. Shelton, AFSWP; Maj H.T. Bingham, USAF; Lt Col W.B. Pohlman, USA; CDR W.M. McLellon, USN; Capt C.S. Adler, USA; CDR C.C. Hoffman, USN; LCDR M.B. Dahl, USN; Maj E.C. Jenkins, USAF; Maj C.W. Bankes, USA; Lt Col J.G. James, USAF; Lt Col W.M. Sheahan, USA; Lt Col H.S. Heaton, USAF; Mr. R.A. Burgin, DWET; LTJG R.J. Culp, USN; Mr. J.R. Kelso, AFSWP; LCDR W.J. Christensen, USN; Dr. V.A.J. Van Lint, DWET; and Dr. D.C. Sachs, Stanford Research Institute.

CONTENTS

TABLES

Chapter 1
INTRODUCTION

1.1 BACKGROUND

During early nuclear tests at the Nevada Test Site (NTS), the Department of Defense (DOD) conducted military-effect-test programs on certain Atomic Energy Commission (AEC) developmental shots on a noninterference basis to the weapon-development program. However, because of their experimental nature, such developmental shots were frequently not suitable for some military-effect programs; thus, the DOD requested and obtained authority for the detonation of several nuclear devices in order to best study the basic blast, thermal radiation, and nuclear-radiation phenomena and their effects on structures, military equipment, biomedical specimens, etc.

During Operation Buster-Jangle (Reference 1), two devices of approximately 1-kt yield were thus detonated: one on the surface and one at 17 feet below the surface. Measurements were made on these two shots to obtain (1) basic data on blast, cratering, and thermal and nuclear radiation; (2) effects information on surface and subsurface structures; and (3) data with which to evaluate the residual nuclear-radiation hazard from fallout.

During Operation Tumbler-Snapper (Reference 2), the military-effect programs were designed primarily to obtain height-of-burst-blast data that was required for operational planning.

During Operation Upshot-Knothole (Reference 3), the military-effect programs were concentrated on two air bursts. General effects information was sought on many critical items of military equipment, idealized structures, and other targets of military significance, along with extensive measurements of the fundamental parameters of blast, and thermal and nuclear radiation. The extensive structures and military equipment that were exposed on these two shots provided a wealth of information in this field and clearly demonstrated the excessive damage effects on drag-sensitive structures located within the dust-laden-precursor region.

1.2 TECHNICAL PROGRAM

In the early part of October 1953, the Armed Forces Special Weapons Project (AFSWP) recommended that a high-altitude test be conducted to provide information relative to the air-defense problem. Subsequently, AFSWP requested the services to submit military-effect proposals for Operation Teapot, which had been announced by the AEC for autumn, 1954.

Project proposals from the services were received by Headquarters, AFSWP, during January, 1954, and reviewed carefully to eliminate duplication and to ensure that all proposals were technically sound and feasible for the planned test series. After numerous conferences with the services, an integrated DOD-effects program was formulated that included: (1) a high-altitude shot of about 1 kt at 40,000 feet; (2) a surface shot of at least 10 kt; and (3) an underground shot of approximately 10 kt at a depth of 135 feet.

This program was submitted to the Joint Chiefs of Staff and to the Assistant Secretary of Defense, R&D. On 19 May 1954, the program was approved by the Joint Chiefs of Staff subject to the review and approval of funds by the Assistant Secretary of Defense, R&D; however, during the time that the latter had the Operation Teapot program under consideration, the AEC

stated that the 10-kt surface and underground detonations were not compatible with the AEC safety criteria which had been established for future operations at NTS. Therefore, a new AFSWP program was prepared to be compatible with the AEC safety criteria.

The new program retained the high-altitude shot, reduced the yield of the underground shot to about 1 kt at a depth of 67 feet, and substituted the military-effect tower shot (MET, Shot 12) with a yield of 15 to 30 kt at a height of 300 to 500 feet for the surface shot. The MET-shot conditions of yield, tower height, time of firing, etc., were designed to accommodate the drone-aircraft Project 5.1, "Destructive Loads on Aircraft in Flight," (Reference 4). This project required the exposure of drone aircraft to a single-shock wave, with symmetrical loading under accurately known dynamic pressures. To verify these conditions, projects were included to verify the closure of the primary- and reflected-shock waves and to measure pressure versus distance on two of the AEC developmental shots of similar scaled heights of burst.

In addition to the drone-aircraft program, an extensive surface-blast program was planned for the MET shot to obtain further information on the behavior of shock waves along the ground surface, particularly those unusual and unexpected phenomena observed on Shot 10 of Operation Upshot-Knothole.

Although the majority of the military-effect experiments were to be conducted during the three shots just mentioned, a number of important effects experiments could be carried out only on AEC developmental shots; therefore, maximum use was made of these shots.

The revised DOD test program was approved by the Joint Chiefs of Staff and the Secretary of Defense in August 1954.

1.3 ORGANIZATION

On 17 September 1954, the Chief AFSWP assigned the responsibility for implementing the test program to the Directorate of Weapons Effects Tests, Field Command, Armed Forces Special Weapons Project (now designated Office of the Deputy Chief of Staff, Weapons Effects Tests, Field Command, Defense Atomic Support Agency). A budget breakdown was supplied which described the preliminary funds advanced to the participating agencies. The organization for the planning phases of the operation is shown in Figure 1.1, while the integrated AEC-DOD organization which became effective at NTS on 1 February 1955, is illustrated in Figure 1.2. An overall breakdown of the costs of Operation Teapot, to date, is shown in Table 1.1.

1.4 SHOT SCHEDULE

The original plans for Operation Teapot had included one high-explosive and twelve nuclear detonations, the high-explosive test to serve as a dry run for the nuclear high-altitude shot. Nine of the nuclear shots were to have been primarily weapon-development experiments, with the remaining three intended mainly for weapon-effect purposes. However, as the plans for the development program became firm, the Los Alamos Scientific Laboratory (LASL) proposed to the DOD that two of their devices [redacted] be utilized for the high-altitude and MET shots. The predicted yields of these devices were well within the limits desired. Therefore, the DOD agreed to the proposal with the reservation that stockpile weapons could be substituted if last-minute calculations indicated that the performance of the experimental devices would not meet military-effect specifications. There was a definite advantage in using the Wasp device for the high-altitude shot, since an identical device in a slightly different ballistic case was planned for detonation at a low altitude just prior in the schedule to the high-altitude shot. A correlation of basic effects at low and high altitudes would thus be possible, as well as easier yield measurement. In addition, the low-altitude detonation would serve as a prooftest of the device before it was committed to the high-altitude test.

The actual air-drop detonation of the low-altitude Wasp device (Shot 1) resulted in a yield

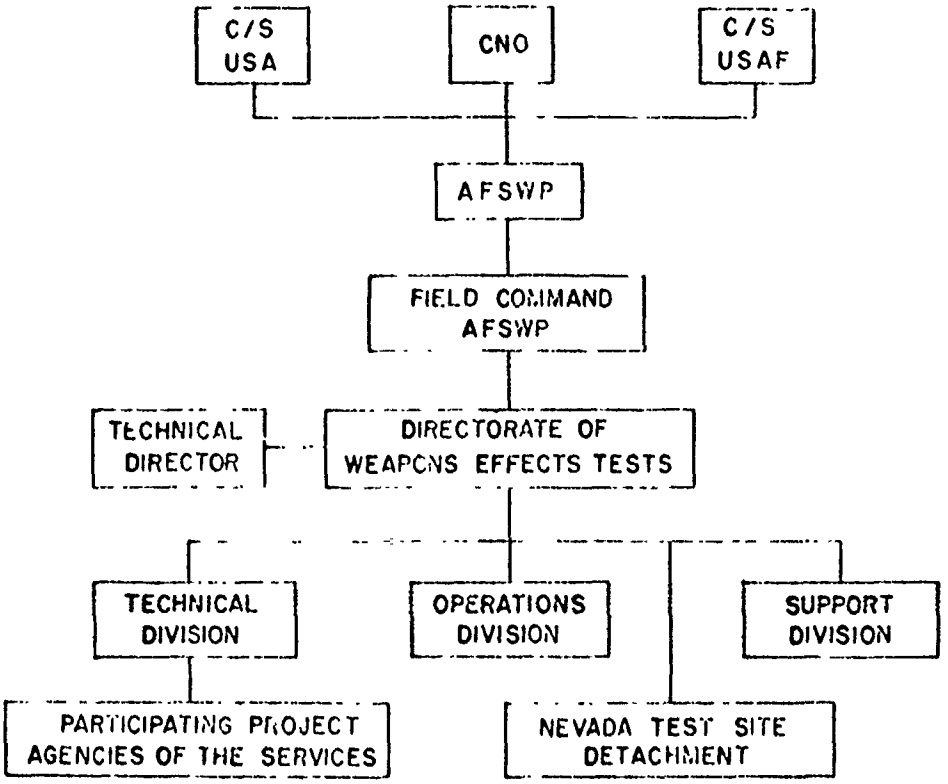

Figure 1.1 Organization, planning phase.

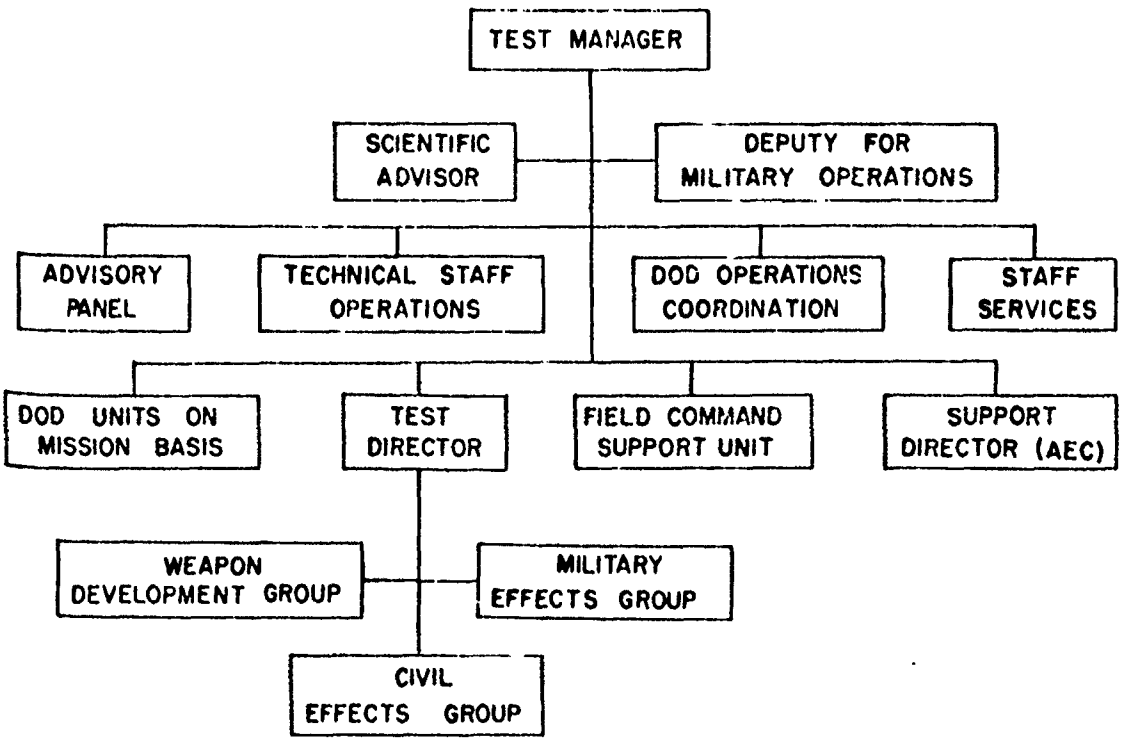

Figure 1.2 Organization, operational phase.

TABLE 1.1 TEAPOT R&D BUDGET

Project	Funds	Project	Funds	Project	Funds	Project	Funds
1.1	$175,680	2.3a	$ 40,508	3.6	$ 22,127	6.3	$101,695
1.2	85,057	2.3b		3.7	280,973	6.4	25,000
1.3	11,098	2.4	98,269	3.8	32,574	6.5	2,500
1.5	109,190	2.5.1	42,658	3.9	1,813		
1.6	61,114	2.5.2	9,279	3.10	123,746	8.1	18,556
1.7	94,692	2.6	22,853			8.2*	166,000
1.9	17,919	2.7	15,794	5.1	2,007,341	8.3	143,467
1.10	296,398	2.8a	19,000	5.2	521,823	8.4a	276,321
1.11	72,505	2.8b		5.4	106,367	8.4b	
1.12	127,719			5.5a	340,125	8.4c	
1.13	179,297	3.1	133,076	5.5b		8.4d	
1.14a	130,111	3.2	64,640			8.4e	
1.14b		3.3.1	62,539	6.1.1a	17,963	8.4f	
2.1	56,779	3.3.2	28,185	6.1.1b			
2.2	127,061	3.4	28,517	6.1.2	8,819	9.1	76,123
				6.2	1,501	9.4	69,934

* Joint effort with LASL Project 18.2.

TABLE 1.2 SUMMARY OF SHOT DATA

Shot	Date	Time	TNT-Equivalent Yield			Zero-Point Environment						Atmospheric Pressure		Air Temperature	
			Hydrodynamic	Radiochemical	Recommended	Support	Area	Nevada State Grid Coordinates		Height of Burst	Scaled Height of Burst*	Ground Zero Elevation	Ground Zero	Height of Burst	Ground Zero	Height of Burst
		PST	kt	kt	kt			North	East	ft	ft	ft MSL	mb	mb	C	C
1. Wasp	16 Feb	1159 59.157	1.32	1.16 ± 0.03	1.2 ± 0.1	Air	T-7-4†	851,123.89	668,674.34	761 ± 5	662	4,196	880	846	−3.0	−6.8
2. Moth	22 Feb	0545:00.019	2.4 ± 0.3	2.39 ± 0.10	2.4 ± 0.2	Tower	T-3	837,926.05	668,416.41	300	213	4,026	890	871	−7.8	−4.2
3. Tesla	1 Mar	0530:00.272	7.0 ± 0.2	6.85 ± 0.35	6.9 ± 0.2	Tower	T-9b	865,221.60	669,566.60	300	150	4,301	876	868	−3.9	3.3
4. Turk	7 Mar	0520:00.200	43 ± 2	43 ± 2‡	43 ± 2	Tower	T-2	869,840.42	660,066.18	500	136	4,401	868	869	5.2	5.6
5. Hornet	12 Mar	0519:59.802	3.6 ± 0.4	3.61 ± 0.1	3.6 ± 0.2	Tower	T-3a	834,301.10	667,164.30	300	187	4,006	881	873	−1.0	7.0
6. Bee	22 Mar	0504:59.930	8.4 ± 0.4	7.76 ± 0.2	8.1 ± 0.3	Tower	T-7-1a	834,123.94	667,562.18	500	266	4,245	876	871	1.0	5.0
7. Ess	23 Mar	1230 00.01	‡	‡	1.2‡	Underground	T-16a	850,656.60	661,461.66	−67	---	4,296	871	---	16.3	---
8. Apple I	29 Mar	0445.00.075	17.6 ± 2	14.2 ± 0.5	15 ± 2	Tower	T-4	854,233.66	664,663.56	500	196	4,300	867	854	9.1	11.2
9. Wasp'	29 Mar	0959:54.815	3.3 ± 0.3	3.16 ± 0.16	3.2 ± 0.2	Air	T-7-4¶	851,123.89	668,674.34	720 ± 10	475	4,196	871	849	13.4	12.6
10. HA	6 Apr	1000:04.065	3.0 ± 0.1	3.3 ± 0.4	3.2 ± 0.2	Air	T-5**	829,987.36	677,714.65	36,645 ± 30 (MSL)	13,103	4,036	662	222	18.3	−47.7
11. Post	9 Apr	0430:00.176	1.6 ± 0.2	1.45 ± 0.1	1.5 ± 0.1	Tower	T-9c	864,645.60	664,336.66	300	181	4,236	874	863	1.0	10.3
12. MET	15 Apr	1115 00.327	24.5 ± 1.5	22.0 ± 1.0	23.6 ± 1.5	Tower	FF	746,240.96	716,000.29	400	137	3,977	908	895	19.5	18.9
13. Apple II	5 May	0410:00.013	31.6 ± 2.0	28.5 ± 1.5	30 ± 3	Tower	T-1	838,780.31	664,358.64	500	186	4,236	871	855	7.5	15.6
14. Zucchini	15 May	0359:59.983	30.0 ± 1.5	28.2 ± 1.4	29 ± 2.0	Tower	T-7-1a	854,123.94	667,562.18	500	155	4,245	866	851	3.0	2.1

* 1-kt sea level, radiochemical yield.
† Actual ground zero 36 ± 15 ft North, 428 ± 15 ft West of T-7-4.
‡ Total yield, primary yield, 36 ± 1.6.
¶ Actual ground zero 96 ± 10 ft North, 62 ± 10 ft West of T-7-4.
** Actual ground zero 36 ± 50 ft South, 397 ± 50 ft West of T-5.
‡ Diagnostic measurements not made; yield based on previous performance of Ranger A.

TABLE 1 3 PROJECT PARTICIPATION

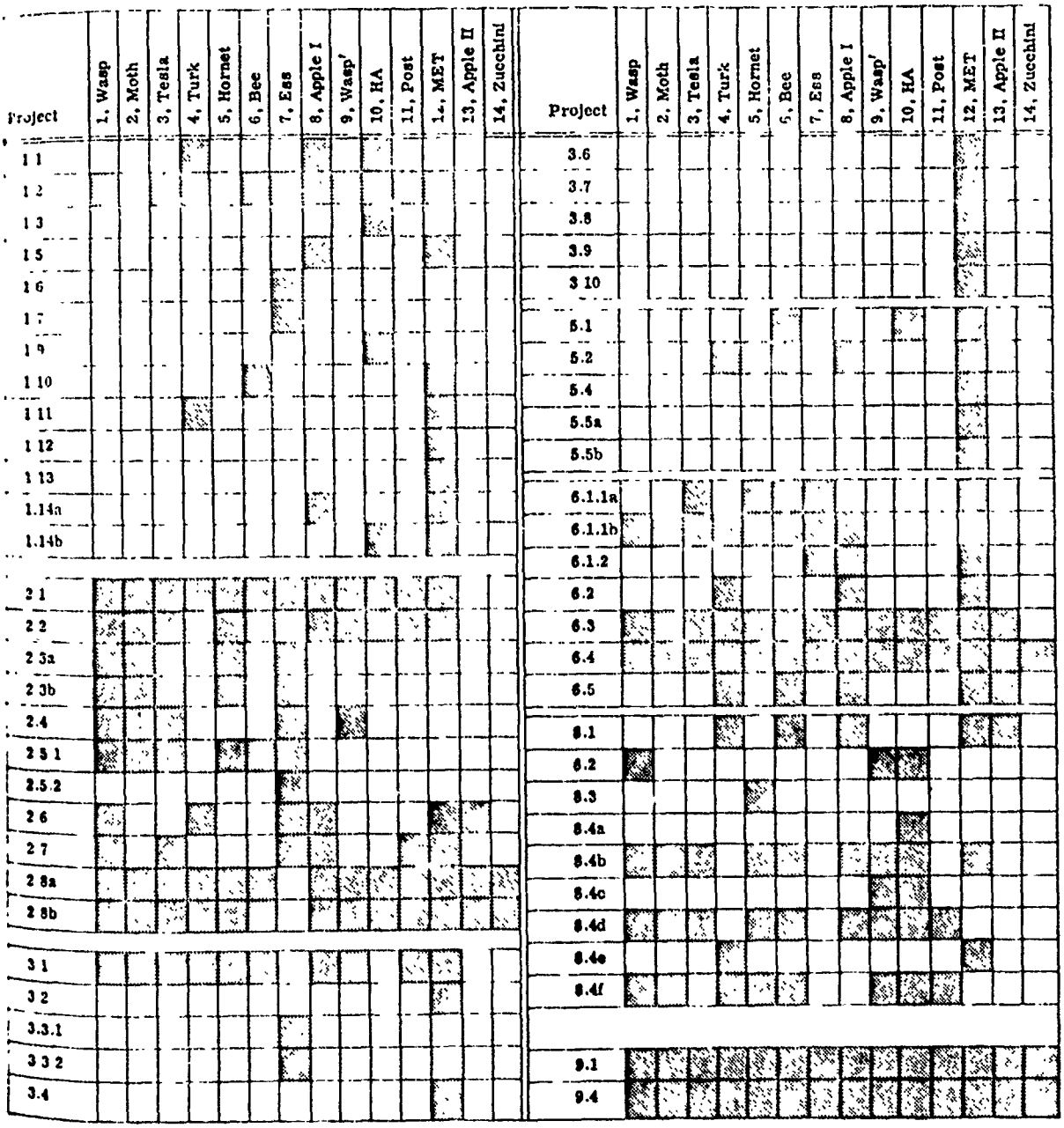

Indicates participation

which was considered too low for the high-altitude experiment. Therefore, the device was redesigned to increase the yield and the revised device, called Wasp Prime (Wasp'), was also air dropped (Shot 9). The resultant yield was entirely satisfactory. Thus, the same device was used for the high-altitude shot (Shot 10).

The Apple device, a development test (Shot 8), failed to give satisfactory performance. Because of the importance of this device to future development tests, a second, identical device designated Apple II was added to the schedule (Shot 13).

Thus, the final-shot schedule included fourteen nuclear detonations: eleven development; two combined development and effects (high-altitude, Shot 10; and MET, Shot 12); and one purely effects (ESS, Shot 7). Detailed information on Operation Teapot shot series is presented in Table 1.2. In general, three yield values were obtained: the fireball yield; the radiochemical yield; and a weighted average of these recommended by the Director, Weapons Development Group.

The shot participation of the military-effect projects is summarized in Table 1.3. The project numbers in this table reflect the organization of Operation Teapot weapon-test report series, as does the organization of the appendix to this summary report; e.g., Project 2.8 reported its findings in two reports, designated the report of Project 2.8a and 2.8b, even though there was no such subdivision formally in effect during the field phase.

Chapter 2
BLAST MEASUREMENTS

2.1 INTRODUCTION

The blast measurements on the high-altitude shot (Shot 10, or HA) and on the underground shot (Shot 7, or ESS) are covered in Chapters 5 and 6 of this report, respectively. All other blast measurements are covered in this chapter. Principal emphasis is placed on the results of the MET shot (Shot 12) on which the majority of the measurements were made.

2.1.1 Ideal Case. Frequent reference will be made herein to the ideal case, which is defined and discussed at some length in Reference 3. Briefly, the ideal case is defined as that which would exist for a nuclear detonation with no thermal effects over a perfect reflecting surface with no particulate matter which can be picked up by the blast wave. Figures 2.1 and 2.2 present ideal peak values of overpressure, p, and dynamic pressure, q, for 1-kt, sea-level conditions (from Reference 3). In the ideal case, the blast wave is characterized by a sharp or instantaneous rise of pressure and other blast parameters followed by a smooth and systematic decay in the classical-wave-form characteristic of TNT detonations.

In addition to the ideal height-of-burst curves for peak pressure, it is useful to refer to ideal arrival time versus slant range and ground range for various burst heights. These curves are presented in Figures 2.3 and 2.4, where the surface-level-arrival times for an ideal surface are presented. The curves were computed as follows: A-scaled (See discussion in Section 2.2) ground range for the onset of the Mach reflection was calculated from the ideal-critical angle (Reference 3) and the ideal-arrival time at the corresponding slant range found from a composite, nuclear, free-air arrival-time curve. In order to calculate arrival times at ground ranges between Mach-reflection onset and those included in Figure 2.1, the ideal height of the Mach stem was found and the arrival times at Mach-stem height taken from the composite free-air curve. The ideal wave was assumed to be perpendicular to the ground surface, so that arrival times at ground level corresponded to this computation. At ground ranges beyond the range at which ideal overpressures equaled 200 psi, the ideal-arrival times were computed by referring to Figure 2.1 (the highest pressure plotted in Figure 2.1) to obtain the curve for ideal pressure versus ground range. Overpressure was converted to shock velocity using the Rankine-Hugoniot relations, and arrival times were found by integrating numerically the relation

$$t - t_0 = \int_{r_0}^{r} \frac{dt}{dr}\, dr = \int_{r_0}^{r} \frac{1}{v}\, dr \qquad (2.1)$$

where t_0 and r_0 refer to time zero and ground zero, respectively.

The curves for 100-foot burst height were almost coincident with those for 200 feet. Determination of the ideal arrivals for scaled-burst heights below 100 feet by this method was not attempted; the assumption that the wave was perpendicular to the ground surface was probably tenuous for the low-burst case.

2.1.2 Background. Several prior nuclear-test series have shown marked departures from ideal behavior. In particular, relatively low bursts at NTS have shown extreme departures

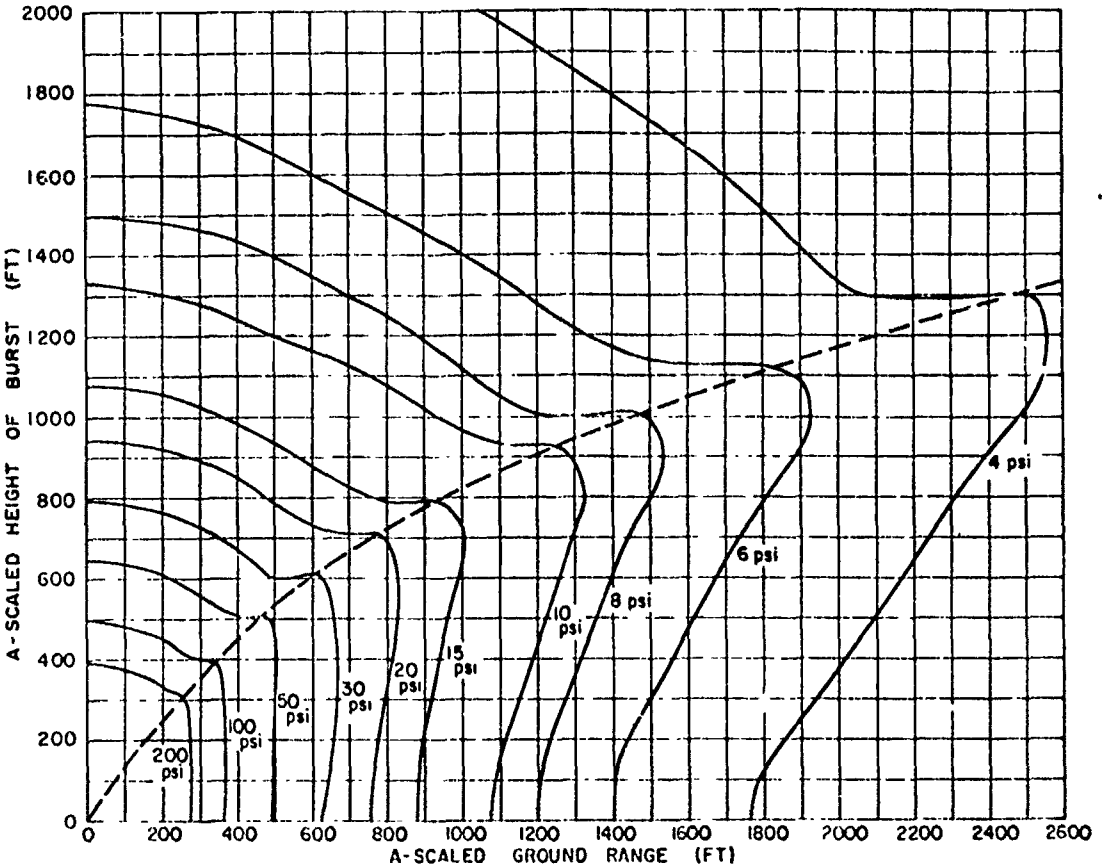

Figure 2.1 Ideal peak overpressure for 1 kt at sea level.

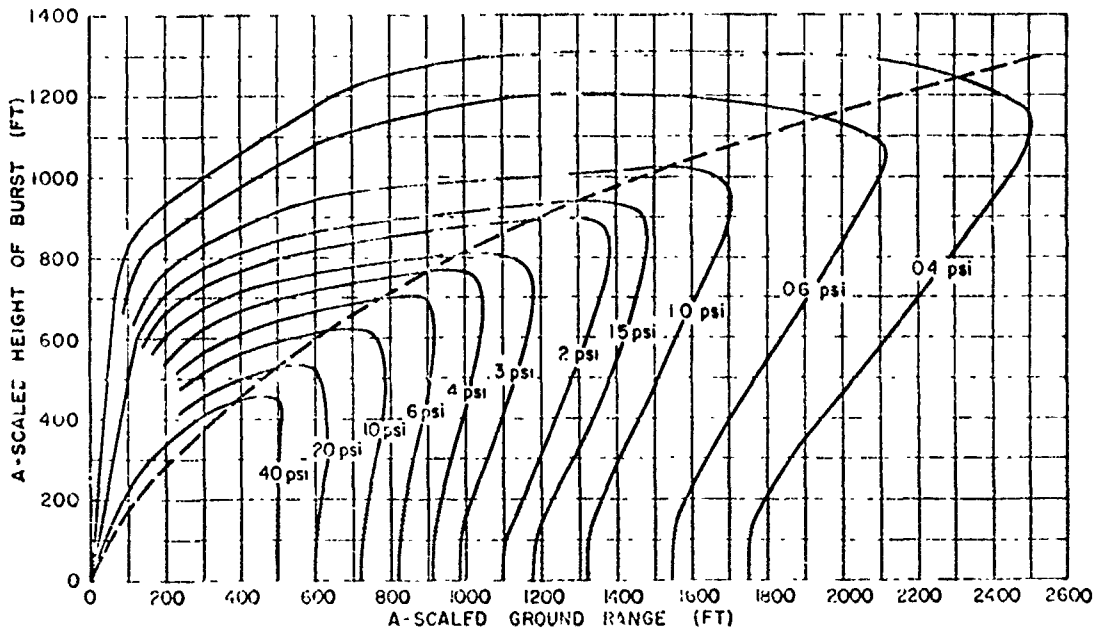

Figure 2.2 Ideal peak dynamic pressure for 1 kt at sea level.

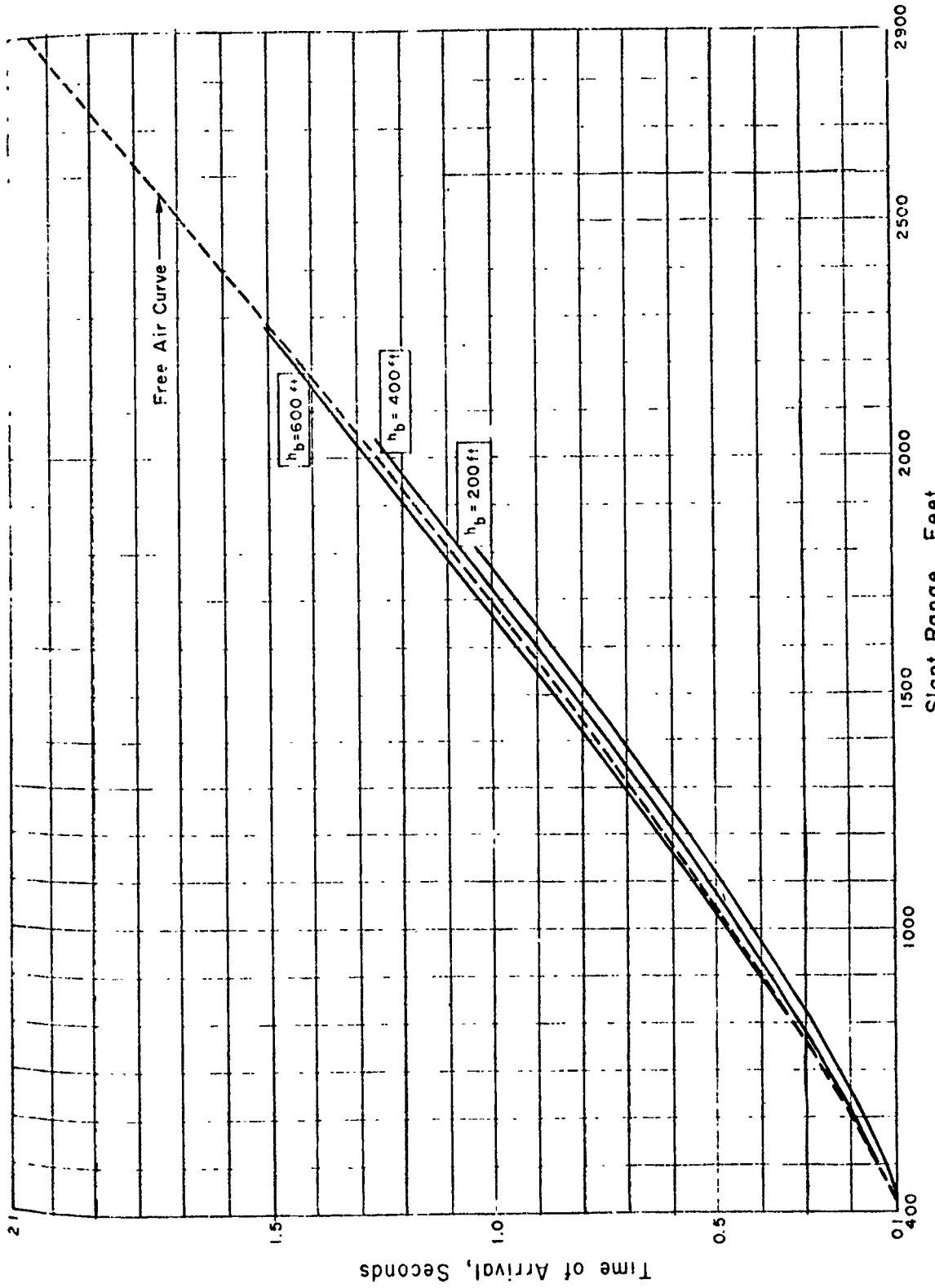

Figure 2.3 Ideal overpressure arrival time versus slant range for 1 kt at sea level.

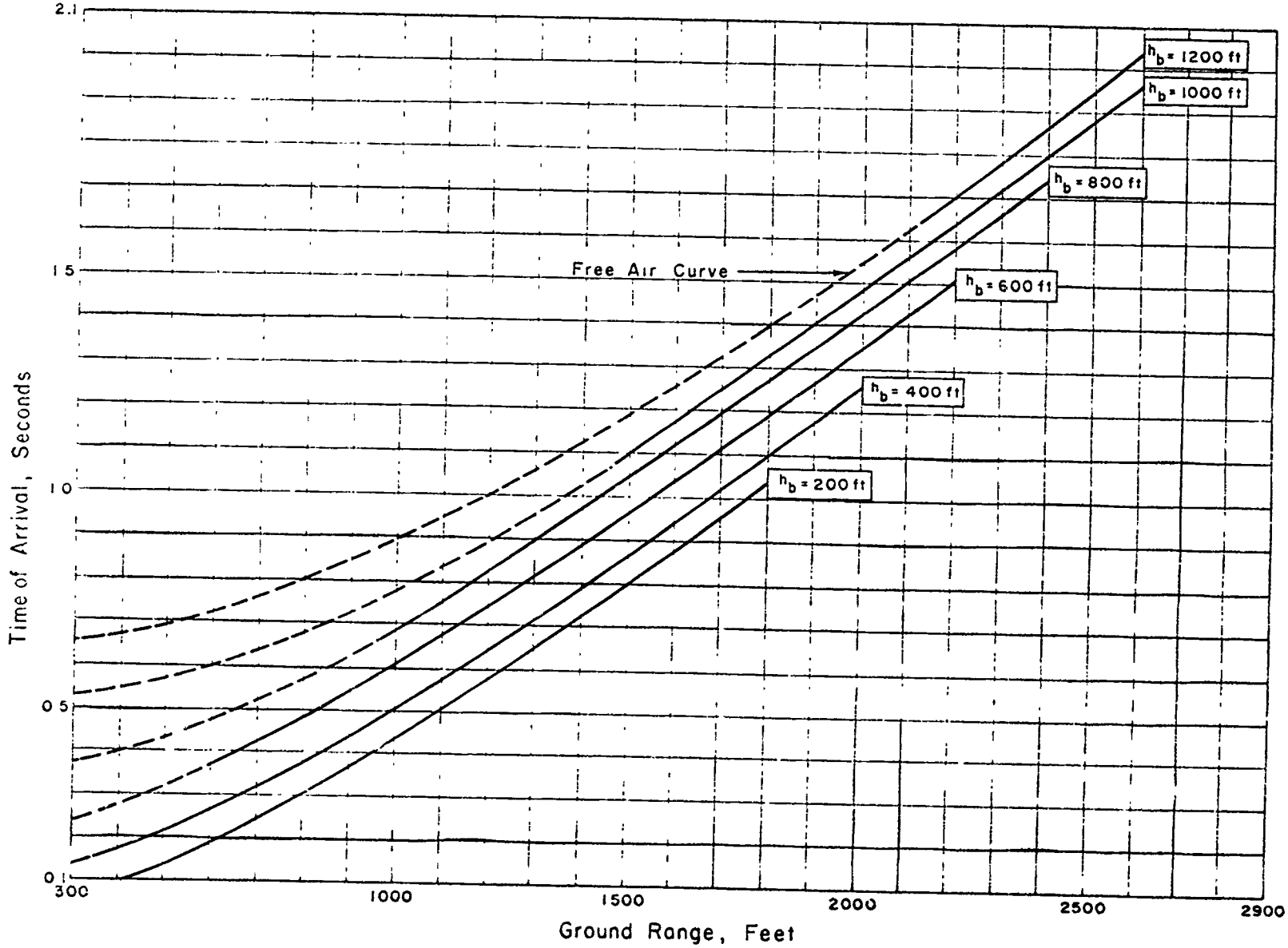

Figure 2.4 Ideal overpressure arrival time versus ground range for 1 kt at sea level.

from ideal. Such non-ideal blast behavior has generally been associated with the existence of a precursor-pressure wave, presumably resulting from the existence of a surface layer of hot air generated by the interaction of the thermal radiation with the ground surface. Where precursors have been developed, it has been noted that the blast wave returns to ideal at overpressures around 6 psi for conditions scaled to sea level.

During Operation Upshot-Knothole (Reference 3) Shot 10, the damage characteristics of a low burst in the precursor region over a desert surface were clearly demonstrated. In this region it was observed that the overpressures were substantially below ideal but that the damage to drag-sensitive targets was much greater than would be expected for the measured values of overpressure. Very few dynamic-pressure measurements were obtained in the precursor region, but the data available indicated that the measured dynamic pressures in the precursor region were equal to or greater than ideal and much greater than would be calculated from the measured overpressures using the classical Rankine-Hugoniot relationship applicable across a shock front. It was further observed that the dust behind the shock front was extremely pronounced in the precursor region. Specific contribution of the dust to drag forces was not determined.

Unfortunately, previous nuclear tests had not permitted the evaluation of the effects of a non-precursor-forming low burst, since the available test surfaces consistently gave rise to the precursor wave on low bursts. There remained a need for a more definite delineation of the various blast parameters in the precursor region plus a determination of their effects on targets and the relative effectiveness of different surfaces in producing precursor effects. In particular, it was not clear that a precursor-forming low burst would be more or less effective in producing damage than would a similar low burst over a non-precursor-forming surface or a surface burst over a precursor-forming surface, with or without dust.

It was clear that an extensive and complex blast program would be required to resolve some of the uncertainties concerning blast effects in the precursor region. In particular, two test detonations would be required: a surface burst of greater than 10 kt, and a low-air burst of greater than 10 kt.

It would further be required or desirable to study the effects of these test detonations over three test surfaces: a dusty, precursor-forming surface (desert), a non-dusty-precursor-forming surface (vegetation), and a non-dusty, non-precursor-forming surface (ideal). In addition, it would be desirable to measure individually as functions of time the various important parameters of the blast wave, such as overpressure, dynamic pressure, total density, air density, particle (dust) density, particle velocity, velocity of sound, direction of particle flow, air temperature, etc., as functions of height above the surface and as functions of ground range. Actual effects on representative targets would have to be observed in order to determine the significance of the various blast parameters under investigation. It would also be desirable to investigate the preshock, thermal-induced characteristics of various test surfaces intermediate between the extremes chosen for the principal studies.

As explained in Chapter 1, it was not possible to include a suitable surface burst during Operation Teapot. Because of the experimental and operational requirements of the aircraft drone Project 5.1 (Chapter 8), the MET shot (Shot 12) was included. For planning purposes, this shot was specified at 28 kt at a height of 400 feet. Within the limitations of time, funds, and available experimental techniques, it was decided to use Shot 12 to investigate the precursor-blast effects discussed above.

2.1.3 Shot 12 Blast Program. Shot 12 was planned for the Frenchman Flat area of NTS where extensive military-effect tests were conducted during Operations Tumbler-Snapper (Reference 2) and Upshot-Knothole (Reference 3). The untreated surface was satisfactory as the dusty, precursor-forming test surface (desert). There remained the problem of specification of the material and geometry for the other two test surfaces.

Ideally, perhaps, each test surface should have occupied a 120-degree sector of the ground plane, with a blast line of measurements along the central axis of each sector. Even this arrangement would not have represented a test detonation over an infinite surface nor guaranteed the elimination of boundary or cross-feed effects. In addition, engineering and economic considerations prohibited the consideration of such extensive artificial-test surfaces. It was decided that smaller, essentially rectangular test surfaces would be adequate if observations were limited to the early portion of the blast wave where boundary and cross-feed effects would be minimized. A width of 800 feet was chosen for each test surface, with the expectation that the first 0.1 to 0.2 second of the blast wave along the center of each surface would be relatively free of external perturbations. Because of such a choice it was recognized that the total effects on exposed targets might not be exactly representative of the effects to be expected over an infinite test surface. It was anticipated that the blast measurements as functions of time would permit an evaluation of cross-feed effects on exposed targets.

Based on Operation Upshot-Knothole Shot 1 and Shot 10 results, it was estimated that the most-significant-precursor region would extend to a ground range of approximately 3,000 feet on the desert. Consequently, it was decided to extend the test surfaces to a ground range of 3,000 feet. It was recognized that some precursor effects would exist to about 4,000 feet on the desert and that precursor effects might extend to an even greater distance on the organic surface. Nevertheless, economic considerations limited the test surfaces to a length of 3,000 feet.

The geometrical arrangement of the desert and test surfaces near the shot tower presented a design problem. A symmetrical arrangement, illustrated in Figure 2.5, was adopted. A four-guy shot tower was chosen, with the guy cables oriented midway between centers of the test surfaces and the centers of the desert test region.

For the organic surface, black asphalt sprayed over a gravel-asphalt-mix base was chosen. Laboratory experiments showed that such a surface gave pronounced thermal effects. Small-scale TNT experiments showed a reasonable insensitivity to mechanical blast effects. It was expected that the asphalt surface would be relatively dust free as compared to the untreated desert or lake bed (Reference 5).

For the ideal surface, water was chosen. Laboratory experiments had shown a water surface to be a good thermal reflector, with little thermal-surface effects. Operational considerations limited the depth of the water bed to an average of about 3 inches. It was recognized that this water surface might not be truly ideal because of the possibility of water loading behind the blast wave and the possibility that the blast wave would lift and carry large quantities of mud. Some Operation Castle results (Reference 6) indicated some water loading over deep water, but the effect of waves was not delineated. Even though water could not be expected to behave as a truly ideal surface at all ranges, it was hoped that it would approach ideal, at least by comparison to the desert and asphalt surfaces, at the outer limits of the water line. No other suitable ideal surface was practical under the operational and economic limitations of NTS. In fact, only good fortune permitted the attainment of a reasonably satisfactory test-water surface at shot time. Uncontrollable and unpredictable shot delays because of radioactive-fallout considerations made the limited water supply at NTS marginal.

Data Requirements. It was planned that the principal emphasis on blast measurements would be in the precursor, or non-ideal, region along the three blast lines. In previous blast measurement programs it was generally assumed that the blast-wave characteristic would be ideal and, consequently, only a single blast-parameter measurement would be required at a given point. For this program, however, it was evident that no such assumptions could be made and measurements of all possible blast-wave parameters would be desirable. In addition, it would be desirable to make measurements of the thermal and other surface effects which were presumed to have the perturbation influences on the blast wave. It would be desirable to investigate (as functions of time) overpressure, total-dynamic pressure, dynamic pressure of the

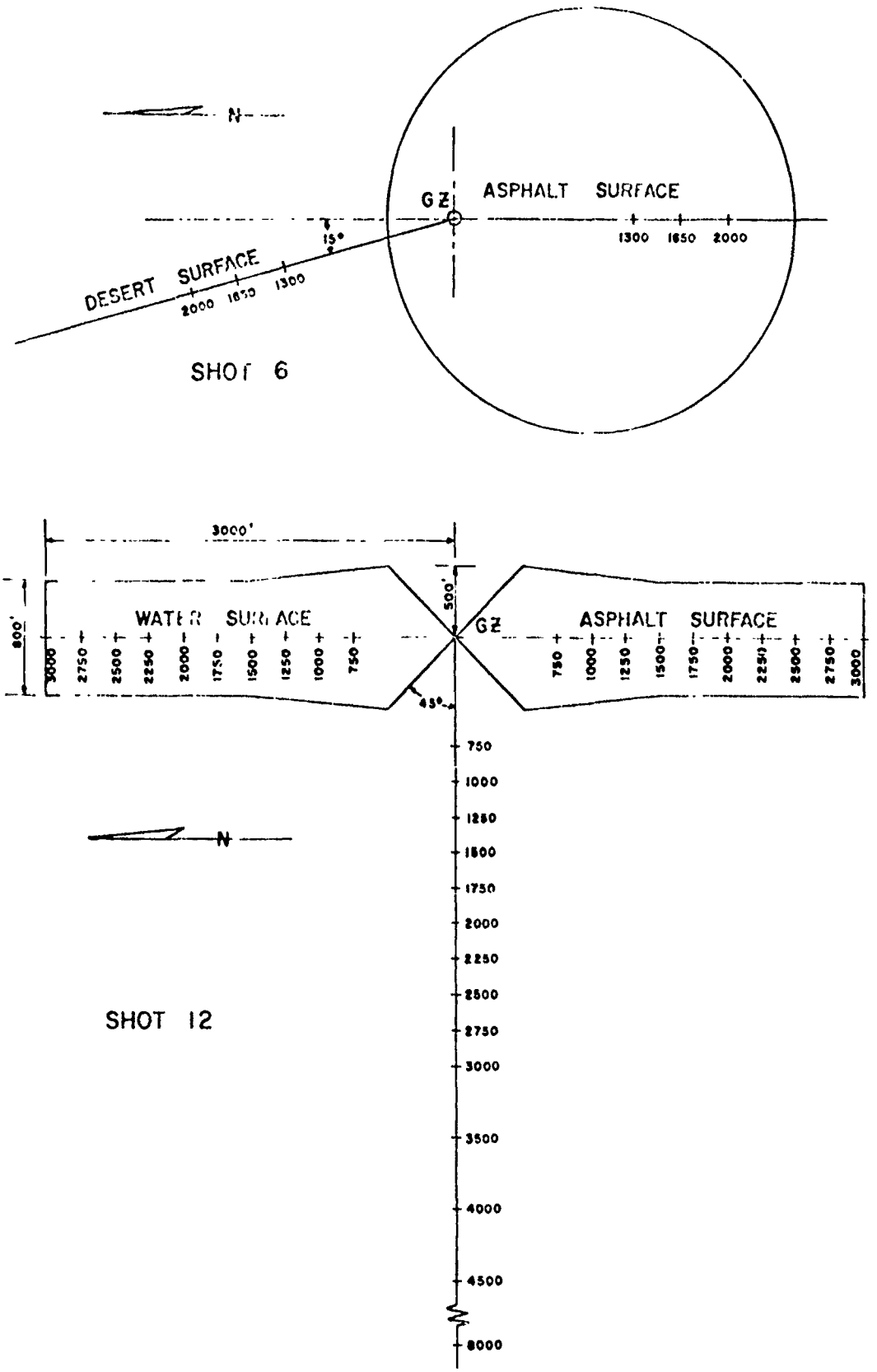

Figure 2.5 Area layouts, Shots 12 and 6.

gaseous medium, dynamic pressure of suspended-particulate matter, particle velocity of the gaseous medium (both in direction and in amplitude), particle velocity of the suspended-particulate matter (both in direction and in amplitude), total density, density of the gaseous medium, density of the suspended-particulate matter, gas temperature, velocity of sound, and perhaps other parameters. In some cases, preshock measurements would be desirable, while in others it would be necessary to make measurements throughout the history of the blast wave. In a few cases the total history would be desired. In general, the various parameters should be examined as functions of distance and height along each of the three blast lines, and additional preshock temperature and sound-velocity measurements should be included over small test surfaces representative of conditions intermediate between the three principal test surfaces chosen for the experiment. Unfortunately, in many cases suitable experimental techniques did not exist for the desired measurements. In general, there were insufficient funds to include an extensive investigation of some of the test parameters for which suitable measurement techniques may have existed. The final test program included extensive measurements of some of the more-fundamental blast parameters for which presumably dependable instrumentation had been developed previously; it included a limited number of exploratory measurements of some of the other parameters for which limited or expensive techniques were available or under development.

The blast program ultimately adopted placed principal emphasis upon blast photography and measurements of overpressure, dynamic pressure, and pitch (the angle of flow in the verticle plane) as functions of time.

Instrumentation. The primary overpressure measurements were on surface-level baffles essentially identical with installations used on previous nuclear tests. These measurements were intended to permit correlation with previous test data. Aboveground measurements were used with similar baffles oriented in a vertical plane and with the side-on ports of the pitot-static tubes used for dynamic-pressure measurements. The dynamic-pressure measurements, q, utilized the pitot-static q-gage previously developed and used by Sandia Corporation. This instrument had been used on previous nuclear tests. Limited data were available for the precursor region, with considerable data available for the ideal region. Tests had indicated that this instrument responded to the particulate matter, or dust loading, although its exact dust response and the relation to the forces developed on targets were still uncertain. Nevertheless, pending extensive new instrumentation development coupled with unlikely extensive application to full-scale nuclear tests, it was clear that an attempt must be made to correlate these so-called q′ measurements with the total blast effects.

The pitch, or angle of particle flow in the vertical plane, measurements were made by a relatively simple instrument designed by Sandia Corporation.

Blast photography was utilized to examine the general character and the time history and geometry of the precursor and other shock-front phenomena, such as Mach-stem formation and triple-point path. It was doubtful that such photography would be of significant value along the water line because of interference by the blast wave passing over the surrounding desert surface. Since it was believed that the blast wave would travel rapidly along the asphalt line, it was hoped that the photography over this surface would have some value. Aerial photography from directly over the shot point was planned to observe the progress of the blast over the three test surfaces.

Secondary blast measurements included special dynamic-pressure instruments developed by Sandia Corporation. An instrument designated as Greg was expected to respond to the total dynamic pressure of the air and the dust, while the Snob instrument was expected to respond only to the dynamic pressure of the air. A few, special, air-density-and-velocity instruments developed by Sandia Corporation were included. Dust measurements by the Army Chemical Center (ACC) included beta densitometers and snap samplers.

The presumed preshock-thermal layer was investigated by sound-velocity measurements by the Navy Electronics Laboratory (NEL) and direct air-temperature measurements by NRDL.

In addition, small test plots of concrete, wood, ivy, and fir were included, with associated air-temperature and sound-velocity measurements, in an attempt to investigate the thermal-layer characteristics as a function of surface properties.

A limited drag-force program was included. Drag forces were measured on 3- and 10-inch-diameter spheres by the Naval Ordnance Laboratory (NOL) and BRL. These measurements were to be compared to the dynamic-pressure (q') measurements at the same locations, and would possibly permit later correlation with extensive laboratory, wind-tunnel, and shock-tube experiments to investigate the drag forces developed by the precursor-blast waves characteristic of the three test surfaces. In addition, jeeps were installed on all three blast lines to investigate the damage characteristics of each of the three blast lines for correlation with the extensive previous test results on jeeps.

Instrument Location and Mounting. On previous test series, with few exceptions, the only reliable blast measurements in the precursor region were of surface-level overpressure. Attempts to make aboveground measurements of overpressure, dynamic pressure, and other phenomena were frequently impaired because of structural failure of the gage mounts or gage towers as a result of blast effects. For Operation Teapot completely new, rugged, and expensive gage-mounting towers were designed. Because of the gage-mounting problem the principal emphasis was devoted to a height of 3 feet above ground, although extensive measurements were made at a height of 10 feet. In the interests of gage-tower stability and economy, the closest aboveground measurements were at a ground range of 1,250 feet while the surface measurements began at a distance of 750 feet from ground zero. These measurements included the intensive shock region, and it is doubtful that the expense associated with more complete investigation of the high-intensity region would be warranted. The gage towers as ultimately designed were completely successful and permitted measurements throughout the blast wave in the precursor region where successful measurements had heretofore been generally unavailable.

In general, identical measurements were made at various locations out to the 3,000-foot limit imposed by the two artificial test surfaces. Along the desert line some additional measurements were included at greater distances to delineate completely the precursor characteristics over the desert and to give limited data on the ideal region for comparison and correlation with previous blast data.

Mechanical overpressure gages along a 200-degree arc, radius 2,500 feet, through the three blast surfaces were included to investigate the overall symmetry of the blast wave. In addition, some dynamic pressure and horizontal direction-of-flow (yaw) measurements were made on one side of the water line in order to investigate cross-feed effects from the principal desert surface to the limited-water-line surface.

The total blast measurements program for the MET shot (Shot 12) is shown in the blast-instrumentation chart of Table 2.1.

2.1.4 Supporting Blast Program. In addition to the program outlined above, limited blast measurements were made on a number of the development shots of Operation Teapot. Mechanical or self-recording overpressure and dynamic-pressure instruments were included on a number of shots to establish the limits of precursor generation and to support the program on blast effects on vehicles. Similar instruments were used to investigate the effects of a limited smoke layer on blast during Shot 5. A summary of the blast measurements made during Operation Teapot shots, other than Shot 12, is included in Table 2.2.

Free air-blast photography using smoke trails was included in support of the aircraft-structures-test-drone program and is described elsewhere in this chapter. Blast photography was included on Shots 1, 2, 3, 6, and 9 to investigate the limiting characteristics of precursor generation.

TABLE 2.1 BLAST INSTRUMENTATION, SHOT 12

Pt - 0', 10' — pressure-time, at 0' and 10' elevations
q' — total dynamic pressure-time (of medium)
p — pitch of medium-time
Y — yaw of medium-time
ρa — air density-time
ρt — medium density-time
q — air dynamic pressure-time
F — force plate (12-inch baffle)
G — force plate (range)
W — particle velocity (of medium)
$C_{3,10}$ — total force on 3- and 10-inch spheres
D — soap-sampler (dust)
β — light transmissometer
AV — acoustic velocity - preshock
T — temperature, preshock

	Surface	750 ft	1,000 ft	1,250 ft	1,500 ft	1,750 ft	2,000 ft	2,250 ft	2,500 ft	2,750 ft	3,000 ft	3,500 ft	4,000 ft	4,500 ft	5,000 ft
Stanford Research Institute, Project 1.10															
Desert	Pt-0	Pt-0	q'-3	Pt-0,10 q'-3,10	q'-10	Pt-0,10 q'-3,10 (Beam)	q'-10	Pt-0,10 q'-3,10,25, 40 (Beam)	q'-3	Pt-0 q'-3,10	Pt-0 q'-10	q'-10	Pt-0 q'-3		
Water	Pt-0	Pt-0	q'-3	Pt-0,10 q'-3,10 q'-2 at 3	q'-10	Pt-0,10 q'-3,10	q'-10	Pt-0,10 q'-3,10,25,40 q'-2 at 3	q'-3	Pt-0 q'-3					
Asphalt	Pt-0	Pt-0	q'-3	Pt-0,10 q'-3,10	q'-10	Pt-0,10 q'-3,10	q'-10	Pt-0,10 q'-3,10,25,40	q'-3	Pt-0 q'-3					
Sandia Corporation, Project 1.11															
Desert			p-3	p-3,10	p-10	p-3,10 ρa-3 ρt-3 F-3 q-3 G-3	p-10	p-3,10,25,40 ρa-3 ρt-3 F-3 q-3 W-3 G-3	p-3	p-3	p-10				q' tube-10 Pt-10
Water			p-3	p-3,10 Y-2 at 4	p-10	p-3,10 ρa-3 q-3 F-3 G-3	p-10	p-10 Y-2 at 4 ρa-3 q-3 F-3 G-3	p-3	p-3					
Asphalt			p-3	p-3,10	p-10	p-3,10 ρa-3 q-3 F-3 G-3	p-10	p-3,10,25,40 ρa-3 q-3 F-3 G-3	p-3	p-3					
Naval Ordnance Laboratory, Project 1.12															
Desert								C_3-2 at 3 C_{10}-3		C_3-2 at 3 C_{10}-3	6-by-6-inch cylinder				C_3-2 at 3 C_{10}-2 at 3
Water								C_3-2 at 3 C_{10}-3							
Asphalt								C_3-2 at 3 C_{10}-3		C_3-2 at 3 C_{10}-3					
Ballistic Research Laboratories,* Project 1.14															
Desert						$C_{3,10}$-3		$C_{3,10}$-3		$C_{3,10}$-3 C_3-3					$C_{3,10}$-3
Water						$C_{3,10}$-3		$C_{3,10}$-3		$C_{3,10}$-3					
Asphalt						$C_{3,10}$-3		$C_{3,10}$-3		$C_{3,10}$-3					
Army Chemical Center and Chemical and Radiological Laboratory, Project 1.13															
Desert						D-3,10		β-3 D-3,10		β-3 D-3,10					
Water															
Asphalt						D-3,10		β-3 D-3,10		β-3					
Naval Electronics Laboratory, Project 1.8															
Desert		AV-1½,3,6				AV-1½,3,6									
Water		AV-1½,3,6													
Asphalt		AV-1½,3,6				AV-1½,3,6									
Naval Radiological Defense Laboratory, Project 8.4															
Desert		T-½,1½,3,6,10				T-½,1½,3,6,10									
Water		T-½,1½,3,6,10													
Asphalt		T-½,1½,3,6,10				T-½,1½,3,6,10									

* BRL, Project No. 1 Mechanical Pt gages at zero elevation along 120 degrees of a circle at 2,500 foot range.

A moderate blast program, including measurements of overpressure, dynamic pressure, and pitch was included on Shot 6 because of the unusual associated surface characteristics. The geometrical arrangements of this shot, which was 7.76 kt on a 500-foot tower, are shown in Figure 2.5. It is to be noted that the asphalt surface, which existed in Yucca Flat from a prior nuclear-test series, was much greater in lateral extent than that planned for Shot 12. Consequently, the blast wave over the asphalt surface could be assumed to be more nearly representative of that existing over an infinite surface of this characteristic. The measurement locations were chosen to be representative of the most interesting precursor region for correlation with the results of Operation Upshot-Knothole Shot 10 and the far more extensively instrumented Operation Teapot Shot 12.

TABLE 2.2 BLAST MEASUREMENTS OTHER THAN MET SHOT 12

Project	Shot Participation													Type of Measurement
	1	2	3	4	5	6	7	8	9	10*	11	13	14	
1.1														Free-air data
1.2														Smoke--rocket grid
1.2														Shock photograph
1.11														Instrument check
1.10														Pressure measurement
3.1														Pressure measurement
1.14a														Pressure measurement
1.5														Preshock sonic
1.6														Underground measurement
1.7														Underground measurement

*Shot 10 data and analysis discussed in Chapter 5.

2.2 SCALING FACTORS

For purposes of comparison with other nuclear detonations, it was convenient to normalize the blast data for individual shots in Operation Teapot to a common base by a method usually referred to as A-scaling. This procedure involved reducing the data to a standard atmosphere at sea level for 1 kt of radiochemical (RC) yield. Conventional cube-root-yield scaling was used in conjunction with Sachs correction factors for atmospheric pressures and temperatures at burst heights. The following A-scaled factors apply:

$$\text{Pressure: } S_p = \frac{14.7}{P_0}$$

$$\text{Distance: } S_d = \left(\frac{P_0}{14.7}\right)^{1/3} \left(\frac{1}{W}\right)^{1/3}$$

$$\text{Time: } S_t = \left(\frac{T_0 + 273}{293}\right)^{1/2} \left(\frac{P_0}{14.7}\right)^{1/3} \left(\frac{1}{W}\right)^{1/3}$$

$$\text{Impulse: } S_I = \left(\frac{T_0 + 273}{293}\right)^{1/2} \left(\frac{14.7}{P_0}\right)^{2/3} \left(\frac{1}{W}\right)^{1/3}$$

where: P_0 and T_0 = the ambient pressure and temperature at burst height in lb/in^2 and °C

W = the finally determined total yield in kilotons

The Sachs burst-height-correction factors and radiochemical yields were specified for use by all test groups to permit direct comparison of the test results with those from previous test series which were normalized in this manner.

Table 1.2 presents the pertinent data from which the A-scaling factors may be computed.

2.3 BLAST PARAMETERS

2.3.1 General Character of Results. Disturbed wave forms typical of a non-ideal, precursor-forming-low burst were observed in varying degrees on all three test surfaces of Shot 12. These results indicated thermal and mechanical disturbances related to the properties of each surface. In general, the wave forms along the desert line showed the generation of the precursor at close range, its customary development as the blast wave moved out along the line, and a final cleanup at around 4,000 feet. Along the asphalt line the wave forms were similar out to around 1,250-foot ground range. Between 1,250 and 2,000 feet the wave form along the asphalt line developed precursor characteristics much more rapidly than along the desert line, indicating the presence of a much stronger thermal layer. Between 2,000 and 3,000 feet the wave form along the asphalt line remained relatively constant, while the desert-line wave form continued to develop through the precursor cycle. It was apparent that even at 3,000 feet a strong precursor was still present over the asphalt, with overpressure considerably below ideal. The water-line records out to about 1,250 feet showed a wave form similar to the initial wave forms along the desert and asphalt lines but indicated slower perturbation development. Beyond 1,250 feet all overpressure wave forms on the water line showed a sharp shock arrival. The wave form seemed to clean up around 1,750 feet and approached the classical form with only slight hash. However, the wave form again became disturbed around 2,000-foot ground range on the water line and cleaned up again around 2,500 feet. From this range out to the end of the water line a classical wave form was observed, with peak overpressures and dynamic pressures nearly in accord with the Rankine-Hugoniot relation. A similar pattern of development of wave forms along the desert and asphalt lines was observed for Shot 6. Again, on Shot 6 the wave form disturbances along the asphalt line persisted to a much greater range than on the desert line, indicating that thermal effects were relatively stronger over the asphalt. A detailed analysis of wave forms for both Shot 6 and Shot 12 is presented in the report for Project 1.10, WT-1109 (Reference 7). The wave-form-classification system for overpressure-time measurements comprised nine types, the first and last of which were equivalent; that is, there were 8 distinct forms. On shots which produced a strong precursor, e.g., Upshot-Knothole Shot 10 and Teapot Shot 12, one was likely to observe examples of all types (Types 0 through 8). The wave forms, examples of which are shown in Figures 2.6 and 2.7, showed a somewhat cyclic behavior with increasing ground ranges, that is, Type 0 was very much like a classic form while Types 1, 2, and 3 indicated successively more pronounced deviation from the classic. Types 4, 5, 6, and 7 progressively lost the non-classic characteristics, and were sometimes called the cleanup forms. Finally, Type 8 was the classical wave form, not unlike Type 0. Generally, Types 3, 5, and 7 could be considered as transition types between the more pure Types 2, 4, 6, and 8.

For this summary report all wave forms presented were smoothed to eliminate short-duration spikes, overshoot, and electronic hash to obtain more representative records of significant military interest. Wave forms for only 0.3- to 0.4-second following shock arrival

are shown, since this is the period of the principal perturbations, with reasonably normal behavior thereafter.

2.3.2 Time of Arrival. A comparison of arrival times of the blast wave over the various surfaces illustrates many of the differences introduced by the surface. Figure 2.8 presents a

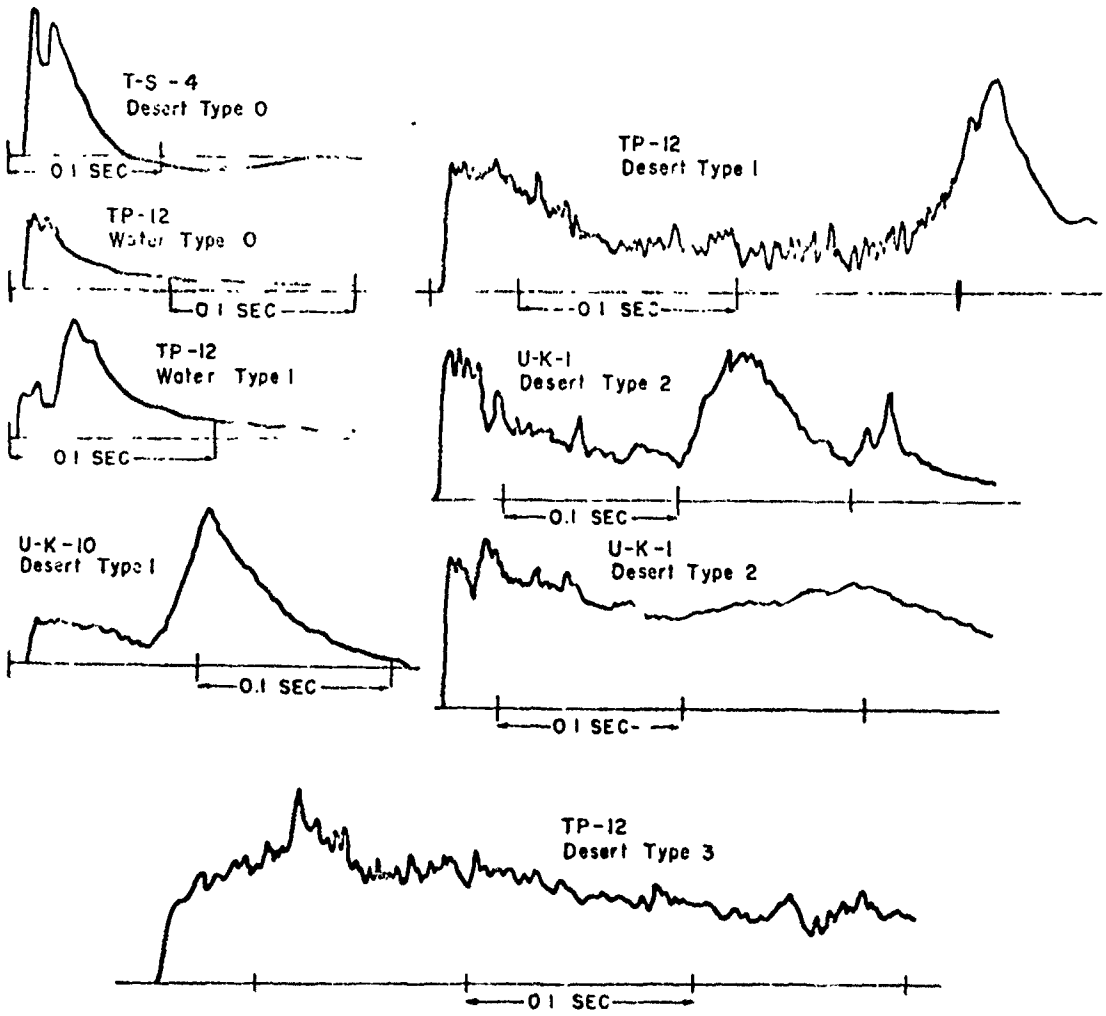

Figure 2.6 Overpressure wave forms; Types 0, 1, 2, and 3.

plot of the first arrivals versus ground range for the three blast lines on Shot 12. Also included in Figure 2.8 is the ideal arrival-time curve for Shot 12. The arrival times along the asphalt line were the earliest, while those along the water line were the latest. It is believed that these differences were caused by differences in the preshock-sound velocity near the ground surface. In the absence of particulate matter and medium change the preshock sound velocity was directly related to air temperature. It appeared that the water line was efficient in reducing the effective temperature of the thermal layer as compared to that which occurred over the desert line. Referring to Figure 2.8, the arrival at the first water-line gage (750 feet) was almost ideal. Similarly, the early arrivals on the asphalt line indicated higher effective temperatures and, consequently, a much stronger thermal layer over the asphalt sur-

face as compared to the desert. It may be noticed, however, that there was an inflection occurring in the arrival-time curve along the water line between 1,500 and 2,000 feet, which corresponded with the disturbances noticed in wave form in this same region. It is possible that cross-feed effects in this region from the desert tended to speed up the arrival of the initial disturbance. Beyond 2,000 feet the speed of the initial disturbance along the desert appeared

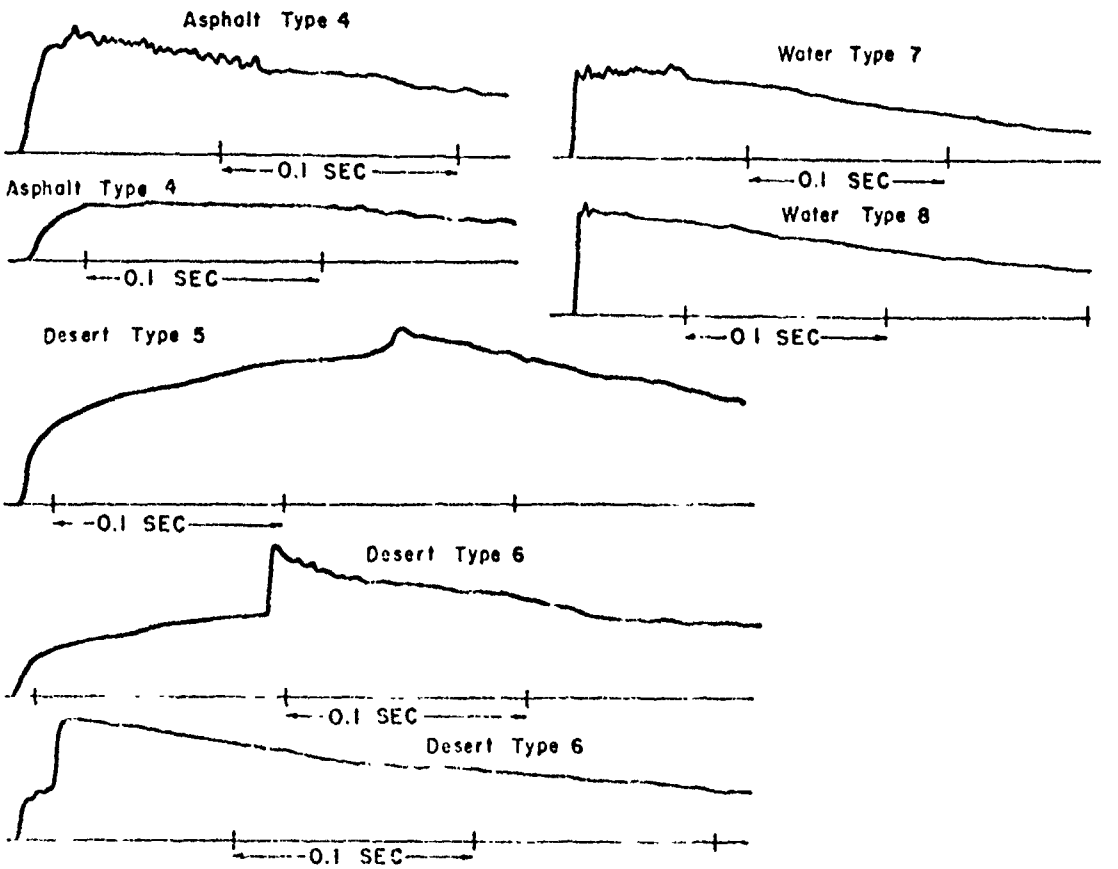

Figure 2.7 Overpressure wave forms; Types 4, 5, 6, 7, and 8.

to slow down as compared to the asphalt line, and the arrival-time curve for the desert approached that for the water line. The convergence of the desert and water line arrival-time curves around 3,000 feet was probably due to reduced thermal effects at long ranges along the desert line, in addition to the higher shock strengths on the water line beyond 2,500 feet. Furthermore, it was apparent that the arrival times over these two surfaces agreed well with the ideal curve. It may be noticed that at 750-foot ground range the arrival times on all three lines were quite similar, although some thermal effects were apparent even at this distance over the desert and asphalt. A similar trend in arrival times along the asphalt and desert lines was observed for Shot 6.

An examination of the electronic gage-records indicated that it was sometimes possible to identify a pronounced second arrival at certain ranges. An attempt was made by Project 1.10 to determine the significance of these second arrivals. When second arrivals were clearly apparent on the observed wave forms they were recorded and plotted as a function of ground range. If the assumption were made that the second arrivals corresponded with the undisturbed

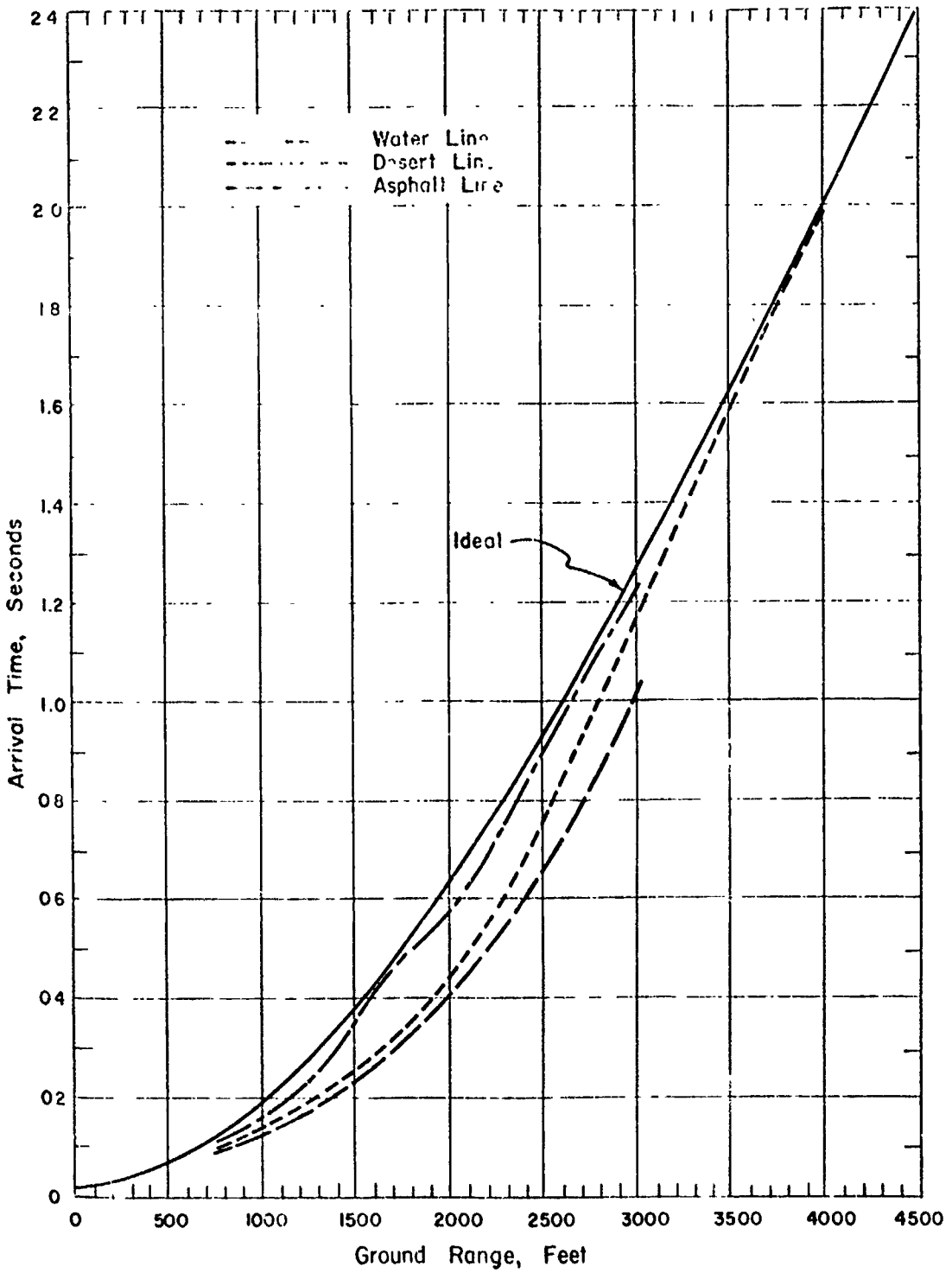

Figure 2.8 Time of arrival of surface overpressure, Shot 12.

main shock, the curve of second arrivals would approximate the arrival time curve over an ideal surface. The difference between curves showing the first and second arrivals represented the duration of the precursor. As was the case in previous tests, this duration was difficult to define in the intermediate precursor region because of the absence of definite arrivals of the so-called main shock. It was interesting to note that, on comparing these second arrivals on all three surfaces, an inverse order was observed as compared to the first arrivals. Consequently, the second shock arrived earliest along the water line and latest along the asphalt line, but the time differences were small. A similar situation was present on Shot 6. This trend was also apparent on Upshot-Knothole Shot 10, when the second arrivals tended to be later than would be expected if the Mach stem observed above the thermal layer were extrapolated to the ground. It would seem that either the second arrival could not be associated with the main wave or some phenomena associated with the thermal layer caused a delay in arrival of the main blast wave over a thermal-absorbing surface dependent on the temperature of the thermal layer, despite the increase in propagation velocity of the precursor under such conditions.

The horizontal-shock velocity versus ground-range curves are presented in Figure 2.9. To obtain these curves it was necessary to differentiate the time of arrival curves of Figure 2.8. Also included in this figure, for comparison purposes, is the ideal-shock-velocity curve from which the ideal time-of-arrival data were derived. Referring to Figure 2.9, the asphalt and desert curves, both well above ideal, have the same general form, showing asphalt-line-shock velocities consistently higher. However, at 3,000-foot ground range, asphalt- and desert-line velocities are approximately equal and nearly the same as the ideal velocity. Actually, at ranges beyond 2,300 feet many of the shock velocities over the desert and asphalt lines appear to be less than ideal. This result is not inconsistent with the depressed-peak overpressures measured on these same blast lines. The water-line velocity curve, exhibiting a pronounced inflection in the 1,500-foot region, deviates markedly from the ideal curve at the close-in ranges. While the ideal-shock velocity at 750 feet would be about 3,300 ft/sec, the water-line data indicate a velocity of about 6,000 ft/sec. The inflection in the water-line curve is followed by velocity data which agree well with desert-line velocities at 2,000 and 2,250 feet. This behavior suggests a feed in phenomenon or some other unusual condition occurring on the water line at these ranges (Section 2.3.5; Cross-Feed, SRI, Water). Finally, reference to Figure 2.9 and the gage records from Shot 12 point up the fact that the agreement of an experimental-shock velocity with the ideal velocity is not a sufficient criterion for the existence of undisturbed ideal-blast waves.

2.3.3 Overpressure. Surface Level Overpressure at Various Distances. The peak air-blast overpressures as a function of time measured by Wiancko gages in ground baffles at 750 feet from ground zero on each of the three test surfaces for Shot 12 are presented in Figure 2.10. At this close range the effects of thermal disturbances are already becoming apparent. The asphalt and desert records show the front-porch characteristic of early-precursor development, although the maximum overpressures are not yet significantly depressed.

Figure 2.11 presents the surface level-overpressure data at 3,000-foot ground range over each of the surfaces for Shot 12, along with the ideal-peak value scaled from Figure 2.1. The maximum-peak overpressure at this range was measured over the water line, with the lowest peak value recorded over the asphalt line. At this range thermal effects on the blast were more pronounced over the asphalt line than over the desert line and were essentially nonexistent over the water line. Reference to the overpressure-time records from the water and desert lines, shown in Figure 2.11, illustrates an inherent limitation imposed by maximum overpressure versus ground range plots. It is apparent in this case that the maximum overpressures measured over the two surfaces were comparable. However, the wave forms were widely divergent.

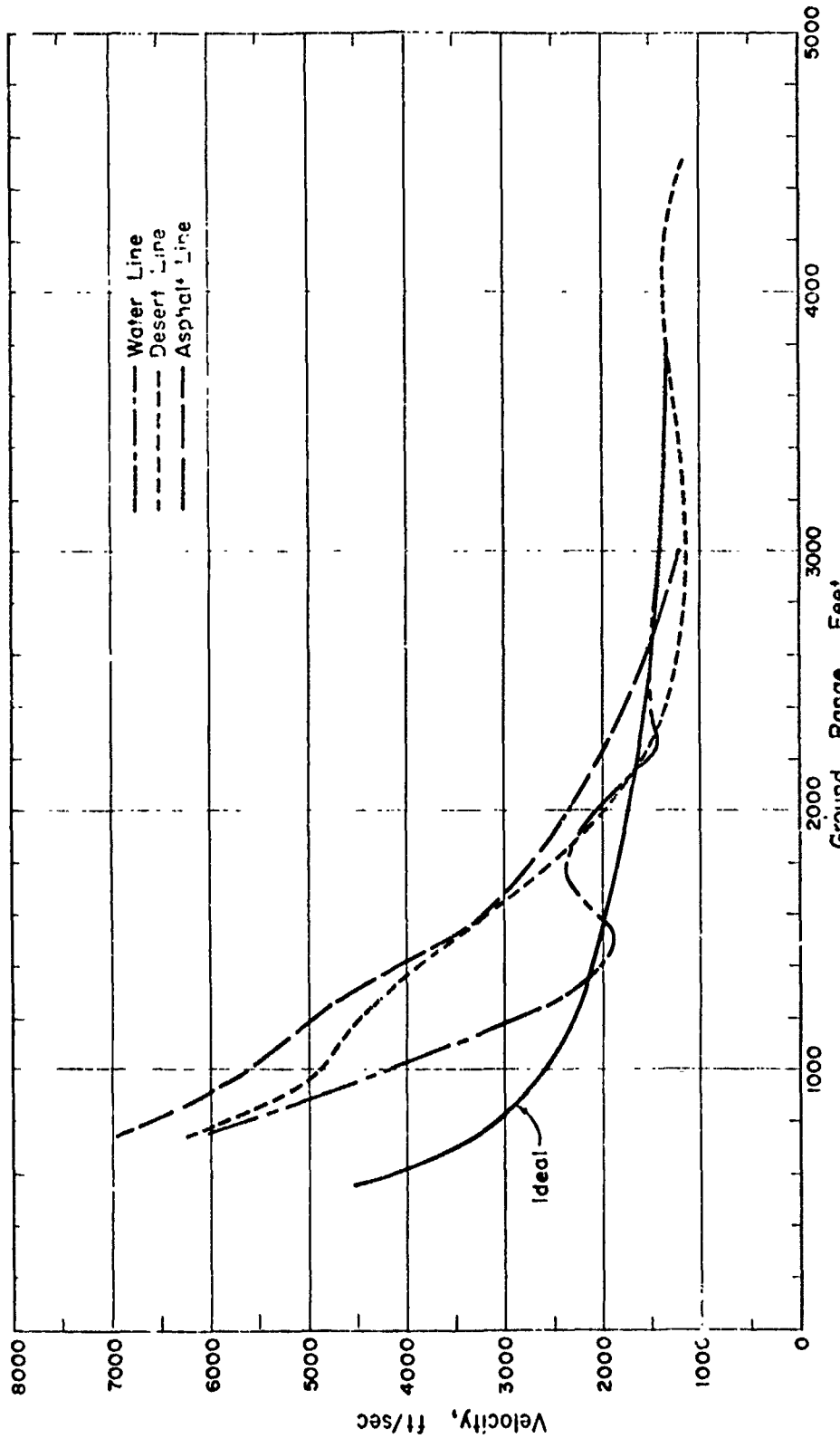

Figure 2.9 Horizontal shock velocity for surface overpressure, Shot 12.

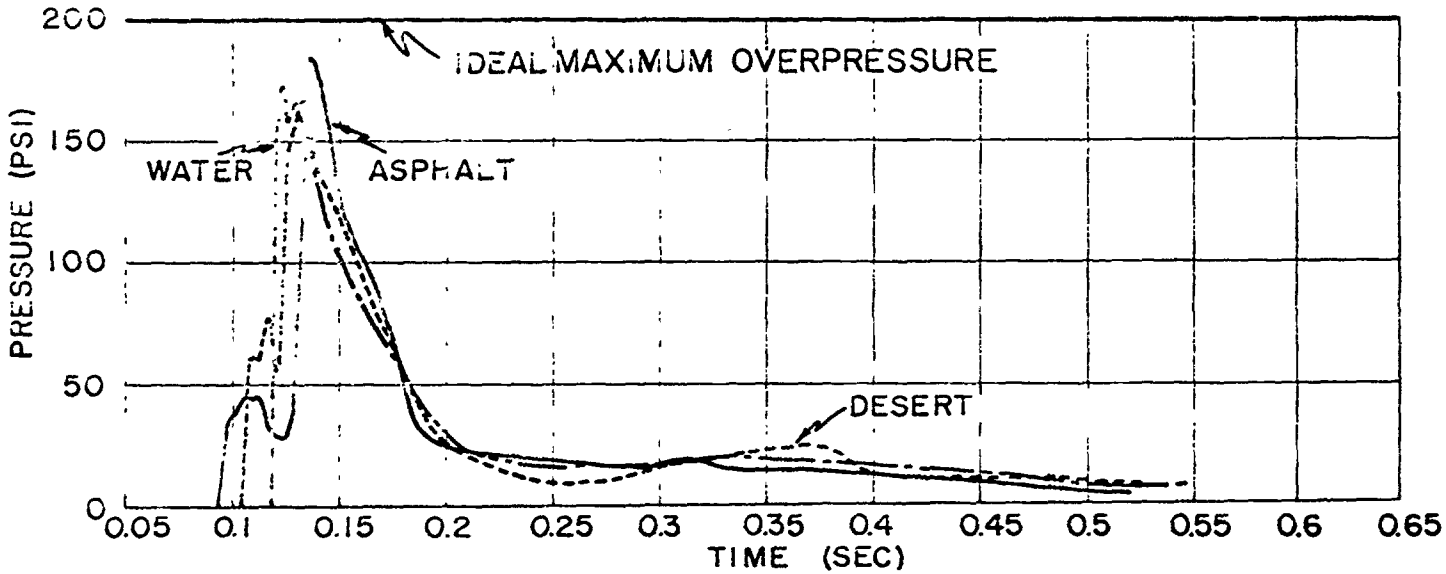

Figure 2.10 Surface level overpressures at 750-foot ground range, Shot 12.

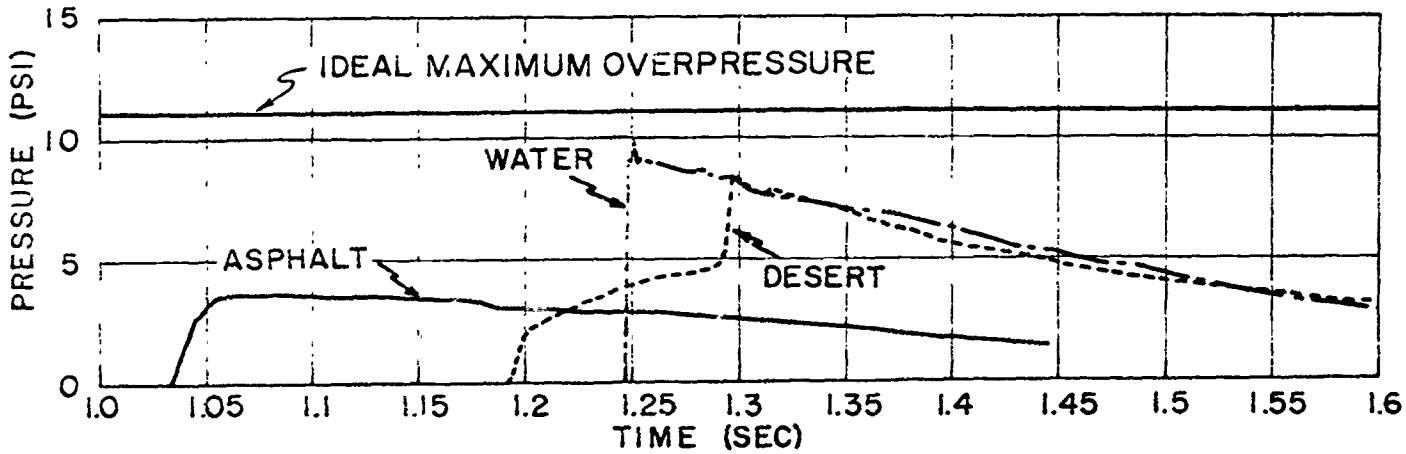

Figure 2.11 Surface level overpressures at 3,000-foot ground range, Shot 12.

When these data were plotted on maximum pressure-versus-range coordinates this divergence was ignored.

The maximum surface-level overpressures as measured along the three main blast lines for Shot 12 are presented as functions of ground range in Figure 2.12. The influence of a

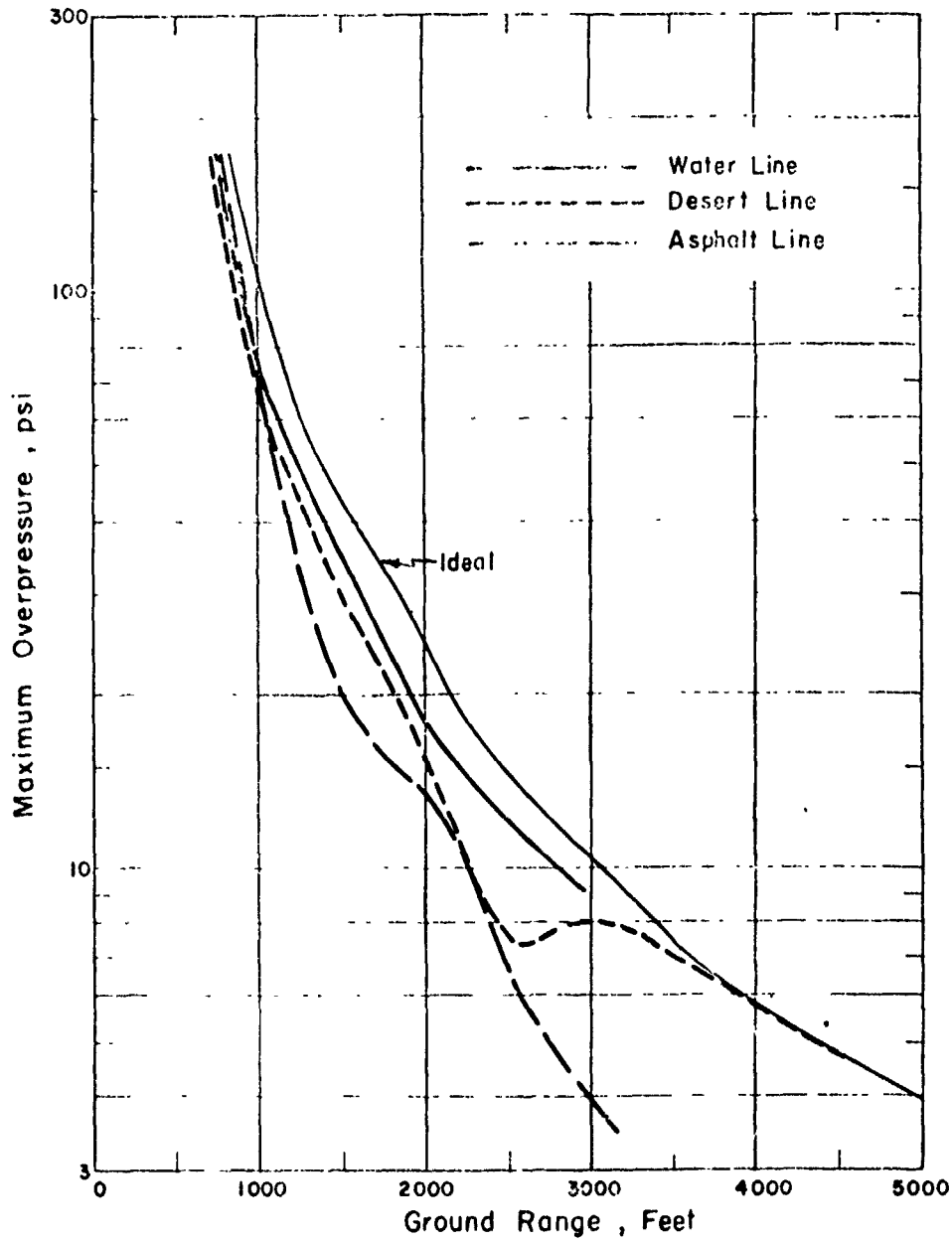

Figure 2.12 Maximum surface level overpressure versus ground range, Shot 12.

stronger thermal layer in depressing peak pressures along the asphalt below those over the desert is clearly indicated by this figure. The maximum deviation occurred around 1,500 feet where the peak overpressure measured on the asphalt was about half that recorded over the desert.

It is apparent from Figure 2.12 that the water and desert curves are similar out to about

2,000 feet, with the desert being somewhat lower, particularly at 1,000 feet. The usual inflection of the pressure-distance curve characteristic of the precursor cycle occurs around 1,500 feet on the asphalt line and around 2,500 feet on the desert line, but the same effect is not apparent over the water line. It should be noticed that, while the desert line curve recovered at about 3,000 feet with pressures on both the desert and water lines approaching ideal, the asphalt-line-pressure curve was still diverging at this range. It is believed that the pressure-distance curve would have recovered at somewhat greater range if the asphalt line had been longer, based on measurements made by BRL with self-recording gages over an asphalt surface on Shot 6. The data points on these curves at 2,500 feet were well documented, as will be discussed in the next section.

In general, overpressures measured by ground-level baffles were somewhat lower than overpressures measured above the ground with pitot-static tubes, with those at 3 feet usually being the maximum. The largest differences were observed over the desert line within 3,000 feet from ground zero and appeared random in nature, indicating local thermal disturbances and accompanying turbulence in the non-ideal or precursor region.

Overpressures at 2,500 Feet. A comparison of overpressure versus time at 2,500 feet along the three main blast lines is presented in Figure 2.13 for measurement at surface level, 3, 10, 25, and 40 feet in height. It is seen that the relative time of arrival is consistent as a function of height over all three surfaces. The arrival time on the asphalt line was ahead of that for the desert line, with that of the water line being last. The wave form comparisons in this figure indicated a relatively steep shock front for the water line at all heights. For the asphalt and desert lines a rounded wave form was observed, which became sharper with increase in height above the ground. The water-line records appeared more ideal in wave form, although a slight flattening of the peak was evident which fell somewhat below the maximum value of the ideal-predicted pressure at this range. Extrapolation to eliminate the flattened peaks would give peak overpressures on the water line nearly equal to the ideal value shown. The desert-line overpressures were somewhat higher than those for the asphalt line at all heights. The overpressure on the water line was usually higher than that on the desert and asphalt lines, except at 10 feet, where the peaks were comparable.

A comparison of overpressure versus time at 2,500 feet as a function of height on each line is made in Figure 2.14. Examination of the records over the asphalt surface showed that an increasing lag occurred in arrival time as the height was increased, indicating the backward inclination of the shock front. The wave forms were generally similar at all heights. The maximum overpressure occured at the 3-foot level. Over the desert surface the times of arrival were closer together, indicating a relatively steeper shock front as compared to the asphalt. The maximum overpressure was recorded at the 10-foot level, with that for the ground baffle and the 40-foot pitot static tube consistently low. Over the water surface the time of arrival was practically identical for all heights, indicating a vertical shock front. It is noticed that the overpressure versus time record at the 3-foot level decayed more rapidly than did the others. The wave forms in general were much cleaner over this surface, showing more conventional behavior as compared to the other surfaces.

Wave-Front Orientation. Using shock photography techniques, it was possible to document the wave-front orientation as a function of ground range. These results are presented in Figure 2.15. Also, using the shock velocity curves of Figure 2.9 and the arrival-time data of aboveground gages, it was possible to determine the orientation of the wave fronts at several ground ranges over the three blast lines for Shot 12. Lastly, if it is assumed that the initial particle flow behind the wave front was perpendicular to the front, a determination of the initial pitch angle also yielded the wave-front orientation.

The results of these three separate wave-front-orientation measurements are presented in Figure 2.16. For the desert line the shock photography and arrival-time-orientation results

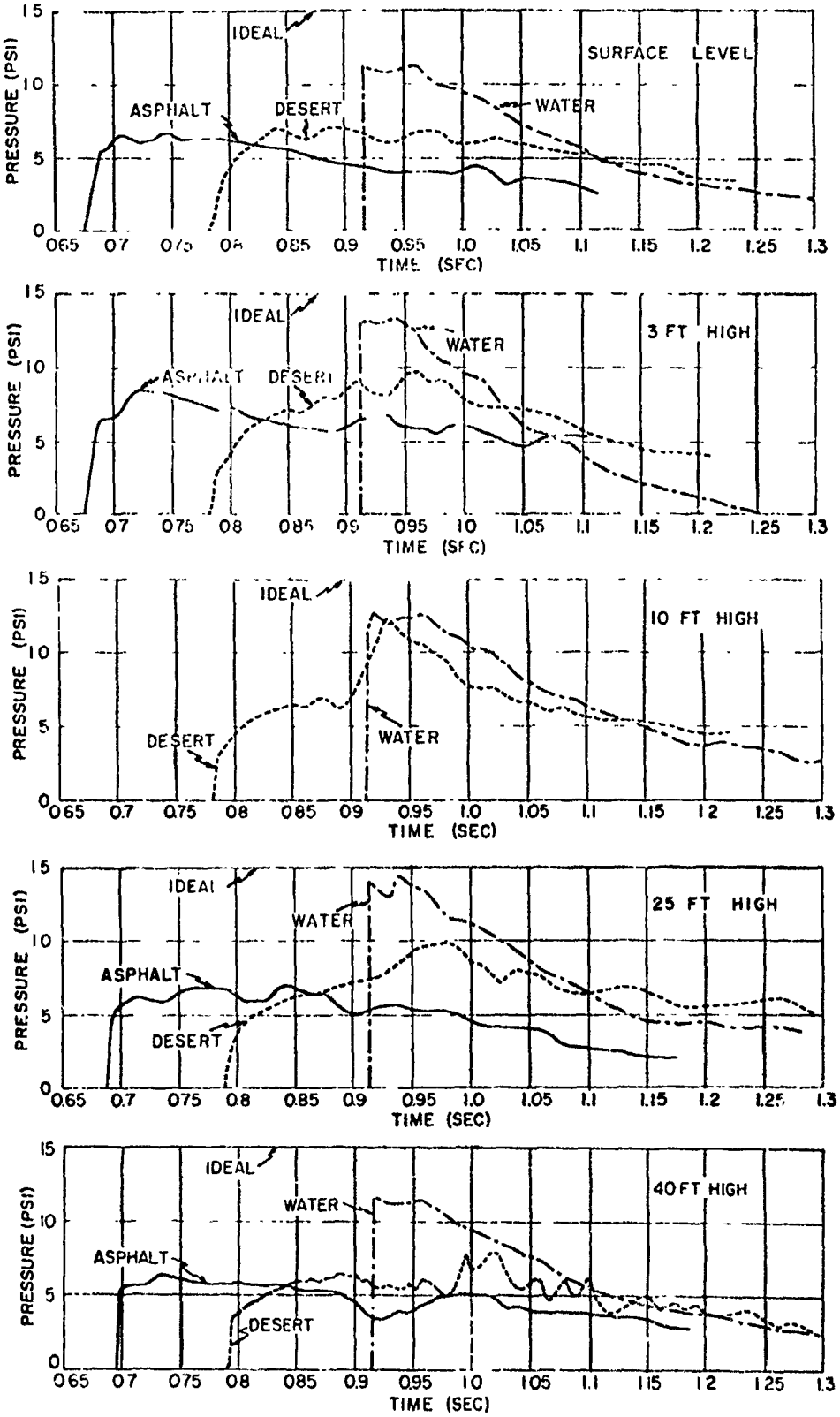

Figure 2.13 Overpressures at 2,500-foot ground range, Shot 12.

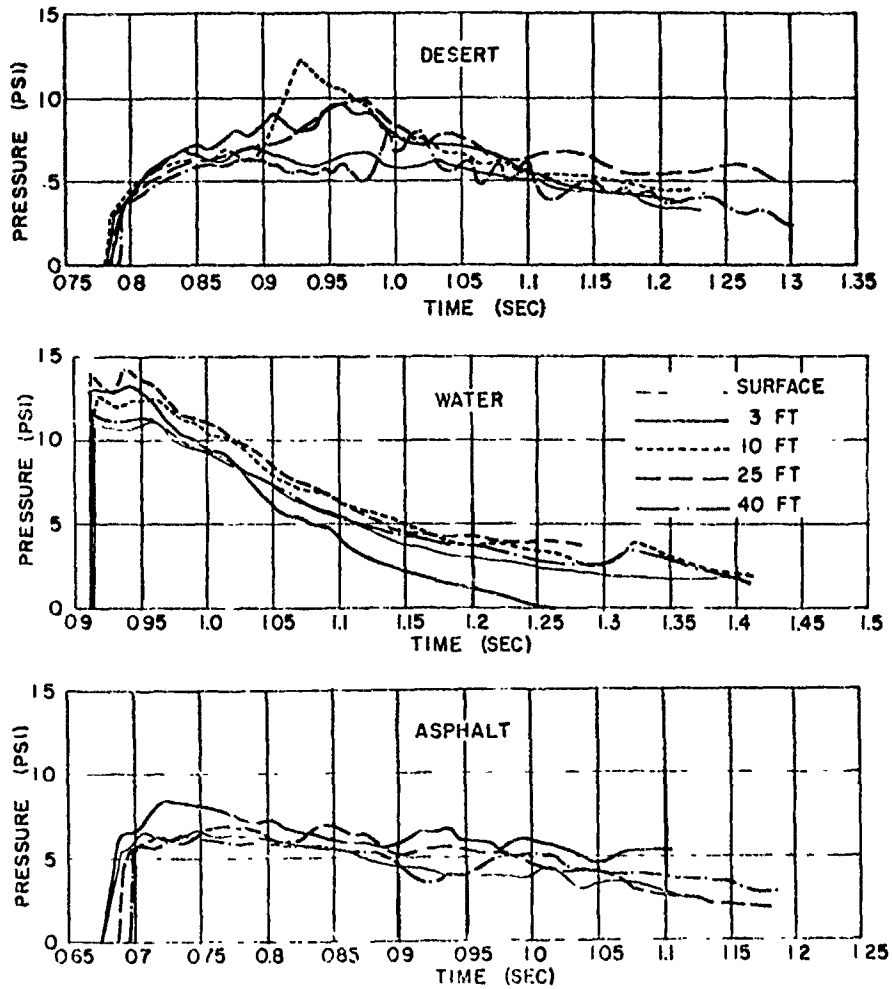

Figure 2.14 Overpressures at 2,500-foot ground range, Shot 12. No record at 10-foot gage over asphalt line.

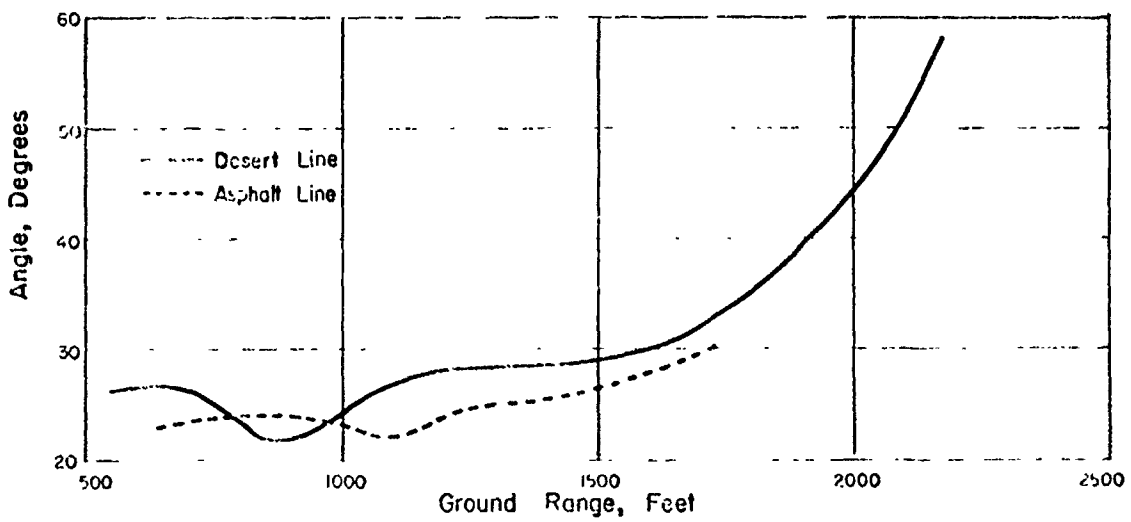

Figure 2 15 Angle of wave front orientation versus ground range, Shot 12.

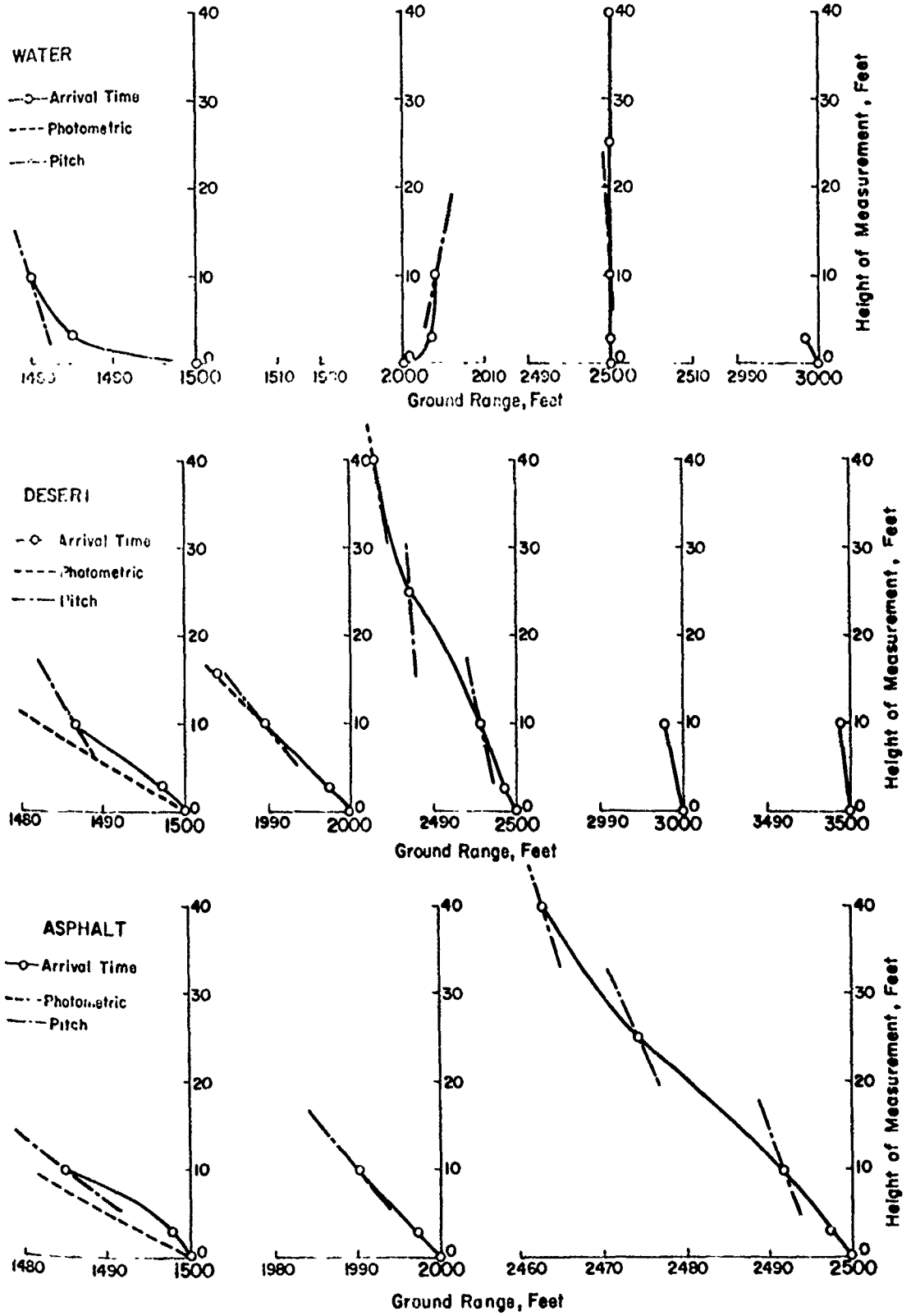

Figure 2.16 Wave-front orientation over various surfaces, Shot 12.

agreed quite well. The small difference in orientation at 1,500 feet may be explained by the fact that the wave fronts observed on the photographs were often obscured by dust near the ground surface. Thus, since the angle determined by the 3- and 10-foot level gage arrivals was nearly equal to the photographic wave-front angle, it can be said that the two methods gave essentially equivalent data. The results from initial-pitch-angle measurements deviated markedly at 1,500 feet but agreed at 2,000 and 2,500 feet. Over the asphalt the agreement was, in general, good for all three methods. Finally, since no shock photography was obtained over the water line, wave-front orientations for only the pitch angle and arrival-time methods could be compared. The results at 1,500 and 2,000 feet for these two methods agreed quite well.

In general, Figure 2.16 shows how the wave-front orientation changed as the wave traveled out to increased ranges. The angle between the front and the ground surface gradually increased so that beyond 3,500 feet the front was, in all cases, approximately perpendicular to the ground. The water line wave-front data were quite different from those over the other two lines. At 1,500-foot range, the front orientation indicated a pronounced toe near the ground surface and at 2,000 feet the front orientation appeared to be completely inconsistent with usual precursor behavior. However, it should be noted that the initial pitch angle at this water-line ground range agreed well with the anomalous behavior. In a sense, this unusual behavior over the water line near 2,000 feet was consistent with other anomalies such as shock velocity (Figure 2.9) at this same ground range.

2.3.4 Dynamic Pressure. **Dynamic Pressure at Various Distances.** The dynamic pressures recorded by 3-foot high pitot-static tubes at 1,250 feet from ground zero over each of the test surfaces for Shot 12 are presented in Figure 2.17. The peak values were approximately the same over the asphalt and desert lines but occurred at slightly different times after shock arrival. The wave forms for asphalt and desert were quite similar in shape but differed in magnitude out to about 0.37 second. At this close range differences in thermal characteristics over the three surfaces had begun to manifest themselves insofar as time of arrival was concerned, with the earliest time of arrival occurring over the asphalt line and with the latest occurring over the water line.

Figure 2.18 presents the dynamic pressure data measured at 3 feet at the end of the water and asphalt lines (3,000 feet) as compared to those recorded on the desert line at the same range. It is noted that the relative times of arrival are the same as those at the close-in station at 1,250 feet. The maximum-dynamic pressure at 3,000 feet is that recorded over the water line.

The peak-dynamic pressure as a function of distance at the 3-foot level over all three surfaces is presented in Figure 2.19, along with the ideal curve scaled from Figure 2.2. In drawing these curves, individual records were smoothed and evaluated to determine peak-pressure values of significant military interest. In particular, the 3-foot q′ record obtained by Project 1.10 at 2,000 feet on the water line was considered to be questionable, since it gave abnormally high values not consistent with other instrumentation at this location. However, the 3-foot Snob and Greg gages gave abnormally low values again inconsistent with other instrumentation. Although an intermediate value was chosen for Figure 2.19, it should be noted that the water-line curve between 1,500 and 2,500 feet on this figure is possibly unreliable. Dynamic pressures recorded on the desert line were generally higher than those on the asphalt and water lines out to 2,750 feet, where there was good agreement over all three surfaces and with the ideal. Beyond this range the curves reversed their position with respect to the ideal. It is expected that the dynamic pressures over the asphalt line would approach ideal if this surface had been longer. This tendency was observed in the measurements taken over the asphalt and desert surfaces on Shot 6 by both Stanford Research Institute (SRI) and BRL. The desert curve departure from ideal beyond 3,000 feet at this height was dependent on the reliability of one data point at 4,500 feet.

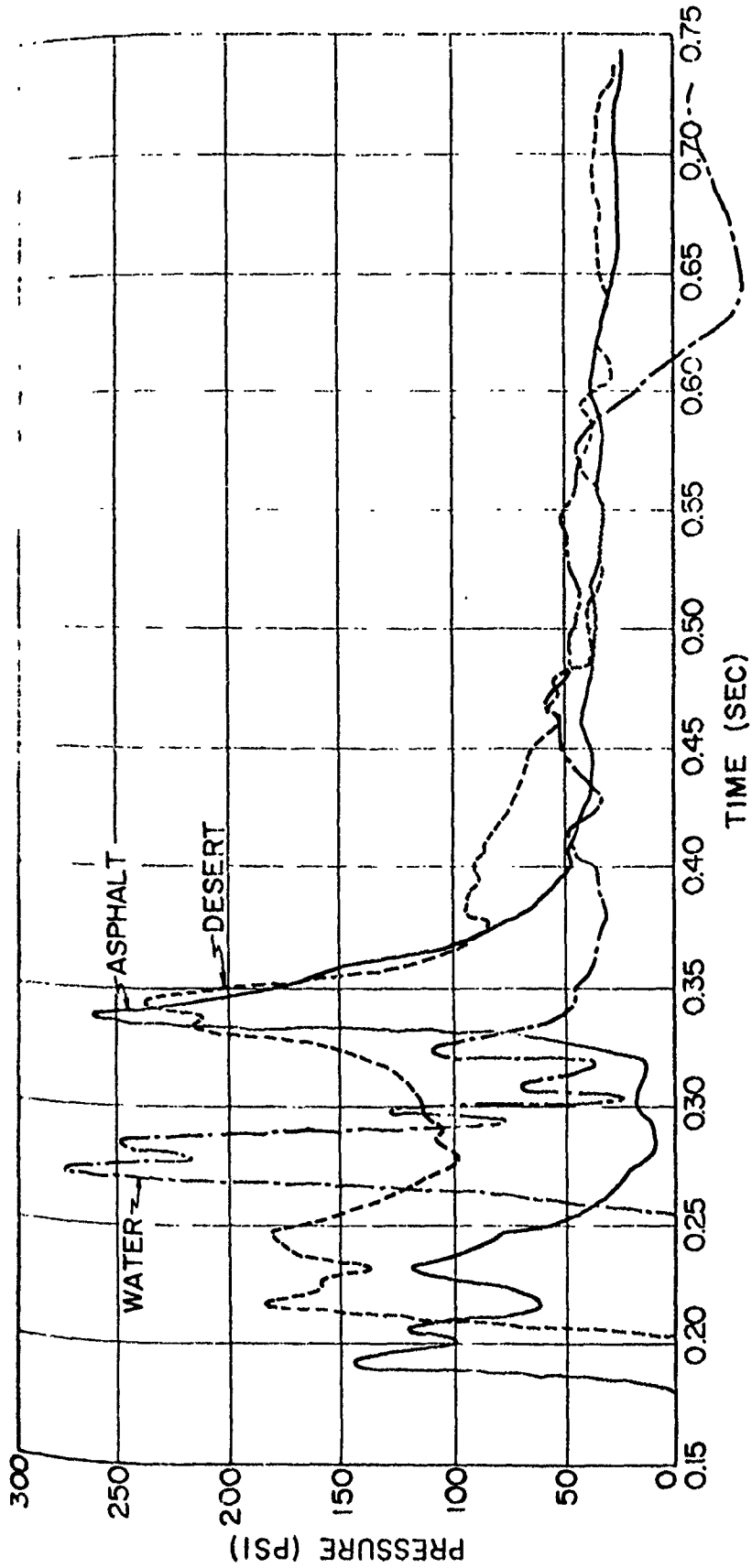

Figure 2.17 Dynamic pressures (q') at 1,250-foot ground range, (3 feet high), Shot 12.

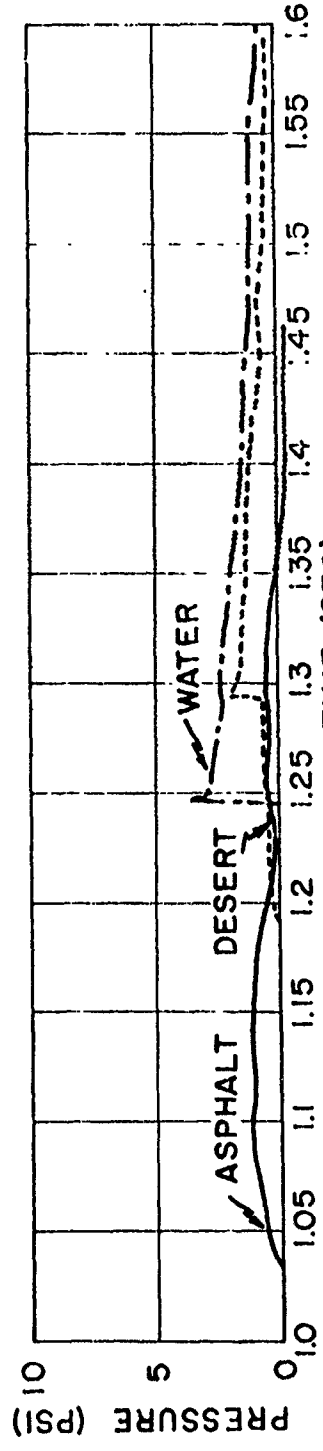

Figure 2.18 Dynamic pressures (q') at 3,000-foot ground range (3 feet high), Shot 12.

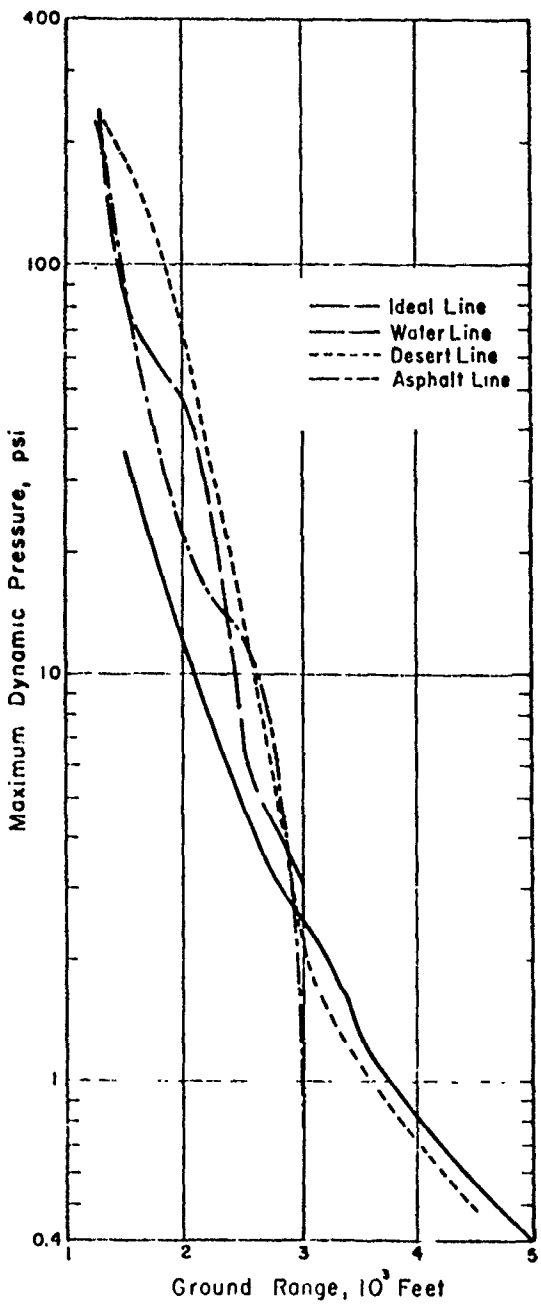

Figure 2.19 Maximum dynamic pressure (q') versus ground range (3 feet high), Shot 12.

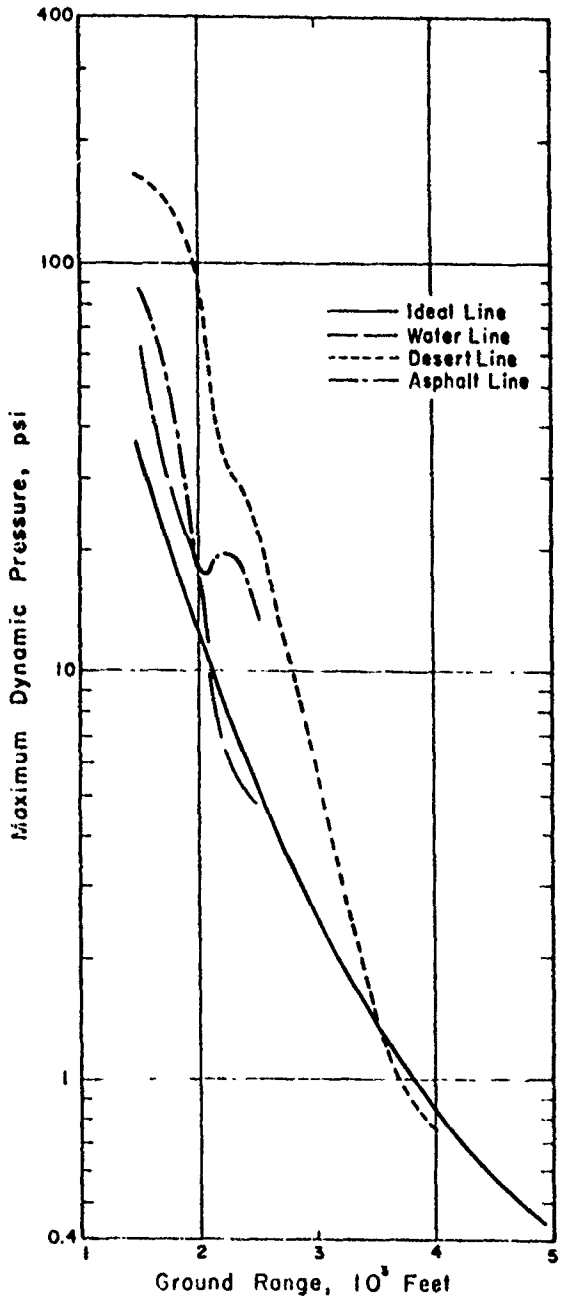

Figure 2.20 Maximum dynamic pressure (q') versus ground range (10 feet high), Shot 12.

Peak-dynamic pressures measured at 10 feet are presented in Figure 2.20 along with the ideal curve scaled from Figure 2.2. Again, the highest pressures were recorded over the desert line, with the lowest being measured over the water line. The asphalt line dynamic-pressure curve was higher than ideal throughout the entire range over which measurements were taken, while the water-line curve was again somewhat lower than ideal to 2,500 feet. The desert-line curve was essentially ideal between 3,000 and 4,000 feet, as contrasted to the uncertain 3-foot curve of Figure 2.19.

Similar trends in dynamic-pressure measurement were recorded over asphalt and desert surfaces for Shot 6. The dynamic pressures over the desert were larger than those over the asphalt and considerably above ideal at close-in ranges. However, at greater ranges measured-dynamic pressures over both the asphalt and the desert surfaces agreed with ideal.

Dynamic Pressures at 2,500 Feet. Comparison of dynamic pressure versus time measurements at various heights above the three test surfaces at a range of 2,500 feet is shown in Figure 2.21. The time of arrival was earliest on the asphalt and latest on the water line. The maximum value of q was recorded over the desert for all heights, but occurred at a later time with an increase in height. The wave forms were generally irregular, although those over the water had a steep front and appeared more conventional at 25 and 40 feet than at 3 and 10 feet. The peak values of dynamic pressure on the water line were somewhat lower than the indicated peak ideal value at this range.

A comparison of dynamic pressure versus time as a function of height on each line is made in Figure 2.22. The extreme irregularity of the records over the desert and asphalt lines is quite apparent as compared to the generally more conventional appearance of the water line records, except for the 3- and 10-foot traces beyond about 1.03 seconds. The steep shock front on the water line is particularly evident on this figure. The times of arrival over the desert and asphalt lines again indicate that the shock front over the desert line was steeper than that over the asphalt at this range.

Pitch Measurements. Measurements of angle of flow in the vertical plane (pitch) versus time were obtained on Shot 12 by Project 1.11 (Reference 8) at most stations where dynamic pressure (pitot-tube gages) was measured. The pitot-tube gage calibration was strictly valid for flow along the axis of the gage tube, i.e., zero angle of pitch. Although corrections could be applied to the gage calibrations for angles of pitch different from zero, the corrections were small for angles less than 15 degrees. Some representative pitch versus time records at 2,500 feet over the three surfaces at different heights are presented in Figure 2.23.

In Figure 2.23a the 10-foot level pitch versus time records obtained on the three blast lines are compared. The general form of these records in an initial-positive pitch (corresponding to upward flow, away from ground surface) followed by a reversal to negative pitch values, whereupon the pitch angle assumes a small constant value. The maximum pitch at the 2,500-foot range was measured on the asphalt line, with decreasing peak values recorded over the desert and water surfaces. Figures 2.23b and 2.23c show the variation in angle of pitch with height over the desert and asphalt surfaces at 2,500-foot ground range. Referring to Figure 2.23b for the desert, the records at the different levels have about the same form, with the 3-foot record displaying significantly lower-pitch angles than the others. Similar behavior is evident over the asphalt line (Figure 2.23c); however, the magnitudes of the pitch angles for levels above 3 feet are higher along this line than along the desert, indicating a more definite upward flow.

Some of the pitch-versus-time measurements on the desert and asphalt lines registered extremely high (up to 60 degrees) initial positive pitch in the form of a short-time-duration pulse. On first sight it was thought that these sharp peaks were caused by flying particles striking the instrument vane. However, reference to Figure 2.16, in which wave-front orientations from the pitch measurements are compared with independent wave-front data, makes it apparent that the initial peaks of pitch are probably real.

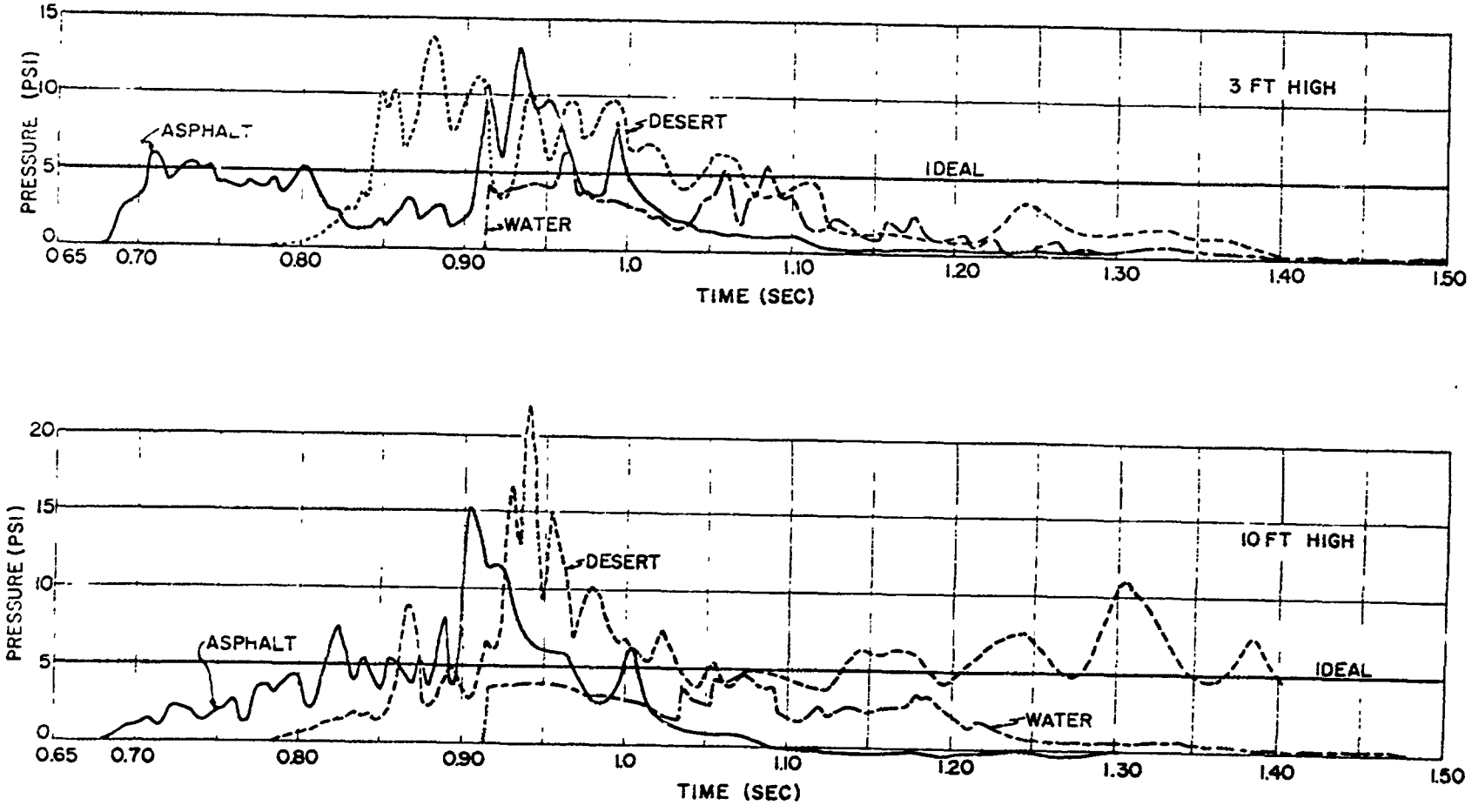

Figure 2.21 Dynamic pressures (q′) at 2,500-foot ground range, Shot 12.

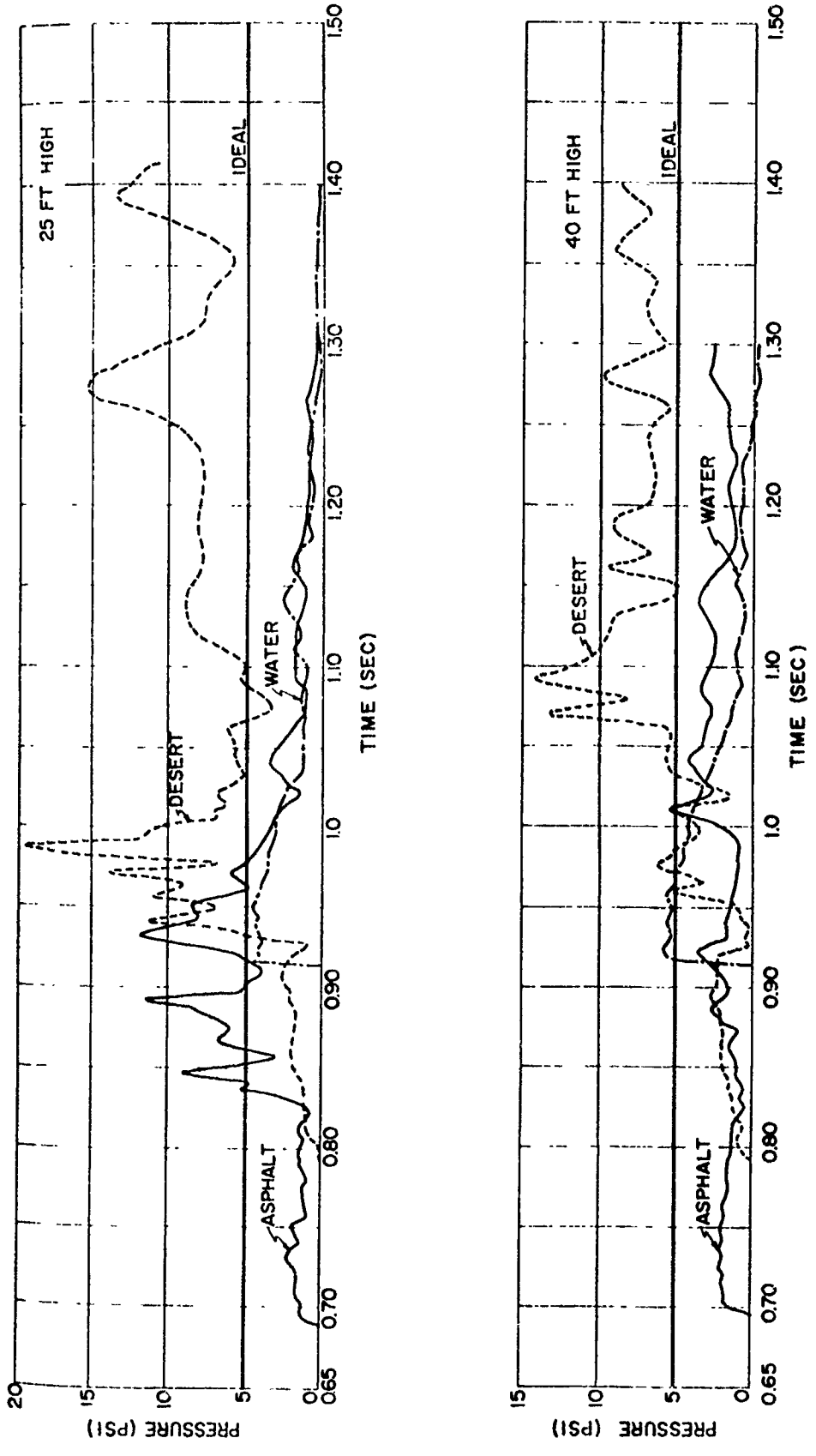

Figure 2.21 Continued.

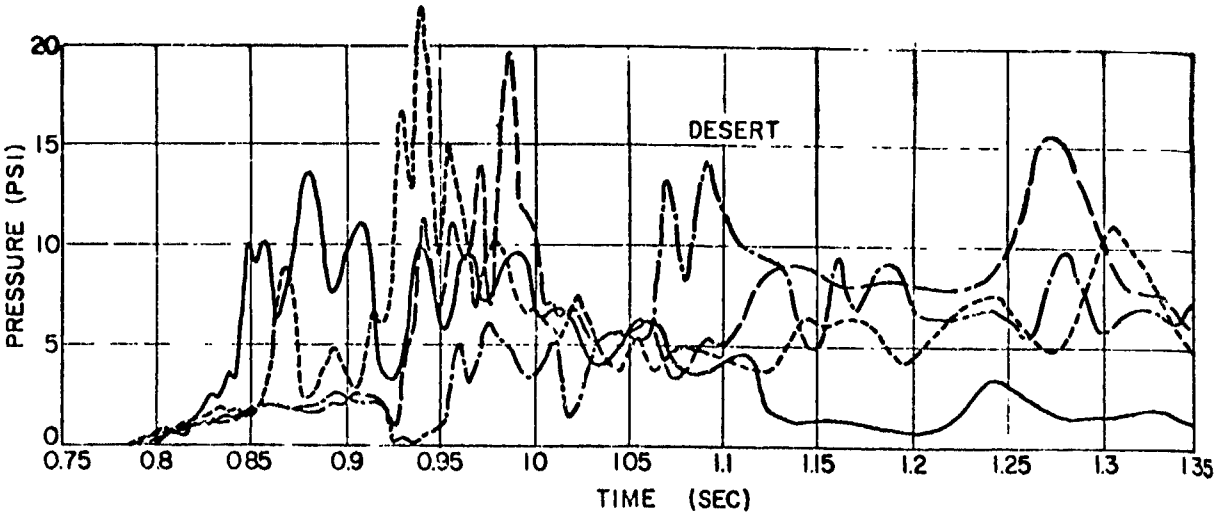

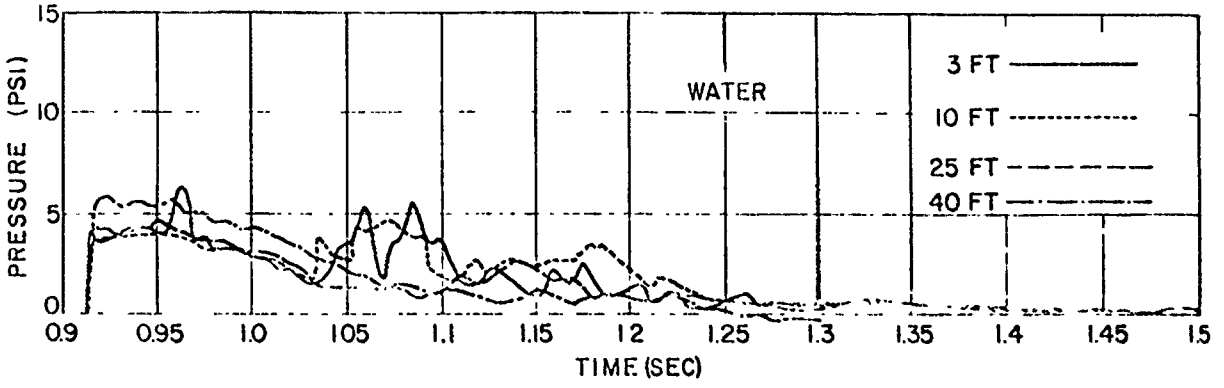

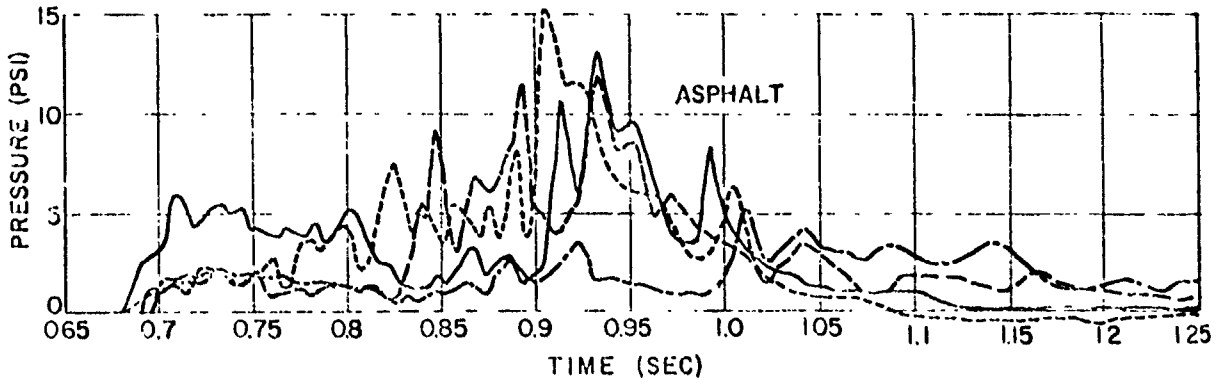

Figure 2.22 Dynamic pressures (q') at 2,500-foot ground range, Shot 12.

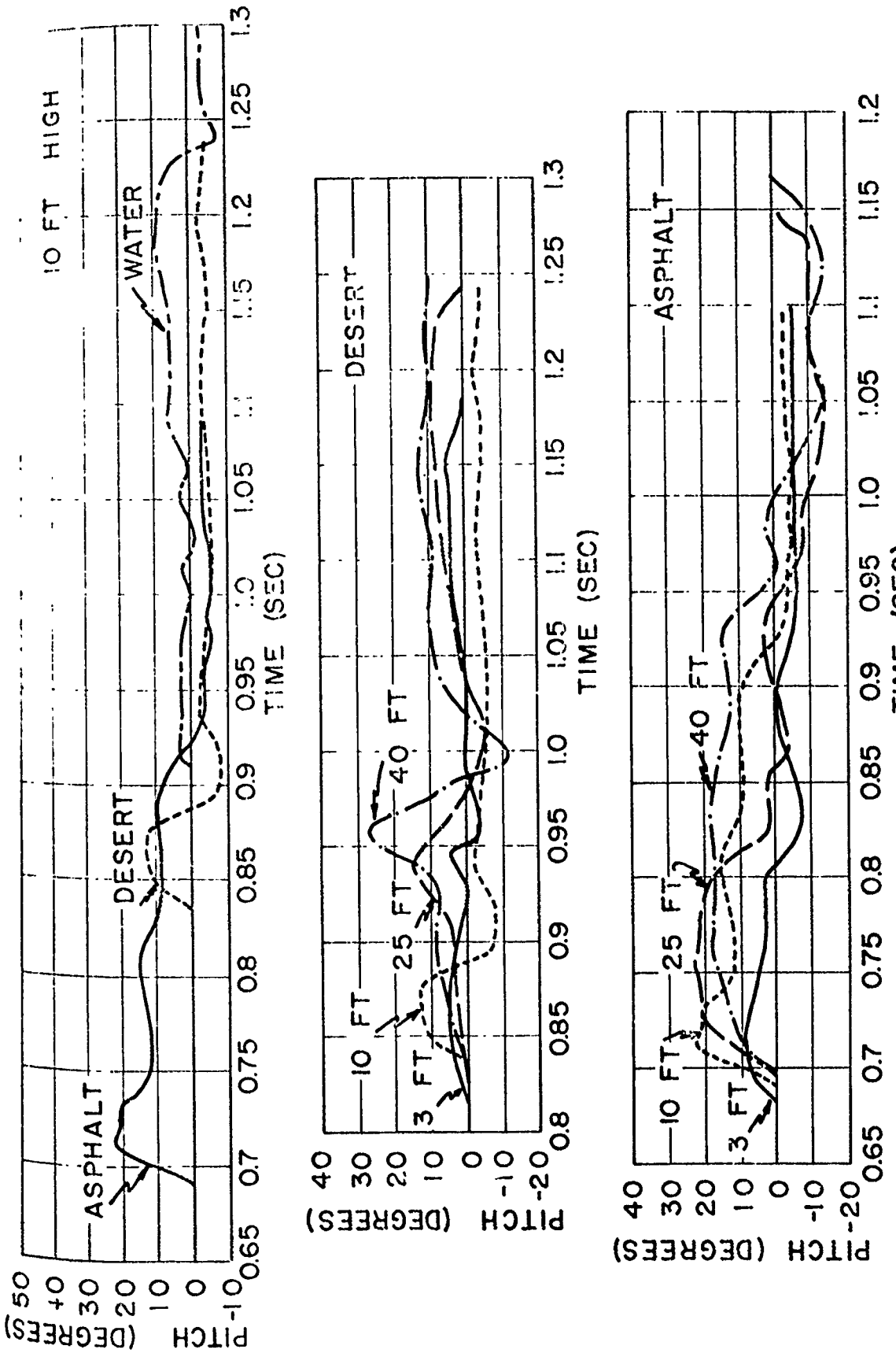

Figure 2.23 Angle of pitch at 2,500-foot ground range, Shot 12.

The dynamic pressures at 2,500-foot range on the three-blast lines of Shot 12 are compared with their corresponding pitch measurements in Figure 2.24. The general conclusion from these figures is that, at this ground range, the dynamic pressure records would not be changed significantly because of corrections for angle of pitch. It may be noted that the peak-pitch angles did not occur at the same times as the peak dynamic pressures. However, a word of caution should be included; that is, it is pointed out that, although the peak value of pitch may not coincide with the peak-dynamic pressure, it is possible that a lower value of q' coupled with a large-pitch angle may transmit significant overturning moments to an aboveground target. Examples which illustrate this situation are included in Figure 2.25.

Snob and Greg Measurements. The Snob and Greg gages, because they supplement each other, are considered together. The Snob gage actually was a small orifice pitot-static arrangement; and the Greg gage was used as a diaphragm type head-on pressure instrument. The Snob gage was designed to register the side-on overpressure and the dynamic pressure of the air alone, while the Greg registered both air- and dust-dynamic pressure. The total pressure measured by the Greg gage may be represented by

$$P_t = \Delta P + q_a + q_d \tag{2.2}$$

where: ΔP = the side-on overpressure

q_a and q_d = the dynamic pressures associated with the air and dust, respectively

In terms of the above quantities, the Snob gage measures both ΔP and q_a separately.

Peak air-dynamic pressures (Snob gage) at equal distances were highest over the desert, lower over asphalt, and lowest over water at both 2,000- and 2,500-foot stations. Only at 2,500 feet on the water line did the peak air-dynamic pressure agree with the Rankine-Hugoniot relations. This station experienced a nearly classical overpressure-wave shape. At all other stations air-dynamic pressure was higher than would be expected from measured overpressure, usually by a substantial factor. When compared with dynamic-pressure maxima derived from ideal overpressure, the measurements were still significantly larger than expected.

An interesting rough comparison can be made to determine the relative magnitude of the dust effects (q_d) on the desert and water lines. This is done by transposing Equation 2.2 to obtain

$$P_t - (\Delta P + q_a) = q_d \tag{2.3}$$

When the appropriate gage records are manipulated to correspond to the above relation, the result is an approximate q_d versus time record. These q_d records over the desert and water lines are shown in Figure 2.26, along with q_a versus time records obtained by the Snob for dynamic pressure of air alone at the same ranges and elevations. In a gross sense, the results show the dust effects over the desert to be as much as five or six times more severe than over the water.

Another comparison that can be made is between the Project 1.10 dynamic-pressure measurements (assumed to be $q_a + q_d$) and the differential Greg-Snob (side-on) measurements ($P_t - \Delta P$). These comparisons appear in Figure 2.27 for the desert and water surfaces. For the desert surface, the comparison of peak-dynamic pressure was fair; however, the wave forms were significantly different. The comparison over the reflecting surface showed good agreement in both amplitude and wave form between the SRI record and the differential Greg-Snob data. These results, although limited, lend some confidence to the hypothesis that the conventional pitot-static dynamic pressure gage measures the effect of the air and the dust.

Implications of q' Pressure Measurement. In the attempts to correlate

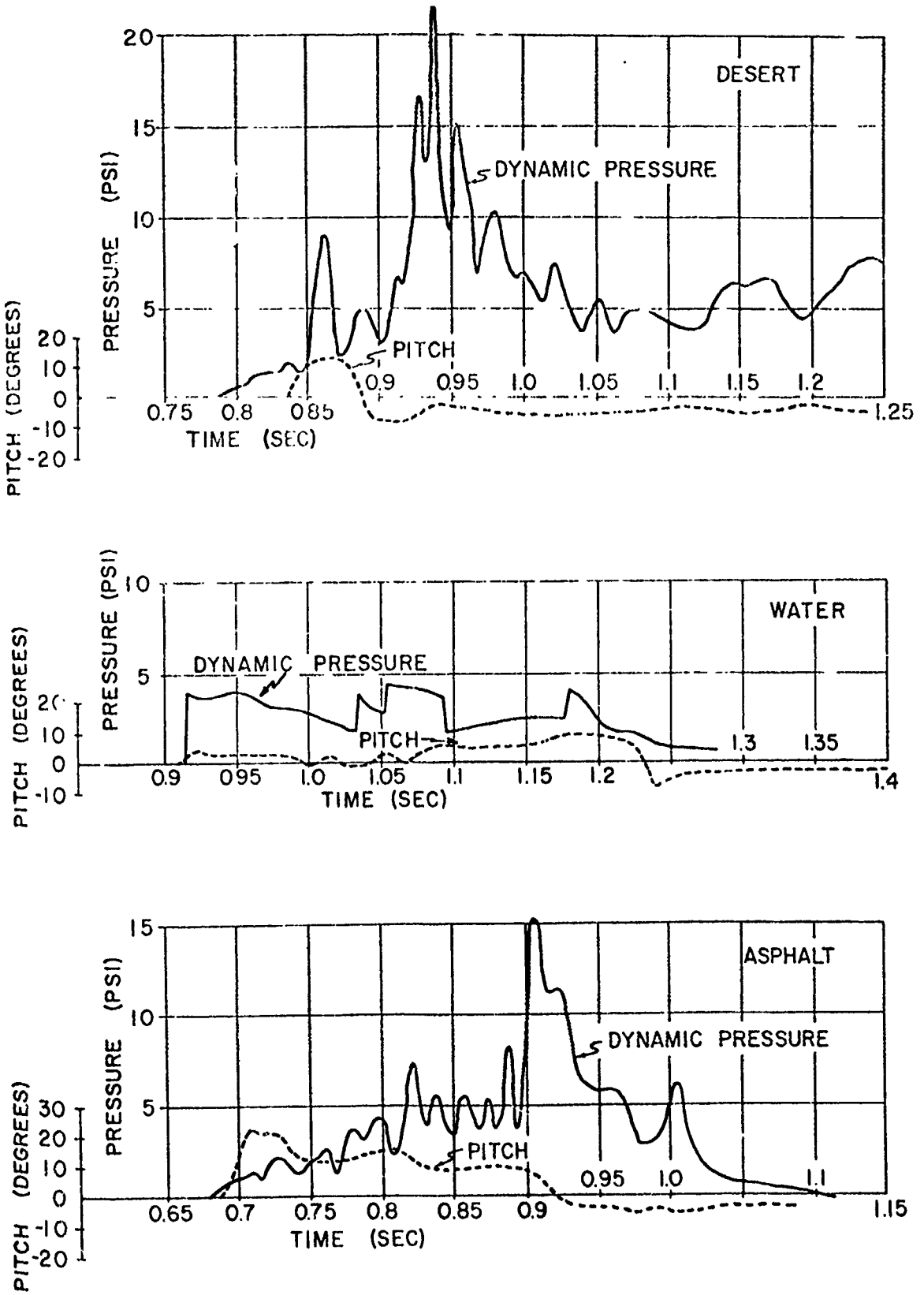

Figure 2.24 Angle of pitch and dynamic pressure (q') at 2,500-foot ground range, Shot 12.

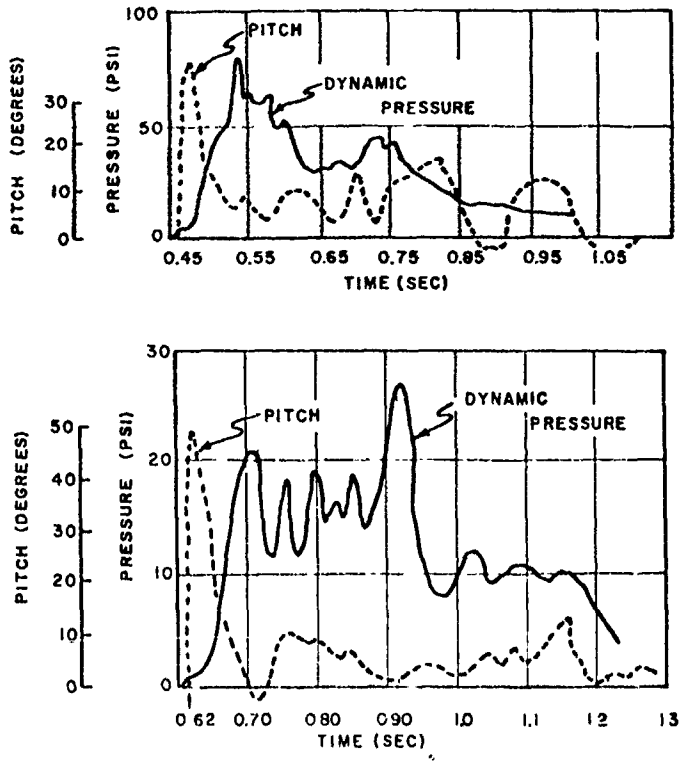

Figure 2.25 Angle of pitch and dynamic pressure (q′) at 2,000- and 2,250-foot ground range, Shot 12.

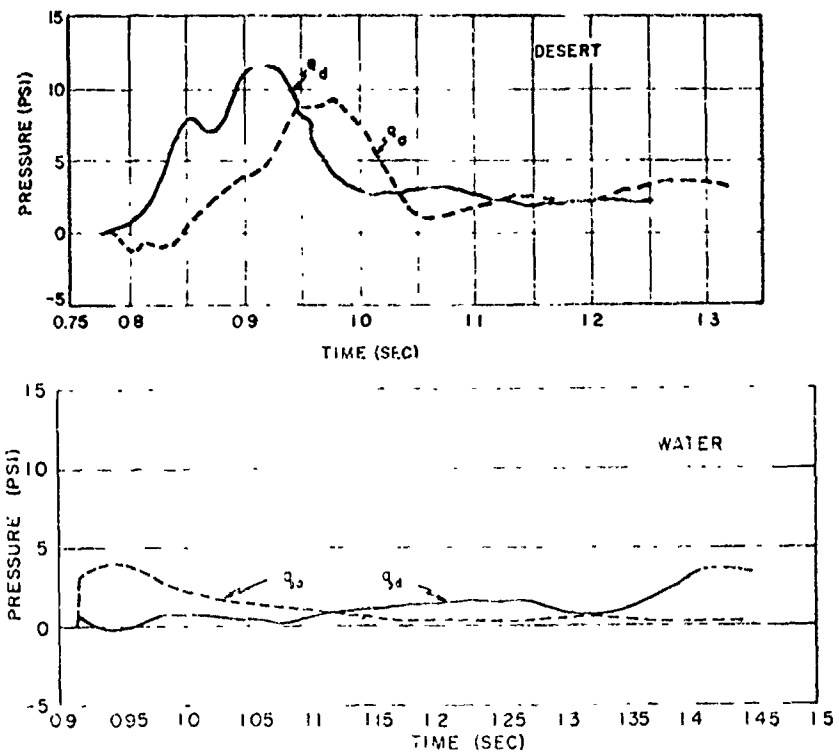

Figure 2.26 Dust dynamic pressure (q_d) derived from Greg and Snob air dynamic pressure (q_a) at 2,500-foot ground range (desert, 3 feet high), Shot 12.

free-field air-blast data with target damage, measurement of dynamic pressure in the region of disturbed blast waves has acquired added significance. The measurement of dynamic pressure for clean air-gas-phase flow (isentropic) is well established. Corrections for the compressibility of the gas have been devised, and designs of gages for minimizing the effect of angle of attack have been investigated thoroughly. The conventional pitot-static tube may be employed in both subsonic and supersonic flow; however, when the flow is supersonic (Mach

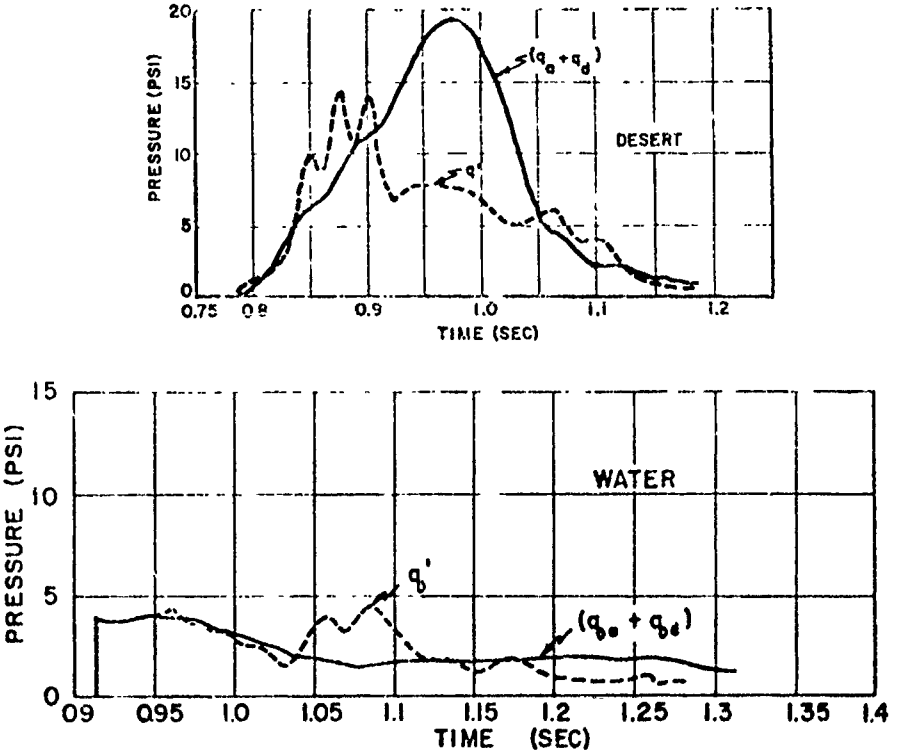

Figure 2.27 Derived total dynamic pressure (Greg, side-on; $q_a + q_d$) compared to pitot-tube dynamic pressure (q') at 2,500-foot ground range (desert, 3 feet high), Shot 12.

number greater than 1) the deceleration at the nose of the impact tube cannot be isentropic because a shock wave must form in front of the tube.

In order to determine the Mach number and flow-direction (pitch and yaw) correction to be applied to the pitot-tube measurements, Cornell Aeronautical Laboratory (CAL), under contract to Sandia Corporation, undertook a testing program in their subsonic wind tunnel. CAL used a scale model of the Sandia pitot tube employed in the field. It was found that the static-pressure measured for this pitot-tube design was larger than the true static pressure. This is consistent with theory. In fact, CAL wind-tunnel tests revealed that the static measurement was much more sensitive (i.e., larger correction factors) to increased Mach number and pitch angle than was the total head measurement. Two ways of computing the instantaneous Mach numbers suggest themselves. The first method was to substitute the pitot-tube side-on measurement and the ambient-reservoir pressure into the appropriate pitot-tube equation, i.e., depending on presence of subsonic or supersonic flow. The second method was to compute Mach number using the equation $q' = \gamma p/2\ M^2$ and the measured p(pitot) and q'. This was equivalent to assuming $(P_0 - P)$ is identical to q'. Thus the second method was restricted to subsonic flows.

Dynamic-pressure measurements obtained in the precursor region led to the conclusion that pressures were equal to or greater than ideal and much greater than would be calculated from measured overpressures using the classical Rankine-Hugoniot relationship applicable across a shock front. Whatever the mechanism responsible for these non-classical, abnormally large q′ pressures, it became immediately apparent that calculations of Mach numbers based upon classical gas-phase flow would be in error. Consequently, it was difficult to apply unambiguous compressibility corrections to the measured results.

One explanation for the high q′ measurements in the region of disturbed blast waves was based on the contribution of suspended particulate matter to the measurement. That is, in addition to the influence of the gas-phase-stagnation pressure, the particles carried by the air would transfer their momentum to the still air in the gage channel. It was at once apparent that the particle-collection efficiency of the particular gage would be dependent on such variables as nose shape, particle size distribution, and gas-phase-flow velocity The latter two variables, under actual field conditions, would probably change drastically with time and range. Also, it must be agreed that particulate matter may be only one of many factors leading to the high q′ measurements.

From this discussion, it can be said that all dynamic-pressure measurements in a region of disturbed-blast waves are intimately connected with the gage design employed. For this reason, gage design and gage calibration take on added significance. For measurements in regions of high-speed non-classic flow, a total head-impact tube is particularly applicable. In supersonic flow, the static pressure measured in the vicinity of an impact tube is, in general, not the free-stream-static pressure; therefore, the static orifice of the conventional differential tube does not measure the free-stream-static pressure, because the orifice is affected by the shock wave associated with the pitot tube. Also, the Mach number and pitch corrections to be applied to data from a well designed pressure tube can be made much smaller than those for the differential tube configuration.

2.3.5 Symmetry and Cross Feed. Symmetry; BRL, 2,500 Feet. BRL installed a 220-degree arc of surface level, self recording, or mechanical, pressure gages at a radius of 2,500 feet on Shot 12. These gages were installed to investigate the symmetry of the blast wave at that radius and to obtain some information concerning the perturbations caused by the test surfaces. The spacing between gages was closest where the arc crossed the water and asphalt surfaces.

Although the time of arrival of the blast wave as determined by the self-recording gages was subject to some error, the measurements had value for establishing general trends. The arrival times recorded on the 2,500-foot gage ring are shown in Figure 2.28. Allowing for some unavoidable data scatter, the arrival times are shown to be earliest in the sector representing the asphalt area and latest in the sector representing the water area. However, it would be expected that the arrival times would be more uniform over the broad area representing the desert area. Shown in this figure are the arcs subtended by the Shot 12 water and asphalt surfaces at the 2,500-foot radius and also the arcs over which the blast wave presumably traveled over a portion of the water and asphalt surfaces near ground zero. It is clear that in the lightly shaded areas the arrival times would be those characteristic of transmission across one of the artificial surfaces for part of the distance and across the desert surface for the remainder.

For comparison purposes, the Project 1.10 blast-arrival times, determined by precise electronic instruments, are shown at the center of the water, desert, and asphalt areas. These data do not deviate significantly from the BRL self-recording-gage data. In a few cases, arrivals of secondary shocks are clearly defined on the BRL records; these data are included in Figure 2 28. It is evident that, where discernible, these second arrivals are more nearly uniform throughout the instrumented arc, which is compatible with the general trend observed on Shot 12 (Section 2.3.2).

The peak pressures recorded on BRL self-recording gages on the 2,500-foot gage ring are shown in Figure 2.28. Also included in the figure are the Project 1.10 electronic-gage peak-pressure measurements at the same ground range and the wave form classification to be assigned to each pertinent pressure-time record.

The maximum overpressures shown in Figure 2.28 indicated that the BRL and Project 1.10 results, where comparisons were possible, agreed quite well; however, the overall picture was confusing. The figure shows a rather orderly behavior across the asphalt surface, with the ex-

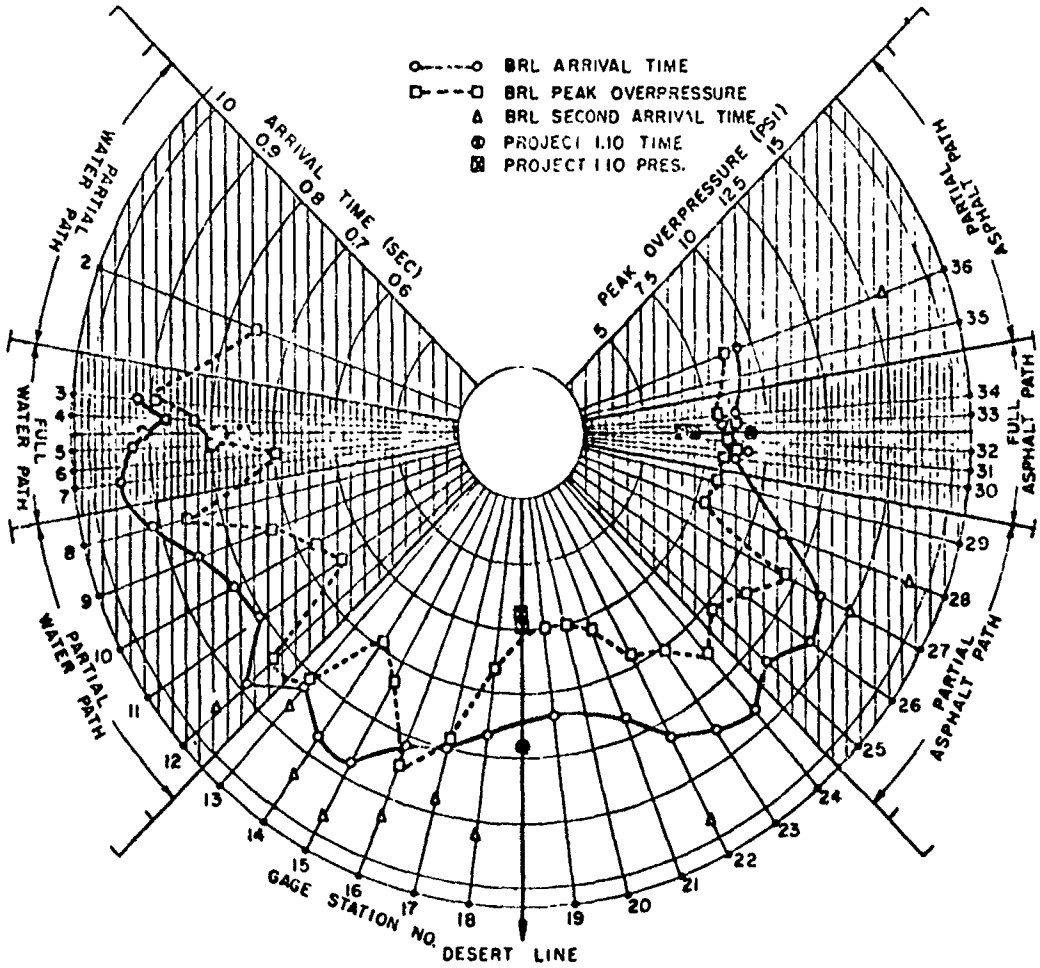

Figure 2.28 Peak surface level overpressure and arrival time at 2,500-foot ground range, from BRL self-recording gages, Shot 12.

pected depressed-peak pressures in evidence; however, the BRL gages at their Stations 27 through 22 indicate an abrupt increase in peak pressure in the desert-asphalt-transition sector. Continuing around the gage arc toward the main desert blast line, it is obvious that both the BRL and Project 1.10 pressures were again depressed. In fact, peak pressures measured here are not unlike those measured near the center of the asphalt surface. Proceeding around toward the water surface, both BRL and Project 1.10 static-pressure data show large variations in magnitude, even from pressure gages located near the water-blast line. Referring to the BRL-gage records included in Figures 2.29 and 2.30, it is apparent that there was some correlation be-

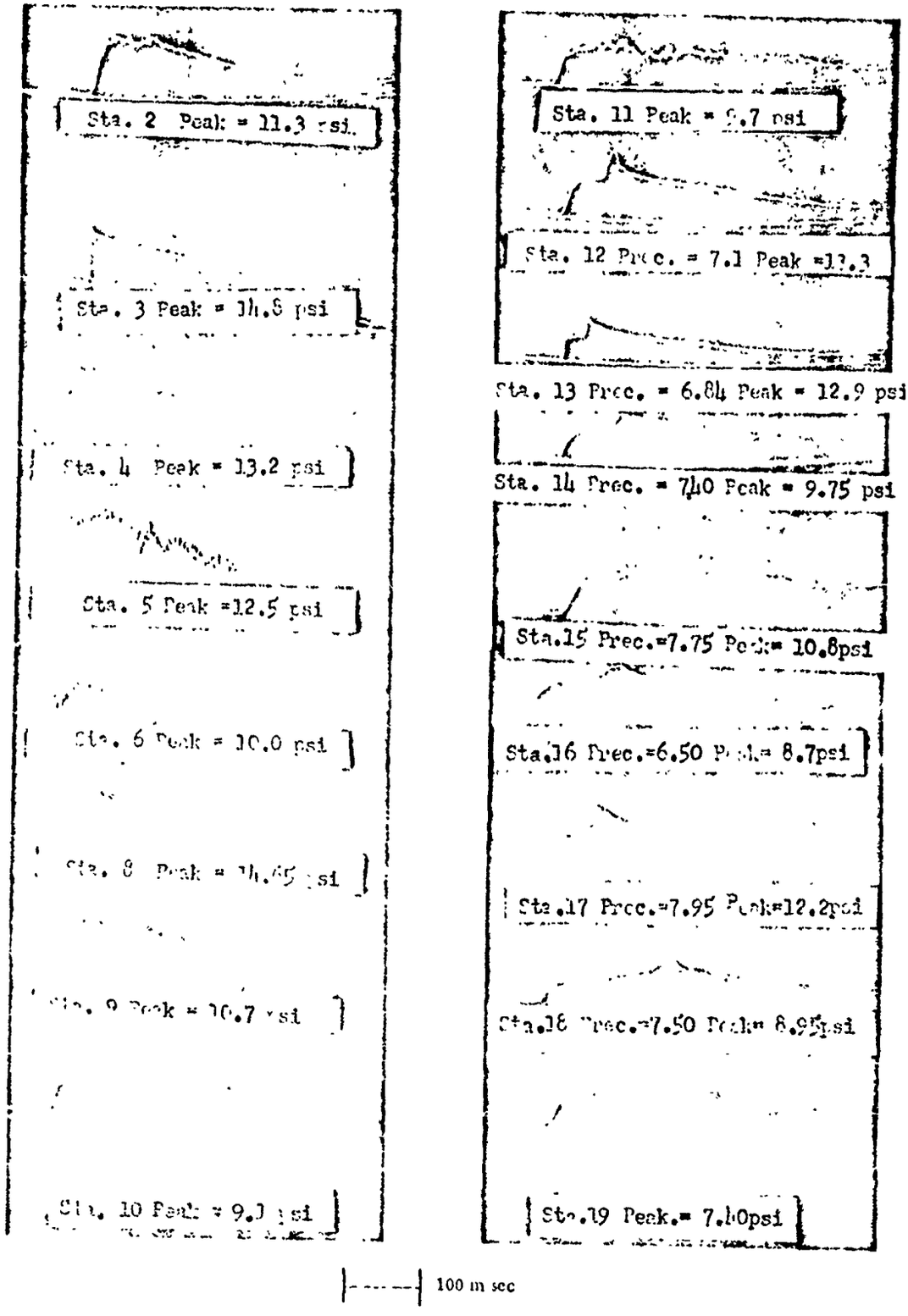

Figure 2.29 Surface level overpressures at 2,500-foot ground range, from BRL self-recording gages (see Figure 2.28 for station locations), Shot 12.

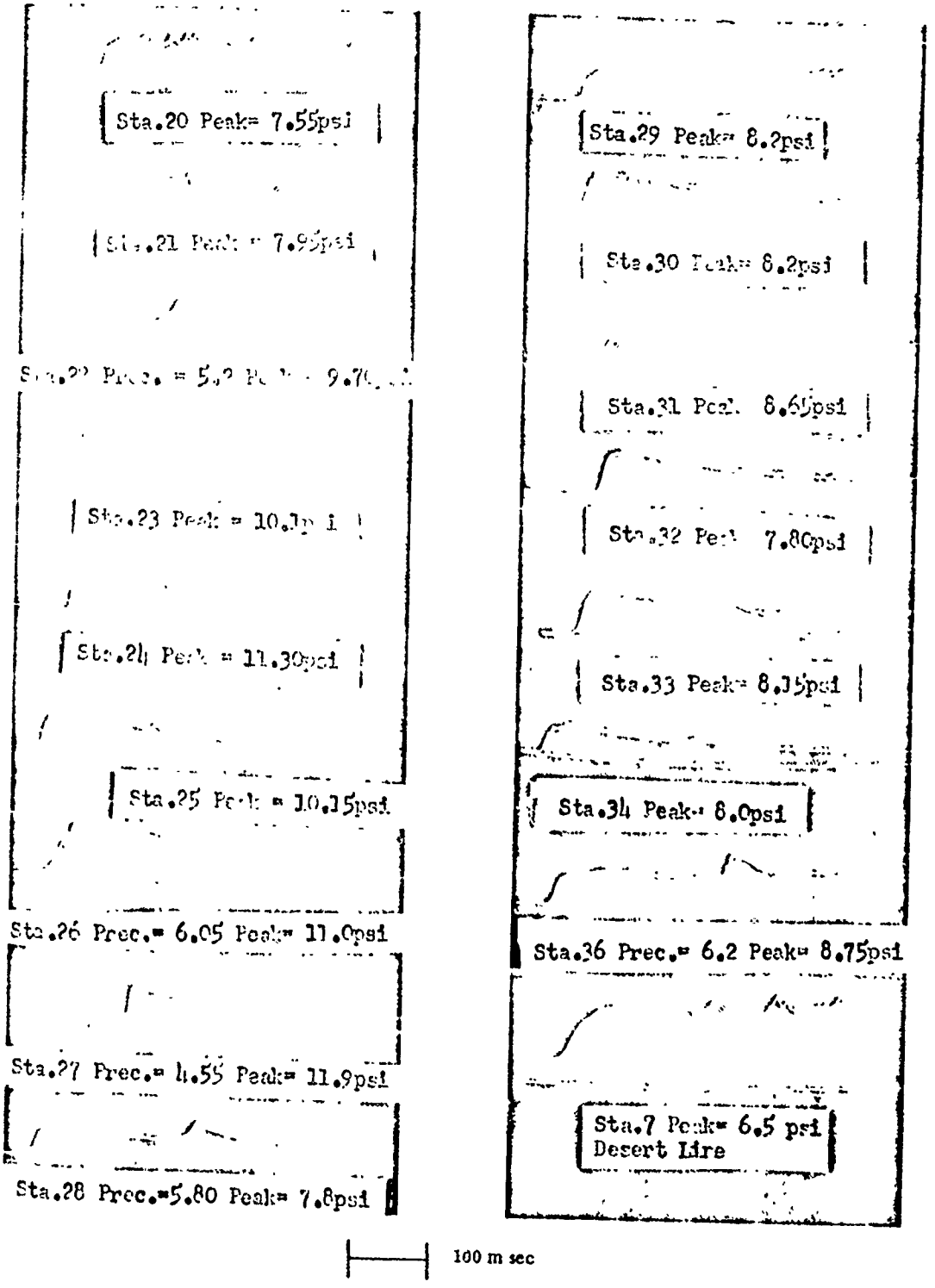

Figure 2.30 Surface level overpressures at 2,500-foot ground range, from BRL self-recording gages (see Figure 2.28 for station locations), Shot 12.

tween the higher-peak pressures and the gage records which exhibited more advanced wave forms, i.e., Types 6 and 7. This result is thought to be characteristic of the so-called cleanup region of the disturbed blast-wave evolution.

The phenomena observed by the BRL instrumentation might be related to the fact that portions of the Frenchman Flat test area have undergone soil stabilization for Operation Teapot and previous operations. It may be significant that most of the BRL gages which recorded the higher-peak overpressures were those located near or on a stabilized-soil pad. The conclusion is that abrupt localized changes in the characteristics of the surface over which a blast wave is traveling may have significant effects upon the peak overpressure and time history of a measurement taken in the near vicinity of the altered surface. Nonetheless, it should be emphasized that caution must be used when attempting to generalize from these symmetry measurements taken at a ground range where the blast wave disturbances were cleaning up. As a matter of fact, a similar gage-ring layout was used on Operation Teapot Shot 14, and no unusual deviations from blast symmetry were observed. The instrumentation on Shot 14 was located at a shorter-scaled ground range and, therefore, the measurements were taken in a region of strong precursor effects.

Cross Feed; SRI, Water. At radii of 1,500 and 2,500 feet, pitot-tube pressure- and horizontal-flow-direction (yaw) instruments were installed on the water line 125 and 225 feet in from the desert-water boundaries, where the water line was 800 feet wide. These gages were installed for the purpose of detecting the possible feed-in of blast disturbances from the desert area to the water area.

If a disturbance which was traveling over the desert surface was to feed in energy across the desert-water interface, this energy would be propagated over the water with the local sound velocity. Arrival-time data at the 570-, 1,000-, and 1,250-foot water-line gage stations yielded propagation velocities which were greatly in excess of sonic velocity. Therefore, it could be concluded that a major portion of the pressure-time history observed at these stations was free of cross-feed effects. However, at 1,500-foot range, the offset gage nearest the interface yielded an arrival time which suggested cross feed at this gage. It was probable, although not readily observable, that cross feed was manifest at times after blast arrival on records obtained at 1,500 foot stations farther removed from the desert-water interface. Analysis of the pressure-time wave forms obtained at 2,000-foot range produced additional evidence of cross feed from desert to water surface. After the first 100 msec following blast arrival the water-line gage record took on the appearance of the record which was recorded at the same ground range over the desert.

In summary, it can be established with some assurance that the observations at close-in ground ranges (less than 1,500 feet) on the Shot 12 water line were free of cross-feed effects.

2.3.6 Artificial Test Surfaces. In general, it can be said that the two artificial test surfaces satisfied the requirements for which they were designed. Factors of economy and practical engineering precluded more effective surfaces, especially in the case of the water area.

Asphalt. The basic requirement was to obtain a thermally absorbing surface, to produce a heated layer of air immediately above a surface which would be relatively dust free.

Data from blast instrumentation indicated that preshock temperatures were higher over this surface than over either of the other two lines, but no direct air-temperature measurements were obtained and the direct NEL sound-velocity results were the same as for the water and desert areas. Arrival times were earlier, and characteristics of recorded wave forms showed evidence of an extensive precursor formation. Although the surface did pick up in spots and instrumentation showed signs of impingement on the forward surfaces of particles of moderate size, the data seemed to indicate a smaller air-borne particulate-matter (dust) effect than was

obtained on the desert area. Dust-sampling equipment which would have given direct data to support this observation failed to function successfully.

A word about the effects of the shot on the surface itself is in order. It had been determined by tests before the shot that a thin-oiled surface could be used on the Frenchman Flat soil. The specifications as finally written called for application of a penetration asphalt directly to the subgrade, followed by a layer of crushed gravel, rolled to a depth of ¾ inch. The surface was given a final spray, as late as practical before shot time, to obtain a completely black finish. The access road down this area, from the shot tower to the 3,000-foot boundary (Figure 2.31), was surfaced with a 2-inch thick road-mix asphalt. Postshot observation revealed appreciable me-

Figure 2.31 Postshot view of asphalt surface looking toward ground zero, Shot 12.

chanical damage to the main surface, but the road did not appear to be disrupted at any point in its length. It was obvious from visual observation of the shot that the thermal action was intense. However, the surface showed little thermal effect. Further evidence to support the thermal action was strikingly shown by the separated cloud which photography showed as originating at approximately 2,500 feet from ground zero on the asphalt surface, rising hundreds of feet into the air. The instrument towers were blackened at this range, while those at 2,000 feet did not appear to be subjected to as much burning.

It is estimated that about 20 percent of the asphalt surface was destroyed by the blast. No strips of asphalt, as such, were torn up, but the action showed itself in the form of patches, a sort of chipping action as shown in Figure 2.31.

Water. The water surface was flooded for the first time on 7 April in anticipation of detonation of Shot 12 on 8 April. On the morning of 8 April the shot was postponed for operational reasons, and it was again postponed on the morning of 9 April. No additional flooding was attempted until the evening of 14 April in anticipation of detonation on 15 April. All of the available water was pumped into the water line during the evening of 14 April. A helicopter survey flight was conducted on the morning of 15 April several hours prior to shot time. Nearly the entire surface of the water area was flooded prior to shot time. A few small, muddy but unflooded patches were observed. However, it was believed that these patches were scattered and so small that they had no influence on the blast phenomena observed along the center of the water area. No significant dry spots were observed near the central axis. Another helicopter

flight was made a few hours after the detonation on 15 April. It was evident that a considerable amount of water had been either evaporated or blown from the surface. However, even at that time most of the water line was still flooded. It seemed safe to conclude that, for all practical purposes, the water line was flooded at shot time and that the amount of water lost was not significant for this test.

The water-line blast data showed that the blast wave along the water surface was by no means ideal. At a range of approximately 1,750 feet the recorded pressures and dynamic pressures were reasonably representative of ideal amplitudes and wave forms. However, some gross perturbations were recorded in the region from 1,750 to 2,500 feet which could not be simply explained by cross feed from the surrounding desert area. Beyond 2,500 feet the blast behavior appeared to be essentially ideal. Postshot examination of gage mounts, gage towers, and other target elements along the water line showed that a substantial quantity of mud apparently was carried by the blast wave. This effect was particularly evident out to a range of 2,000 feet, with a lesser effect at greater ranges. Loading, caused by mud and possibly water, undoubtedly caused some undesirable effects on the aircraft components of Project 5.5. It is quite likely that even a substantially deeper water area, which would be a most uneconomical and difficult engineering task at NTS, would not produce a truly ideal surface. Snow or ice would, perhaps, be a more satisfactory ideal surface. It is unlikely that any other representative hard- and dust-free surface could be achieved without substantial associated thermal effects.

2.4 SURFACE EFFECTS

2.4.1 Thermal Layer. Sound Velocity. Figure 2.32 shows the Project 1.5 (Reference 9) sound-velocity measurements prior to shock arrival at a distance of 1,000 feet on the three blast lines. Not only is a relatively small difference shown between the blast lines, but the sound velocities over the water line are shown higher than over either the asphalt or desert lines. Furthermore, the temperatures represented by these sound velocities, assuming no change in the medium, are very low indeed. The maximum temperature rise indicated is about 130 C. Figure 2.33 shows similar data obtained at 2,000 feet on Shot 12. Again, the calculated temperature rise is quite low, and there is substantially no difference between the desert and asphalt lines. No measurements were made at this distance on the water line. It is to be noted that these sound-velocity measurements showed substantially the same results at distances of 1,000 and 2,000 feet. The estimated thermal input normal to the ground surface prior to shock arrival at 1,000 feet was 37 cal/cm^2, while at 2,000 feet it was 15 cal/cm^2. The sound-velocity measurements at a distance of 2,000 feet over the small test surfaces of ivy, fir, and concrete gave results similar to those of Figure 2.33.

Following the field activities during Operation Teapot, the Project 1.5 instrumentation was subjected to a series of instrument checks at the home laboratory (NEL). All these experiments indicated that the instrumentation used during Operation Teapot operated satisfactorily and, in reality, measured sonic velocity. In the opinion of Project 1.5 personnel, their instrumentation used on Operation Teapot was much superior to similar devices used on Operations Tumbler-Snapper and Upshot-Knothole. For these reasons, although much higher sonic velocities were observed during these other two operations, they believe the Operation Teapot data to be the most reliable.

Air Temperature. The direct air-temperature measurements on Shot 12 appeared erratic. Unfortunately, many of the anticipated data were not obtained because of various equipment failures. Those data which were obtained were difficult to understand when compared to the anticipated phenomena or when compared to the sound-velocity measurements. The only direct correlation was made over the concrete-test plot at 2,000 feet. Figure 2.34 presents the

air-temperature data and the sound-velocity data from this location. It is to be noted that most of the recorded air temperatures dropped to ambient and remained at ambient long before shock arrival, while the thermal-radiation pulse still had a considerable amplitude. It is also worth noting that one air temperature record, at 1.5 feet, showed no response during the period of principal output from the others and showed its principal response just prior to shock arrival. These results were characteristic of the air-temperature measurements on Shot 12. Most of the records indicated a temperature drop to ambient long before shock arrival, with an occa-

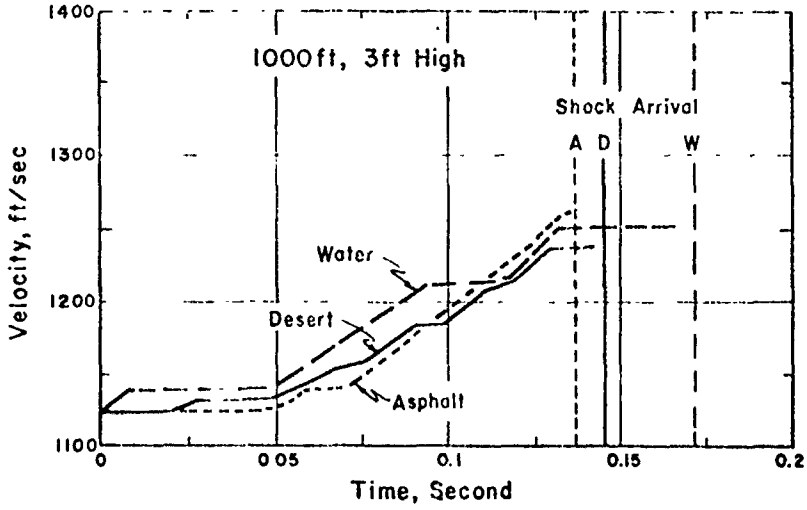

Figure 2.32 Sound velocities (NEL) at 1,000-foot ground range (3 feet high), Shot 12.

sional intermediate elevation giving a temperature rise at a later time with a substantial amplitude at shock arrival. Furthermore, the peak temperatures indicated were many times greater than those which would be deduced directly from the sound-velocity measurements at the same location, as shown on Figure 2.34. There was also relatively little difference in the air-temperature measurements over the various test surfaces at corresponding distances.

The basic character of these air-temperature measurements was extremely difficult to reconcile with any rational interpretation of the anticipated phenomena. It was possible that they could demonstrate extreme turbulence, but the steady nature of the temperatures following their fall to ambient long before shock arrival would have contradicted a turbulence explanation. If the majority of the air temperature measurements were accepted as fact, it was not possible to support the existence of a thermal layer prior to shock arrival. It is suggested that these results should not be used to form a conclusion that there is no thermal layer to affect the blast wave at shock arrival. It is probable that these temperature measurements are not suitable for a quantitative understanding or even a qualitative understanding of the character of the thermal layer or of the differences between the thermal layers developed over various surfaces.

A few direct-air-temperature measurements were made on Shot 4. These results appeared to be more compatible with expectations, since the indicated temperatures rose to a peak at about shock arrival. The results were also more consistent internally. Peak temperatures on the order of 1,000 C were recorded over the Yucca Flat desert surface at a distance of 1,500 feet, from 43 kt on a 500-foot tower.

Sound Velocity and Air Temperature Comparisons. The calculated shape of the thermal pulse and the percent of total thermal emission as a function of time are shown in Figure 2.34. These calculations make no allowance for obscuration by dust, and it is not

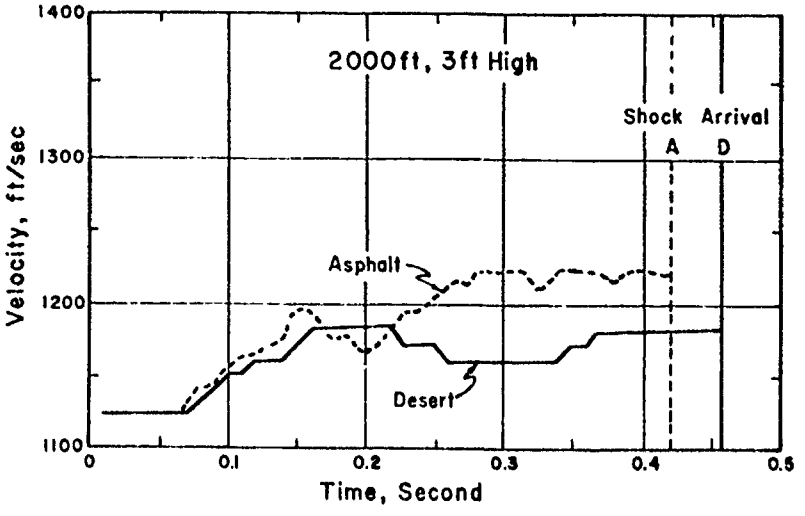

Figure 2.33 Sound velocities (NEL) at 2,000-foot ground range (3 feet high), Shot 12.

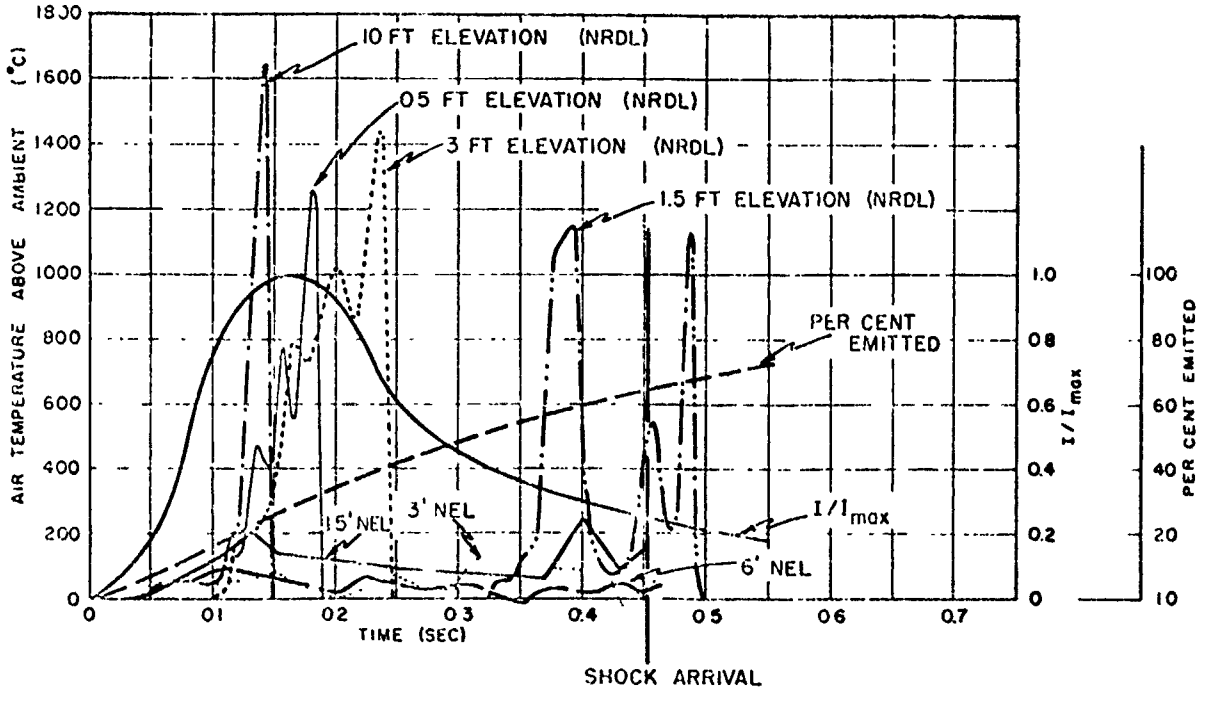

Figure 2.34 Air temperatures (NRDL), air temperatures from sound velocity (NEL), and thermal pulse (TM 23-200), over concrete test surface at 2,000-foot ground range, Shot 12.

possible to estimate what this effect would be in the 0.5-second period following detonation. It would appear inconsistent, however, to use obscuration as an explanation of the unusual air-temperature measurements, in view of the fact that significant air-temperature rises were recorded at a few elevations following the substantially complete decay of the other temperature measurements.

It can only be stated that the sound velocity and air-temperature measurements appeared to be incompatible. Neither set of these data appeared to adequately describe the thermal layer characteristics expected from Shot 12. Any explanation presently conceived for either set of data appears to be incompatible with the other set of data. It is suggested that these data cannot be used to prove, disprove or describe the existence of the thermal layer previously hypothesized as a basic requirement for the generation of a precursor-blast wave from a low-nuclear detonation.

Temperatures Deduced from Blast Data. If one assumes that a thermal layer exists prior to shock arrival, in order to explain the blast phenomena, it is possible to set up some simple analytical relationships which can be used to deduce the general characteristic of the thermal layer from the observed blast behavior. For instance, at the ground level where the particle flow must be parallel to the ground surface, the horizontal velocity of the blast wave is analytically related to the temperature or velocity of sound of the ambient air into which it propagates. The exact relation is somewhat uncertain because the blast wave is not of an ideal nature, but it may be estimated within reasonable limits in terms of the pressure level of the observed blast wave. In this manner, it is possible to estimate the air temperatures which would be required at the ground level to produce the velocities observed for the blast wave at ground level in terms of the overpressures measured at ground level.

The deduced temperatures based upon blast parameters can be divided into three main classifications: (1) those using shock-wave equations, measured initial overpressures, and some average wave-front orientation angle (called pressure calculation); (2) those using the assumption that wave-propagation velocity equals the sonic velocity characteristic of the medium (called sonic calculation); and (3) those using only angles of the shock-wave front orientation (called angle or front calculation). Using shock-wave photography-data, time of arrival from electronic gages, and overpressure-time measurements, one can compute, using these various methods, the preshock, near-surface temperatures. From these calculations it is possible to choose the best value of computed temperature; this choice is based upon the type of pressure-time record observed at each station; i.e., a shock-type pressure rise would suggest that the best temperature calculation is either the pressure method or the angle-of-front method, whereas a compression type pressure-time history points to the sonic method. Naturally, the so-called transition form of record presents a problem. However, since the angle-of-front method is equally applicable to the shock or compression cases, this type of calculation should influence the choice of best value in the transition region.

Figure 2.35 presents the best value, near surface, preshock temperatures plotted against ground range for the three blast lines of Operation Teapot Shot 12. Although the data were meager, some general statements could be made. The near-surface, preshock temperatures at ground ranges between about 650 and 1,000 feet were comparable over the asphalt and desert blast lines. The greatest discrepancy of computed preshock temperature over the desert and asphalt surfaces occurred at 1,500-foot ground range. The 1,500-foot computed preshock temperature over the water surface was not significantly less than the desert-line surface temperature; however, at 2,500 feet the value over water was severely depressed with relation to the desert data.

Since the computed temperature was determined on the basis of conditions obtained at shock arrival, it was obvious that the computations over the different blast lines, although they referred to the same ground range, corresponded to different absolute times. Therefore, a legitimate

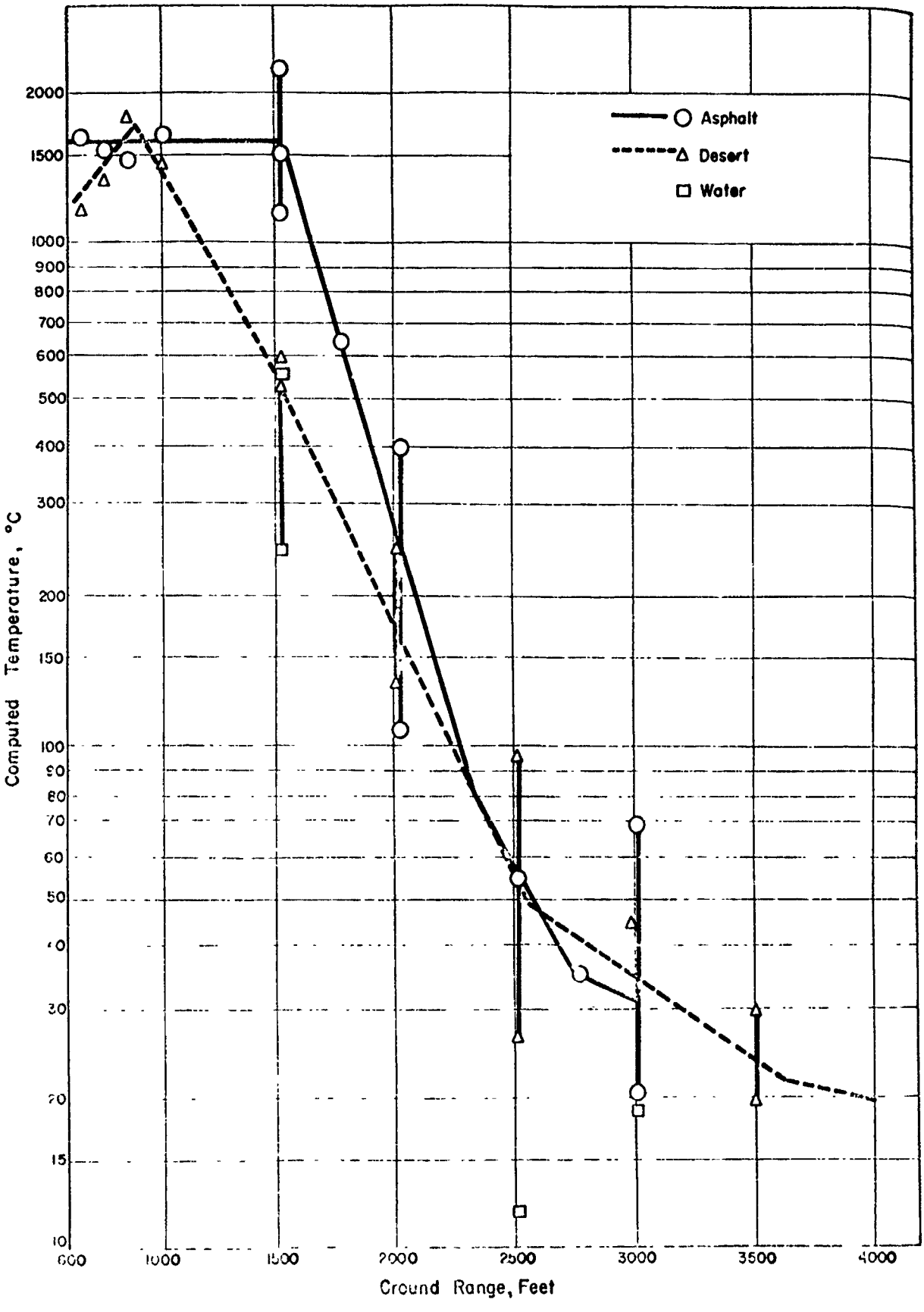

Figure 2.35 Computed preshock temperature versus ground range, Shot 12.

criticism of the presentation of temperatures in Figure 2.35 was that at the same ground ranges temperatures over asphalt were determined at times significantly earlier than those computed over desert. To complete the analysis, Figure 2.36 presents the computed temperatures as a function of arrival time for Operation Teapot Shot 12. This presentation indicates a rather consistent behavior over the three blast line surfaces; that is, it is possible to draw a single average curve which agrees well with the derived temperature data. It is noteworthy that on the time plot of Figure 2.36 the asphalt temperature of nearly 2,000 C and the temperatures over water near 400 C appear quite compatible; only at later arrival times do the water-line preshock temperatures fall significantly below the average curve.

It is obvious that the computed temperatures deduced from blast data (Figures 2.35 and 2.36) are inconsistent with the Teapot Shot 12 near-surface temperatures obtained by sound velocity- and direct-air temperature measurements. The fact that the direct-air-temperature measurements, where available, are incompatible with air temperatures deduced from sound-velocity measurements makes the problem of correlation extremely difficult. The only connection that is valid at this time is that the deduced preshock temperatures based on blast data are consistent with the hypothesis that a thermal layer exists at the ground surface prior to shock arrival, whereas the direct air temperature and sonic velocity measurements do not support this theory.

2.4.2 Mechanical Effects. Dust Loading. The mechanical-effects theory which was proposed after Operation Buster-Jangle to account for disturbed wave forms in the non-ideal region was in general superseded, after Operations Tumbler-Snapper and Upshot-Knothole, by the hot-air-boundary-layer hypothesis for precursor generation. However, the contribution of dust loading of the shock wave to damage in the precursor region remained unanswered after Shot 10 of Upshot-Knothole.

In order to determine the relative significance of the dust in the shock wave, an attempt was made to measure the dust density and particle-size distribution as a function of time, as well as the total-air density during the passage of the shock wave.

Isokinetic sampling of the air during the passage of the shock wave was performed by Project 1.13 (Reference 10) over the desert and asphalt surfaces. Data obtained at 2,000 feet on the desert line in the period from 40 to 340 msec after shock arrival gave ratios of dust density to total density between 0.12 and 0.77 at 3 feet and about 0.42 at 10 feet above ground. Density ratios at greater ranges over the desert were considerably smaller. The best estimate of the dust-density ratios over the asphalt at 2,000 feet was 0.30. This ratio could correspond to about 0.25 mg of dust per cm^3. These results are considered accurate to about 50 percent. It was noted that the dust concentration increased during the sampling interval to 0.34 second after shock arrival. The mean particle-size distribution of the dust collected over the desert line had a median diameter of 1.2 μ, with 95 percent of all particles being less than 5 μ in diameter. The mass mean diameter of the distribution was 15 μ. It should be noted that the aforementioned characteristics of the particle-size distribution correspond closely to those found in the near-surface soil in Frenchman Flat.

Density. In an attempt to measure as many parameters of the shock wave in the precursor region as possible, some attention was given to the density of the medium. Measurements of total density by Project 1.13, using beta densitometers at 2,500 and 3,000 feet on the desert and asphalt lines were not successful, since the detectors were saturated by excessive gamma radiation. Total density measurements by Project 1.11 at 2,000 and 2,500 feet on the desert line were likewise unsuccessful. Measurements of air density only with a centripetal-density gage, by this project, met with limited success. The air-density records on the water line were about as expected, despite the unusual shape of the pressure-time wave. The pressure and air density increased and decreased together and appeared to obey the Rankine-

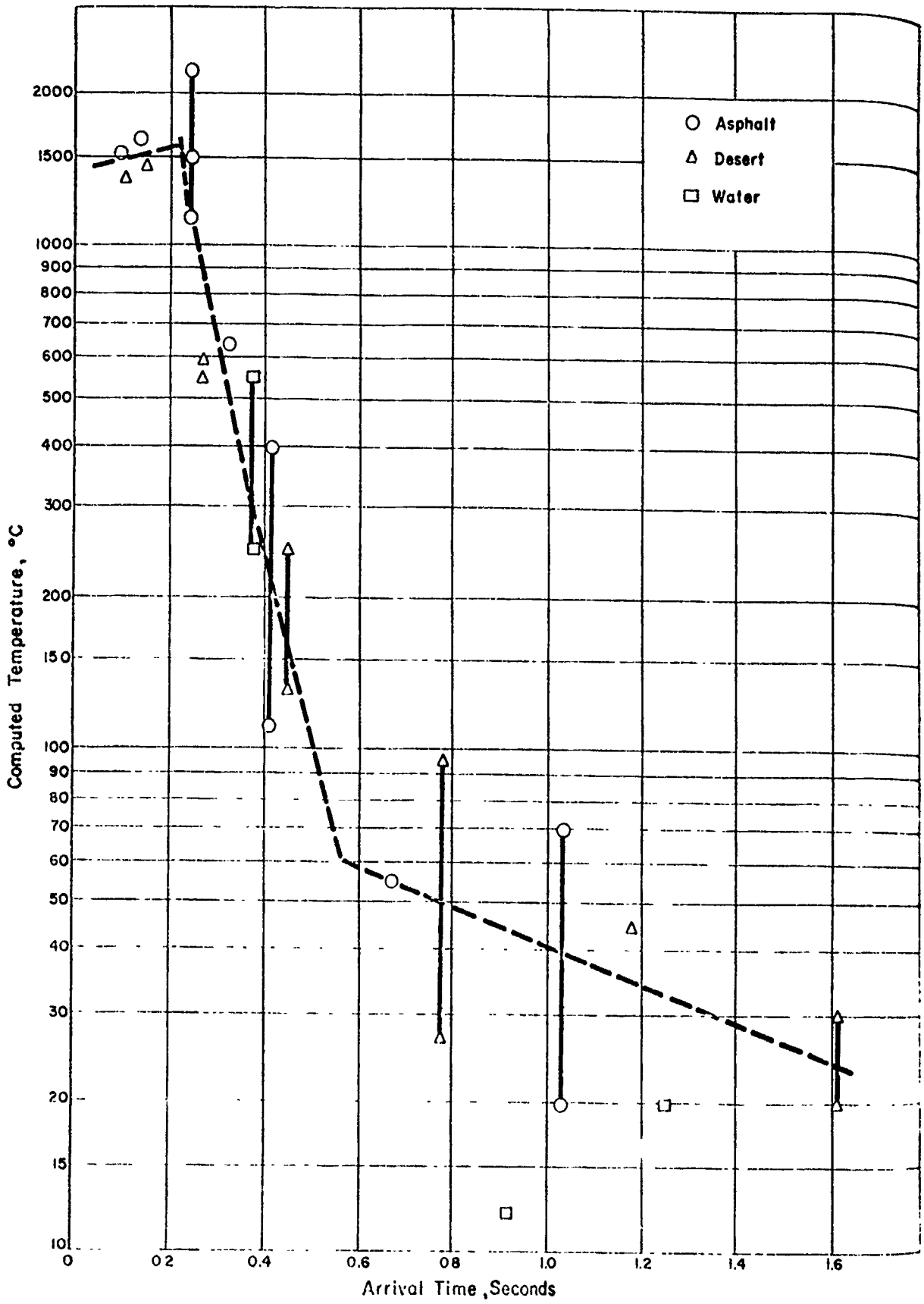

Figure 2.36 Computed preshock temperature versus shock arrival time, Shot 12.

Hugoniot relations. On the asphalt and water lines the air density showed an initial increase, after which it fell below the preshock density level for most of the remainder of the blast-wave history. The results showed no consistent density decrease attributable to heating of the air prior to shock arrival.

Dust Data from Snob and Greg. The dynamic pressure of the dust alone has been discussed in an earlier section. Further analyses of these data for correlation with dust densities reported by Project 1.13 yield the fact that, while the gages (Project 1.11) indicate larger dust densities at 2,500 feet than at 2,000 feet on the desert, the opposite is indicated from the isokinetic-sampling techniques (Project 1.13). As it happens, this was the only comparison that could be made using data obtained from the two projects.

It is generally assumed that the particle velocity of the dust will approach that of the air behind the shock if the particles are small. It was hoped that the particle velocity of the medium (air plus dust) could be measured by means of a wind-velocity gage developed by Sandia Corporation. Wind tunnel tests in clean air appeared promising. However, the electronics appeared too delicate to withstand the zero transient, and only one gage was activated for Shot 12. No useful results were obtained.

Loading of the Shock Wave over the Three Surfaces. On all three areas near the ground for Shot 12, analysis of direct-shock photography indicated that the blast wave was loaded with some material raised by the passage of the shock along the surfaces.

Shock photography indicated that the dust cloud over the desert surface began to lag behind the precursor front at about 1,900-foot ground range; the dust ceased to propagate horizontally at about 3,100-foot ground range. Over the asphalt line a dense cloud of material was lifted and carried along by the flow behind the precursor. The makeup of this cloud appeared quite different from that over the desert. It is believed that it was composed of smoke and particles of dust and asphalt. In the water area a column of material rose to a height of 200 feet behind the Mach stem. This column lagged farther and farther behind as the triple point rose in height. This column appeared to be composed of a fairly dense material such as water vapor or smoke but was smaller and less dense than that over the desert line.

The possibility of correlating photometric data on the motion of the dust cloud with gage results has been investigated. It was thought that the differential pitot-tube gage (q′) was sensitive to the arrival of the dust front. Viewing the records, it appeared that shortly after the first disturbances arrived at the gage there was a sharp increase in apparent dynamic pressure. If one identifies the time delay between first disturbances and this sharp rise with the lag of the dust front behind the precursor front, and assumes an average precursor velocity, one obtains dust-front orientations shown in Figure 2.37. It is obvious from this figure that in the early stages of formation the dust front is coincident with the precursor front near the ground surface. However, as the precursor front progresses to larger ground ranges the dust lags farther and farther behind, assuming an angle near 20 degrees to the horizontal. The most interesting aspect of this method of determining dust front orientation is that the identification of the dust-front arrival on the dynamic pressure-gage records appears to correlate well with the photometric data, which points up the profound influence suspended matter has upon the q′ measurement.

Force Plate. To obtain information on the effect of dust loading over a larger area than the Greg, Project 1.11 installed force plates at 2,000 and 2,500 feet on the water, desert, and asphalt lines. This instrument measured the total-stagnation pressure, P_t, imposed by the mixture of dust and air on a sizable object. A large diaphragm-type-pressure gage with a sensitive area of $7\frac{3}{8}$-inch diameter was mounted in a baffle head onto the blast. Satisfactory results were obtained on five of the six stations. In the absence of dust, the force plate and Greg results should have been substantially the same. A comparison of these two gages at 2,500 feet at 3 feet in elevation is made in Figure 2.38 and Figure 2.39.

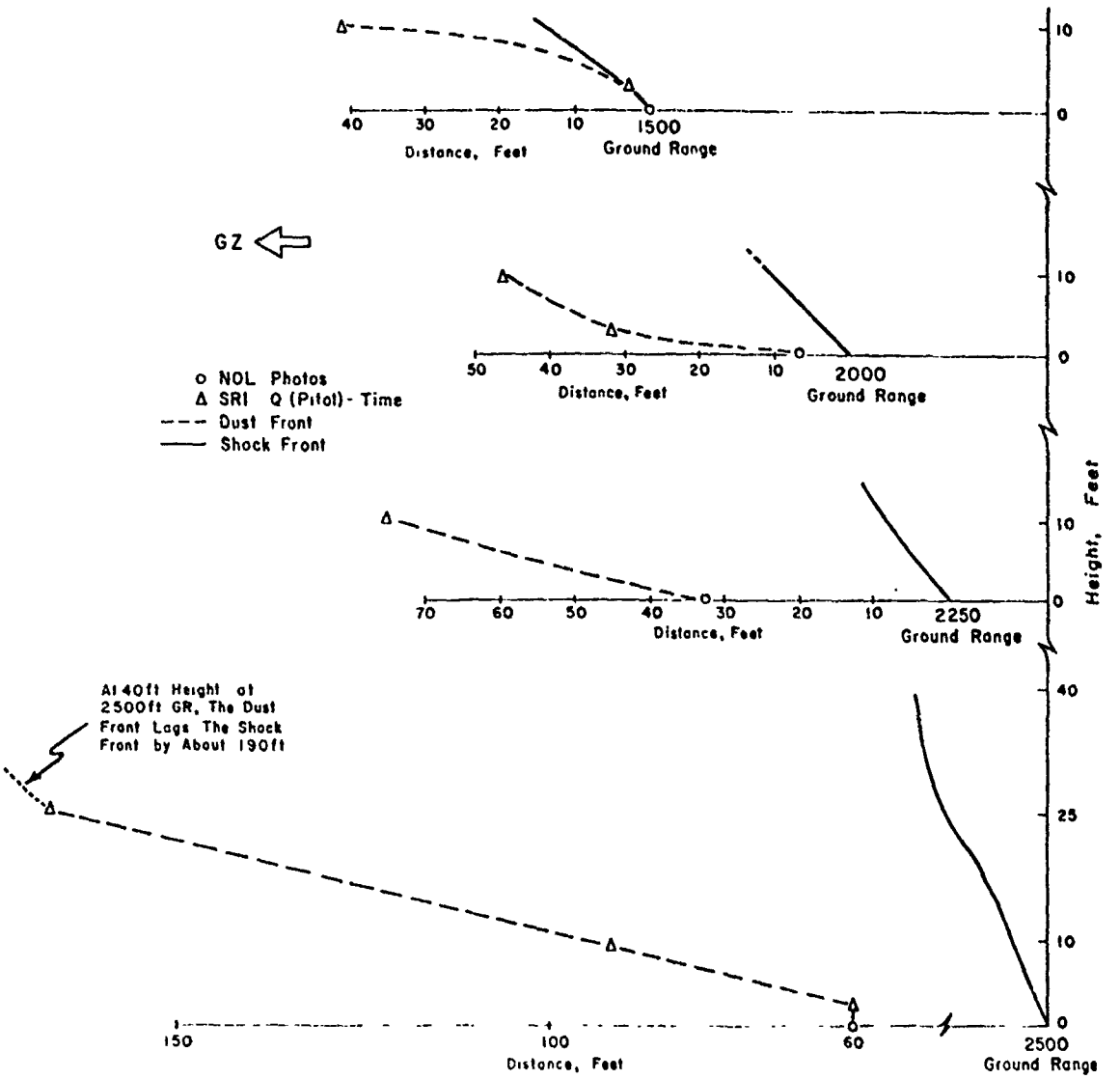

Figure 2.37 Dust-front orientation, Shot 12.

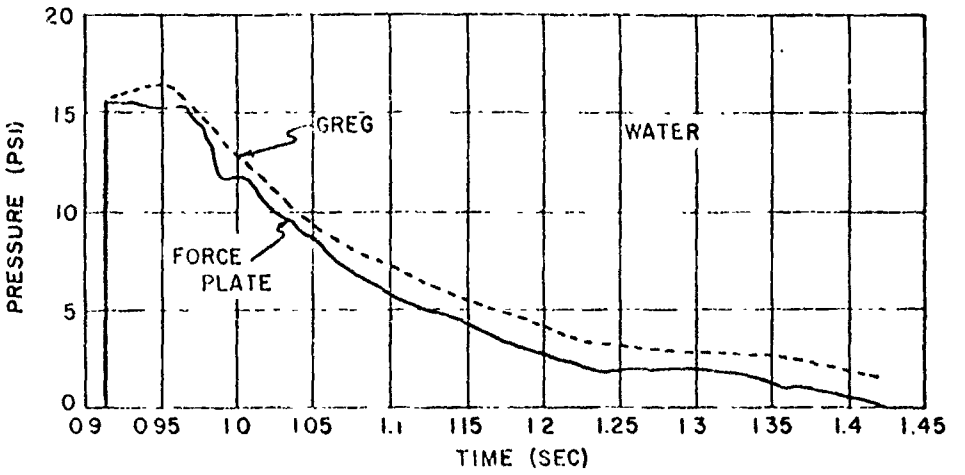

Figure 2.38 Total stagnation pressure. Comparison between Greg (small diaphragm) and force plate (large diaphragm), 2,500-foot ground range (water, 3 feet high), Shot 12.

2.4.3 Triple-Point Data On Shot 12 the height of the triple point was measured over the three surfaces as a function of ground range. These data are shown in Figure 2.40. Comparison of the path of the triple point over the three areas indicates that the Mach stem grew much faster over the asphalt area than over the other two areas. The path of the triple point over the desert area was not too different from the ideal and fell between those for the water and asphalt areas. The maximum heights of the precursors over these areas followed the same relative pattern. Though the reflection coefficients for these three surfaces were slightly different, it is believed that the large differences in the thermal layers over these surfaces accounted for the

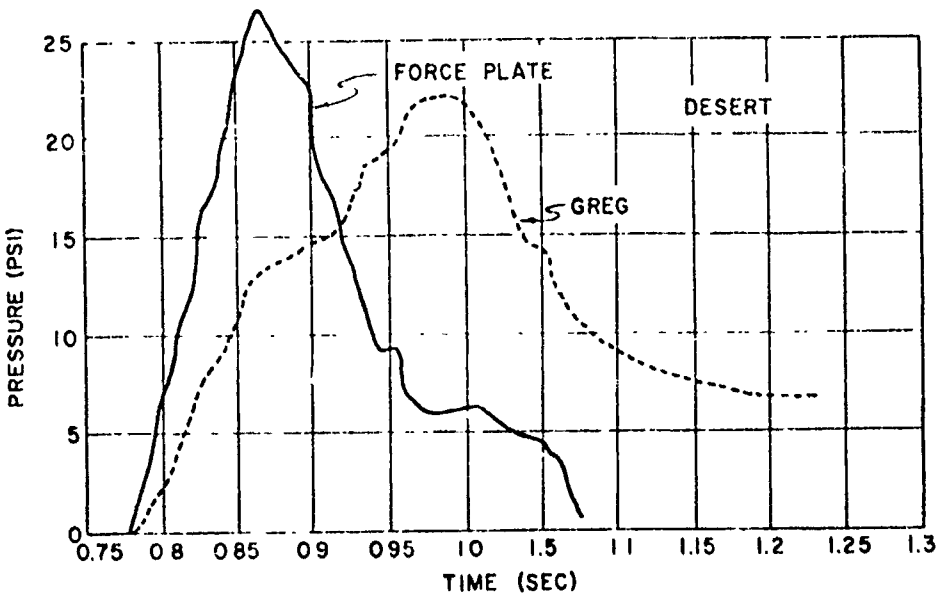

Figure 2.39 Total stagnation pressure. Comparison between Greg (small diaphragm) and force plate (large diaphragm), 2,500-foot ground range (desert, 3 feet high), Shot 12.

radical differences in triple-point trajectories. In a sense it was rather disturbing that the triple-point trajectory over the desert line agreed so well with the ideal trajectory as given in AFSWP-510, as the reference presented the ideal trajectories as those which would obtain under conditions of no thermal disturbances. It would appear that the triple-point data obtained over the water line should have agreed more closely with an ideal curve.

An analysis of triple-point data on Shot 4 showed slight differences in the triple-point path as measured on either side of ground zero at 180 degrees. The growth of the Mach stem appeared normal above 50 feet and correlated well with other nuclear shots on an A-scaled basis.

2.5 PRECURSOR

2.5.1 General. The term precursor is generally used to describe the existence of an auxiliary-pressure wave which has been observed to form for nuclear bursts at low heights. This pressure wave travels ahead of the incident shock to a range where thermal effects on the blast wave are no longer significant. The existence of a precursor wave can be related to specific conditions of yield, height of burst, and thermal properties of the reflecting surface over which the detonation takes place. The characteristics of the precursor in the non-ideal blast region have been described in detail in WT-782 (Reference 3). For most precursor-forming

detonations observed to date, peak overpressures appeared suppressed out to ground ranges corresponding to pressures of 6 to 7 psi, while dynamic pressures (pitot-static tube measurements) were considerably higher than those calculated from measured overpressures by the Rankine-Hugoniot equation. It is generally believed that the existence of a layer of air close to the surface with a high-sonic velocity is required for precursor formation and propagation. Assuming no change of medium, this boundary layer would consist of air at high temperature. The exact mechanism of heat transfer into the air to create such a layer is not fully understood. Prior to Operation Teapot it was believed that this heat-transfer process would take place in several different ways, although popcorning was the more common explanation, over the desert. The asphalt surface was expected to give a much more intense thermal layer without the presence of loose surface dust or particulate matter, for direct comparison with the desert and the so-called ideal or water surface.

There appears to be some confusion regarding the distinction between a precursor and a disturbed wave form. It has been shown to be possible under both laboratory-controlled conditions and field-test conditions to produce disturbances in wave forms which deviate from the classical behavior. However, the term precursor will be understood to be applied only to that definite wave which travels ahead of the main shock wave and is separate from it. Thus, the criterion for whether a precursor has formed or not will be the existence of the separate and distinct wave designated as the precursor wave. Detection of this precursor wave may be by shock photography, pressure-time wave form appearance, or arrival-time analysis.

2.5.2 Criteria for Precursor Formation. As discussed in WT-782, there are two sets of criteria in existence by which the occurrence or formation of a precursor may be predicted. The first is that formulated after Operation Tumbler-Snapper by AFSWP and NOL, which appears in the Tumbler Summary Report, WT-514 (Reference 2). These criteria, based on empirical data, set limits on scaled height of burst, yield, actual height-of-burst relation (W/h^3), and the time required for shock arrival at ground zero. The second precursor-formation criteria are found in a Sandia Corporation (Reference 11) report by F. H. Shelton, SC 2850(TR), and are based partially upon empirical data and partially on theoretical analysis. Both the AFSWP and the Shelton criteria apply to surfaces whose characteristics are essentially the same as those found at NTS. For comparison, these criteria are presented in Figure 2.41. The formation of a definite precursor wave on Shots 1, 10, and 11 of Operation Upshot-Knothole would have been predicted by either of these two sets of criteria. In addition, it was found that Operation Upshot-Knothole did not produce much pertinent data from which more realistic prediction criteria could be developed. In comparing these two sets of criteria, several interesting differences were apparent. The AFSWP criteria predicted precursor formation for low-yield devices (1 to 2 kt) at a scaled height of burst from 50 to 400 feet, while Shelton's curves indicated that no precursor was formed for these weapons at any burst height. The other significant difference between the two sets of criteria was found in the region of 500- to 600-foot scaled-burst height for yields larger than 30 kt, where there were no available data.

Realizing that Operation Teapot afforded an opportunity to check differences between the two sets of criteria illustrated in Figure 2.41 in the low-yield range, it was decided to obtain data on a number of development shots primarily on a go-or-no-go basis. Two methods of determining the existence of a precursor were employed. The first was by means of BRL self-recording pressure-time gages to obtain the pressure-time data and the peak-pressure-versus-distance curve. Examination of wave forms at various ranges would determine the various stages of development in the precursor cycle, and observation of peak pressure would indicate the relative influence of the thermal layer in depressing peak pressures below ideal values. The second method used to determine the existence of a precursor was to examine the shock contours, at

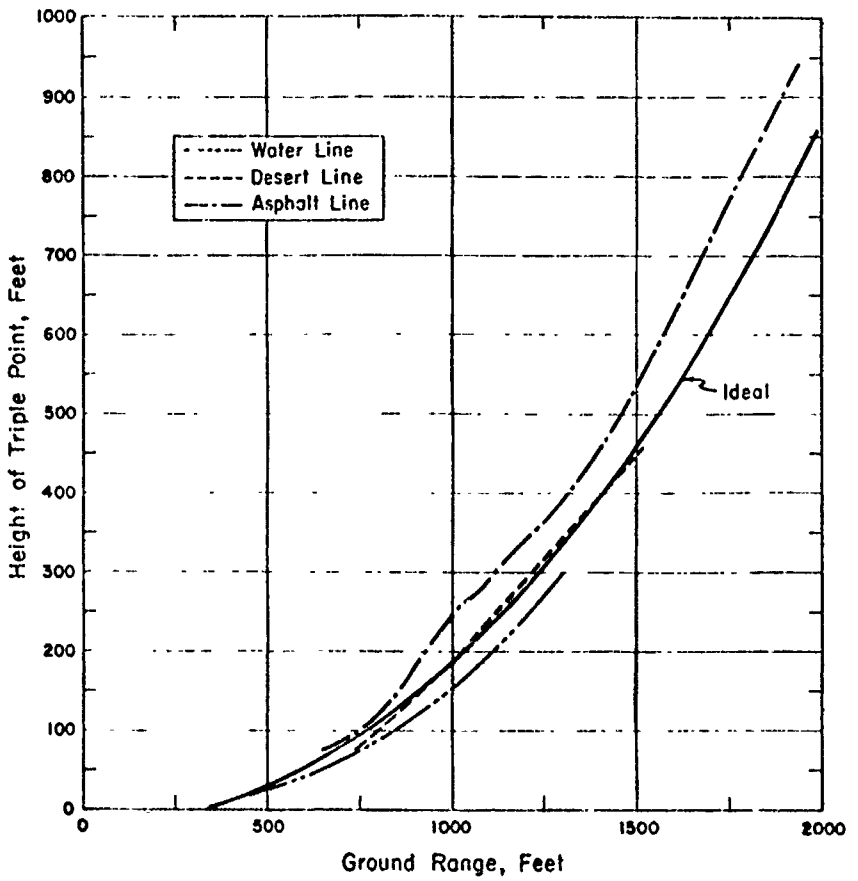

Figure 2.40 Triple point path, Shot 12.

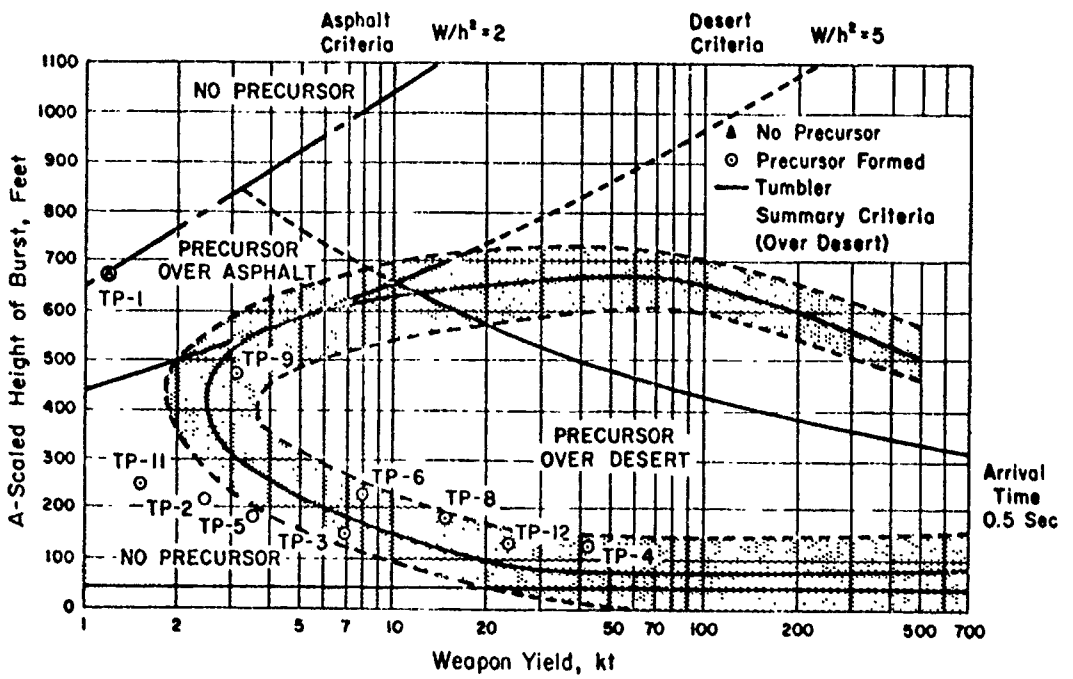

Figure 2.41 Precursor chart from WT-782.

various times, obtained by NOL direct-shock photography. The results obtained from these two projects are discussed below.

2.5.3 BRL data. Project 3.1 (Reference 12) participated in a total of 10 shots during Operation Teapot. These shots are indicated in Figure 2.41 in their A-scaled position relative to the precursor criteria discussed in Section 2.5.2. Using pressure-time wave form distortions as indicating the presence of a separate precursor wave, all shots instrumented produced precursors except Shot 1. On Shot 1 only peak pressures were obtained and the wave shapes are unknown. Photographic data from which Shot 1 arrival times may be determined indicate that a precursor wave was not produced over the desert surface; however, photographs of the shock wave over the nearby asphalt pad indicate that a weak precursor disturbance may have propagated over this surface. Examination of Figure 2.41 shows that all shots except Shot 1 fall within the AFSWP criteria for which precursors would be predicted, including Shots 2, 5, and 11, which fall outside the limits of Shelton's precursor criteria. It should be mentioned that the aforementioned prediction criteria make no claim to predict the relative strength of the precursor wave after formation.

2.5.4 NOL Data. Analysis of direct shock photography by NOL revealed definite evidence of precursor formation on Shots 4, 6, 8, and 12. A slight precursor on Shot 9 was noted, as well as some thermal disturbance on Shot 2. There were indications that a precursor was present on Shot 2; however, because of the excessively high yield, the photography for this shot was not satisfactory. No information was obtained on Shots 5 and 11. It is considered that the NOL data, except for Shot 2, were consistent with those obtained from BRL.

On Shot 1 a weak precursor formed over an asphalt area in the vicinity and to one side of ground zero. On the other side of ground zero over the desert surface no precursor was observed. On Shots 6 and 12, where asphalt surfaces were also involved, much larger precursors were observed over the asphalt than over the desert areas. (These precursors were larger in the sense that the disturbed wave form characteristic of precursor formation persisted out to larger ground ranges over the asphalt surface.) Presumably, a smaller thermal input was required over a more absorbing surface such as asphalt than over the more reflective desert surface to produce a sufficiently intense thermal layer for precursor formation. Based on this information, an extension of the AFSWP chart has been made. Since the Shot 1 precursor over the asphalt was so weak, it was considered justified to use this point as a lower limit on the prediction chart, for it corresponded to minimum-energy-input condition over a higher absorbing surface capable of causing the formation of a sufficiently intense thermal layer for precursor development. The appropriate extension of the precursor criteria to highly absorbing surfaces is shown in Figure 2.41. The results obtained on precursor formation by NOL and BRL are summarized in Table 2.3.

2.5.5 Smoke Layer on Shot 5. On Shot 5, which was a 3.6 kt detonation on a 300-foot tower, a smoke screen was employed. Since the lowering of the peak overpressure on the smoke line was less than on the desert in the clear, it can be concluded that the thermal effects causing precursor formation were diminished because of the smoke. The time of arrival was later, the positive phase duration was shorter, and the intensity of the precursor effect appeared to be reduced over the smoke line, although wave forms indicated the existence of a precursor over both lines. These results did not differ a great deal from those obtained under a smoke screen for Upshot-Knothole Shot 10, an air burst of 14.9 kt at 524 feet, where peak pressure and wave forms measured in the smoke compared favorably with the ideal. For Teapot Shot 5, beyond the precursor zone, peak overpressures on the smoke line were above the overpressures recorded on the clear line.

2.5.6 Precursor Formation on Shot 12 Water Line. The question of whether a precursor formed over the water surface on Teapot Shot 12 or whether the observed disturbances were simply the result of feed-in effects from the desert surfaces was not fully resolved by the film records obtained for Project 1.2. Unfortunately, obscuration by dust made the films useless in this regard. However, using the pressure-time and arrival-time data of Project 1.10, as was pointed out in Section 2.3.5 (Cross Feed; SRI, Water) it can be deduced that feed-

TABLE 2.3 PRECURSOR DATA

Shot	Actual Height	Yield	Scaled Height	Prediction Criteria		Precursor Existence	
				Tumbler	Shelton	BRL	NOL
	ft	kt	ft				
1	762	1.2	675	No	No	No*	—
2	300	2.5	210	Yes	No	Yes	Some thermal effects noted
3	300	7	149	Yes	Yes	Yes	Good possibility†
4	500	43	136	Yes	Yes	Yes	Yes
5	300	3.6	186	Yes	No	Yes	—
6	500	8.1	237	Yes	Yes	Yes	Yes
8	500	15	192	Yes	Yes	Yes	Yes
9	739	3.1	478	Yes	Yes	Yes	"Slight" precursor observed
11	300	1.53	247	Yes	No	Yes	—
12	400	24	133	Yes	Yes	Yes	Yes

*Based on study of peak pressures only, wave forms not available.
†Based on preliminary study of limited photographic data.

in from the desert surfaces to the water line was first evidenced at 2,000-foot ground range on the water-blast line. This hypothesis appears to be consistent with the results obtained on the offset-gage measurements obtained at 1,500-foot ground range. Therefore, it is concluded that the disturbed precursor-like wave forms and earlier-than-ideal arrival times observed on the water blast line at 750, 1,000, 1,250, and possibly 1,500 feet were due to disturbances generated over the water surface without influence of feed-in energy from the desert.

2.6 DRAG-FORCE MEASUREMENTS

2.6.1 General. It was recognized from previous nuclear tests that the drag forces and the damage to drag-sensitive targets in the precursor region of low bursts did not correlate with the results anticipated from utilization of measured overpressures. The limited dynamic-pressure (q′) measurements available indicated that, in general, in the precursor region q′ is substantially higher than would be calculated by the classical relationships from the existing side-on pressure at the location of measurement. Operation Teapot involved extensive measurements of dynamic pressure in the precursor region over different test surfaces using the pitot-static tube previously applied to nuclear-blast measurements. However, there remained a great uncertainty concerning the application of the resultant dynamic-pressure measurements to the calculation of drag forces on objects exposed to the blast wave. Within the limitations of the existing funds and experimental techniques, it was decided to make direct drag-force measurements on simple shapes for direct correlation with the companion dynamic-pressure measurements and for future correlation with combined dynamic-pressure and drag measurements in shock tubes and wind tunnels.

The test program was limited to 3-inch diameter and 10-inch diameter spheres at distances of 2,000, 2,500, 2,750, 3,000, and 4,500 feet, over the three principal test surfaces on Shot 12, all at a height of 3 feet above the ground. The measurements at 4,500 feet would pre-

sumably be in the ideal region and would be the most useful for later direct correlation with shock-tube and wind-tunnel results, although it was hoped that future laboratory programs would permit the development of some unusual conditions which would simulate some of the precursor characteristics of a nuclear detonation. The force-versus-time instruments, employing two different transducer principles, were developed expressly for the Teapot program and were designed to measure the three principal orthogonal components. The program was divided between Project 1.12 (NOL) and Project 1.14 (BRL). Table 2.4 presents a summary of the force-gage layout for Teapot Shot 12. Both projects utilized 3- and 10-inch spheres and, as shown in the table, both projects made adjacent measurements at ground ranges of 2,500 and 4,500 feet, for correlation.

Project 1.10 (SRI) made dynamic-pressure measurements using pitot-static-tube gages, as close as possible to each of the principal drag-sphere installations, at a height of 3 feet. It was expected that the pitot-static tube would perhaps respond to dust and other particulate matter with a different registering coefficient than would the test spheres, and consequently it might be difficult to relate the sphere forces to a simple-drag coefficient in terms of the dynamic-pressure measurements. Nevertheless, such data were considered desirable because only these particular dynamic-pressure measurements, designated as q′ to indicate the characteristic of the pitot-static tube in registering the dust component, could be expected in sufficient quantity to describe the drag-producing characteristics of Operation Teapot and previous nuclear-test series. It was hoped that similar pitot-static-tube dynamic pressure gages and similar drag-force gages would be used in close proximity for shock-tube and wind-tunnel experiments, in order to establish a more precise correlation.

2.6.2 Results on Spheres. It must be recognized that the drag-force instruments for the measurements on the spheres were developed expressly for Operation Teapot. Consequently, their application on Shot 12 of Operation Teapot was both a gage-development test and an attempt to obtain useful drag-force information. Fairly satisfactory, although not completely successful, results were obtained. Unfortunately, a number of gage records were either completely lost or appeared to be unreasonable. The missing data prohibited many of the intercomparisons between the 3- and 10-inch spheres, between the various test surfaces, and between the two projects, which would be desirable to evaluate the validity of the results.

It is worth noting that only the horizontal component along a radial line passing through the sphere and ground zero proved to be of significance. In general, the vertical and transverse components were small by comparison. These results are consistent with the pitch measurements made by Project 1.11. In this report only the axial or principal force component is discussed.

On consideration of the drag-force data for general evaluation, it was found that the degree of reproducibility for measurements of the same size spheres at the same station increased as the ground range increased. At the 2,000- and 2,500-foot stations the force-versus-time records appeared to deviate most markedly. Figure 2.42 presents some comparisons of Project 1.12 and Project 1.14 results. It is noted that the greatest deviation occurred over the asphalt surface at 2,500-foot ground range, while on the desert at this same ground range, although the wave forms of the two records differed, the peak forces compared quite favorably. The data-evaluation picture was clouded by the ambiguity associated with corrections due to air leakage at the seal between the sting and the sphere; in most cases it was impossible to determine how much leakage occurred during the actual test. In addition, it was known that the presence of a sting would prevent the normal shedding of vortices from the surface of the sphere, which would introduce other unknown corrections.

Table 2.5 presents a summary of the peak drag-force measurements obtained on Teapot Shot 12. From this table it is seen that, generally speaking, the peak-drag force decreased

TABLE 2.4 FORCE GAGE LAYOUT, TEAPOT SHOT 12

All spheres at 3-foot height.

Ground Range	Water		Asphalt		Desert	
ft						
2,000	3-inch sphere 10-inch sphere	BRL	*3-inch sphere 10-inch sphere	BRL	3-inch sphere 10-inch sphere	BRL
2,500	*3-inch sphere *10-inch sphere	BRL	*3-inch sphere 10-inch sphere	BRL	3-inch sphere 10-inch sphere	BRL
	3-inch sphere 3-inch sphere 10-inch sphere	NOL	3-inch sphere 3-inch sphere 10-inch sphere	NOL	3-inch sphere 3-inch sphere 10-inch sphere	NOL
2,750	*3-inch sphere *10-inch sphere	BRL	3-inch sphere *10-inch sphere	BRL	†3-inch sphere 10-inch sphere	BRL
3,000	None		3-inch sphere 3-inch sphere 10-inch sphere	NOL	*3-inch sphere 3-inch sphere 10-inch sphere	NOL
3,500	None		None		†Cylinder gage	NOL
4,500	None		None		3-inch sphere 3-inch sphere 10-inch sphere †3-inch (bellows) gage 10-inch sphere	NOL
					3-inch sphere *10-inch sphere	BRL

*Data uncertain.

†Experimental gage.

TABLE 2.5 PEAK AXIAL DRAG-FORCE MEASUREMENTS, SHOT 12

Ground Range	Project	3-Inch Spheres			10-Inch Spheres		
		Desert	Asphalt	Water	Desert	Asphalt	Water
feet		lb	lb	lb	lb	lb	lb
2,000	1.14	101	*	25	1,390	199	252
	1.12						
2,500	1.14	37	*	*	407	376	*
	1.12	40	18	16	650	62	175
2,750	1.14	18	12	*	84	*	*
	1.12						
3,000	1.14						
	1.12	5	3.2	—	35	20	—
4,500	1.14	4.2	—	—	*	—	—
	1.12	1.5	—	—	21	—	—

*No record

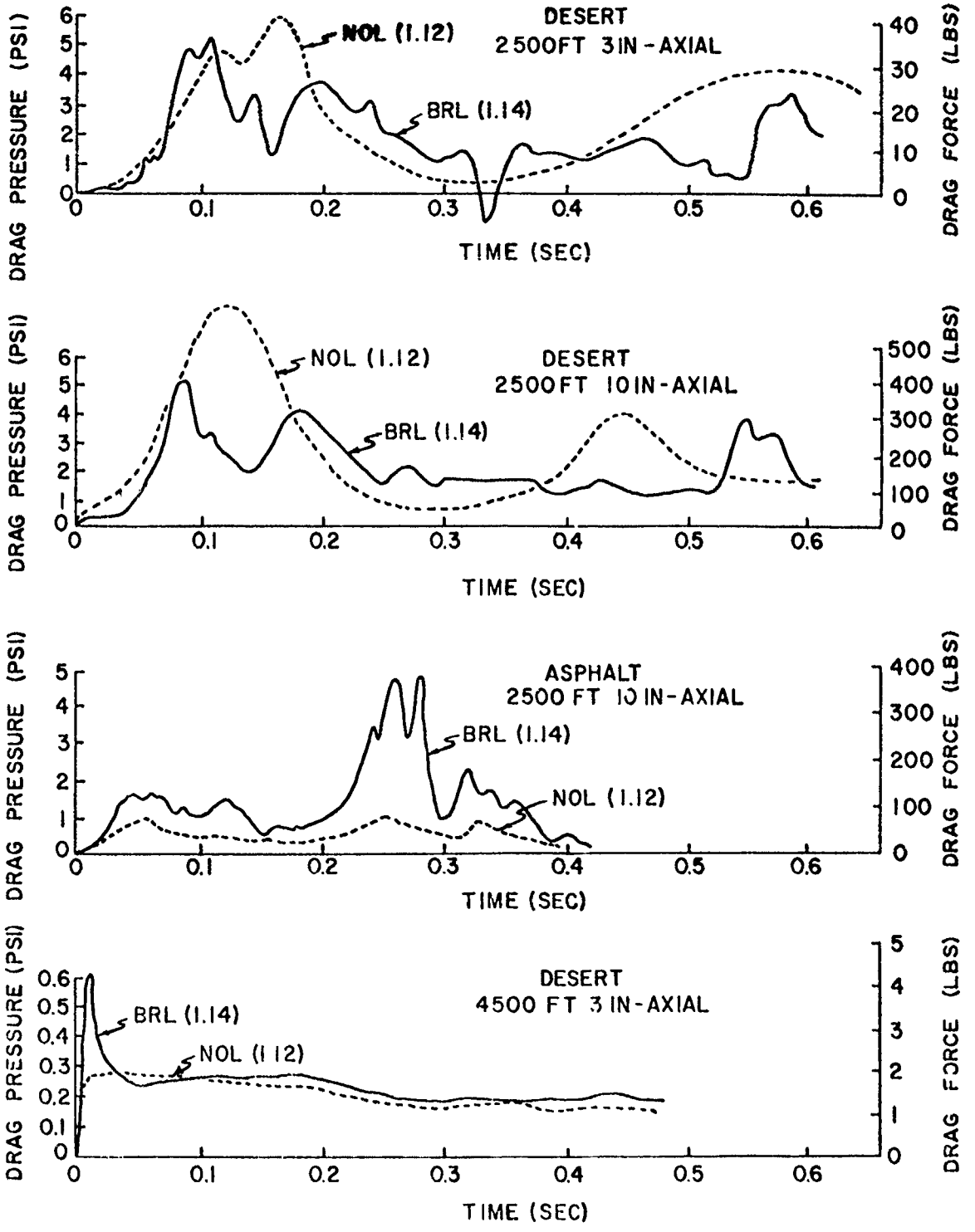

Figure 2.42 Comparisons of NOL and BRL drag force measurements, Shot 12.

with ground range over all the test surfaces; only one apparent anomaly (2,500 feet on the asphalt line, 10-inch sphere) appeared to be present. For the clean-air case it would be expected that the drag-force measurements on the two size spheres would be in the ratio of their projected areas, or approximately 11 : 1. This ratio appeared to hold quite well in most cases documented in Table 2.5. In general, the drag forces developed on the desert line were substantially greater than on the asphalt or water lines at corresponding distances. In some cases the drag pressures on the asphalt line were greater than on the water line and in other cases the results were opposite. Comparisons of this nature are limited and relatively inconclusive because of the loss of a number of data which would have been of primary significance. Furthermore, this table presents only the reported peak values without any consideration of the associated wave forms, with

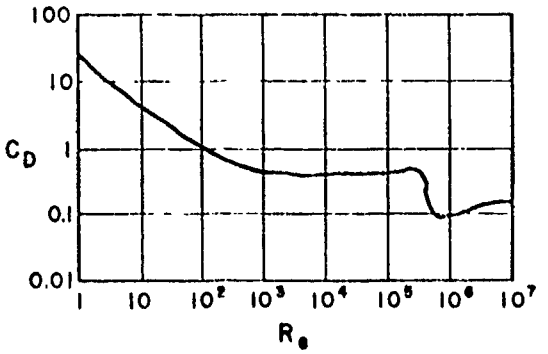

Figure 2.43 Drag coefficient versus Reynold's number.

the possibility that the peaks being compared occurred at substantially different times in the time history of the blast wave. With respect to pitch and yaw effects, scouring and denting of the force spheres was distributed symmetrically about the horizontal axis. Some localized inhomogeneities in the flow were revealed by a few abnormally high vertical and transverse force-time records.

2.6.3 Drag Coefficients. In the conventional sense, it is possible to define a drag coefficient as the ratio between the drag pressure developed on an object and the input dynamic pressure. In steady-state conditions, the relationship between drag coefficient and Reynolds number for a sphere can be presented as shown in Figure 2.43. This curve is obtained for Mach numbers less than 0.5 and laminar flow. At a Reynolds number value of about 4×10^5 the curve is seen to drop suddenly (defined as critical Reynolds number). The critical Reynolds number increases with Mach number, but at the same time the severe drop in the curve is diminished and at Mach 0.8 it disappears completely. Because of the disturbed blast-wave conditions existing on Shot 12 and the fact that parameters such as Mach number and medium density were not determined directly, it was not possible to make a direct comparison between Operation Teapot drag coefficients and those documented in Figure 2.43. Therefore, at best, one could convert the available data into approximate drag coefficient-versus-time plots at the various gage stations. A summary of the most pertinent data is presented in Figure 2.44. If the drag-force-versus-time and the dynamic-pressure-versus-time records at a specific station had exactly the same time history (wave form), one would expect that the drag coefficient would be a constant and that the curves presented in Figure 2.44 would be merely straight lines parallel to the time axis. From the curves presented it is obvious that in most cases the drag-force peaks did not occur at the same time as the dynamic-pressure peaks. These differences might have been caused by instrumental difficulties, turbulence, or large pieces of particulate matter or missiles in the flow. The figure indicates that in most cases the drag coefficient fluctuated as a function of

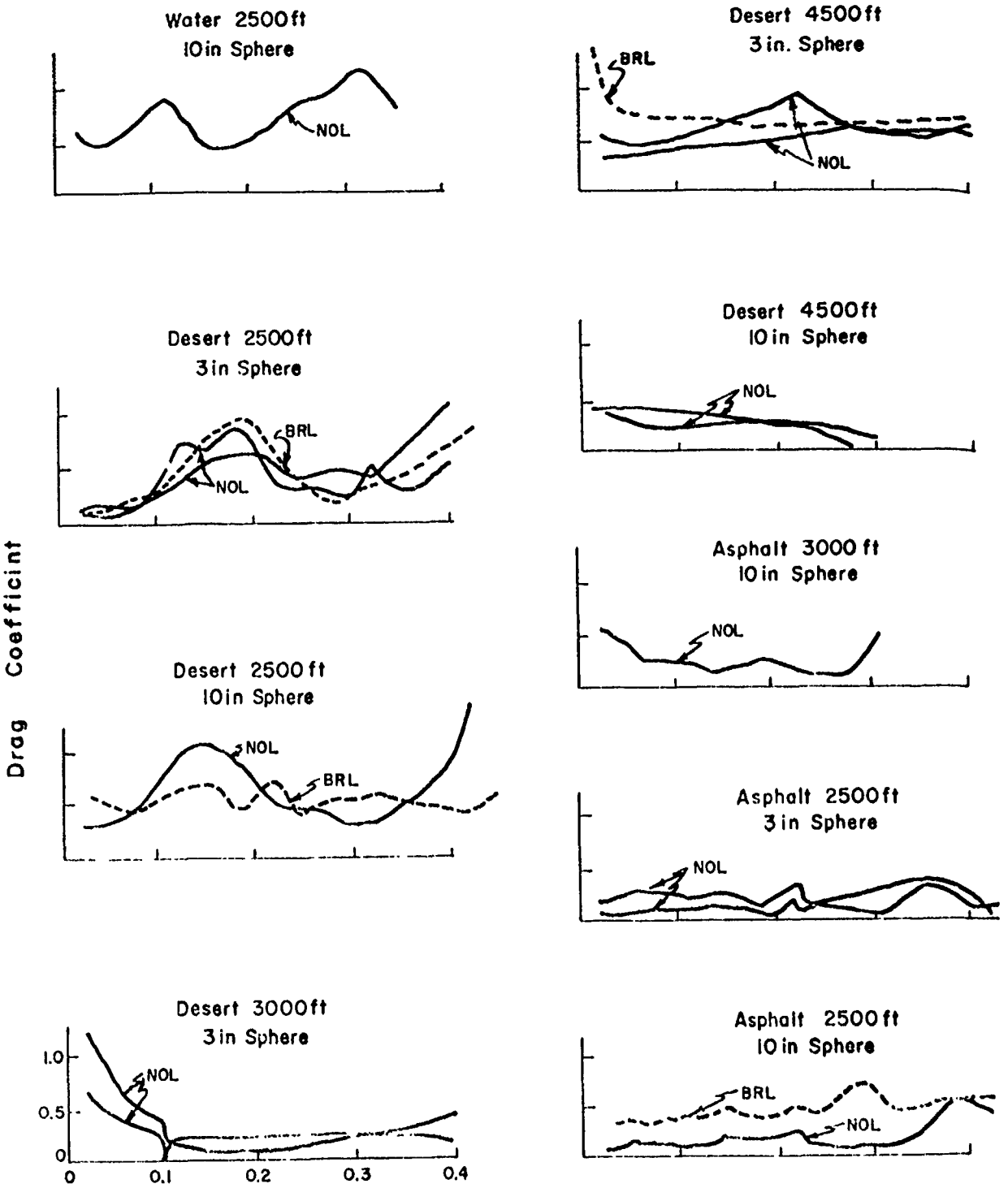

Figure 2.14 Drag coefficient versus time, Shot 12.

time; generally the fluctuations appeared to decrease at larger ground ranges. It was virtually impossible to make quantitative comparisons for the results over the three different surfaces. Referring to the stations at which comparisons between Project 1.12 and Project 1.14 results may be made, it is evident that the fluctuations of drag coefficient versus time may be quite large for a so-called equivalent measurement.

There is, of course, no reason to presume that the drag coefficient of a sphere or any other object will be constant throughout the time history of a blast wave. Even if the transient characteristic of the formation of boundary layers before reaching steady-state flow is ignored, it is clear that the Reynolds number and the Mach number change during the decay of a blast wave. Consequently, a constant-drag coefficient could be expected only on objects having drag coefficients insensitive to Reynolds number and Mach number. Furthermore, it is quite likely that the pitot-static gage (q′) responded differently to dust- or particulate-matter loading than did a sphere, and consequently the drag coefficient changed during the time history of a blast wave if the dust or particulate matter density changed.

2.6.4 Laboratory Investigations. Subsequent to the Teapot field operations, NOL undertook as a part of Project 1.12, a program of laboratory investigations of their force-gage instrumentation in an effort to correlate results with those obtained in the field. These measurements were conducted using the following facilities: (1) the 24-inch-diameter-shock tube, BRL; (2) the 6-inch-diameter-shock tube, Armour Research Foundation; (3) the 40-by-40-cm wind tunnel, NOL; (4) and the 7-by-10-foot transonic wind tunnel, David Taylor Model Basin.

These investigations were designed to determine the effects upon drag force of variables such as Mach number, Reynolds number, wave shape, shock overpressure, surface roughness, gage-frequency response, angle of attack, and sting configuration. No attempt was made to determine, under laboratory conditions, the effect of suspended-particulate matter in the flow impinging upon the force-gage spheres. The results of the drag coefficients obtained in the wind-tunnel experiments are summarized in Figure 2.45 and the shock-tube results are collected in Figure 2.46. A tentative conclusion was drawn that wind tunnel and shock tube drag coefficients are the same after some 75 transit times have elapsed. However, it must be noted that this time for establishment of the drag phase was not well established and that there was much scatter in the Operation Teapot laboratory data.

Drag coefficients obtained in the field could not be compared legitimately with the shock tube and wind tunnel drag coefficients because the condition of each gage in regard to the leakage of pressure into the model was unknown at the time of the field test; the effect of dust loading could not be subtracted from the total-recorded force to show the net-aerodynamic force; and variability in aerodynamic loading of spheres, as indicated by extensive laboratory tests, was so high as to render the results obtained by two or three gages at a station of poor statistical significance. The Operation Teapot laboratory program had value as the first well-organized effort to understand the fundamental phenomena of drag forces on simple shapes. It is evident that further work along these lines, as well as additional field efforts, should be encouraged.

2.6.5 Jeep Program. Test jeeps were installed at identical locations between 2,000 and 3,000 feet on all three surfaces of Shot 12. The postshot survey indicated the maximum damage to jeeps on the desert line, with substantially less blast damage on the water and asphalt lines. The jeeps on the asphalt line showed pronounced thermal effects, presumably due to the flaming characteristics of the surface asphalt. Since the drag data on spheres were conflicting in their comparisons between the water and asphalt surfaces, no clear-cut observations could be made. Nevertheless, it appears that the relative damage to the jeeps on the water and asphalt lines was not in accord with the measured dynamic pressures, q′, which were in general higher on the asphalt line than on the water line. Since it was presumably dynamic pressure that was

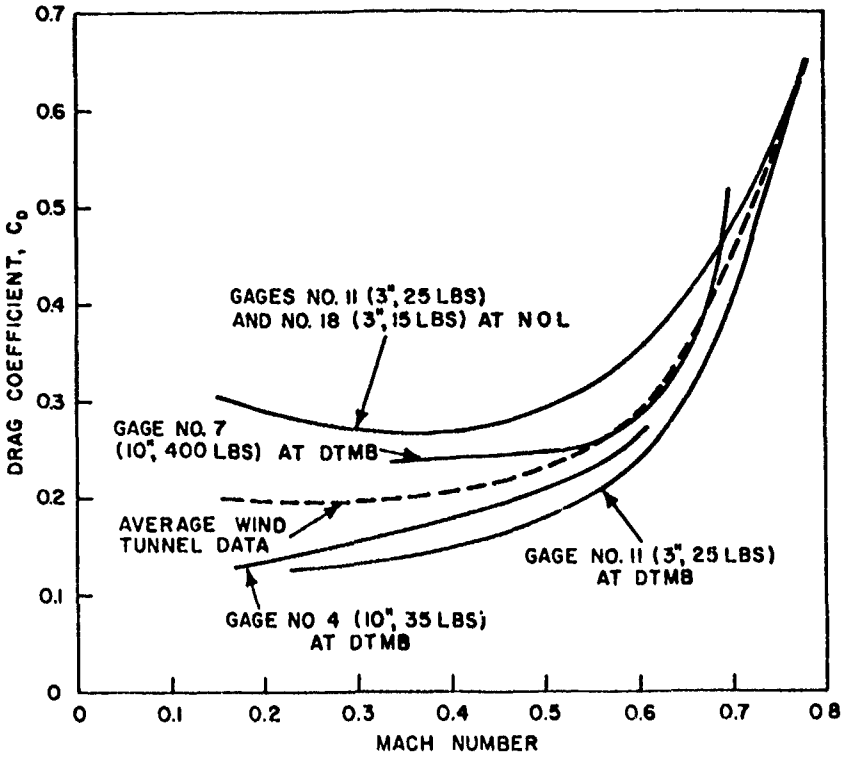

Figure 2.45 Drag coefficients from wind-tunnel experiments.

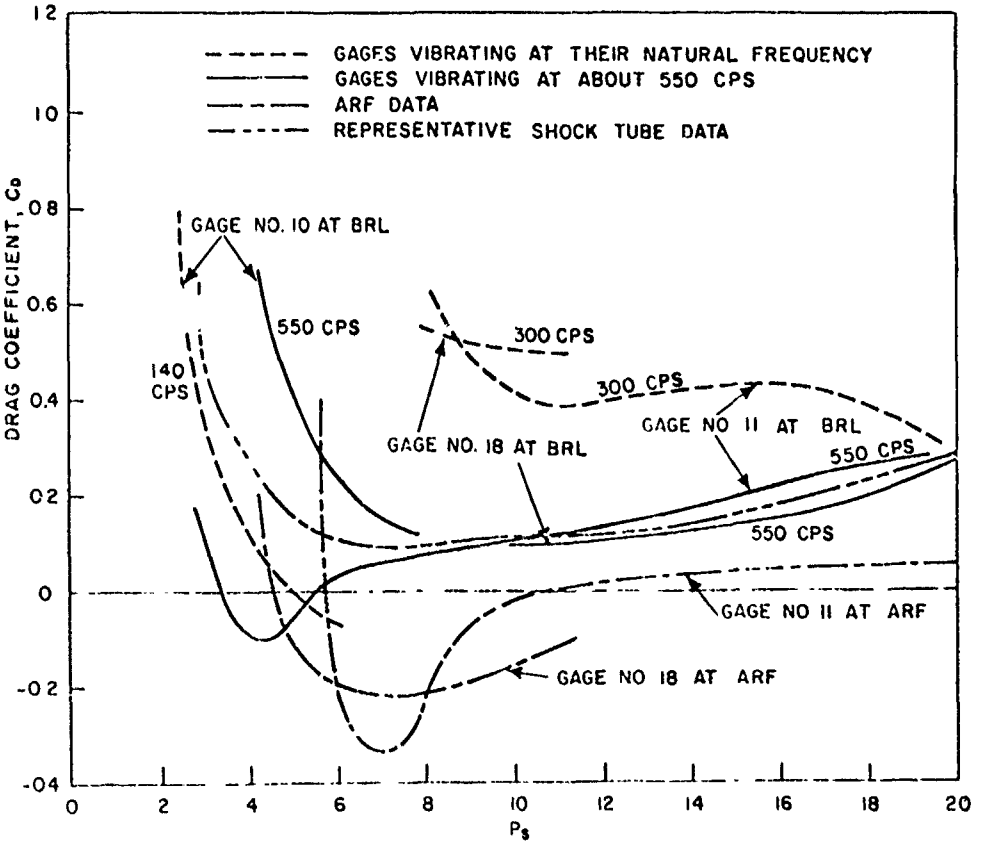

Figure 2.46 Drag coefficient measurements in the shock tube.

principally responsible for blast damage to jeeps, the observed effects on the jeeps were difficult to reconcile with these data.

It appears that it is not possible at this date to say whether force is a parameter of greater significance than dynamic pressure in the establishment of damage criteria for structures. Neither the force gages nor the q′ gages responded to a dust-laden blast with readings that could be used readily for prediction of full-scale loading; the force gage because of size effects (size of model relative to particle size) and variable drag coefficient, the q′ gage because of the design of its nose and shell and the size of the sampling hole. Pending further investigation of the relative merits of force and q′ measurements, it was concluded that both parameters were significant with regard to the damage process.

2.7 DRONE BLAST PROGRAM

2.7.1 Background and Requirement. The most important and critical single project of Operation Teapot was Project 5.1, which utilized three drone aircraft to investigate the lethal effects of blast on aircraft structures in flight. Shot 12 was established principally to permit the conduct of this particular project. The test conditions of Shot 12 were regulated to permit the optimum conduct of Project 5.1.

Project 5.1 required that the wave form of the blast wave at the drone locations be equivalent to that existing from an air burst high above ground surface. In other words, a single peak, ideal type, shock wave was desired in which all reflections or other spurious signals would be minimized. Operational problems eliminated the possibility of using a high air burst for the conduct of this project. The optimum shot choice would have been a surface burst. However, off-site fallout limitations eliminated the possibility of using a surface burst of adequate yield at NTS. There remained the possibility of a relatively low tower shot if the expected reflected wave could be eliminated or reduced. The desired geometry for the drones of Project 5.1 was for them to be located directly over the burst point at shock arrival. Hence, the special interest was in the nature of the blast wave in a relatively narrow cone directly over the burst point.

Heretofore, free-air-pressure measurements by photography to determine shock velocity as a function of time against a background of smoke trails had been made in the horizontal plane of the burst or at relatively small angles above this plane. An examination of similar test results, particularly those from Operation Upshot-Knothole Shots 1 and 11, indicated that the reflected wave might be greatly accelerated during its passage back through the region heated by the fireball. Such an acceleration could have the effect of causing the reflected wave to merge with the incident wave in the region directly over the burst and, if such a merger took place, the test conditions would be suitable for Project 5.1. The available test information did not conclusively prove that these blast conditions would result from a low tower burst. However, some analytical studies coupled with limited experimental data indicated a reasonable possibility that the desired blast configuration would result. Figure 2.47 represents the anticipated shock contours. As a consequence, the height of Shot 12 was specified to be the lowest permissible for the yield in consideration of off-site-fallout restrictions. The yield was specified to be greater than 20 kt, in order to meet the operational limitations for possible position errors established by the drone program. A simple and symmetrical development nuclear device having a reasonably reliable predicted yield of 28 kt was chosen for this shot.

2.7.2 Experimental Plan. Before committing the important and expensive drone program to full participation on Shot 12, it was required that additional experimental information be obtained concerning the possibility of obtaining the desired blast-input conditions directly over

the shot point. There existed an uncertainty concerning shock merger, or the attainment of a single-peaked-shock wave, as well as an uncertainty in the pressure-distance curve in the region directly overhead, which was needed in order to properly specify the positions of the drone aircraft. Free-air-peak-pressure measurements by photography to determine shock velocity against a background of crossed smoke trails was planned for two large development tower shots, Shots 4 and 8, scheduled prior to Shot 12 in the Operation Teapot series. It was expected that such photography would be devoted to the region directly over the burst point and would trace the space-time position of the reflected wave, as well as providing a peak-pressure-

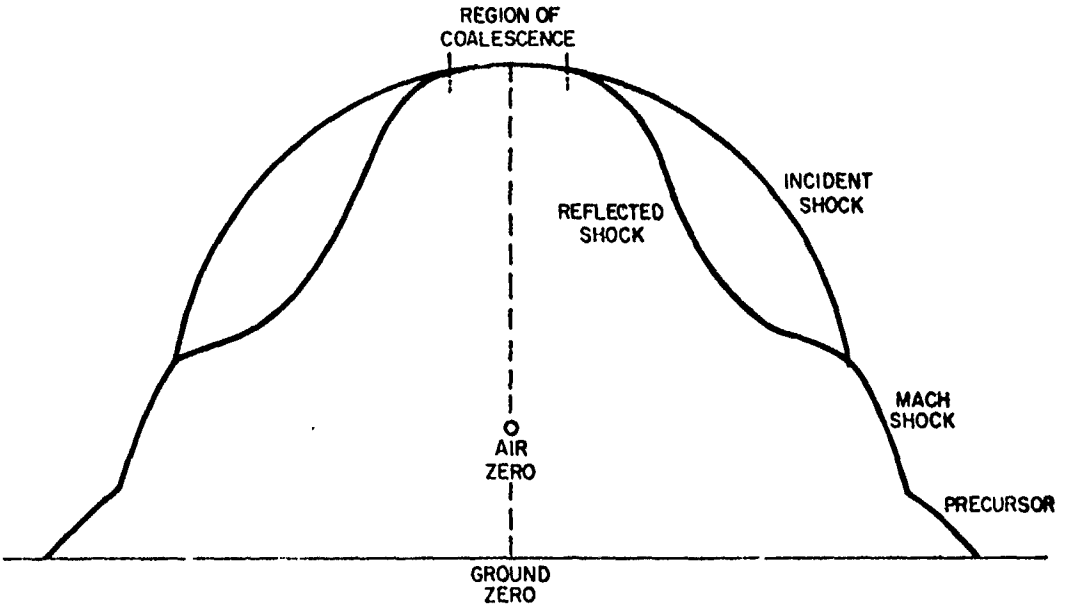

Figure 2.47 Desired shock contours for a low burst.

versus-distance curve in the region of interest. In addition, airborne, parachute-supported, pressure-time instruments were to be suspended in the region directly over these same two development shots, to make pressure measurements in the lower pressure region where the shock photography method was not suitable. For direct correlation with Project 5.1, on Shot 12, the free-air-shock-photography program was also included on Shot 12, but it was not possible, for operational reasons, to include the parachute-suspended-pressure canisters on this shot.

2.7.3 Test Results and Shot 12 Predictions. As it developed, only Shot 4 was utilized for this program, since the yield of Shot 8 fell far below expectations. On Shot 4 the pressure canisters were not properly positioned and none were located in the region of direct interest. However, some of the canisters were close to the region of interest. On these canisters the reflected shock was low in amplitude. Consequently, these measurements suggested that, even if the reflected shock did not truly merge with the incident shock directly above the burst point, it would be of sufficiently low amplitude that the drone project could be conducted satisfactorily on Shot 12.

On the Shot 4 free-air-shock photography it was extremely difficult to identify a reflected pressure wave directly over the burst. A slight moving-density change was observed on the films and when this was plotted in conjunction with the position of the incident wave a distinct closure was indicated. However, the apparent velocity of the reflected wave above the region

heated by the fireball was abnormally high for any reasonable pressure level. On the shock-velocity-versus-distance curve a slight inflection was noticed approximately 2,500 feet above the burst point, which corresponded with the indicated merger of the reflected and incident shock waves. Careful scrutiny of the available films gave the information that the merger extended to approximately 750-foot radius about a vertical axis from air zero. Following the incident wave beyond this point, it was possible to calculate from shock velocity the peak-overpressure-versus-distance curve. The peak overpressures determined by this method are shown in Figure 2.48, as compared to the free-air pressures for this shot as computed from the standard composite free-air curve. In the region of interest, below 20 psi, and in the region directly over the burst point the pressure-distance curve corresponded to a yield of approximately 1.16 times the Shot 4 yield or 1.16W. This is contrasted to an expectation that the shock behavior in this region might be equivalent to that from twice the yield located at the ground surface. The pressures were substantially below those which would be predicted by a two-bomb theory; this result was not inconsistent with those obtained on other tower shots of Operations Upshot-Knothole and Greenhouse. There was some indication that an extrapolation of the pressure-distance curve to the 5 to 2 psi region of particular interest to Project 5.1 could be based on the free-air curve for an equivalent yield of 1.2W.

Since it appeared that the characteristic of the blast wave directly overhead for a large tower shot would be satisfactory for the conduct of Project 5.1, it was decided to implement Project 5.1 on Shot 12. It is worth noting that Shot 4 (a 43-kt shot at 500 feet) was at a higher scaled-height of burst than that planned for Shot 12, 28 kt at 400 feet. It was estimated that if shock merger occurred on Shot 4, it would definitely occur on Shot 12 at a still higher-pressure level and perhaps over a greater vertical sector. There remained the problem of predicting the pressure-distance curve for Shot 12 to permit the proper placement of the Project 5.1 drones.

Pressures were predicted on the basis of the anticipated yield of 28 kt, using a reinforcement factor of 1.2W based on the Shot 4 results. This so-called 1.2W curve is shown in Figure 2.49, and the drone position specifications were made using this curve. It was recognized that there might be some departures from this curve, because of yield variation and because of uncertainties in the method of prediction. An absolute maximum curve was then estimated to be that calculated on a 2W basis, assuming a 10-percent increase in yield and a 5-percent increase in pressure at any given distance because of the possible error in the determination of the pressures on Shot 4. Similarly, an absolute-minimum curve was prepared, on the basis of no reinforcement, i.e., 1W, with a 10-percent reduction in yield and a 5-percent decrease in all pressures. The requirements of Project 5.1 were then examined with respect to the design center 1.2W curve and with respect to the absolute-maximum-and absolute-minimum curves, shown in Figure 2.49. It was decided that a pressure-distance curve anywhere within these limits would be satisfactory for the purposes of Project 5.1.

2.7.4 Shot 12 Results. The free-air-shock photography on Shot 12 showed a relatively clear reflected shock merging with the incident shock approximately 2,600 feet (7-psi level) above burst zero, as compared to the position of the lowest drone at 3,800 feet above burst zero. Once again, the apparent velocity of this reflected shock in the region above the fireball-heated air was high but not as high as observed on Shot 4. The coalescence of the incident and reflected waves extended over a 1,000-foot radius about the vertical axis through air zero. The peak overpressures were then determined on the basis of shock velocity of the shock front to the limit of the available photography. Figure 2.50 shows these peak pressures as compared to the composite free-air curve for the yield of Shot 12, which was 22 kt. It is to be noted that at the lower-pressure levels the actual peak pressures were below those predicted for the free-air case for this shot. In other words, the results were completely contrary to those from Shot 4, where some reinforcement was obtained; however, this deviation appeared to be in no way con-

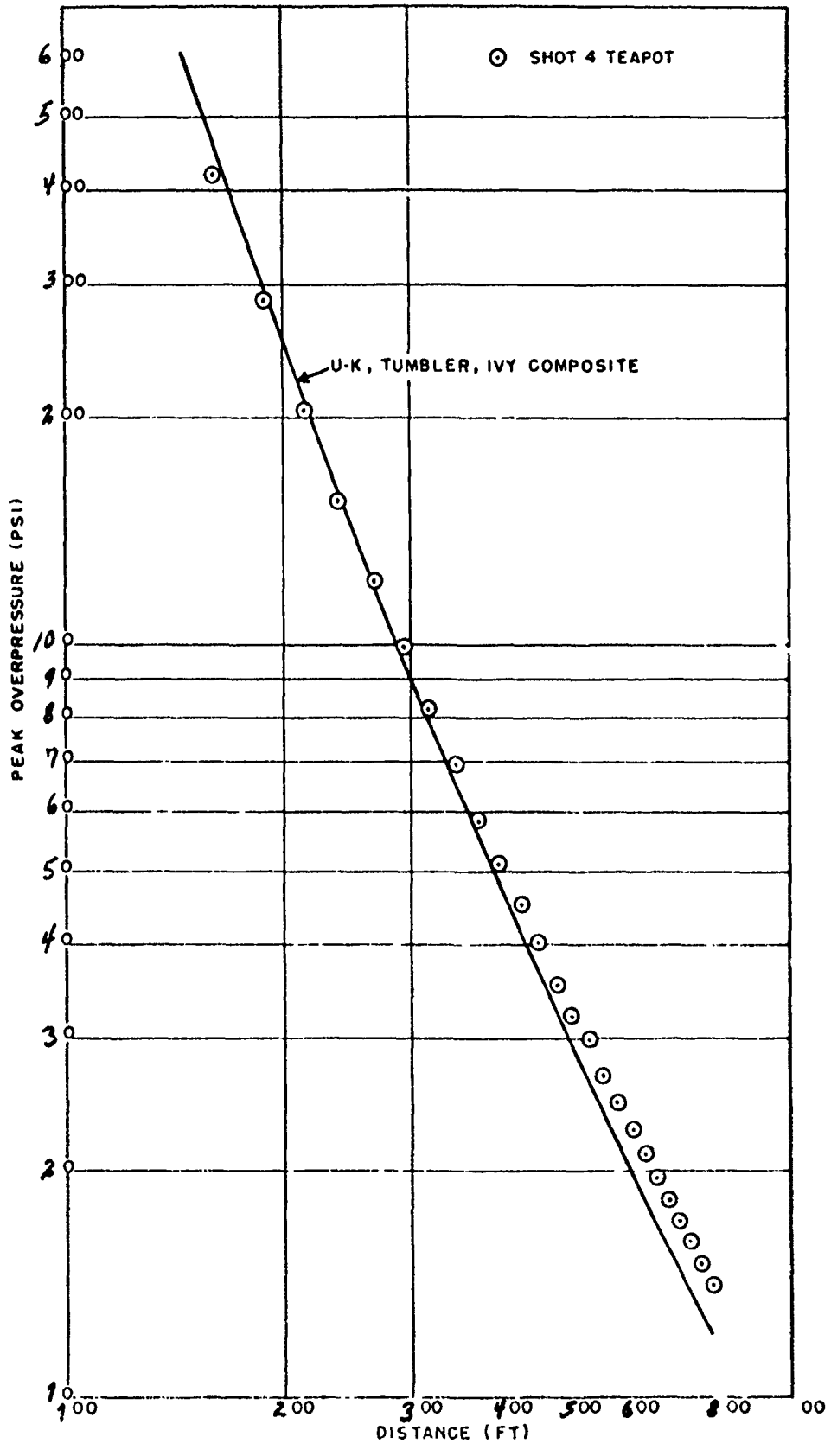

Figure 2.48 Peak overpressure above burst compared to free air (A-scaled), Shot 4.

nected with the problem of shock-wave coalescence. The limited data available for this phenomenon do not permit any adequate explanation of this behavior at this time; however, it has been suggested that the deviation may be attributed to the peculiarities of the present statistical method of treating the arrival-time data. It is sufficient to say that the observations of Shots 4 and 12 were not resolved in this regard.

The peak overpressures as obtained from shock velocities in the region directly over the burst on Shot 12 are also shown in Figure 2.49. Because this shot not only failed to show the

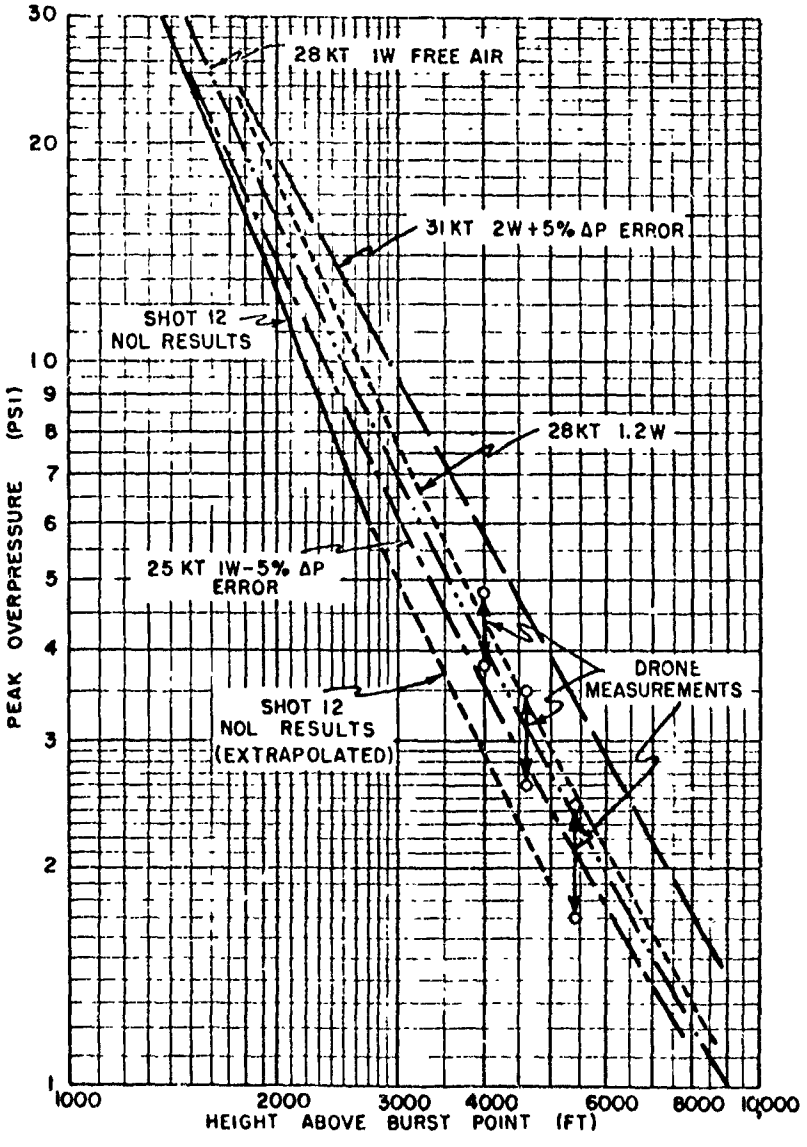

Figure 2.49 Peak overpressure above burst point; predictions and results (Projects 1.2 and 5.1), Shot 12.

reinforcement represented by the 1.2W assumptions but in fact gave pressures substantially below those based on a 1W assumption, and because the yield was a little more than 10 percent below the design center, the overpressures fell outside the limits established in the preshot considerations.

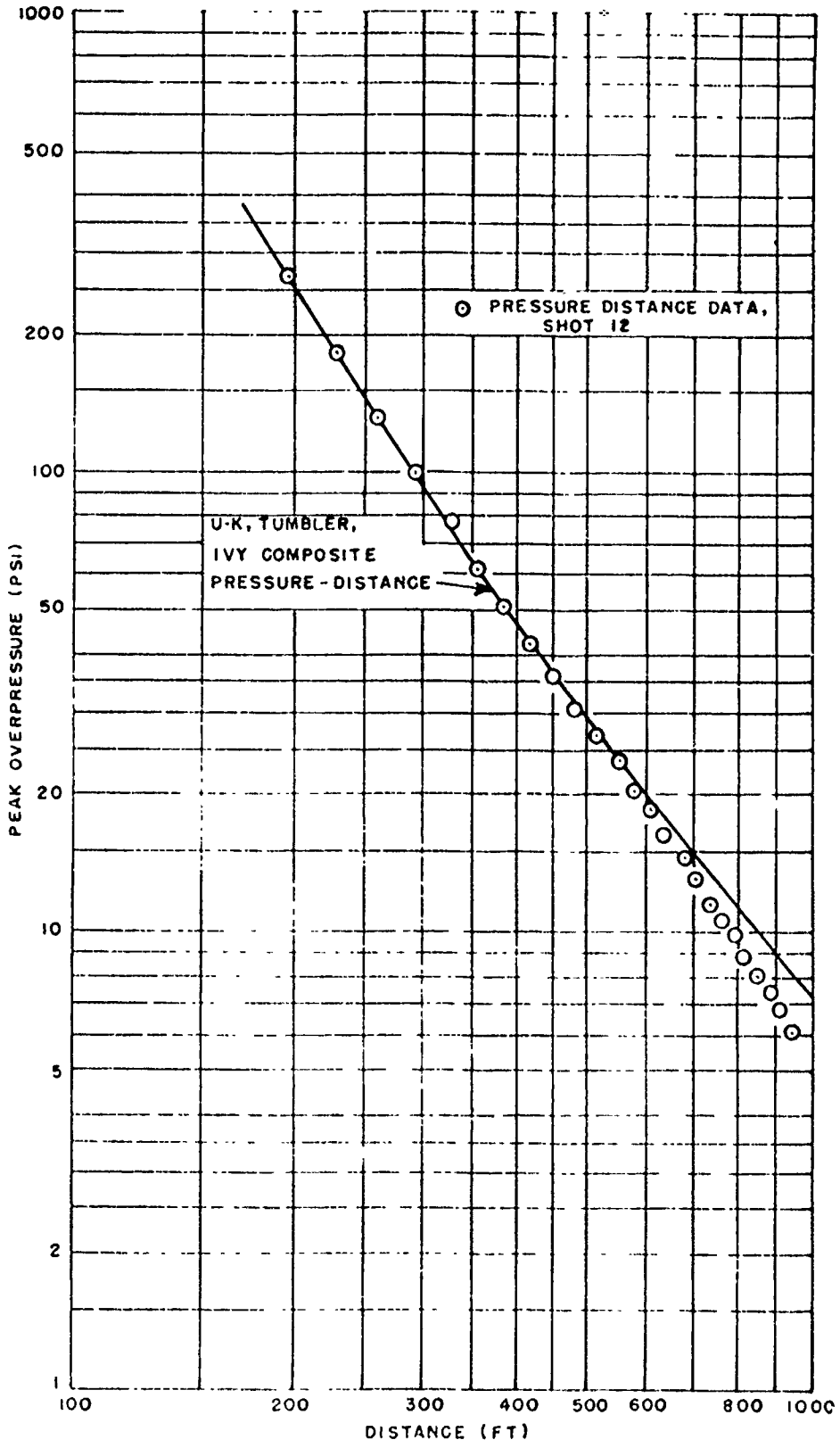

Figure 2.50 Peak overpressure above burst point compared to free air (A-scaled), Shot 12.

Although the Project 5.1 drone-telemetering instrumentation failed shortly after shock arrival and the oscillograph records were not complete, the reported measured-peak overpressures are shown in Figure 2.49. These peak overpressures were substantially greater than those obtained by extrapolation of the NOL results. However, the drone measurements were not grossly inconsistent with the predictions based upon the extrapolation of the composite free-air curve when the low yield of Shot 12 was considered. Further analysis has been unsuccessful in the attempt to reconcile the NOL and drone results of measured overpressures. It should be pointed out that one would be ill advised to attempt to correlate the drone-damage results with the peak overpressures extrapolated from the NOL measurements. Such a correlation would indicate excessive-lethal distances for free-air detonations. A more germane approach would be to use, meager though the data may be, the measured overpressures obtained by drone telemetering on Shot 12.

Chapter 3
NUCLEAR RADIATION

3.1 OBJECTIVES

The objectives of the projects in Program 2 were:

1. To obtain quantitative data on gamma and neutron exposures as a function of distance and to compare the measurements obtained on similar devices detonated under different ambient conditions (References 13 and 14).
2. To determine the degree of shielding protection afforded against gamma and neutrons by different types of field fortifications, above-and below-ground structures, and by earth cover (Reference 15).
3. To determine the relative hazard due to soft gamma and betas on contaminated objects within and without a residual-fission-radiation field (References 16 and 17).
4. To document thoroughly the mechanism by which the residual-radiation field results from an underground shot, i.e., by determination of isodose contours, dose rates as functions of time and distance (including crater and lip samples), the importance of the base surge as a contaminating mechanism, and the gamma-energy spectra of the residual field (References 13, 14, 18, 19, and 20).
5. To document the nature and extent of the neutron-induced field resulting from a low air burst, and further to correlate the measurements with predicted scale values (References 13, 14, 18, and 21).

For information on the extensive instrumentation and measurement techniques the reader is referred to the respective project reports.

3.2 INITIAL NUCLEAR RADIATION

3.2.1 High Altitude and Correlation Shots (Shots 9 and 10). Data for Shots 9 and 10 are presented and discussed in Chapter 5 of this report.

3.2.2 Thin High-Explosive Systems (Shots 1, 2, 5, 6, and 9). Table 3.1 presents data on the size and nuclear composition of these five shots together with yield, zero intercept, and mean-free paths of the gamma radiation. Figure 3.1 presents the gamma exposure in $r \times D^2$ versus D in yards. The curves in this figure have been normalized to an air density of 1 gram/liter. This gamma data has been corrected for neutron blackening of film dosimeters based on the gold-neutron data from Project 2.2 and the method developed by E. N. York. From this figure it can be noted that the slopes, i.e., e-fold distances, are approximately the same which indicates that the effective energies of the gamma spectra of these shots are similar. One further notes that when these normalized curves are reduced to 1 kt (W to the 1.0 scaling) the zero intercepts per kiloton vary with the type of device probably as one would expect.

The Shot 1 device is known to have detonated improperly, and a comparison of Shot 1 with Shot 6 has not been made since the inferences drawn would probably be erroneous.

3.2.3 Linear Implosion Systems (Shots 3 and 11). Four gamma-dosimeter lines were instrumented for Shots 3 and 11 to determine the asymmetry of linear-implosion devices. These lines were in directions:

1. Parallel to the long axis of the device.
2. At a 45-degree angle to the long axis of the device.
3. Perpendicular to the long axis of the device.
4. On a perpendicular line located midway between the Shot 3 and the Shot 11 towers (Figure 3.2). Table 3.1 and Figure 3.3 summarize the results of the measurements obtained on the

TABLE 3.1 DEVICE AND GAMMA DATA

Shot	Yield	Zero Intercept of rD^2 vs D Plot	Mean Free Path (1-gm/liter Air Density)	Zero Intercept Per Kiloton
	kt		yards	
1	1.2	2.3×10^9	415	1.9×10^9
2	2.5	3.0×10^9	420	1.2×10^9
3	7.0	1.8×10^{10}	370	2.7×10^9
5	3.6	8.3×10^9	385	2.3×10^9
6	8.1	2.6×10^{10}	390	3.3×10^9
9	3.1	1.3×10^{10}	345	4.2×10^9
11	1.53	6.0×10^9	350	3.6×10^9
12*	24.0	5.4×10^{10}	395	2.2×10^9

instrument line perpendicular to the line between the towers. The curves in Figure 3.3 of $r \times D^2$ versus D for these two shots compare favorably in having approximately the same mean-free paths and zero intercepts when scaled to 1 kt and are within the accuracy of the gamma instrumentation.

There seemed to be indications of an asymmetry of the gamma radiation on lines 1, 2, and 3 on Shot 11. However, the accuracy of the data was not sufficient to justify a positive statement. Shot 3 data was not usable since the dosimeters were located in a heavily contaminated fallout region.

3.2.4 Neutron Radiation (Shots 3 and 11). The results of the neutron measurements are presented in Table 3.2. The degree of asymmetry for the fast (sulfur) and thermal (gold) neutrons was clearly demonstrated on both shots.

3.2.5 Nuclear Radiation on MET Shot (Shot 12). Figure 3.4 presents the gamma exposure as rD^2 versus D. As described earlier, these data have been corrected for neutron blackening.

Table 3.2 and Figures 3.5 and 3.6 present the neutron data on this shot. It is important to observe that there were large numbers of neutrons whose energies were between thermal (gold) and fast (sulfur) neutrons.

3.2.6 Gamma Radiation (Shot 7). There were no data to present on the initial-gamma radiation resulting from the underground shot because of failure of the timing signal to operate the mechanism designed to drop the gamma-film dosimeters into a protective lead pig, subsequent to the initial-gamma exposure.

3.2.7 Shielding Studies (Gamma and Neutrons). Nuclear-shielding studies were conducted

(Text continued on Page 99)

TABLE 3.2 NEUTRON DATA

Shot	Zero Intercept of nvt × D^2 vs D Plot	E-Fold Distance	Zero Intercept Per Kiloton	Direction to Implosion Axis
		yards		degrees
Gold Neutrons				
1	1.1×10^{16}	295	9.2×10^{14}	—
2	5.0×10^{15}	220	2.5×10^{15}	—
3	8×10^{16}	260	1.14×10^{16}	90
	7×10^{16}	270	1×10^{16}	45
	6×10^{16}	270	8.6×10^{15}	0
5	1.3×10^{16}	250	3.6×10^{15}	—
6	5.0×10^{16}	260	6.2×10^{15}	—
9	2.0×10^{16}	230	6.0×10^{15}	—
11	2.2×10^{16}	210	1.4×10^{16}	90
	2.0×10^{16}	210	1.3×10^{16}	45
	1.5×10^{16}	210	0.98×10^{16}	0
12	1.0×10^{17}	190	4.3×10^{15}	—
Plutonium Neutrons (200 - ev threshold, 1 cm B)				
6	2.1×10^{20}	270	2.6×10^{19}	—
9	5.0×10^{19}	265	1.6×10^{19}	—
12	1.5×10^{20}	260	6.7×10^{19}	—
Plutonium Neutrons (4-kev threshold, 3 cm B)				
1	6.4×10^{18}	294	5.3×10^{18}	—
2	7.0×10^{18}	255	2.8×10^{18}	—
5	1.7×10^{19}	250	4.7×10^{18}	—
6	1.7×10^{20}	260	2.1×10^{19}	—
9	2.4×10^{19}	275	7.7×10^{18}	—
11	4.2×10^{19}	210	2.7×10^{19}	90
	3.2×10^{19}	210	2.1×10^{19}	0
12	1.3×10^{20}	260	5.4×10^{17}	—
Neptunium Neutrons (4-kev threshold)				
11	1.2×10^{19}	220	7.8×10^{19}	90
	1.0×10^{19}	220	6.5×10^{19}	0
Neptunium Neutrons (700-kev threshold)				
1	5.0×10^{18}	270	4.2×10^{18}	—
2	3.0×10^{18}	250	1.2×10^{18}	—
5	6.0×10^{18}	275	1.7×10^{18}	—
6	6.0×10^{19}	265	7.4×10^{18}	—
9	1.3×10^{19}	275	4.2×10^{19}	—
12	5.0×10^{19}	260	2.1×10^{18}	—
Uranium Neutrons (700-kev threshold)				
11	7×10^{18}	220	4.6×10^{18}	90
	5.9×10^{18}	220	3.9×10^{18}	0
Uranium Neutrons (1,500-kev threshold)				
1	1.6×10^{18}	294	1.3×10^{18}	—
2	1.6×10^{18}	260	6×10^{17}	—
5	6.0×10^{18}	250	1.7×10^{18}	—
6	3.4×10^{19}	265	4.2×10^{18}	—
9	7×10^{18}	275	2.3×10^{18}	—
12	2.0×10^{19}	250	8.4×10^{17}	—

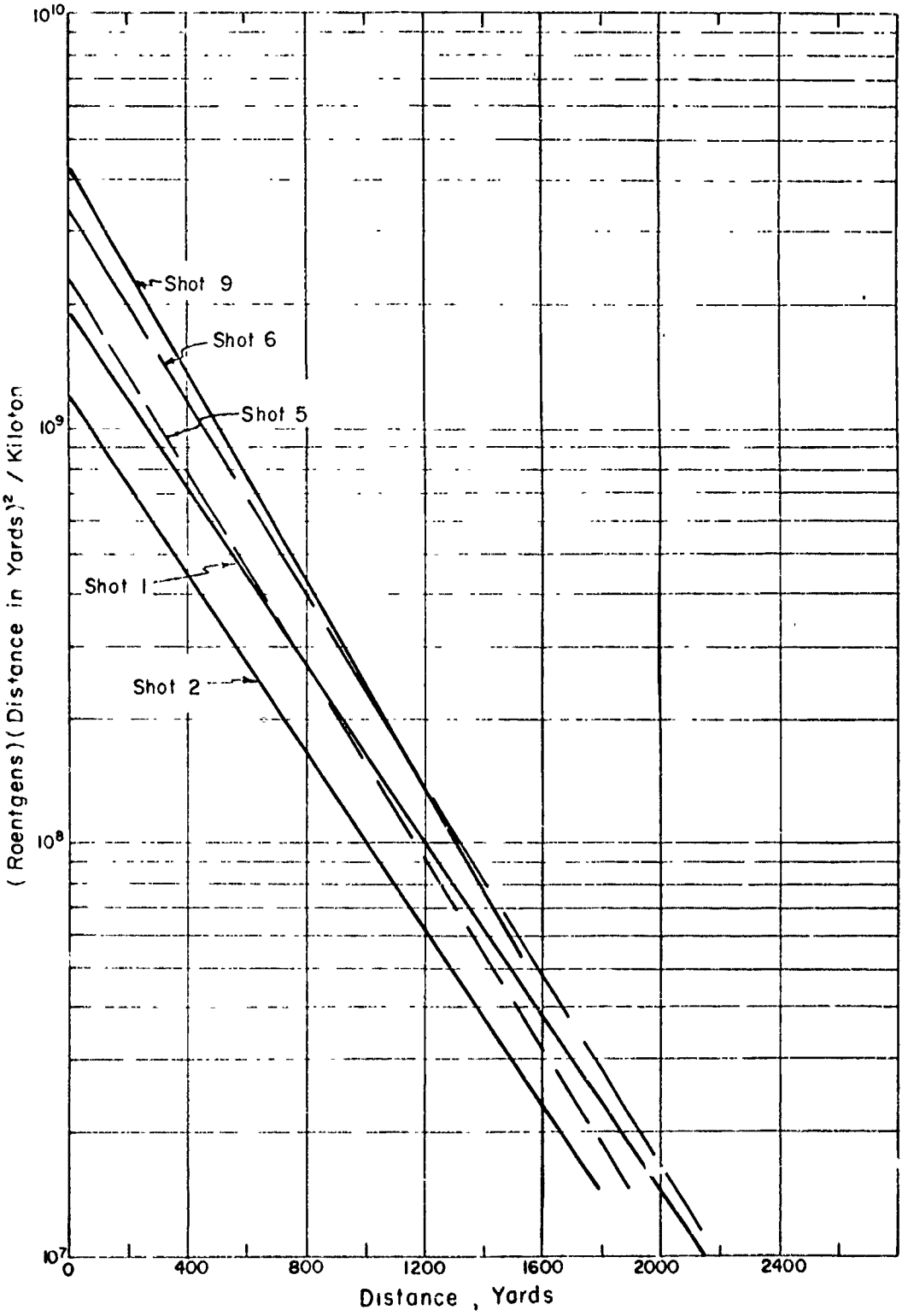

Figure 3.1 Gamma data, Shots 1, 2, 5, 6, and 9 normalized to an air density of 1 gm/liter and scaled to 1 kt.

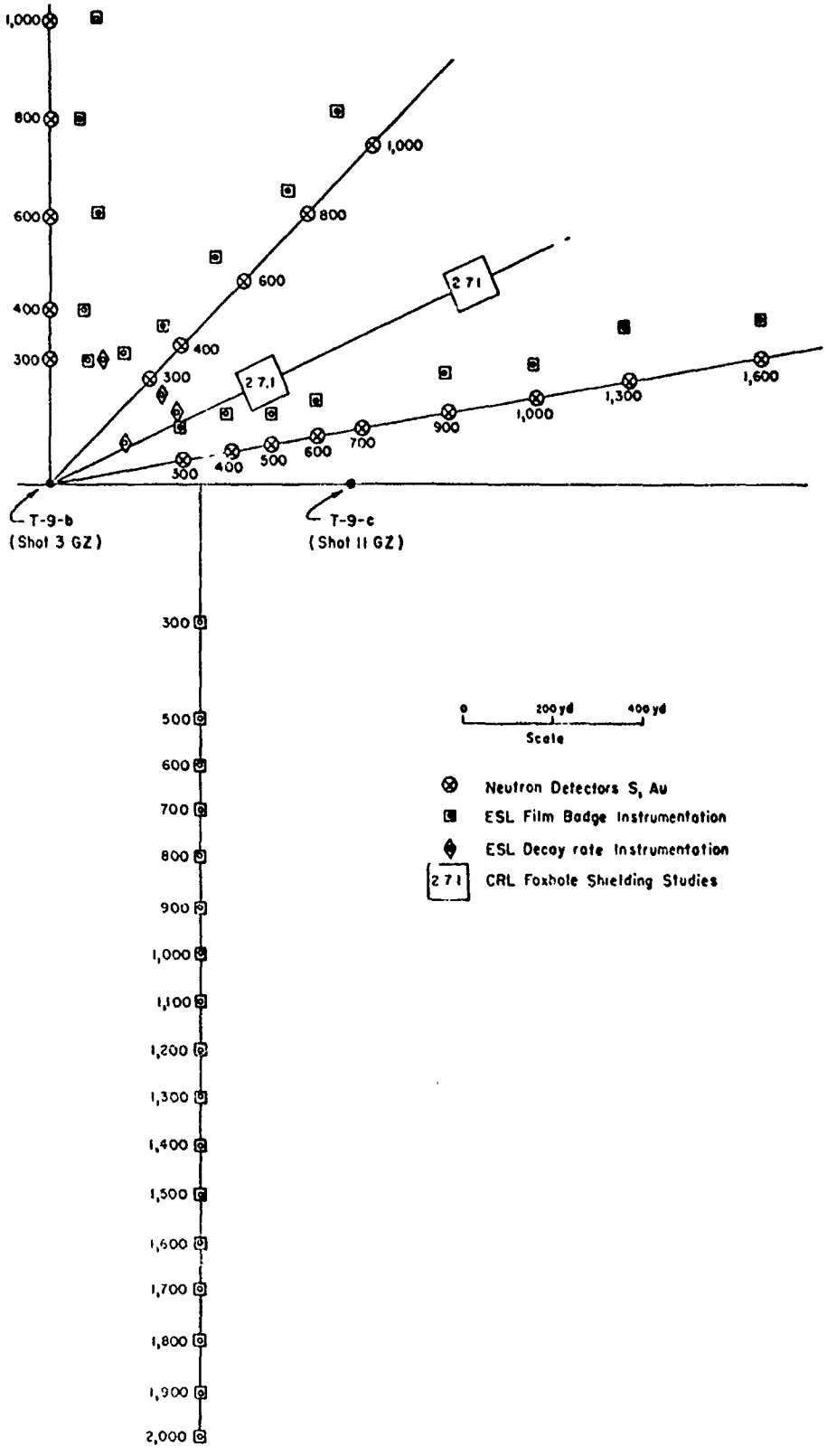

Figure 3.2 Instrument station layout.

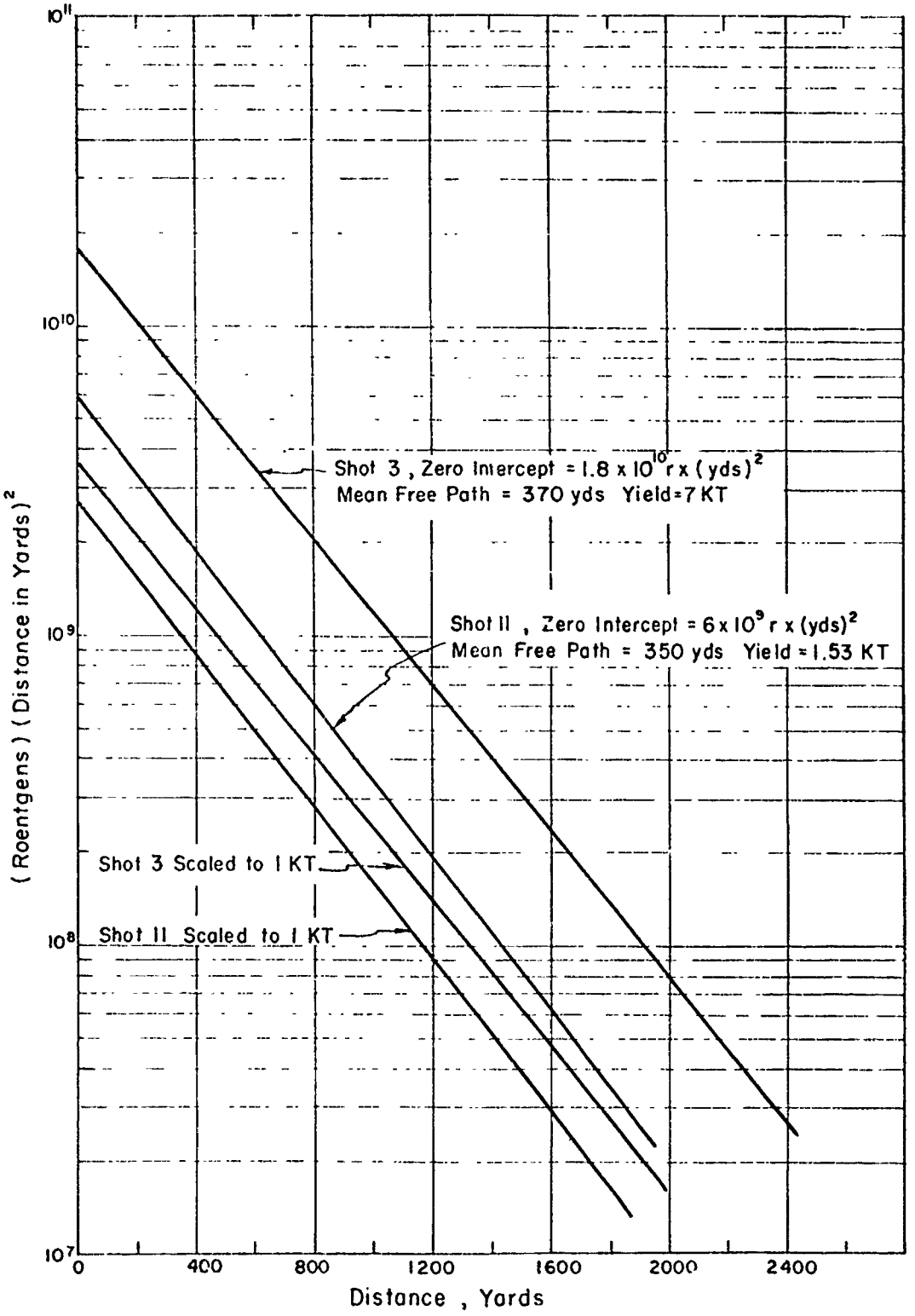

Figure 3.3 Gamma data, Shots 3 and 11 normalized to an air density of 1 gm/liter.

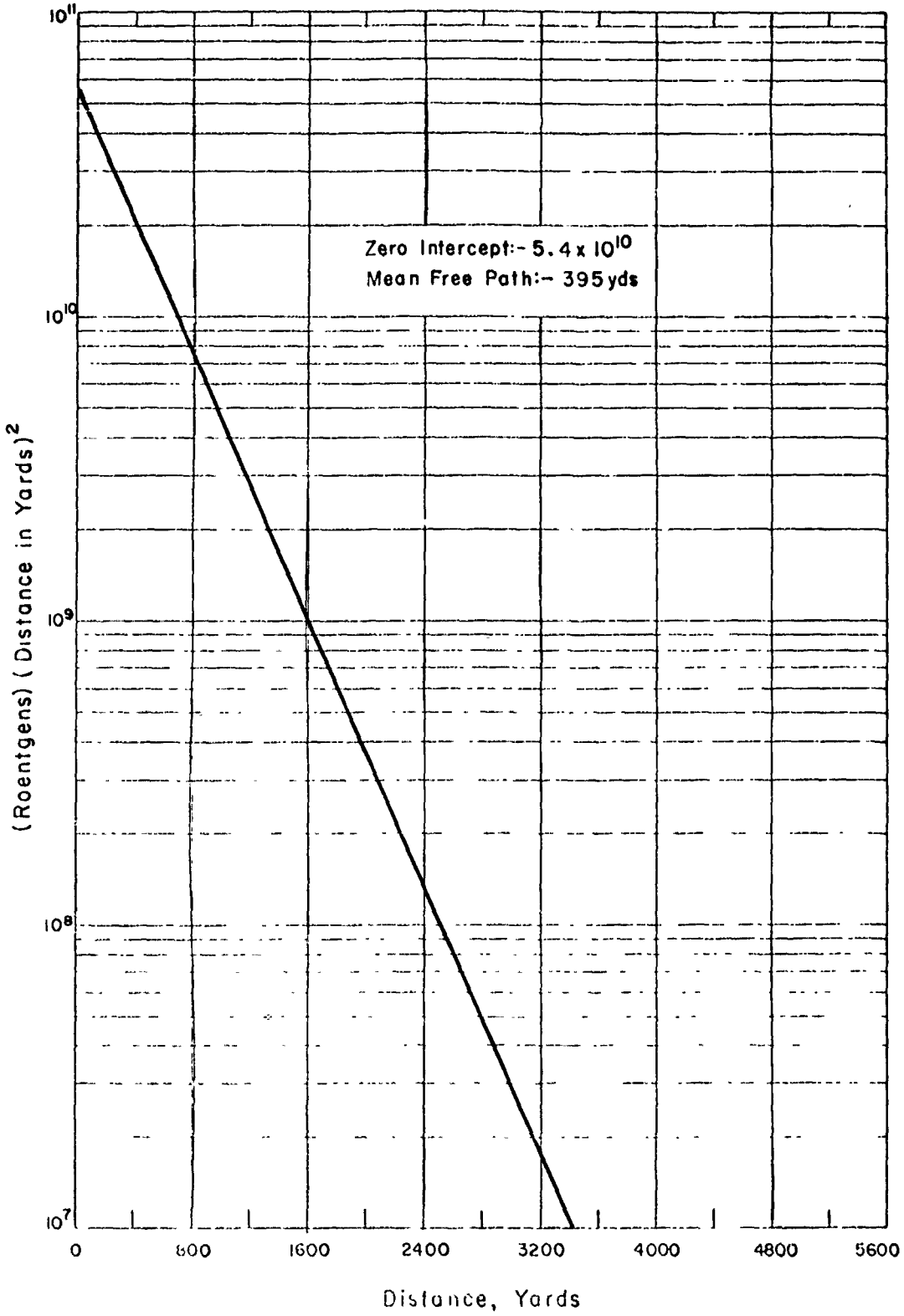

Figure 3.4 Gamma data, Shot 12 normalized to an air density of 1 gm/liter.

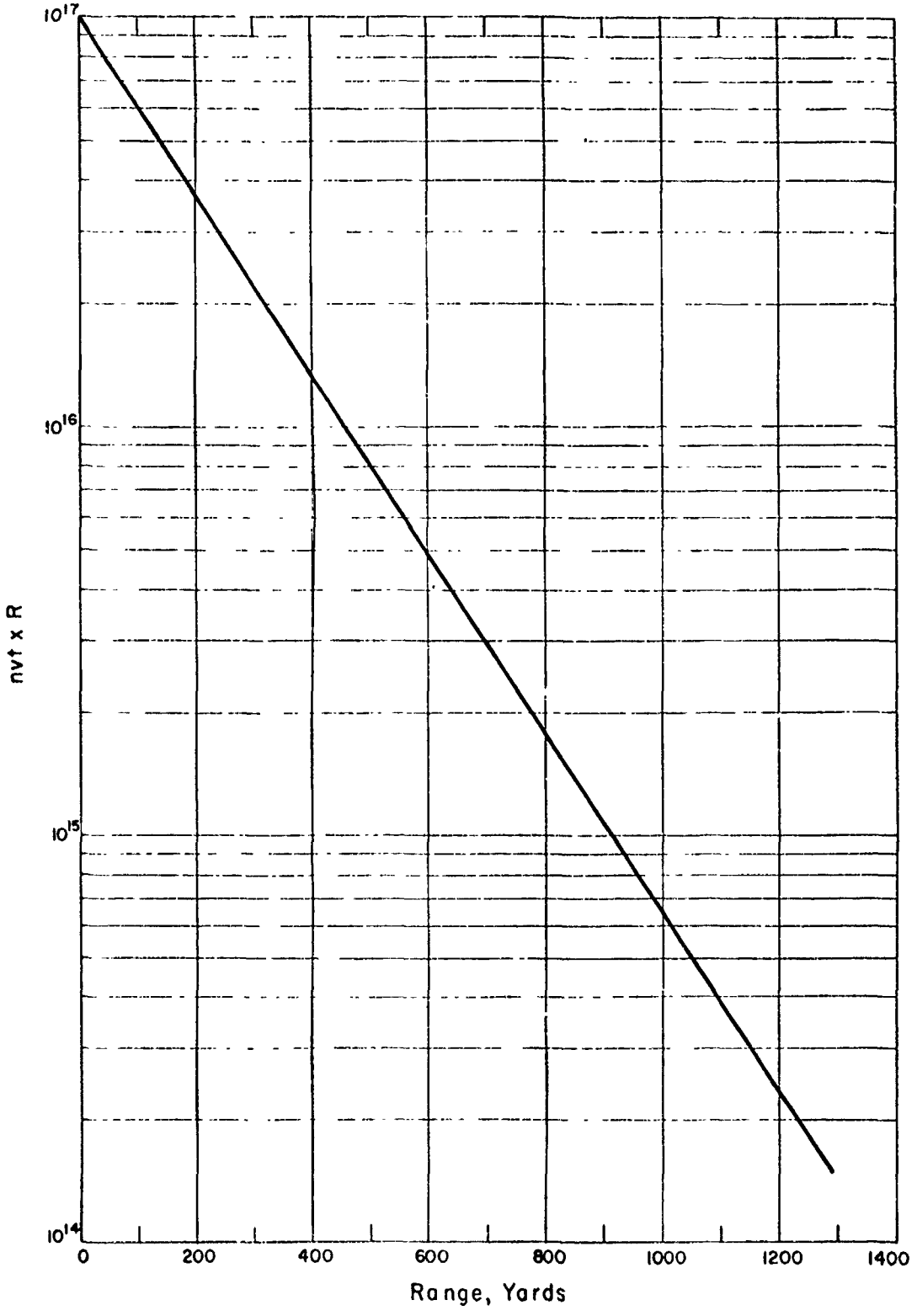

Figure 3.5 Neutron data, Shot 12, Au neutrons normalized to an air density of 1 gm/liter.

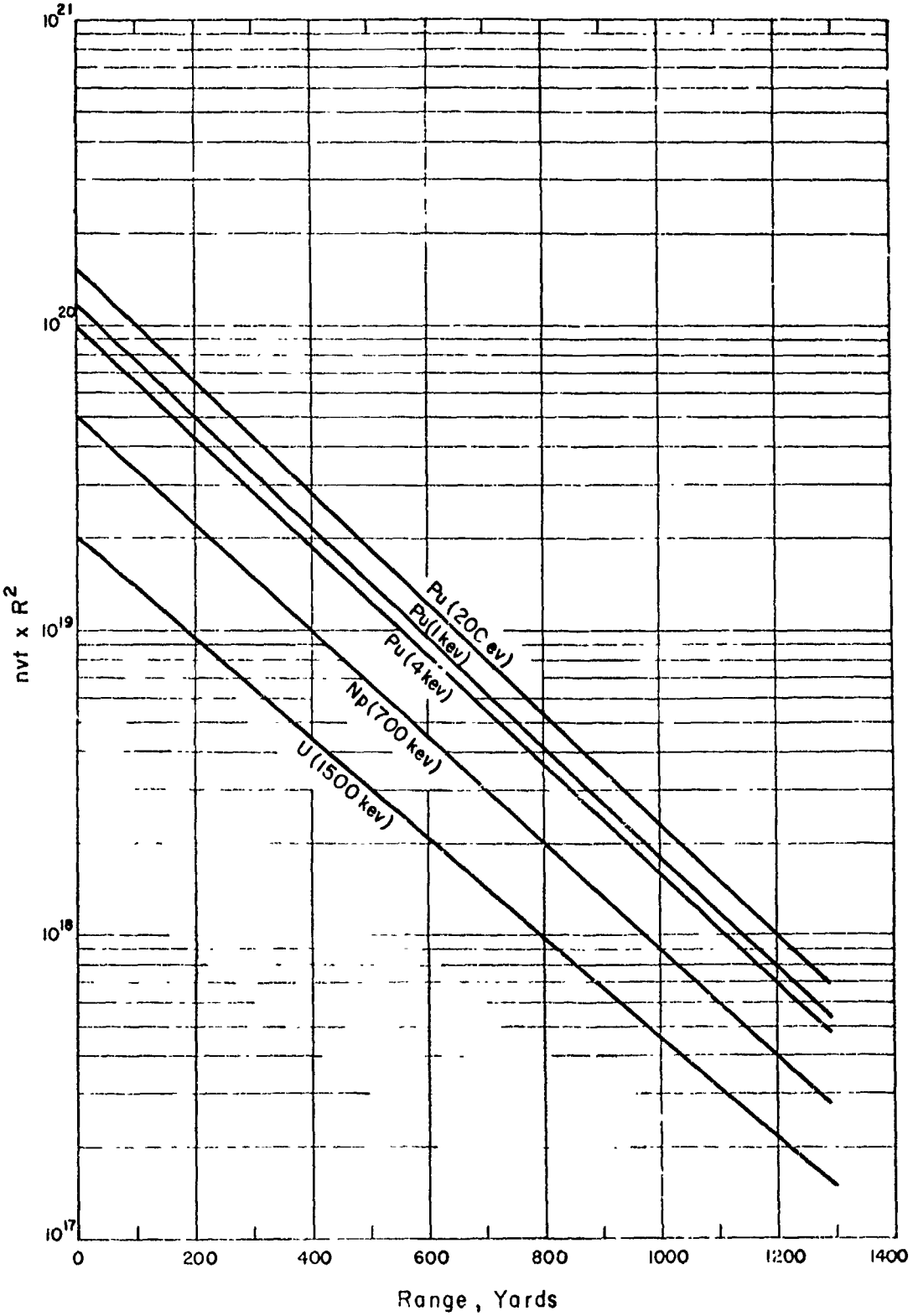

Figure 3.6 Neutron data, Shot 12, Pu, Np, U and S neutrons data normalized to an air density of 1 gm/liter.

by Project 2.7 on a variety of surface and underground structures (field fortifications, foxholes, vehicles, etc.,) on Shots 3, 7, 11, and 12, utilizing film badge and chemical dosimeters for measuring the gamma radiation and sulfur, gold, and fission detectors for measuring the neutron flux. This was a well-conducted experiment that obtained a wealth of informative data. The reader is referred to the project report for a complete presentation of these data. The significant results are discussed briefly in the following paragraphs.

The most important factor for providing shielding protection against gamma and neutrons is the thickness of the intervening material between the source and receiver. Figure 3.7 summarizes attenuation of the gamma and neutrons which can be obtained with various thicknesses of earth, over specific types of shelters.

Shielding factors for initial and residual gamma radiation for vehicles are presented in Table 3.3.

TABLE 3.3 AVERAGE VEHICLE ATTENUATION FACTORS

Type of Vehicle	Average Attenuation	
	Initial Gamma	Residual Gamma
Tank, M-48	0.1	0.2
Gun, T-97	0.6	0.4
Personnel Carriers AIV-M 59	0.7	0.6

It was also observed that baffling in the entranceways of field fortifications, underground shelters, etc., appreciably reduced the gamma and neutron hazards within these structures.

Gold-neutron detectors were wrapped with $\frac{1}{8}$- and $\frac{1}{2}$-inch thicknesses of lithium foil and these two readings compared with nonlithium-shielded-gold detectors. Good agreement was

TABLE 3.4 THERMAL NEUTRON SENSITIVITY OF GAMMA FILM

Type of Emulsions	Sensitivity
	10^{-10} r/(neutrons/cm^2)
Ho 548	1.71
606 (stabilized)	2.85
510	2.78
606	1.63
	Average: 2.24

noted between these readings and the theoretical absorption curve for neutrons under the $Li^7(n, \alpha)He^4$ reaction with cross section of 67 barns. The neutron blackening for several gamma-film emulsions was then evaluated in a similar manner by placing $\frac{1}{8}$- and $\frac{1}{2}$-inch lithium foils between the source and gamma dosimeters and comparing these readings with the nonshielded-gamma-film dosimeters. From these data the film-dosimeter sensitivities to slow neutrons were computed. Table 3.4 summarizes these results, from which an average sensitivity of 2.24×10^{-10} r/(neutrons/cm^2) was obtained.

3.3 RESIDUAL NUCLEAR RADIATION

3.3.1 Underground Shot (Shot 7). Shot 7 was a nuclear device similar to the Operation Buster-Jangle surface and underground devices and was detonated at a depth of 67 feet below the surface. The significant results obtained by Program 2 projects that participated on this shot are briefly summarized in the following paragraphs.

1. Instrument Station Locations: The locations of the nuclear instrumentation on Shot 7

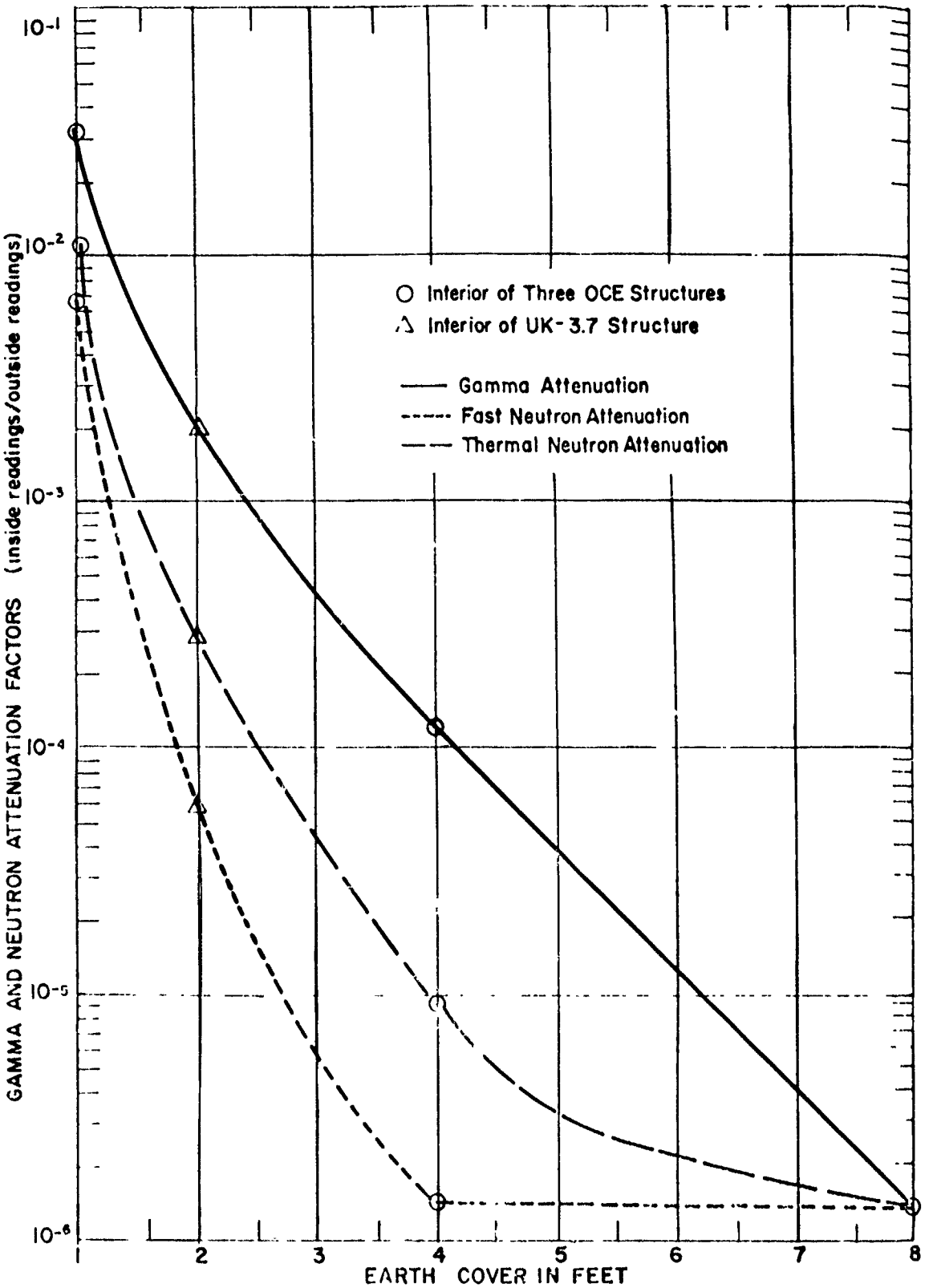

Figure 3.7 Gamma and neutron attenuation factors versus earth cover, Shot 12, 300 yards from ground zero. Outside gamma exposure, 307,000 r; outside thermal neutron flux, 6×10^{13} n/cm^2, outside fast neutron flux, 1.3×10^{13} n/cm^2.

are shown in Figure 3.8. The material and radioactive fallout were documented by sampling of the ground stations which had been deployed to include the major portion of the expected-fallout-residual field. The types of instrumentation used to collect data at these stations are detailed in Table 3.5.

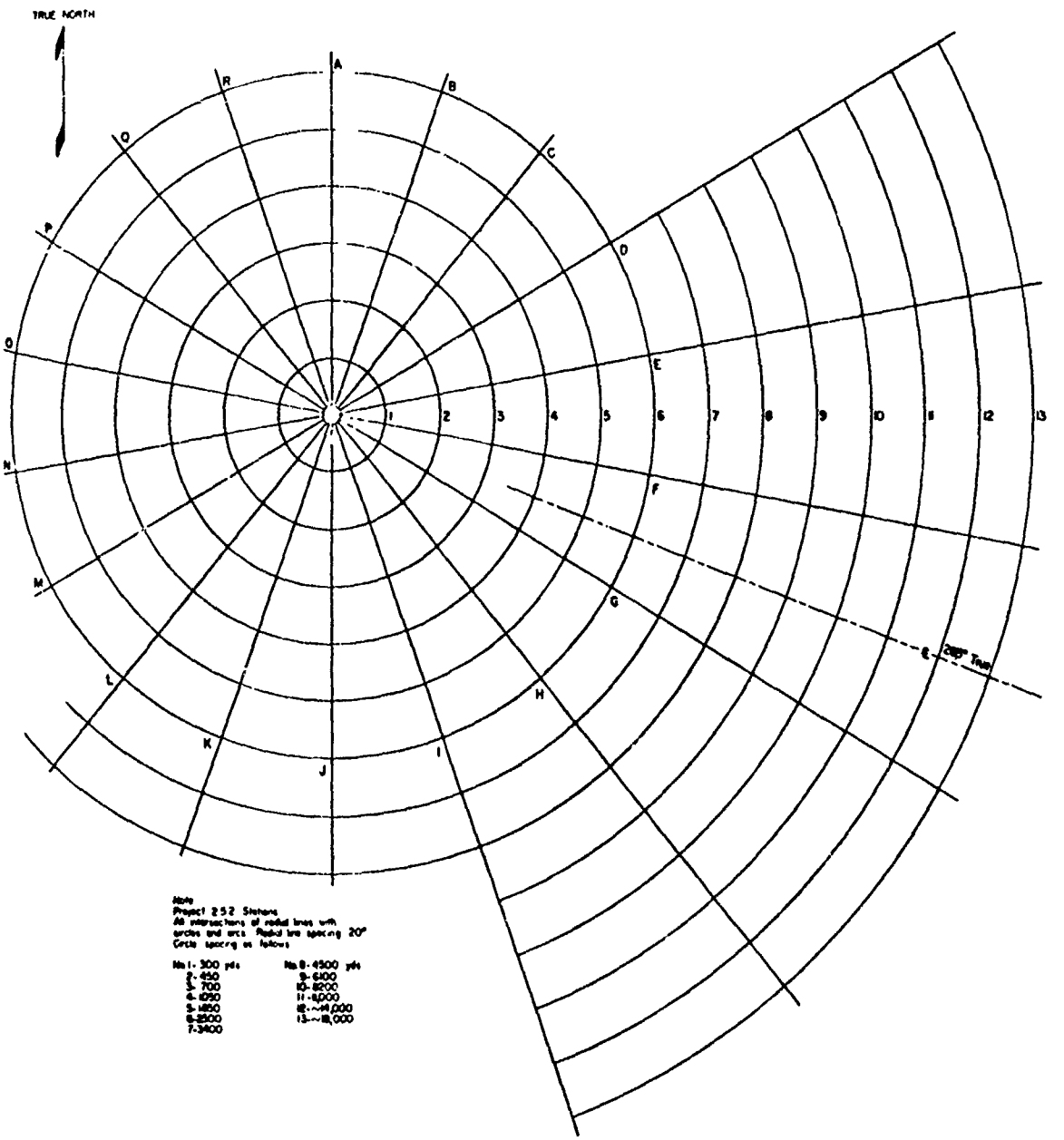

Figure 3.8 Residual radiation instrument station locations, Shot 7.

2. Project 2.5.1 (Army Chemical Center) and Project 2.5.2 (Naval Radiological Defense Laboratory) collected sufficient data which provided a measure of the total mass and total-radioactive mass deposited by the fallout process. The following observations were made concerning the degree of success of this effort: the sampling devices functioned satisfactorily; the station array appeared to have given adequate cover of the fallout pattern; and the weather con-

ditions during the preparatory and the recovery phases were satisfactory.

The weight of the fallout material collected by the total fallout collectors at various times is presented in Table 3.6.

3. Several thousand ground- and aerial-survey readings were taken during the three-week period following the shot at all stations listed in the instrument station-locator chart and extending in a downwind direction to approximately 25 miles. Figures 3.9, 3.10, and 3.11 show the observed gamma-dose-rate-field contours in r/hr computed as H + 1 hour using the $t^{-1.2}$ approximation. The contours listed in Table 3.7 show the area inside the 3,000 r/hr contour to be approximately 30 percent greater than that predicted by existing scaling methods, while the

TABLE 3.5 SHOT 7 INSTRUMENTATION DATA

Instruments	Positions
Total Fallout Collectors	All Stations
Incremental Collectors	F-3, 5, 8, 11
Particle Collectors	All Stations
Multiple Array of Total Collectors	F-5, 8, 11
Duplicate Fallout Stations with Soil Sampling	D-5; E-3, 5, 8, 11, 13; F-3, 5, 8, 11, 13; G-3, 5, 8, 11, 13; H-5; O-3, 4, 5
Radiac Readings	All Stations
Film Badges	All Stations
Gamma Dose Rate vs Time	
Scintillation Detectors	E-1, 3, 5, 7, 8, 9; G-1, 3, 7, 8, 9; L-3; O-3
Ion Chambers	E-8, 9; L-5; O-5; G-7
Cadmium Sulfide Detector	E-1

area enclosed by the 100 r/hr contour is approximately 20 percent greater than predicted.

4. Total Amount of Radioactivity: The areas in square miles enclosed by the various dose-rate contours of Figures 3.9, 3.10, and 3.11 have been obtained by using planimeter integration of the area. Table 3.7 presents the area in square miles enclosed by several representative isointensity lines and a comparison of these areas with predictions based on TM 23-200, 1954, (Reference 22).

Analysis of the data accounts for approximately 85 percent of the total radioactivity produced by the 1.2 kt detonation within the $\frac{1}{10}$-r/hr contour.

5. Activity Decay Rates: The rate of decay of the residual activity was documented at 42 different stations and the values obtained plotted on log-log paper as dose rate versus time. The values of the decay exponent ranged from -0.70 to -1.48 with an average value of -1.18. There is clear evidence to show that the large variations from the average of -1.18 were due to redistribution of the ground activities by wind. The decay rates were followed in most cases for a period of approximately 50 days. The close agreement between the exponent of -1.18 and the value of -1.2, determined by laboratory decay measures of fission product activities, indicated that the relative amount of neutron-induced activities was small. This statement is also further confirmed by the residual gamma-spectra measurements (see following paragraph).

6. Crater and Lip Samples: Core sampling of 16 points on the crater lip showed that the

TABLE 3.6 WEIGHT AND ACTIVITY CONCENTRATION OF TOTAL FALLOUT

Station Location	Weight Collected	Surface Area of Total Collector	Total Sample Activity Corrected to H + 1 Hour	Activity Concentration Corrected to H + 1 Hour	
	gram	ft^2	10^{15} dis/min	10^{15}(dis/min)/gm	mc/gm
G-1	251.1	0.60	430.99	1.72	7.7
G-3	159.6	0.60	359.34	2.25	10.1
G-5	42.6	0.60	296.17	6.95	31.3
G-7	24.1	2.64	46.40*	8.80*	39.7
G-8	Negative	0.60	—	—	—
L-3	30.0	0.60	94.86	3.17	14.2
L-5	Negative	0.60	—	—	—
L-7	Negative	2.64	—	—	—
E-5	3.3	0.60	†	—	25.8
E-7	Negative	2.64	—	—	—
E-8	Negative	0.60	—	—	—
F-7	1.0	2.64	†	—	27.5
F-8	Negative	0.60	—	—	—
F-11	Negative	0.60	—	—	—
H-7	0.7	2.64	†	—	14.9

* G-7 activity concentration has been corrected for collector surface area to put the activity concentration on a comparative basis with other stations, i.e., total collector activity was multiplied by the ratio 0.60/2.64.

† Only a portion of the total sample collected was recovered; therefore, total sample activity could not be determined.

TABLE 3.7 AREAS ENCLOSED BY DOSE RATE CONTOURS OF SHOT 7 COMPARED WITH PREDICTED AREAS FROM TM 23-200*

Dose-Rate Contour at H + 1 Hour	Shot 7 Contour Areas		Ratio: Actual to Predicted
	Field Measurements	TM 23-200 Predictions	
r/hr	mi^2	mi^2	
3,000	0.070	0.052	1.3
1,000	0.261	0.135	1.9
300	0.78	0.49	1.6
100	1.41	1.21	1.2
30	3.2	3.38	0.95

* Capabilities of Atomic Weapons, TM 23-200, December 1954, Armed Forces Special Weapons Project, Washington, D. C., Secret Restricted Data.

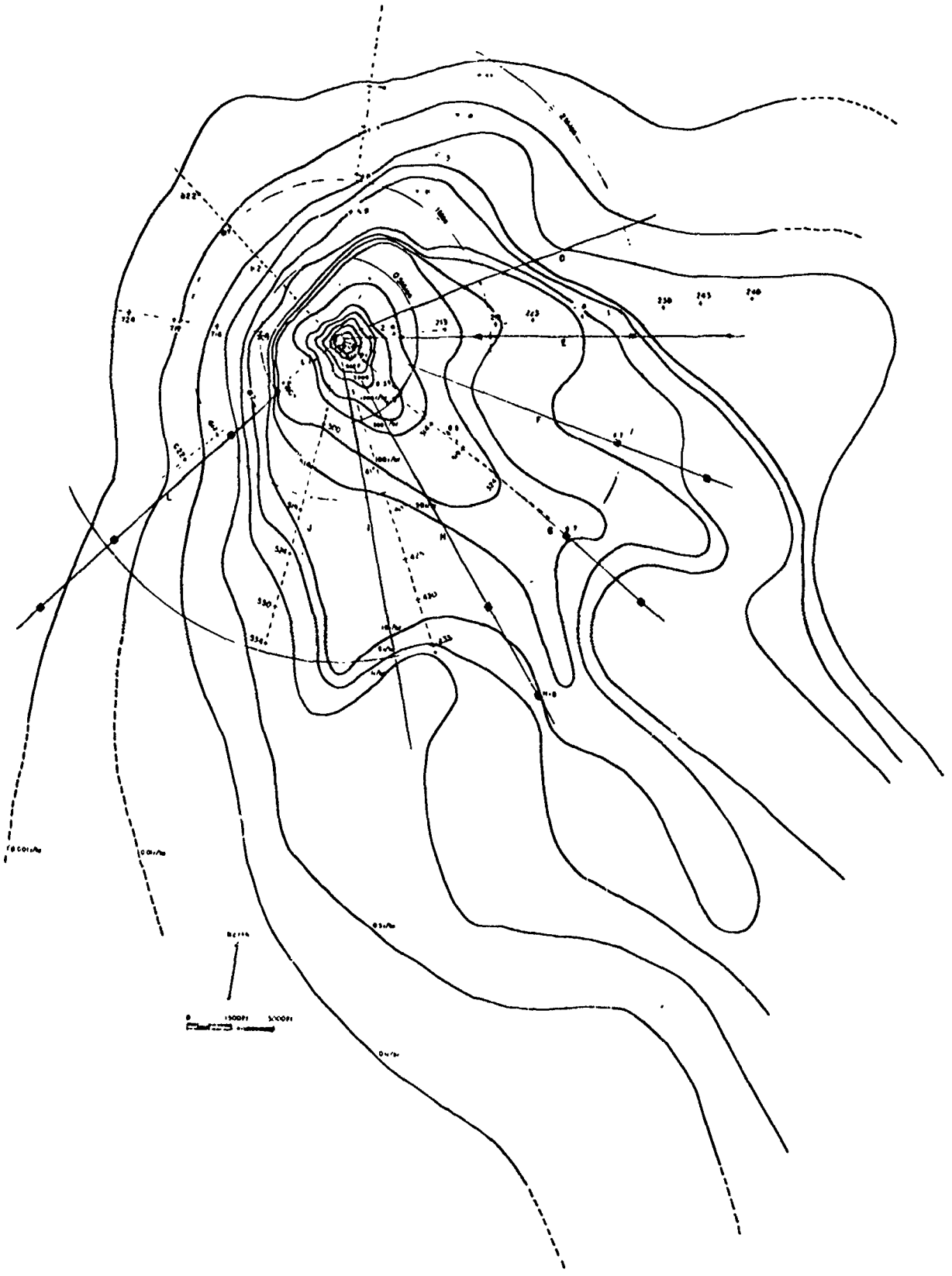

Figure 3.9 Dose-rate contours at H + 1 hour, 10-r/hr line closed.

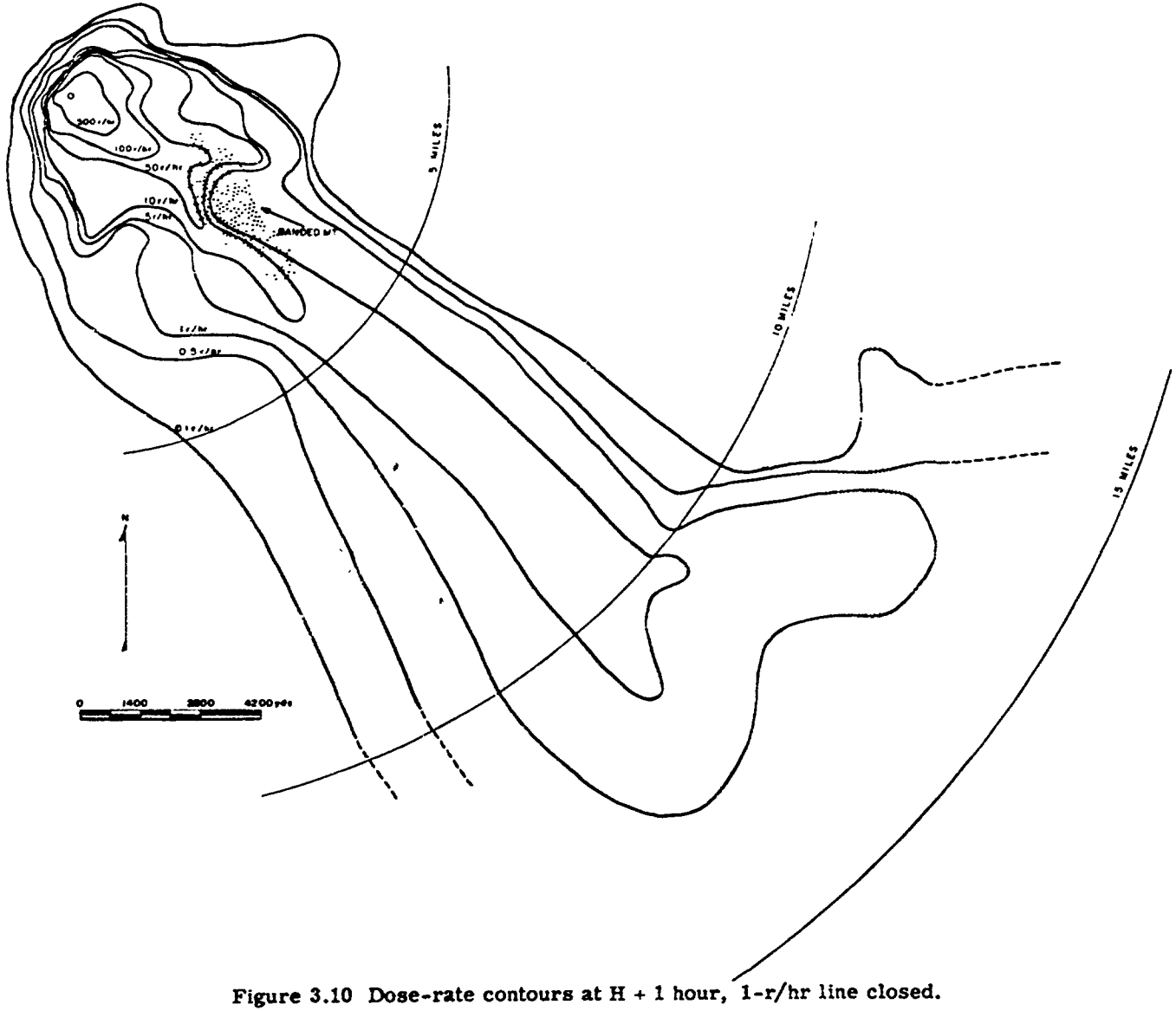

Figure 3.10 Dose-rate contours at H + 1 hour, 1-r/hr line closed.

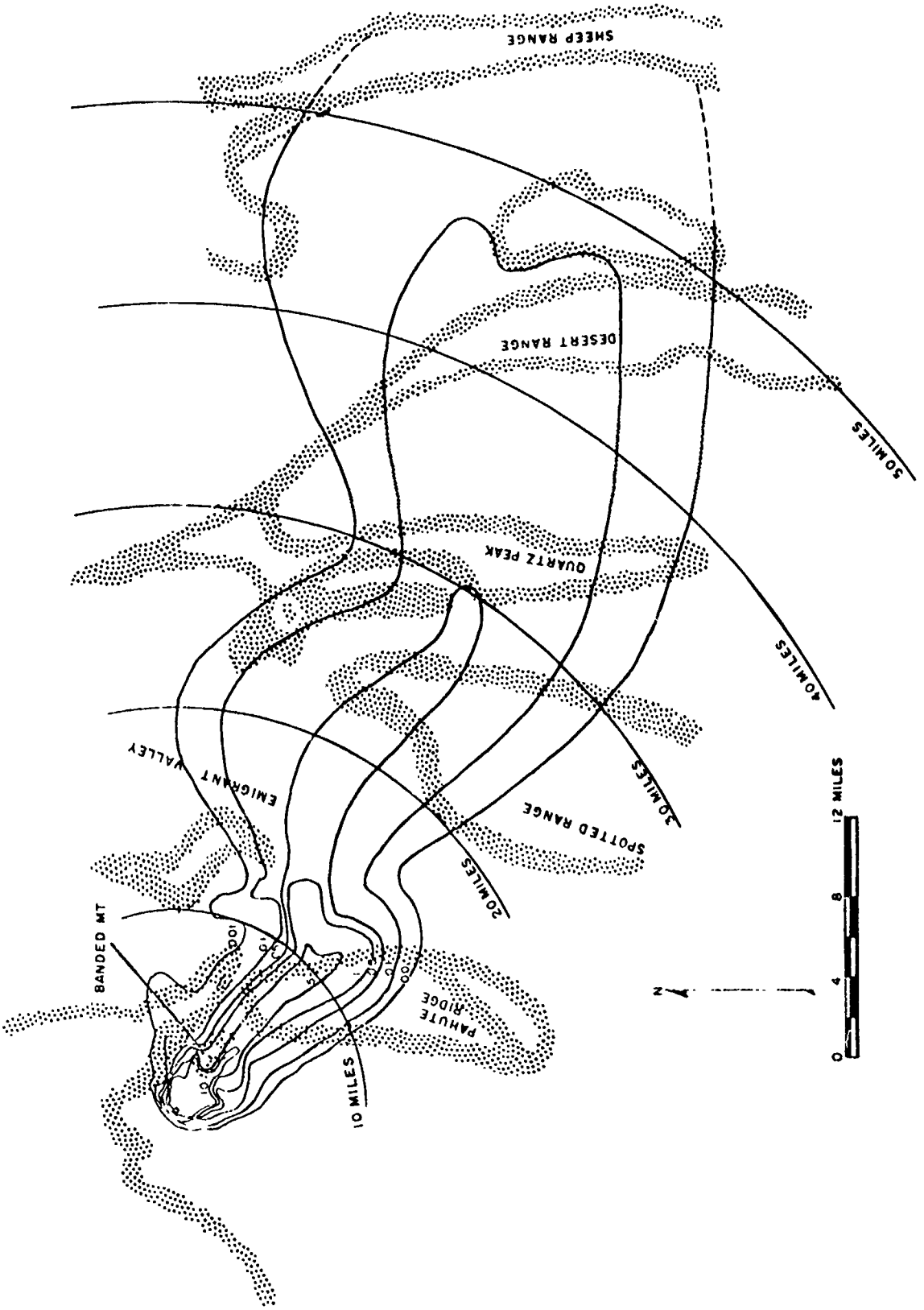

Figure 3.11 Dose-rate contours at H + 1 hour, 0.1-r/hr line closed.

activity was concentrated near the surface with approximately 90 percent contained in the first 12 inches of depth. Intensity measurements on the lip and just inside of the crater at H + 2 hours indicated a dose rate of 6,000 r/hr computed as of H + 1 hour. Later measurements extrapolated to this same value. The intensities increased as the distance increased from the crater on all sides out to at least 150 feet, indicating the spill over of the crater material.

7. Base Surge: An analysis of the time-of-arrival data, technical photography, and other available data definitely indicated that the base surge was a contaminating mechanism (Figure 3.12).

8. Residual Gamma Spectra: The residual-gamma spectra as a function of distance and time were measured in the field by Project 2.3, Naval Radiological Defense Laboratory (NRDL), (Reference 18), utilizing a vehicle-mounted spectrometer on which a nearly total-absorption sodium-iodide-thallium-activated crystal was used, together with a pulse-height analyzer. From

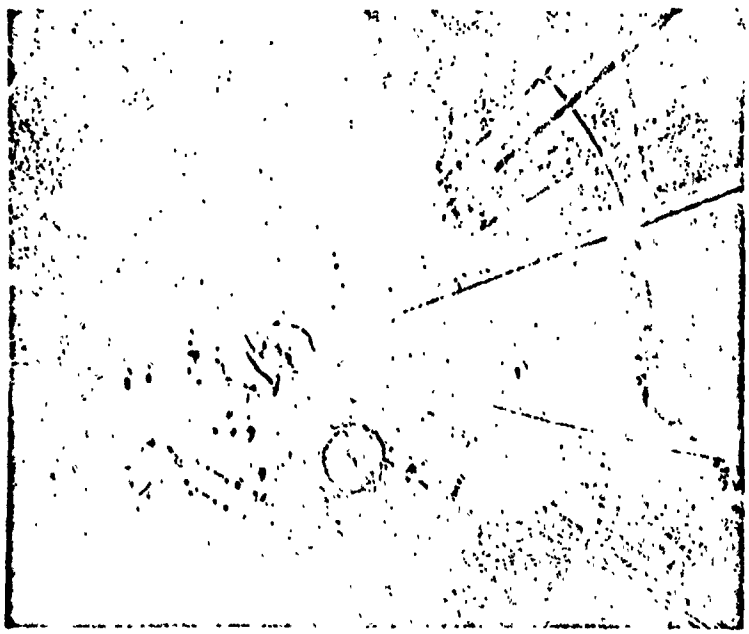

Figure 3.12 Fallout area.

the data obtained, it was concluded that the relative quantities of observed neutron-induced activity to fission-product fallout activity are functions of height, yield, and type of detonation. While only Na^{24} and Mn^{56} induced activities could be definitely found in significant quantities in all soil samples tested, the relative amounts of these two radioisotopes varied over a considerable range, and within reasonable accuracy, were activated in proportion to the amount of sodium and manganese atoms present in the soil samples exposed.

3.3.2 Neutron-Induced Activities, Air Bursts (Shots 1 and 9). One of the objectives of Project 2.3 was to measure the gamma spectra of neutron-induced activities on Shots 1 and 9. Also, one of the objectives of Project 2.4 was to measure the gamma-dose rate as a function of time and distance on these air-burst shots. The significant results obtained by these two projects are summarized in the following paragraph.

The principal neutron-induced activities in the Nevada-type soil are Na^{24} and Mn^{56} with half lives of 14.9 hours and 2.59 hours, respectively. The activities measured on these two shots contained no observable fission-product activity. Project 2.3 had gamma dose-rate instruments positioned at close-in distances in an equilateral triangle about the expected ground zero.

TABLE 3.8 PREDICTED AND OBSERVED INTENSITIES FOR SHOTS 1 AND 9

Shot	Station	Azimuth	Slant Range	Predicted	Observed
		degrees	ft	r/hr	r/hr
1	I	215	1,515	3.6	16.5
1	II	—	—	—	Recorder failed
1	III	95	2,070	0.54	0.45
9	I	335	1,580	7.1	6.1
9	II	215	1,715	4.6	3.5
9	III	95	1,715	4.6	2.5

TABLE 3.9 AVERAGE RATIOS BETWEEN THE DOSE RATE READINGS OF VARIOUS METHODS COMPARED TO THE T1B

Aircraft Components	Juno/T1B	Ion Chamber/T1B	Film Max/ T1B	Film Av/T1B
Air Intake (Rim)	15	96	290	77
Forward Gun Deck	6	22	165	23
Dive Brake Plate	5	19	93	11
Wing Root (Leading Edge)	6	28	110	19
Wing Center (Leading Edge)	15	97	520	172
Wing Tip (Leading Edge)	14	90	554	95
Gas Cap (Outboard Wing)	10	34	65	—
Gas Cap (Tip Tank)	15	40	240	21
Wing Surface (Top center)	7	22	243	19
Wing Surface (Bottom center)	9	22	156	13
Wing Flaps (Inboard)	4	12	40	4
Wing Flaps (Outboard)	6	21	64	—
Rudder Access Door	3	14	68	11
Front of Canopy	10	36	80	19
Grand Averages	9	39	192	40

Table 3.8 summarizes the predicted and observed intensities for these shots. The predicted values are based on Figure 26, Capabilities of Atomic Weapons, revised 1 December 1954, (Reference 22), using the high-neutron-flux weapons curve.

3.3.3 Contact-Radiation Hazard Associated with Contaminated Aircraft. The contact-radiation hazard involved in the decontamination of aircraft that have flown through atomic clouds was investigated. Surface-dose rates were measured with special instrumentation, i.e., a small volume, thin-window ionization chamber dose-rate meter, and photographic film. Surveys were made of the same contaminated areas employing radiological survey instruments: T1B's, Juno's and PDR-27C's. Ratios of dose rates obtained using several of the instruments indicated above to the dose-rate measured using a T1B, placed adjacent to various contaminated aircraft components, are indicated in Table 3.9. The average ratios were compiled from measurements on the identical aircraft component for 17 aircraft. The ratio Film Max/T1B is for the spot on the film emulsion giving the highest reading while Film Av/T1B is for the average reading over the surface of the film. While the contamination collected on aircraft components was far from uniform, the ratio of dosage to be expected by contact with these components to T1B dosages taken at these components was roughly 90 for the direct-impingement surface and 40 for other contaminated surfaces. Biological significance of these higher-physical measurements appears to warrant further study.

3.3.4 Beta and Soft Gamma Hazard. The presence of soft components in the radiation fields resulting from Shots 4, 7, and 8 was strongly indicative of beta radiation. These soft components gave a surface dose, in many cases, 20 times the average-internal dose for a man lying prone. Although the internal doses recorded agreed favorably with radiac equipment readings, the surface dose was significantly greater and it can be concluded that a fallout field delivers a large dose of absorbed energy, which is not usually measured, to the body.

Chapter 4
THERMAL MEASUREMENTS and EFFECTS

4.1 OBJECTIVES

The basic objectives of the thermal measurements and effects program of Operation Teapot were:

1. To determine the basic-thermal characteristics of a nuclear device detonated at an altitude of approximately 40,000 feet MSL and of an identical device detonated at an altitude of approximately 800 feet MSL.
2. To determine the thermal characteristics of other nuclear detonations for the verification and extension of existing thermal-radiation-scaling relationships.
3. To study the contribution of thermal radiation reflected from the earth's surface to the total-thermal energy received by aircraft in flight.
4. To provide a field test of theoretical and experimental studies on thermal-attenuating-smoke screens.
5. To furnish basic measurements of thermal-radiation phenomena required in support of other programs as follows: (1) the mechanisms of formation of heated layers conducive to precursor formation; (2) the thermal energy received by drone aircraft and aircraft components; (3) the thermal energy received by aircraft in flight as a function of the geometry of the aircraft, detonation point, and reflecting surface; and (4) the thermal radiation received outside of the attenuating smoke screens.

Information obtained by the thermal measurements and effects program is conveniently presented under the following broad topics: (1) thermal measurements for the high-altitude detonation, Shot 10, and correlation event, Shot 9; (2) thermal measurements for devices having yields between 1 and 10 kt, of particular importance for thermal-scaling purposes, were those measurements for devices having mass-to-yield ratios of less than[illegible] (3) thermal measurements from aircraft and drones; (4) thermal radiation-attenuating cloud studies; and (5) thermal and air-temperature measurements performed on the military-effects tower shot.

The extensive measurements program proposed for Operation Teapot is summarized in Table 4.1, which indicates the measurements made or attempted, instruments used, and project performing the measurement for each Operation Teapot shot. An indication is given where the measurements were only partially successful or failed to produce adequate data.

4.2 SUMMARY OF DATA FROM SHOTS 9 AND 10

Data are summarized in Table 4.2 which gives total radiant energy received at various ground stations and at the delivery aircraft, various characteristics of the thermal pulses, atmospheric transmissivities, and yields for the correlation shot, Shot 9, and the high-altitude experiment, Shot 10. Pulse-shape data for these two devices obtained from bolometer measurements by NRDL are presented in Figures 4.1 and 4.2 and from bolometer measurements by Naval Research Laboratory (NRL) in Figures 4.3 and 4.4.

The data given in Table 4.2 is discussed further in Chapter 5 of this report. Spectral data is also discussed in that chapter because of the importance of this data to an understanding of the

TABLE 4.1 SUMMARY OF THERMAL-RADIATION MEASUREMENTS BY PROJECT

Measurement	Project Performing Measurement											
	1	2	3	4	5	6	8	9	10	11	12	13
Total radiant energy from a distance, cal/cm²												
NRDL MK6F calorimeters:												
90° field of view	8.4	8.4	8.4	—	8.4	8.4	8.4	8.4	—	—	5.1,5.5	—
180°, 45°, 22°, 11° fields of view	8.4	8.4	8.4	—	8.4	8.4	8.4	8.4	—	—	—	—
180° field of view under smoke	—	—	—	—	8.3	—	—	—	—	—	—	—
180° field of view under smoke goniometric measurements	—	—	—	—	8.3	—	—	—	—	—	—	—
90° field of view under smoke	—	—	—	—	8.3	—	—	—	—	—	—	—
Minneapolis-Honeywell thermopiles, 90° field of view	—	—	—	—	—	—	—	—	8.4	—	—	—
NRDL MK7F calorimeters, 90° field of view	—	—	—	—	—	—	—	—	8.4	—	—	—
NRDL MK8F calorimeters												
90° field of view	—	—	—	—	—	—	—	—	—	—	8.4,5.4*	—
180°, 45°, 22°, 11° fields of view	—	—	—	—	—	—	—	—	—	—	8.4*	—
CRL thermistor calorimeter, 180° field of view	—	—	—	—	8.3	—	—	—	—	—	—	—
Radiant energy in broad spectral bands using Corning Filters, cal/cm²												
NRDL MK6F calorimeters, 90° field of view	8.4	8.4	8.4	—	8.4	—	—	8.4	—	—	—	—
NRDL MK7F calorimeters, 90° field of view	—	—	—	—	—	—	—	—	8.4	—	—	—
Minneapolis-Honeywell thermopiles	—	—	—	—	—	—	—	—	8.4	—	—	—
NRDL MK6F calorimeters under smoke	—	—	—	—	8.3	—	—	—	—	—	—	—
Total irradiance, cal/cm²-sec												
NRDL MK6F radiometer	8.4	8.4	8.4	—	8.4	8.4	8.4	8.4	—	—	8.4,5.1, 5.4,5.5	—
Total thermal radiant power(cal/sec) versus time with high time resolution (50 microsec) NRL type bolometers	8.4	8.4	—	8.4	8.4	8.4	—	8.4,18.2	8.4,18.2	8.4	—	—
Spectral distribution of radiant power for the entire thermal pulse versus time for 22 narrow spectral regions from 0.25 microsec to 2.7 microns with a time resolution of 100 to 200 microns, NRDL spectrometer (Hilger medium quartz spectrometer and baird interference filters)	8.4*	8.4*	8.4*	—	8.4*	8.4*	8.4*	8.4*	8.4*	8.4*	—	—
Radiant power as a function of time in 3 wavelength bands (i.e., filtered photocell invisible, filtered lead sulfide cell for region around 1 micron. Filtered lead selenide cell for region around 3 microns) with high time resolution (50 microsec)	—	—	—	—	—	—	—	18.2	18.2	—	—	—

TABLE 4.1 CONTINUED

Measurement	Project Performing Measurement											
	1	2	3	4	5	6	8	9	10	11	12	13
Spectrum of first pulse in wavelength interval 2,200A UV to 7,800A infrared dispersion 11 angstroms per mm. NRL spectrograph (JACO)	—	—	—	—	—	—	—	18.2	18.2†	—	—	—
Spectrum versus time in wavelength interval 2,800A to 5,300A, dispersion 5 angstroms per mm, time resolution 100 microsec, running time 100 milliseconds. NRL spectrograph (JACO)	—	—	—	—	—	—	—	18.2	18.2†	—	—	—
Spectrum versus time for interval 2,800A to 5,300A, dispersion 5 angstroms per mm, time resolution 2 milliseconds, running time 2 sec.	—	—	—	—	—	—	—	18.2	18.2†	—	—	—
Spectrum versus time, dispersion of 100A per mm at 5,000A, time resolution 2 microsec, running time approximately 1 sec. NRL prism spectrograph	—	—	—	—	—	—	—	18.2	18.2	—	—	—
Spectrum versus time, 5,000 low resolution spectra per sec, running time 1 sec. NRL cine spectrograph	—	—	—	—	—	—	—	18.2	18.2	—	—	—
Time to second maximum of thermal pulse, NRDL photocell	—	—	—	—	—	—	—	—	8.4	—	—	—
Photography of fireball												
NRDL—GSAP cameras	—	—	—	—	—	—	—	—	—	—	—	—
NRL—Bowen cameras with running time 100 microsec	—	—	—	—	—	—	—	8.4	8.4	—	—	—
NRL—Bowen cameras—2 narrow wavelength intervals	—	—	—	—	—	—	—	18.2	18.2*	—	—	—
NRL—telephotography—80 in. focal length camera—48 frames/sec	—	—	—	—	—	—	—	18.2	18.2*	—	—	—
Total radiant energy from aircraft, cal/cm^2												
NRDL MK6F calorimeter, 90° field of view	—	—	—	8.1,5.2	—	8.1,5.2	8.1,5.2	—	—	—	8.1,5.1,5.2	8.1,5.2
NRDL MK7F calorimeter, 90° field of view	—	—	—	—	—	—	—	—	8.4	—	—	—
NRDL thin foil TE-1 calorimeter, 90° field of view	—	—	—	—	—	—	—	—	8.4	—	—	—
Minneapolis-Honeywell thermopile	—	—	—	—	—	—	—	—	8.4	—	—	—
Radiant energy in broad spectral bands from aircraft												
NRDL MK6F calorimeter + Corning filters	—	—	—	8.1,5.2	—	8.1,5.2	8.1,5.2	—	8.1,5.2	—	5.1,5.2	8.1,5.2
Minneapolis-Honeywell thermopiles + filters	—	—	—	—	—	—	—	—	8.4	—	—	—
Irradiance versus time from aircraft												
NRDL MK6F radiometers	—	—	—	8.1,5.2	—	8.1,5.2	8.1,5.2	—	—	—	8.1,5.2	8.1,5.2
Photography of fireball from aircraft												
NRDL—GSAP cameras	—	—	—	8.1,5.2	—	8.1,5.2	8.1,5.2	—	8.4	—	8.1,5.2	8.1,5.2

*Measurements partially successful.
†Measurements failing to produce usable data.

TABLE 4.2 SHOT 9 AND SHOT 10 DATA

Measurements	Shot 9	Shot 10
Total thermal radiant energy normalized to 10.3 nm, cal/cm^2	0.02	0.025
Total radiant energy (NRDL 90 degrees field of view calorimeter) from ground station at slant range of 2,420 feet from air zero, cal/cm^2	18.8	—
Total radiant energy (NRDL MK6F 90 degrees field of view calorimeter at slant range 3,810 feet from air zero), cal/cm^2	7.26	—
Total radiant energy (NRDL MK7F 90 degrees field of view calorimeter) from ground station at slant range 32,565 feet from air zero, cal/cm^2	—	0.061
Total radiant energy (NRDL MK7F 90 degrees field of view calorimeter; NRDL thin foil calorimeter), Minneapolis-Honeywell thermopile (average) from delivery aircraft (slant range 21,500 feet ± 300), cal/cm^2	—	0.17
Time to the second maximum NRDL photocell (delivery aircraft), msec	—	45
Time to the second maximum NRDL MK6F radiometers, msec	73	43
Time to the second maximum NRDL bolometers (improved NRL type), msec	69	42.5
Time to the second maximum NRL bolometers, msec	70	60
Time to minimum NRDL bolometers, msec	6.2	4.5
Time to minimum NRL bolometers, msec	5	4.7
Time to first maximum NRDL bolometers, msec	0.140	0.225
Time to first maximum NRL bolometers, msec	0.500	0.22
Ratio of first maximum radiant power to second maximum radiant power, NRDL bolometers	1.1	1.1
Ratio of first maximum radiant power to second maximum radiant power, NRL bolometers	1.95	1.08
Ratio of radiant power at minimum to second maximum radiant power, NRDL bolometers	0.07	0.14
Ratio of radiant power at minimum to second maximum radiant power, NRL bolometers	0.07	0.19
Ratio of energy of first pulse to total energy measured; NRDL bolometers, percent	0.63	1.2
Atmospheric, transmissivity (1/Beta broad band approximately 5,500A), (miles)$^{-1}$	0.078	0.0535
Device yields (Radiochemical), kt	3.1 ± 0.1	3.1 ± 0.1

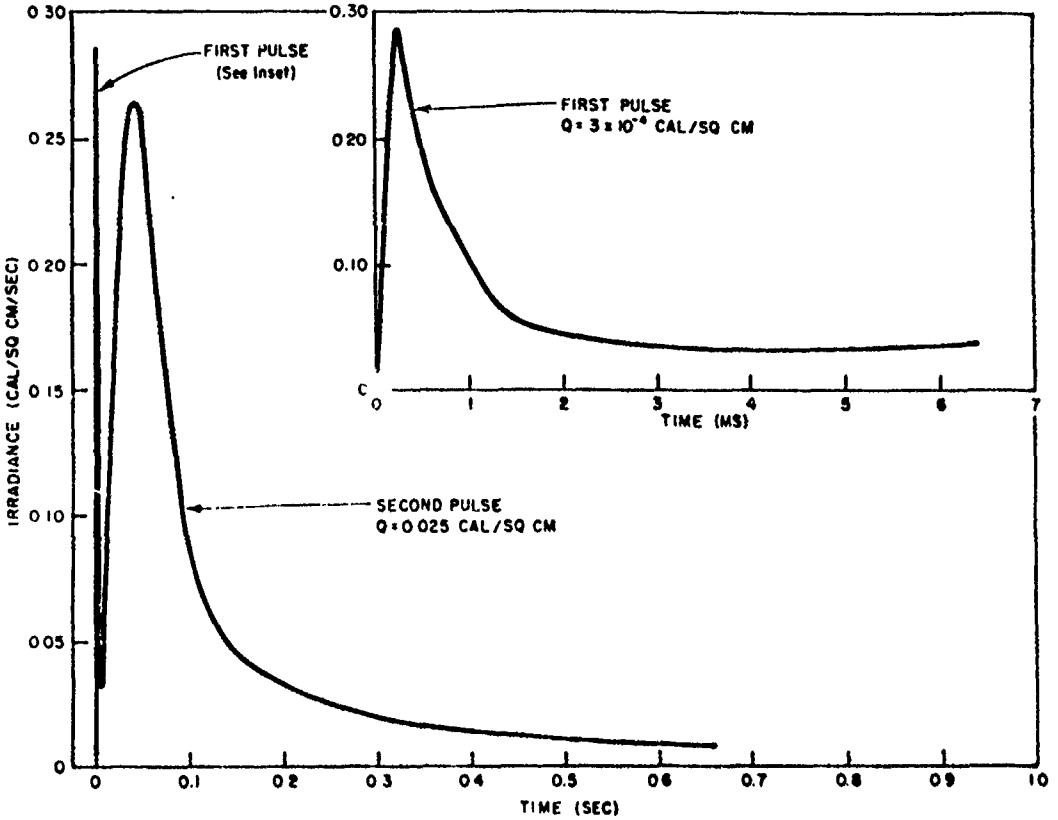

Figure 4.1 Irradiance as a function of time for Shot 9.

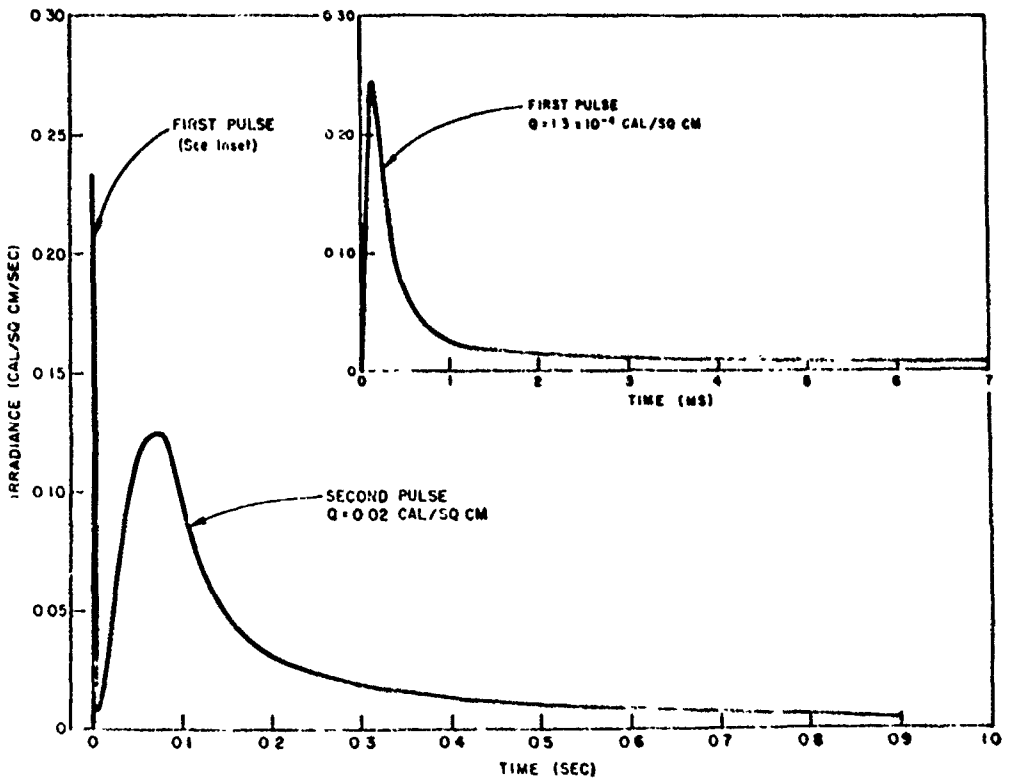

Figure 4.2 Irradiance as a function of time for Shot 10.

variation in the partition of energy as the altitude of a nuclear detonation is significantly increased. A final Project 18.2 (Reference 24) report is still not available for consideration in this chapter.

4.3 DATA FOR DEVICES HAVING YIELDS BETWEEN 1 AND 10 KT

Devices in this category were detonated as Shots 1, 2, 3, 5, 6, 9, and 11. Shots 1 and 9 were air bursts of approximately 800-foot height of burst. Because of the possible influence of the mass-to-yield ratios on thermal characteristics, Table 4.3 presents the shot number, yield, weight of device, weight of cab materials and weight of tower.

Data derived from radiant power versus time (bolometers) and irradiance versus time (NRDL Mk 6 F radiometers) measurements by Project 8.4 are presented in Table 4.4. Specif-

TABLE 4.3 WEIGHTS OF DEVICES, CAB, AND TOWER

Shot	Device Weight	Cab Weight	Tower and Platform Weight
	pounds	pounds	pounds
1		Air drop	
2	*	30,020	89,850
3	*	48,430	129,380
5	*	51,100	165,654
6	*	53,167	268,660
9		Air drop	
11	*	50,030	167,650

* Not significant compared to other material engulfed by the fireball.

ically, the times to the minimum (bolometer data) and the times to the second maximum (bolometer and radiometer data) are presented for Shots 1, 2, 3, 5, 6, and 9. These observations are compared with the empirical scaling laws for the time to the minimum ($t_{min} = 0.0025W^{1/2}$) and for the time to the second maximum ($t_{max} = 0.032W^{1/2}$). From the table it is clear that the observed data are somewhat higher than the predictions given by the empirical scaling laws by percentages varying from 16 to 48 percent for the time to the minimum data and for the time to the second maximum by percentages varying from 1 to 33 percent. It is further clear by comparing the information in Table 4.3 with the data in Table 4.4 that any perturbation of the time to the minimum or time to the second maximum by the mass of material associated with the device was negligible.

Measurements of the total-radiant energy employing 90-degree field of view, NRDL Mk 6F calorimeters for Shots 1, 2, 3, 5, 6, and 9 are summarized in Table 4.5. Calculations of thermal yield and percent of total yield appearing as thermal radiation are included. For the two air bursts, Shots 1 and 9, the thermal yields agreed within experimental errors with those computed using the empirical scaling relationship $E = 0.44W^{0.94}$, where E is the thermal yield and W the total yield. For tower Shots 2, 3, 5, and 6 significantly lower-thermal yields were obtained when a spherical radiating source was assumed. As can be seen in an examination of photographs, the fireball of each tower shot exhibited a hemispherical shape for a substantial length of time during its growth. Thus, recomputing the thermal yield on this basis in an approximate fashion resulted in partition of energy reasonably consistent with that of the air bursts. Further details concerning these results may be found in WT–1146 (Reference 25).

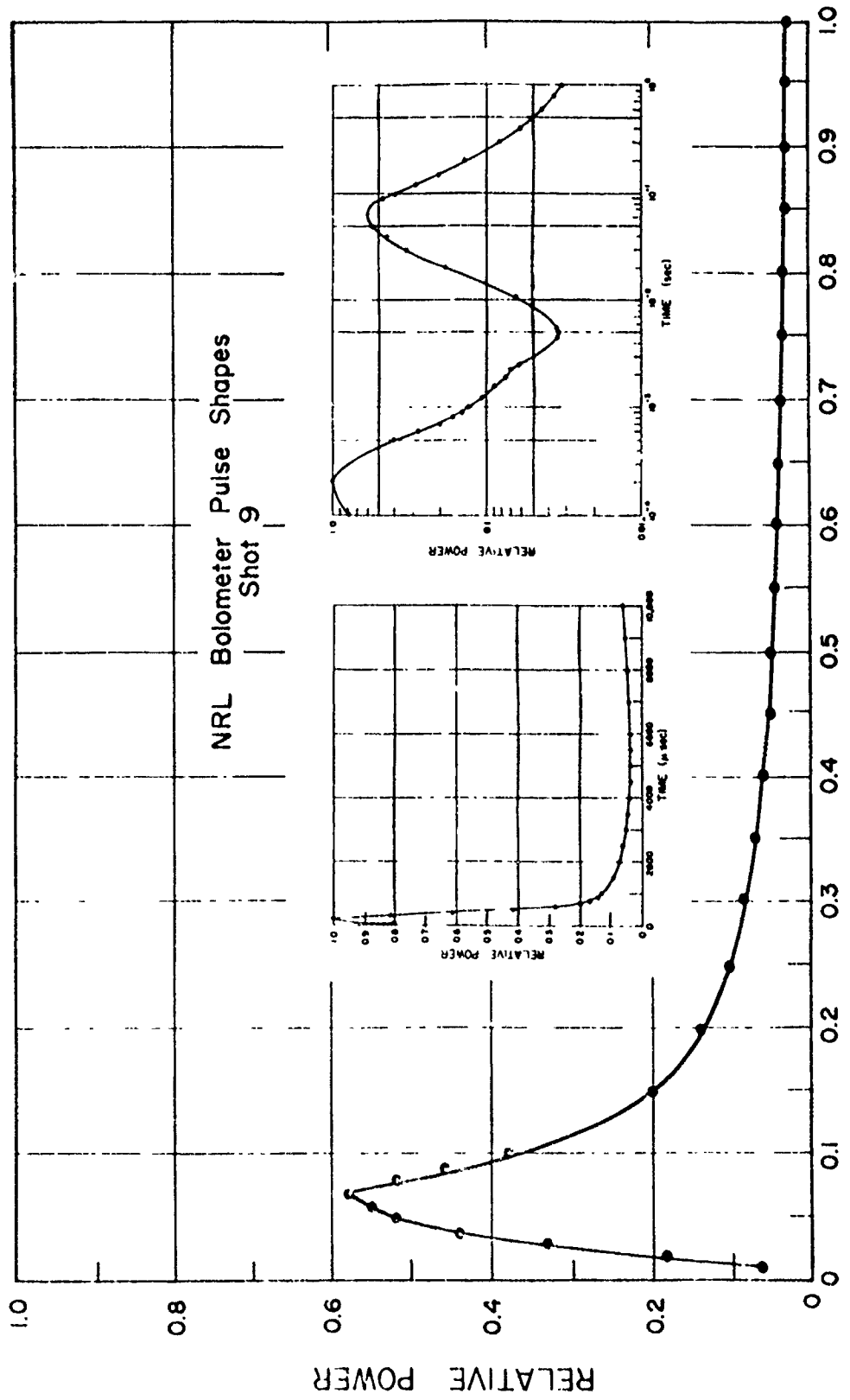

Figure 4.3 Shot 9 thermal pulse shapes, NRL bolometers.

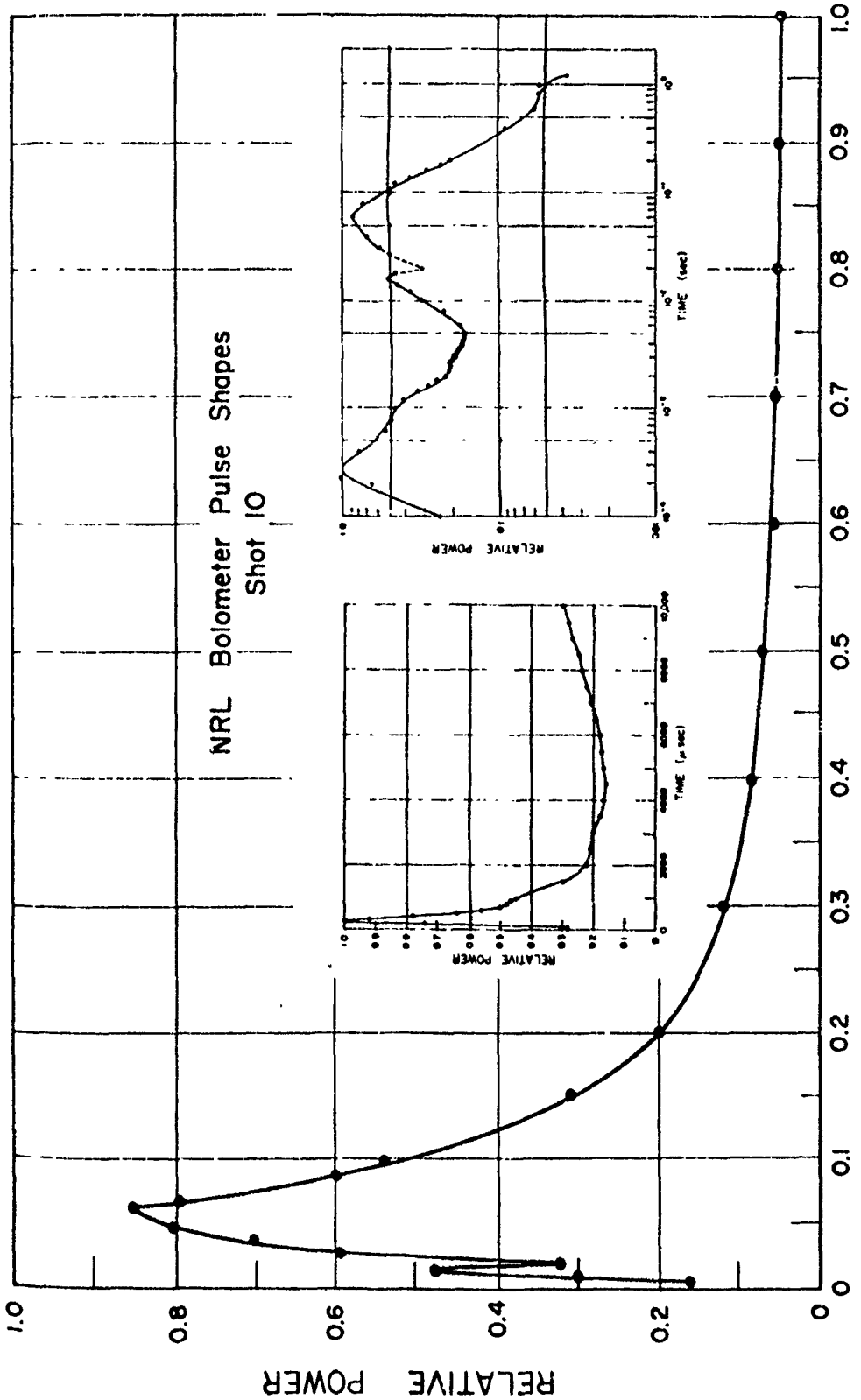

Figure 4.4 Shot 10 thermal pulse shapes, NRL bolometers.

TABLE 4.4 BOLOMETER AND RADIOMETER DATA

Shot	Time to minimum, t_{min}		Increase over predicted t_{min}	Time to second maximum, t_{max}			Increase over predicted t_{max}
	Bolometer	$0.0027W^{1/2}$		MK6F Radiometer	Bolometer	$0.032W^{1/2}$	
	msec	msec	percent	msec	msec	msec	percent
1	3.3	2.8	18	48	44	34	33
2	5.00	4.3	16	68	64	50	32
3	—	—	—	85	—	84	01
5	7.7	5.2	48	71	77	60	20
6	—	—	—	102	110	90	18
9	6.2 5.00*	4.7	32	73	69 70.0*	58	22

*NRL data.

TABLE 4.5 TOTAL RADIANT ENERGY

Atmospheric attenuation assumed to be 5 percent.

Shot	Slant Range	Total Radiant Energy	Thermal Yield	Yield Partition: Thermal/Total	Thermal Yield	
					E	$0.44\,W^{0.84}$‡
	feet	cal/cm²	kt			
1	2,428	6.83	0.52†	0.45		0.46
2	5,005	2.05	1.02*	0.43		—
3	4,960	4.84	2.37*	0.35		—
5	4,676	3.21	1.40*	0.39		—
6	5,270	5.55	3.08*	0.39		—
6	6,698	3.29	2.99*	0.39		—
9	2,397	17.3	1.29†	0.41		1.28
9	3,808	6.66	1.27†	0.40		—

*Tower shots; computed assuming hemispherical source.
†Air bursts; computed assuming spherical source.
‡Pertains to air bursts.

4.4 THERMAL MEASUREMENTS FROM AIRCRAFT

Details of the experiments constituting Projects 8.1, 5.1, and 5.2 are to be found in the appendix to this report and in WT-1143, WT-1132, and WT-1133 (References 26, 4, and 27). The shot participation and instruments used are summarized in Table 4.1. All measurements were made with 90-degree field-of-view instruments, whose receiving surfaces were substantially perpendicular to the line of sight between the fireball and instrument, with the exception of certain instruments with the same field of view oriented to observe radiation reflected from the earth's surface.

The total radiant energy received on a unit area at a given point in space is given, to first approximation, by calorimeters oriented on the fireball. Table 4.6 presents aircraft positions and the calorimeter data obtained at these positions. Examination of gun-sight-aiming-point (GSAP) camera photographs of the fireball indicated that no correction was required for deviations between the normal to the detector's surface and line of sight between detector and fireball. However, in using this data, the reader is reminded that the thermal instruments had 90-degree fields of view and, therefore, recorded only reflected radiation from a portion of the ground plane and only a portion of the scattered radiation. Further, with varying surface and atmospheric conditions, the thermal energy received at a given point in space relative to ground zero could be substantially modified.

Since Project 8.1 had as its objective a determination of the contribution of thermal radiation reflected from the earth's surface to the total-thermal energy received by an aircraft in the vicinity of a nuclear detonation, the test aircraft were also equipped with thermal instruments to observe essentially reflected radiation. These instruments had 90 degree fields of view and were, in general, oriented so that their receiving elements were parallel to the reflecting surface. Unfortunately, several factors involved in the design of this experiment complicated the analysis of the experimental data, i.e., instruments oriented to observe the fireball also viewed a sizable portion of the reflecting plane. In addition, instruments oriented to observe reflected radiation viewed only a portion of the reflecting plane. Further, in some cases, the instruments oriented to observe the reflected plane also viewed at least portions of the fireball. The instruments used by this project consisted of calorimeters to measure total-radiant energy and energy in several spectral bands and irradiance. The reader is referred to WT-1143 (Reference 26) for details as to the comparison of analytical and experimental work. While it is quite straightforward to compute the thermal energy received, directly neglecting attenuation and scattering, the most general case requires knowledge of the atmospheric attenuation and scattering and the reflecting properties of the reflecting ground surface. The latter two considerations are somewhat uncertain.

4.5 RESULTS OF THERMAL RADIATION ATTENUATING CLOUD STUDIES

In the detonation of a nuclear device in a clear atmosphere, the thermal radiation is received on an object primarily on a direct line from the source. The introduction of an oil-fog smoke screen between the source and objects inside or beneath the smoke cloud scatters the incident radiation so that the amount of energy reaching the object is reduced sufficiently to minimize burn production or fire ignition. Smoke generators were employed by Project 8.3 (Reference 28) to establish an oil-fog smoke screen over instrumentation located at 1,000, 1,400, 1,900, and 2,400 feet east of ground zero on Shot 5 which was detonated from a 300-foot tower and which had a yield of 3.6 ± 0.1 kt. The maximum height of the smoke screen and average height of the smoke screen have been determined from photography to be approximately 55 feet, and probably 30 to 40 feet, respectively. The measurements made under the smoke screen and the instruments used by Project 8.3 and similar measurements and instrumentation outside the smoke by Project 8.4 are given in Table 4.1. Total radiant energy, radiant energy in broad

spectral bands, and thermal irradiance as a function of time were measured by Project 8.4 outside the smoke screen at a slant range of 4,660 feet from the point of detonation. The area concentration of smoke was estimated to have been 300 to 425 gallons per square mile. Attenuation factors as measured at instrumentation stations located at 1,000, 1,900, and 2,400 feet,

TABLE 4.6 RADIANT ENERGY MEASURED FROM AIRCRAFT

Shot	Project	Altitude MSL	Slant Range	Radiant Energy*
		feet	feet	cal/cm²
4	5.2	11,700	14,118	6.0 – 6.75
6	5.2	7,605	10,343	2.9 – 3.2
8	5.2	12,932	14,113	2.6 – 2.9
12	5.2	10,023	12,879	4.7 – 4.9§
12	5.1	8,880	5,551	36 – 42¶
12	5.1	8,000	4,990	40 – 55¶
12	5.1	7,370	4,050	90 – 100¶
4	8.1	13,500	19,000	3.80
4	8.1	20,000	19,250	4.26
6	8.1	11,500	11,700	2.16†
				0.40‡
6	8.1	19,000	16,500	1.12†
				1.05‡
8	8.1	16,500	11,750	2.3
8	8.1	16,000	16,400	2.7
8	8.1	19,000	20,800	1.04†
				0.67‡
12	8.1	15,500	14,400	4.35
12	8.1	15,000	13,900	5.27†
				3.42‡
12	8.1	15,500	23,300	1.46
13	8.1	10,000	14,500	3.7†
				0.32‡
13	8.1	16,000	18,800	2.4†
				0.73‡

* Data indicated require corrections for angle between line of sight to fireball and normal to sensing element.
† Direct radiation, cal/cm².
‡ Reflected radiation, cal/cm².
§ Aircraft probably not in proper position and orientation to satisfactorily record thermal data.
¶ Data were telemetered.

using 180 degree field of view calorimeters with detecting surfaces normal to the air zero direction, varied from 78 to 90 percent. The angular distribution of radiation was measured at 1,000, 1,400, and 1,900 feet. These measurements revealed maximum radiant energy was received on a vertical surface normal to ground zero and less radiant energy was received on a horizontal surface. Under the latter conditions the radiation was attenuated by 77 percent and 96 percent at ranges of 1,000 and 2,400 feet respectively. These results are consistent with theoretical considerations, and coupled with them, provide an adequate basis for establishing operational doctrine.

An evaluation of experimental data indicates that adequate information was obtained for use

in establishing operational doctrine for thermal-radiation-attenuating clouds and for correlation with theoretical work performed by the Chemical Corps.

4.6 THERMAL AND AIR-TEMPERATURE MEASUREMENTS, SHOT 12

Basic thermal- and air-temperature measurements were performed on Shot 12 in support of the blast program, Program 1. The air-temperature measurements were considered in Chapter 2 of this report and in WT-1149 (Reference 29). Thermal measurements to determine the

TABLE 4.7 RESULTS OF THERMAL MEASUREMENTS ON SHOT 12 PLOTS

Quantity	Surface Measurements			12-Foot Elevation Measurements	
	Asphalt 2,000 ft	Concrete 2,000 ft	Fir Boughs 2,000 ft	Asphalt 2,000 ft	Desert 2,500 ft
Time to First Obscuration of Instrument, sec	0.04	0.05	0.09	0.22	1.01
Maximum Irradiance to Instrument, cal/cm²-sec	90	234	184	*	*
Time of Maximum Irradiance, sec	0.06	0.11	0.10	0.20	0.17
Time of Shock Arrival, sec	0.45	0.51	0.51	0.45	1.01
Total Thermal Energy Received to Time of First Obscuration, cal/cm²	0.9 – 2.0	4.9	6.5	117	*
Total Thermal Energy to Time of Shock Arrival, cal/cm²	6.1	42	41	Off Scale	85
Total Thermal Energy to Surface Until Time of Obscuration of Instrument at 12-foot Elevation, cal/cm²	*	*	*	5.0	*

*Not available.

thermal inputs to various surfaces above which air-temperature measurements were performed are presented in WT-1146 (Reference 25). These measurements consisted of total-radiant energy and thermal irradiance as a function of time using NRDL Mk 8 calorimeters and radiometers, respectively. The measurements were only partially successful because of electromagnetic pickup and recorder failures. Available data are presented in Table 4.7

Chapter 5
HIGH ALTITUDE SHOTS

5.1 INTRODUCTION

The high-altitude shot and, to a lesser extent, the correlation shots were conducted for the purpose of determining the basic effects of a nuclear detonation in a rarefied atmosphere in order to facilitate progress of the air-defense program. To avoid the many uncertainties in scaling effects between weapon yields, size of high-explosive spheres, yield processes, and the total mass of weapons, a concerted effort was made to select a device representative of that anticipated for the air-defense program. The general planning altitude for the high-altitude shot was 40,000 feet MSL. To provide scaling data for changes in only the ambient atmosphere, the correlation shot was a device as nearly identical to the high-altitude device as practical. The correlation device was detonated sufficiently high above the terrain so that the return of the reflected shock had a minimum influence on weapon effects, yet was sufficiently low in elevation to permit making certain necessary diagnostic measurements for weapon development. An acceptable elevation above terrain was 800 feet. Because the nuclear device was a new development, it was deemed prudent to detonate the correlation shot prior to the high-altitude shot in order that an easily obtained and reliable yield could be used to anticipate the performance of the device on the operationally difficult high-altitude event. Briefly, the first shot of Operation Teapot, which was planned to be the correlation shot for the high-altitude test, did not fulfill the air-defense criterion with respect to yield, whereas a redesigned device, detonated as Shot 9 in the operation, was acceptable.

The overall instrumentation of the high-altitude shot and correlation shot was designed to determine each of the weapons effects parameters: blast, thermal and nuclear radiation as a function of distance and time. This would permit direct comparison of these values for a specific-yield device detonated in two substantially different ambient atmospheres. Further, it was planned that these data, along with sufficient diagnostic-type data, such as spectroscopy, would provide scaling trends to allow extrapolation of weapon effects to neighboring atmospheres. That is, it was planned that the instrumentation would be of such a nature as to indicate trends in changes of partition of energy into blast and thermal radiation, and any significant deviations from traditional nuclear radiation scaling.

5.2 OPERATIONS

Operationally, the mission of the high-altitude test was to detonate a nuclear device at the highest feasible altitude consistent with the required instrumentation, safety of the delivery vehicle, and accuracy of burst zero.

Delivery of the nuclear device by a conventional B-36 type aircraft was an early decision. This method of delivery made possible the deployment from a single aircraft of all essential airborne instrumentation along with the nuclear device, thus reducing to a minimum the possibility of positioning errors. In addition, the aircraft tail blister was available for thermal-radiation instrumentation.

The weapon-effects parameter that determined safety of the delivery-aircraft crew was nuclear radiation. A maximum exposure of 5 r was used for planning. To achieve the maximum altitude for the detonation, it was necessary to employ a parachute on the nuclear device.

This permitted a safe separation of the drop aircraft from burst point principally along the horizontal rather than the vertical. Considering the maximum altitude of the drop aircraft, the early planning was for the drop aircraft to deliver the bomb from 50,000 feet MSL, with the detonation occurring at 40,000 feet MSL. A time-of-fall rather than a baro fuze was employed to detonate the weapon, since the latter would not guarantee safety of the drop aircraft in the event of parachute failure. For safety over NTS, the bomb was equipped with a baro-fuze backup to detonate at 20,000 feet MSL in the event of a parachute failure.

To achieve less than 1,500 feet circular error in burst point at a predetermined point in space using a parachute bomb with a time-of-fall fuze, it was necessary to obtain its trajectory by a number of test drops at the Edwards Air Force Base bombing range. Since it was necessary for the instrumentation canisters to parallel the trajectory of the nuclear device, a number of these canisters were also deployed on the practice drops to determine the necessary size of their parachutes. The canisters were deployed after the nuclear device at preset times on an intervalometer. The practice drops of the high-altitude device began in the summer of 1954 and continued through to early spring of 1955. The upper air is reported to be at its greatest density during this time of the year and the B-36 usually achieved a 50,000-foot MSL altitude. However, in the event of an engine failure, 48,000 feet was its near-ceiling altitude. As Operation Teapot extended into late spring 1955, the upper-air density decreased and the altitude ceiling for the B-36 was relaxed to 48,000 feet, with 46,000 feet as an alternate in the event of an engine failure.

On April 6, 1955, the high-altitude operation was conducted with an engine failure on the drop aircraft; hence, the nuclear device was delivered from an altitude of 46,000 feet (Reference 30). Test personnel were informed the previous day to anticipate the burst altitude to be 36,400 feet MSL in the event of an engine failure. Actual burst zero was at 36,620 ± 100 feet MSL; and 397 ± 50 feet west, 36 ± 50 feet south, of intended ground zero. The burst-point accuracy was highly satisfactory, indicating that previous test dropping was fruitful. Correlation Shot 9 had also been delivered with small errors; burst elevation being 739 feet above terrain and 62 feet west, 94 feet north of intended ground zero.

In addition to the B-36 drop aircraft, eight jet aircraft were employed to lay smoke trails 400 feet apart in a horizontal grid 3,000 feet above burst point just prior to detonation time. These smoke trails were to be used in the conventional way to determine free-air pressure versus distance from the high-altitude detonation. The timing and positioning of the smoke-trail aircraft with respect to the drop aircraft and intended burst point required a high degree of timing since it was necessary for the smoke trails to be laid as close to zero time as possible. The necessity for a complete dry run (HADR) of the high-altitude operation except for the nuclear capsule was obvious and was initiated early in the high-altitude planning. The smoke trails were incorrectly spaced on the dry run and action was taken to ensure correct spacing on the live run. The smoke trails were, however, disappointing on the actual high-altitude event in that their homogeneity and density were poor.

An impressive group of aircraft (two B-36's, two B-57's and four F-84G's) was assembled in an all-out effort to successfully sample the high-altitude radioactive cloud. Because a major portion of the test philosophy involved a reliable radiochemical yield for the high-altitude detonation, it was most rewarding to find that the cloud sampling was successful. A radiochemical yield of 3.3 ± 0.4 kt was obtained for the high-altitude Shot 10 and the correlation Shot 9 gave a radiochemical yield of 3.16 ± 0.16 kt. A comparison of the various weapon effects was thus possible for Shots 9 and 10 with the change in ambient atmosphere being the most significant variable.

The remaining portion of the instrumentation for the high-altitude shot was carried out on the ground. This included thermal radiation, photography, and a minor blast program. To obtain high-resolution data, the Project 18.2 thermal instrumentation on the ground required

that some of the receiving mirrors track the nuclear device along its trajectory until detonation. To aid in this optical tracking, the main nuclear unit was equipped with a black and white parachute which made it more visible and further distinguished it from the smaller canister parachutes. However, in spite of this, Project 18.2 was unable to track the main nuclear unit on the high-altitude shot. A minus one-second signal (Reference 24) was supplied to the Project 18.2 thermal instrumentation. This was accomplished by tapping off a highly accurate (± 10 msec) minus one-second signal on the timer fuze in the nuclear unit. This signal was telemetered to the ground.

Operationally, the high-altitude program was difficult, but was carried out with moderate-to-good success.

5.3 BLAST

5.3.1 Ambient Atmosphere and Blast Scaling Factors. High-altitude Shot 10 occurred at an altitude of 36,620 ± 100 feet MSL and the correlation Shot 9 at 4,933 feet MSL. Ambient-air conditions at burst altitude are given in Table 5.1. The ambient atmosphere decreased by a factor of about four in pressure and a factor of three in density between Shot 9 and Shot 10.

Meteorological data in the vicinity of burst zero for high-altitude Shot 10 are recorded in Table 5.2. Similar data recorded over the region from 4,000 to 93,000 feet MSL are given in Figure 5.1. The ambient air densities and pressures given in Figure 5.1 are in terms of sea-level atmosphere (14.7 psi, 15 C), whereas the temperatures are given as absolute quantities. It is observed that two tropopause-like discontinuities existed that day, one at 31,000 to 41,000 feet and a second at 55,000 to 66,000 feet. The high-altitude detonation occurred nearly in the middle of the lower one. Over an altitude of 3,000 feet above or below the detonation, variations in temperature were about 1 C.

Returning to Table 5.2, it is to be noted that almost no shears in wind speed or direction existed for several thousand feet above or below the detonation. Thus, the detonation could be considered as having taken place in a large air mass moving with constant velocity. The latter consideration had a bearing on the method of reducing the canister pressure-distance data.

The characteristics of a nuclear detonation are modified by the ambient atmosphere. Although altitude in terms of feet MSL is one criterion for the burst conditions, the ambient-air pressure and density vary daily at the same altitude. In terms of the National Advisory Committee for Aeronautics (NACA) standard atmosphere the high-altitude detonation occurred at 37,330 feet and the correlation Shot 9 occurred at 6,000 feet, using ambient-air density as the criterion.

The factors by which the ambient atmosphere changed from a standard sea-level atmosphere are given in Table 5.3.

Using the ambient-air conditions at burst altitudes (Table 5.1), conventional scaling factors for distance (S_d), time (S_t) and pressure (S_p) are presented in Table 5.4. Multiplication of observed pressures, distance, and time by the scaling factors reduce the data to the equivalent 1 kt, sea-level values (ambient pressure = 14.7 psi, ambient temperature = 15 C).

5.3.2 Rate of Growth of the High-Altitude Fireball and Yield Determination. The luminous surface of the fireball prior to breakaway is the shock front rendering the air luminous at the high temperatures and densities prevailing immediately behind the shock front. The fireball radius during this phase is the shock-front radius. Extensive use of this radius-time data has been made on previous detonations to obtain what is called a fireball yield. Because of possible changes in the partition of energy into blast (hence changes in radius) with increasing detonation altitude, the fireball yield was not relied upon for yield determination of the high-altitude detonation. The yield of 3.3 ± 0.4 kt was determined by conventional radiochemical

TABLE 5.1 AMBIENT AIR CONDITIONS AT BURST ALTITUDE

P_{0H} = Ambient air pressure at altitude H; T_{0H} = Ambient air temperature at altitude H; ρ_{0H} = Ambient air density at altitude H; C_{0H} = Ambient air speed of sound at altitude H.

Shot	Altitude (H)	P_{0H}	P_{0H}	T_{0H}	ρ_{0H}	C_{0H}
	ft MSL	mb	psi	°C	gm/liter	m/sec
9	4,933	849	12.32	12.6	1.036	340.0
10	36,620 ± 100	222	3.22	−47.8	0.343	302.0

TABLE 5.2 METEOROLOGICAL DATA IN THE VICINITY OF SHOT 10, 1000 PST, 6 APRIL 1955

Sky condition, clear, visibility, unrestricted.

Height	Wind	Pressure	Temperature
10^3 ft MSL	deg/knots	mb	C
30	310/27	301	−47.7
31	310/29	287	−50.0
32	310/31	275	−49.4
33	320/30	262	−47.1
34	320/29	249	−46.8
35	320/27	238	−47.2
36	300/28	228	−47.6
36.620 *	300/28	222	−47.8
37	300/29	218	−48.0
38	300/31	209	−48.2
39	300/38	198	−47.0
40	290/43	190	−45.9
41	290/45	181	−46.0
42	290/47	173	−46.8
43	290/47	166	−48.6
44	300/45	158	−50.9
45	300/44	151	−52.4
46	300/40	143	−53.8
47	290/33	138	−55.0
48	290/30	131	−56.3
49	290/29	125	−58.0
50	290/29	119	−59.0

* Burst altitude.

TABLE 5.3 AMBIENT CONDITIONS AT BURST ALTITUDE IN TERMS OF SEA LEVEL ATMOSPHERE

P_{00} = Ambient air pressure at sea level = 14.7 psi; T_{00} = Ambient air temperature at sea level = 15 deg C; ρ_{00} = Ambient air density at sea level = 1.222 gm/liter. See Table 5.1 for other definitions.

Shot	$\frac{P_{00}}{P_{0H}}$	$\frac{T_{00}}{T_{0H}}$	$\frac{\rho_{00}}{\rho_{0H}}$
9	1.1932	1.0084	1.1832
10	4.5631	1.2780	3.5703

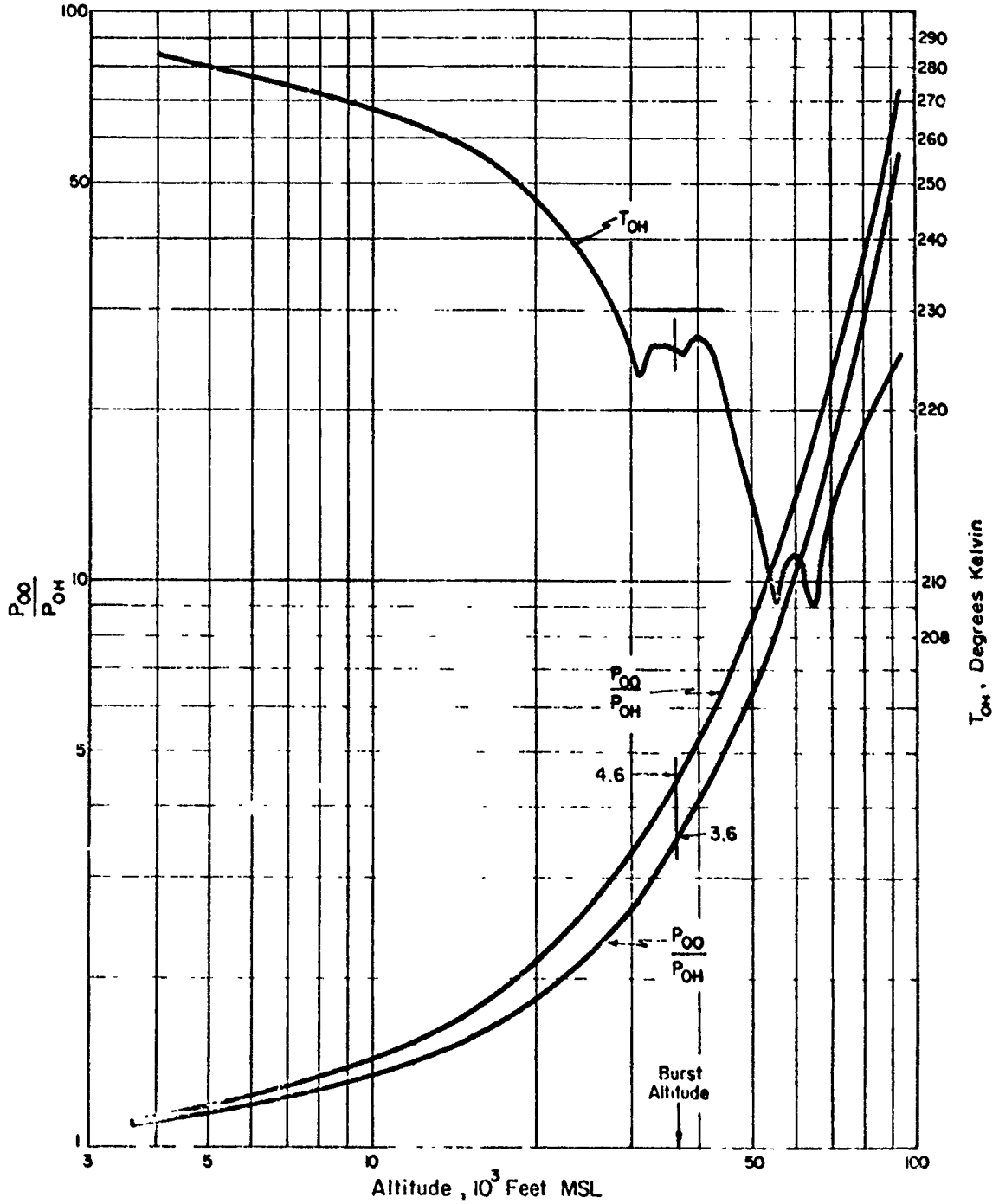

Figure 5.1 Ambient atmosphere, Shot 10.

methods, It is obviously important to compare the fireball yield with the radiochemical yield in order to detect significant changes in partition of energy up until the breakaway point. This comparison can only be rough, since the radiochemical yield has an unusually large uncertainty.

Diameter-time data for the high-altitude Shot 10 and the correlation Shot 9 as reported by Edgerton, Germeshausen and Grier (EG&G) (Reference 31) are given in Table 5.5 and plotted in Figure 5.2.

The EG&G method for fireball-yield determination is given by the following expression:

$$\text{Yield, kt} = 1.272 \times 10^{-8} \rho \phi^5 \tag{5.1}$$

Where ρ is the ambient air density in grams per liter and the quantity ϕ is the diameter of the fireball in meters divided by time (msec) to the two-fifths power. It is noted that the value of ϕ (Table 5.5) becomes nearly constant for Shot 9 after about 6 msec, having an average value of about 47.95. The value of ϕ does not become constant for Shot 10; however, it does

TABLE 5.4 BLAST SCALING FACTORS TO 1 kt AND SEA LEVEL

Shot	Yield	S_p	S_d	S_t
	kt			
9	3.16	1.1932	0.6425	0.6398
10	3.3	4.5631	0.4050	0.3582

have the value of 59.3 near the end of the fireball phase and changes slowly after 11 msec. The yields obtained by substitution into equation 5.1 are 3.3 kt for Shot 9 and 3.2 kt for Shot 10.

The yields obtained by various methods are given in Table 5.6.

Generally, the fireball yield for the high-altitude Shot 10 appeared slightly less than the fireball yield for Shot 9. However, the fireball yields were within the accuracy of the radiochemical yields and no change in partition of energy during the fireball phase could be attributed to the high-altitude shot.

5.3.3 Fireball Surface Conditions. Fireball diameter-time data for Shots 9 and 10 are plotted in Figure 5.2. The data showed little scatter although several camera positions and films were used to obtain the average curves. The curves through the diameter-time data are not straight lines on the log-diameter versus log-time graphs indicating that its equation, if represented by

$$D = \phi t^n \tag{5.2}$$

must have a variable, n.

From radius-time data, fireball pressure versus distance and other shock-front values can be calculated. The equation for radius versus time over a small region can be written as

$$R = \phi' t^n \tag{5.3}$$

where n is the slope of log radius versus log time. The shock-front velocity is then

$$\frac{dR}{dt} = U = n\phi' t^{n-1} \tag{5.4}$$

Substituting ϕ' from 5.3 into 5.4, the shock velocity is

$$U = \frac{dR}{dt} = n\frac{R}{t} \tag{5.5}$$

The values of the slope n can be calculated accurately by computing its difference from the value $^2/_5$ by use of the following equation:

$$n = \frac{\log R}{\log t} = {}^2/_5 + {}^1/_5 \frac{\log (\phi')^5}{\log t} \tag{5.6}$$

The fireball-surface conditions for the high-altitude detonation are given in Table 5.7. Using well-known shock relations and the equation of state of air, the shock velocity versus radius

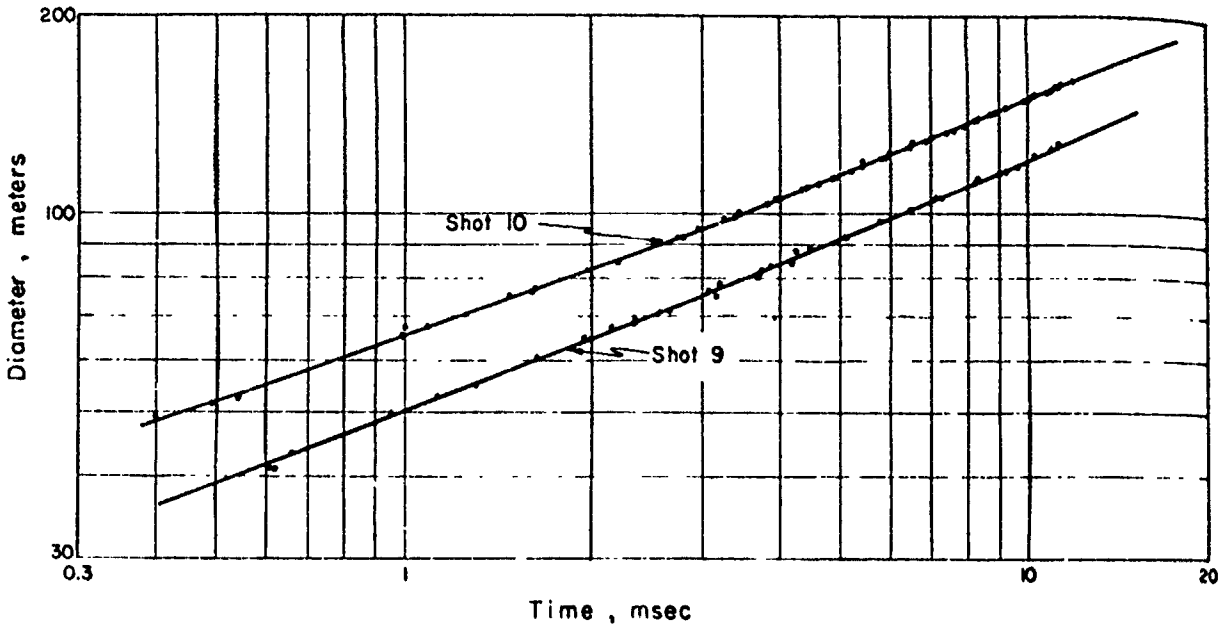

Figure 5.2 Fireball diameter versus time, Shots 9 and 10.

can be related to pressure versus distance and shock temperature versus distance. Because of the interest in possibly using the fireball as a region for kill of hard-missile targets, the values in Table 5.7 serve to give actual data for an air-defense-type warhead. The fireball overpressure versus distance for Shot 10 is given in Figure 5.3. Similar data for Shot 9 are given in Table 5.8 and Figure 5.4.

It is to be noted that the high-altitude Shot 10 fireball grew at a faster rate than the Shot 9 fireball (Figure 5.2). At any given time the Shot 10 fireball was larger than Shot 9. Since the two detonations had nearly the same yield, the rapid rate of growth on Shot 10 was caused primarily by the reduced ambient atmosphere. The Shot 10 diameter versus time would be equal to that of an 11-kt detonation at sea level.

If the overpressure versus distance for Shot 10 (Figure 5.3) is compared with the overpressure versus distance for Shot 9 (Figure 5.4) it is noted that almost exactly the same overpressure versus distance values are found in the fireball region. The shock-front overpressures are nearly inversely proportional to the cube of the radius over the high-pressure region. That high overpressures (and dynamic pressures) at given radii from a fixed blast yield are constant,

TABLE 5.5 SHOT 9 AND SHOT 10 FIREBALL DIAMETER VERSUS TIME

Time	Shot 9 Diameter	Shot 10 Diameter	Shot 9 ϕ	Shot 10 ϕ
msec	meter	meter	$m/msec^{2/5}$	$m/msec^{2/5}$
0.5	39.3	52.0	51.9	68.6
1.0	50.0	65.5	50.0	65.5
1.5	58.0	75.0	49.35	63.8
2.0	64.5	82.8	48.90	62.7
3	75.0	95.4	48.30	61.4
4	84.0	106.0	48.2	60.8
5	91.5	115.0	48.05	60.4
6	98.0	123.0	47.8	60.0
7	104.5	130.3	47.95	59.8
8	110.0	137.0	47.90	59.6
9	115.5	143.2	47.95	59.5
10	120.5	149.0	48.0	59.4
11	125.0	155.0	47.95	59.3

TABLE 5.6 YIELDS FOR SHOTS 9 AND 10

Shot	Radiochemistry	EG&G ϕ^5	LASL J-10 Analytic
	kt	kt	kt
9	3.16 ± 0.16	3.3	3.3
10	3.3 ± 0.4	3.2	3.0

TABLE 5.7 FIREBALL SURFACE CONDITIONS FOR SHOT 10

$U/C_{\theta H}$ = shock velocity divided by ambient sound speed; $P/P_{\theta H}$ = absolute shock pressure divided by ambient air pressure; $T/T_{\theta H}$ = absolute shock temperature divided by ambient air temperature.

Time	Radius	n	U = n R/t	$U/C_{\theta H}$	$P/P_{\theta H}$	Overpressure	$T/T_{\theta H}$	Temperature
msec	meter		m/msec			psi		K
1	32.75	0.3360	11.02	36.5	1,700	5,472	67.5	15,210
1.5	37.5	0.3400	8.50	28.1	1,030	3,227	48.0	10,810
2	41.4	0.3434	7.10	23.5	715	2,297	41.0	9,250
3	47.7	0.3538	5.62	18.6	450	1,447	34.0	7,660
4	53.6	0.3666	4.86	16.1	332	1,067	28.6	6,450
5	57.5	0.3712	4.26	14.1	272	873	24.6	5,550
6	61.5	0.3727	3.82	12.65	210	673	21.0	4,740
7	65.15	0.3774	3.51	11.65	173	553	18.7	4,215
8	68.5	0.3819	3.27	10.82	148	473	17.2	3,880
9	71.6	0.3845	3.06	10.13	130	416	15.8	3,565
10	74.5	0.3855	2.87	9.50	115	367	14.7	3,315
11	77.5	0.3870	2.73	9.05	104	332	13.8	3,135

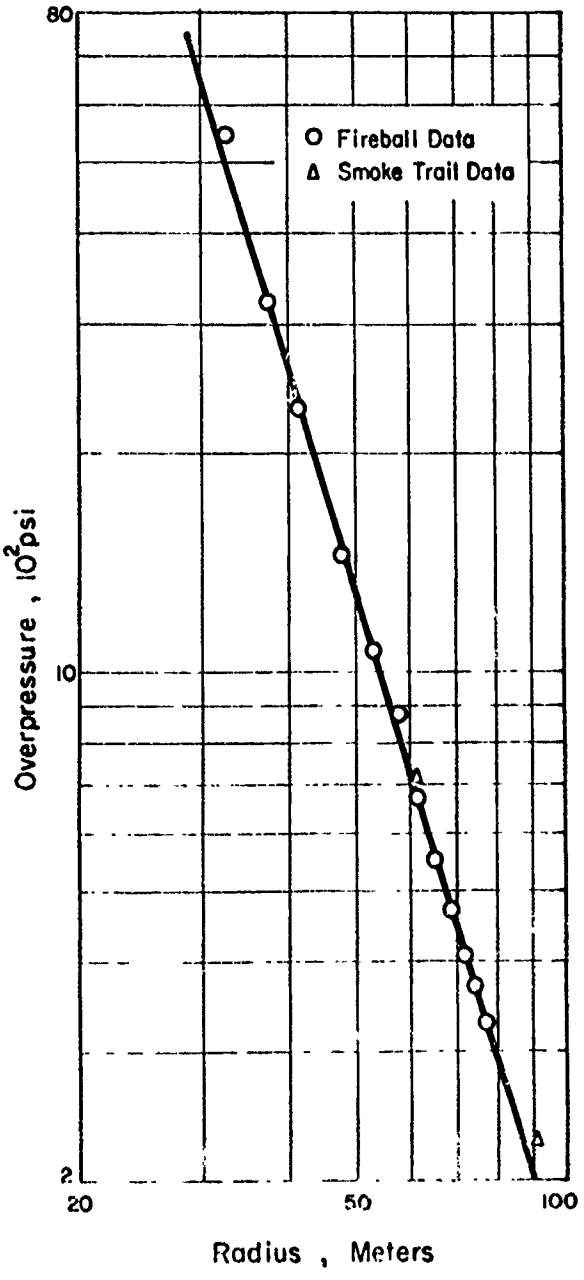

Figure 5.3 Fireball overpressure versus distance, Shot 10 (HA).

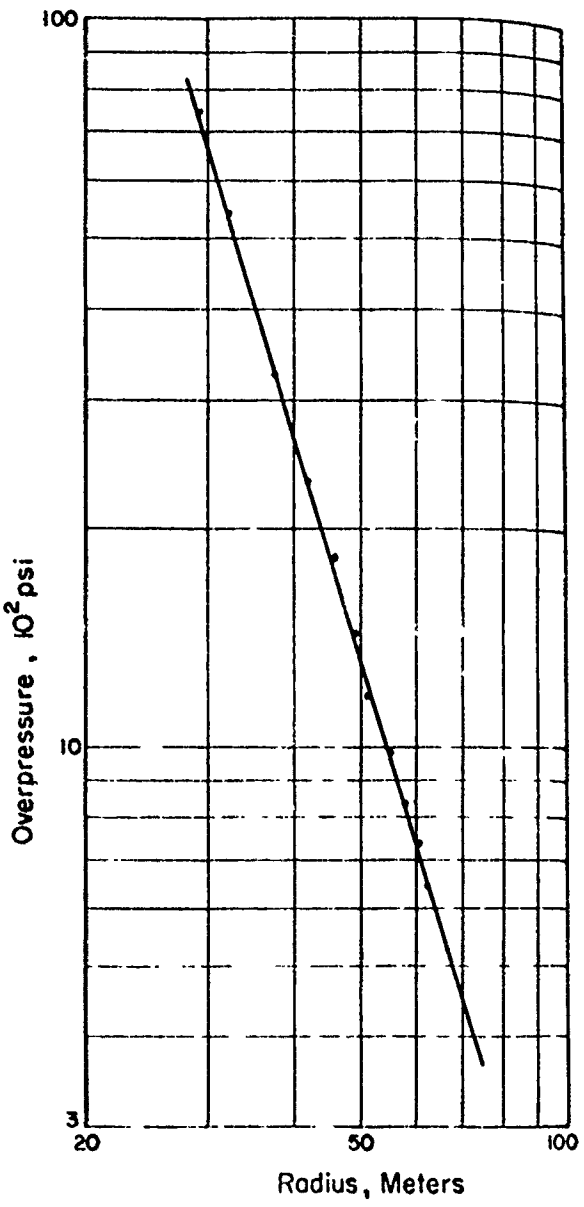

Figure 5.4 Fireball overpressure versus distance, Shot 9 (Wasp').

independent of altitude, is a unique property of Sachs scaling, which has seldom been pointed out in the literature. If an object (such as a missile nose cone) were placed at a distance R from a detonation of yield W at sea level, it would experience the same peak overpressure and dynamic pressure as at the same radius R from a high-altitude detonation of yield W provided the region of interest was high pressure and the change in blast partition of energy was small. It can be shown that at a given distance the overpressure in this high-pressure region is directly

TABLE 5.8 FIREBALL SURFACE CONDITIONS FOR SHOT 9

U/C_{0H} = shock velocity divided by ambient sound speed, P/P_{0H} = absolute shock pressure divided by ambient air pressure; T/T_{0H} = absolute shock temperature divided by ambient air temperature.

Time	Radius	n	U = n R/t	U/C_{0H}	P/P_{0H}	Overpressure	T/T_{0H}	Temperature
msec	meter		m/msec			psi		K
1	25.0	0.3700	9.25	27.2	960	11,828	44.5	12,700
1.5	29.0	0.3810	7.36	21.65	605	7,438	34.9	9,955
2	32.25	0.3915	6.31	18.58	442	5,428	31.0	8,850
3	37.5	0.3940	4.92	14.50	266	3,263	23.4	6,680
4	42.0	0.3970	4.16	12.27	191	2,338	18.7	5,350
5	45.75	0.4	3.66	10.78	148	1,813	15.9	4,540
6	49.0	0.4	3.27	9.61	118	1,440	13.75	3,925
7	52.25	0.4	2.99	8.79	97	1,184	12.15	3,470
8	55.0	0.4	2.75	8.09	81	986	10.85	3,100
9	57.75	0.4	2.57	7.55	69	839	9.85	2,815
10	60.25	0.4	2.41	7.09	61	739	9.15	2,615
11	62.5	0.4	2.27	6.69	54	643	8.50	2,425

proportional to the blast yield. Overpressure changes in the high-pressure region due to changes in blast partition of energy with altitude can be compensated for by proportional changes in the total yield.

The shock-front temperatures are higher for Shot 10 at a given radius or time than for Shot 9 (Tables 5.7 and 5.8). An object at the same distance from the burst points of Shot 9 and Shot 10 would be engulfed during the fireball phase by higher-temperature air at the shock front of Shot 10. At a radius of 50 meters, the shock-front temperature on Shot 10 was 7,100 K and only 3,700 K on Shot 9.

Using the fireball yields and the computed pressure versus distance values for the high-altitude Shot 10 as criteria, it would appear that the high-altitude fireball was performing in a normal, predictable manner for a 3.3 kt detonation. A continuing history of the shock wave was provided by the smoke trail, smoke puff, canister and ground-blast measurements.

5.3.4 Smoke Trail, Free-Air-Shock Arrival and Pressure Versus Distance for Shot 10.

The smoke trails delivered by jet aircraft on the high-altitude Shot 10 were of poor quality. Useful data were obtained by Project 1.2 using direct observation of the shock front as recorded on film. Arrival-time data (Reference 32) for the shock front are given in Table 5.9 and plotted in Figure 5.5. A comparison of the early-time data in Table 5.9 with the fireball data in Table 5.5 or Figure 5.2 shows the Project 1.2 radii to be generally larger than the EG&G values at a given time.

The arrival-time curve was fitted with an equation which could be differentiated with respect to time to obtain shock velocity versus radius. By substitution of the instantaneous velocities into the Rankine-Hugoniot equations, the peak-shock overpressures were calculated. The

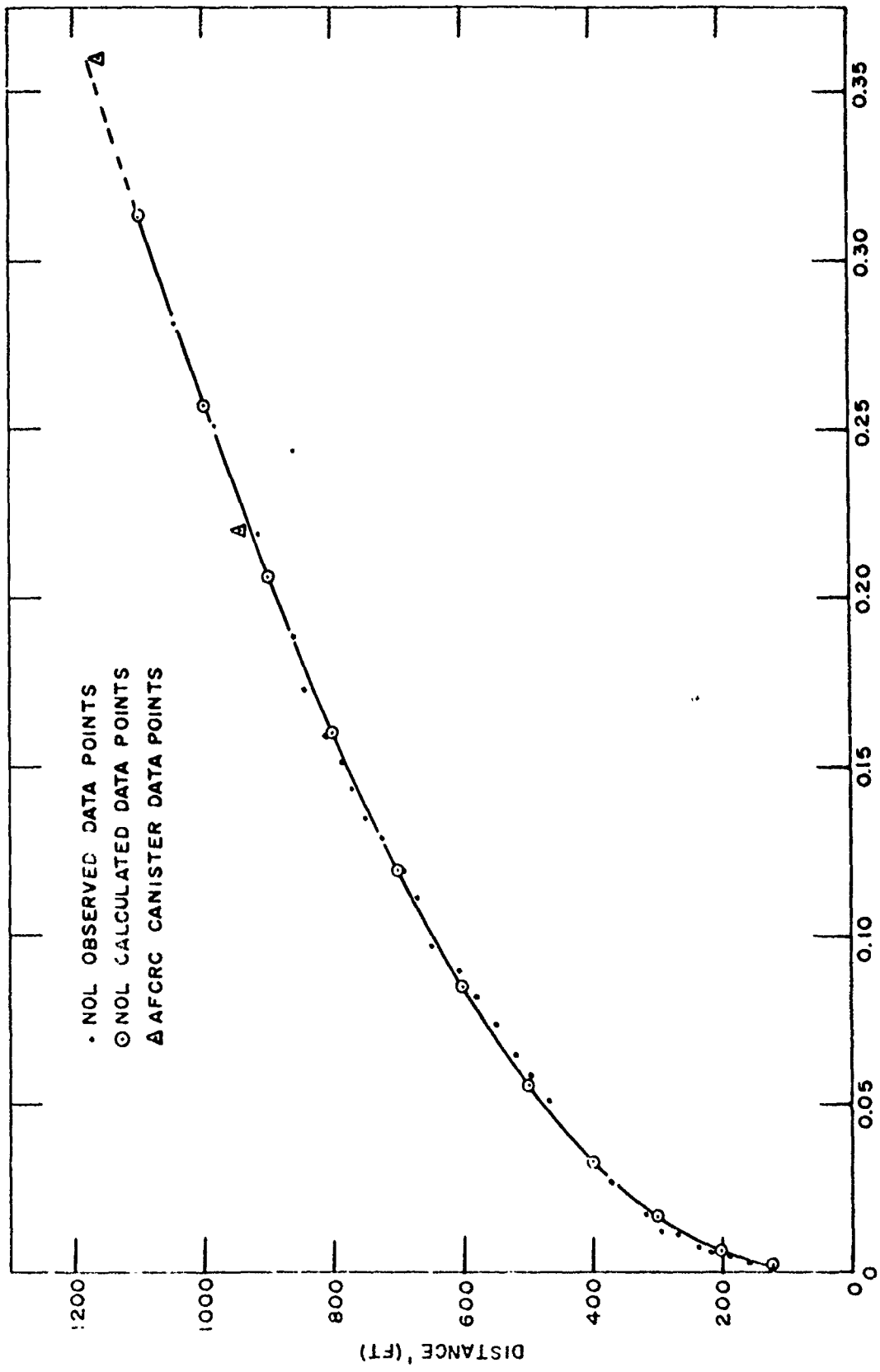

Figure 5.5 Time-of-arrival of free-air incident shock, Shot 10.

peak-shock overpressures as a function of distance are tabulated in Table 5.10 and plotted in Figure 5.6. Also plotted in Figure 5.6 are some of the Project 1.1 canister pressure versus distance data. Generally, the canister pressures were slightly less than the smoke-trail data in the region of overlap.

5.3.5 Canister, Shock Arrival and Pressure Versus Distance for Shot 10. Project 1.1 canisters were deployed from the drop aircraft and their positions with respect to a ground coordinate system were determined by EG&G (Reference 33) at zero time and at shock-arrival

TABLE 5.9 SMOKE TRAIL — SHOCK ARRIVAL, SHOT 10

Radius	Time	Radius	Time
ft	sec	ft	sec
123.400	0.001550	609.179	0.089540
157.700	0.003150	646.934	0.097390
188.500	0.004750	671.423	0.111290
215.300	0.006400	690.811	0.119090
235.200	0.007950	725.504	0.128440
267.400	0.011050	749.994	0.134590
295.916	0.012590	770.402	0.143890
318.365	0.017290	785.708	0.151590
372.446	0.026940	810.198	0.159290
467.343	0.050440	842.850	0.172340
496.935	0.058240	861.218	0.188740
520.404	0.064490	914.278	0.219440
551.016	0.073890	981.625	0.251440
581.628	0.081890	1,044.890	0.280940

time. Since the shock wave, as well as the canisters, moved horizontally with the ambient wind, the effective canister-slant ranges at shock-arrival time were taken with reference to a coordinate system moving with the wind. The peak overpressures were corrected according to the Ballistic Research Laboratories' (BRL) shock-tube calibration. The canister data (Reference 34) are given in Table 5.11. Modified Sachs scaling has been used to reduce the peak overpressures and slant ranges to equivalent values at shot altitude using the meteorological data at shot time (Table 5.2). The canister pressure versus distance data are plotted in Figure 5.7.

5.3.6 Smoke-Puff Measurements on Shot 10. A circular pattern of smoke puffs was ejected from a canister about 1,000 feet from the burst point. The smoke puffs at various distances from the burst were photographed from the ground. Displacement time was recorded (Reference 35) for four of the smoke puffs. Although the results were not entirely satisfactory, the smoke puff-displacement times were smooth and indicated nothing abnormal, such as secondary shocks, in the positive phase. There appeared to be a discrepancy between the burst-point coordinates obtained by this project and the EG&G coordinates.

5.3.7 Overpressure Measurements on the Ground for Shot 10. Project 1.3 made overpressure measurements (Reference 36) in the millibar range on the ground. Modified Sachs scaling of the data resulted in a reasonable extension of the pressure versus distance curve derived from all shots. Propagation of the shock wave over a long distance of varying atmosphere can be predicted fairly well.

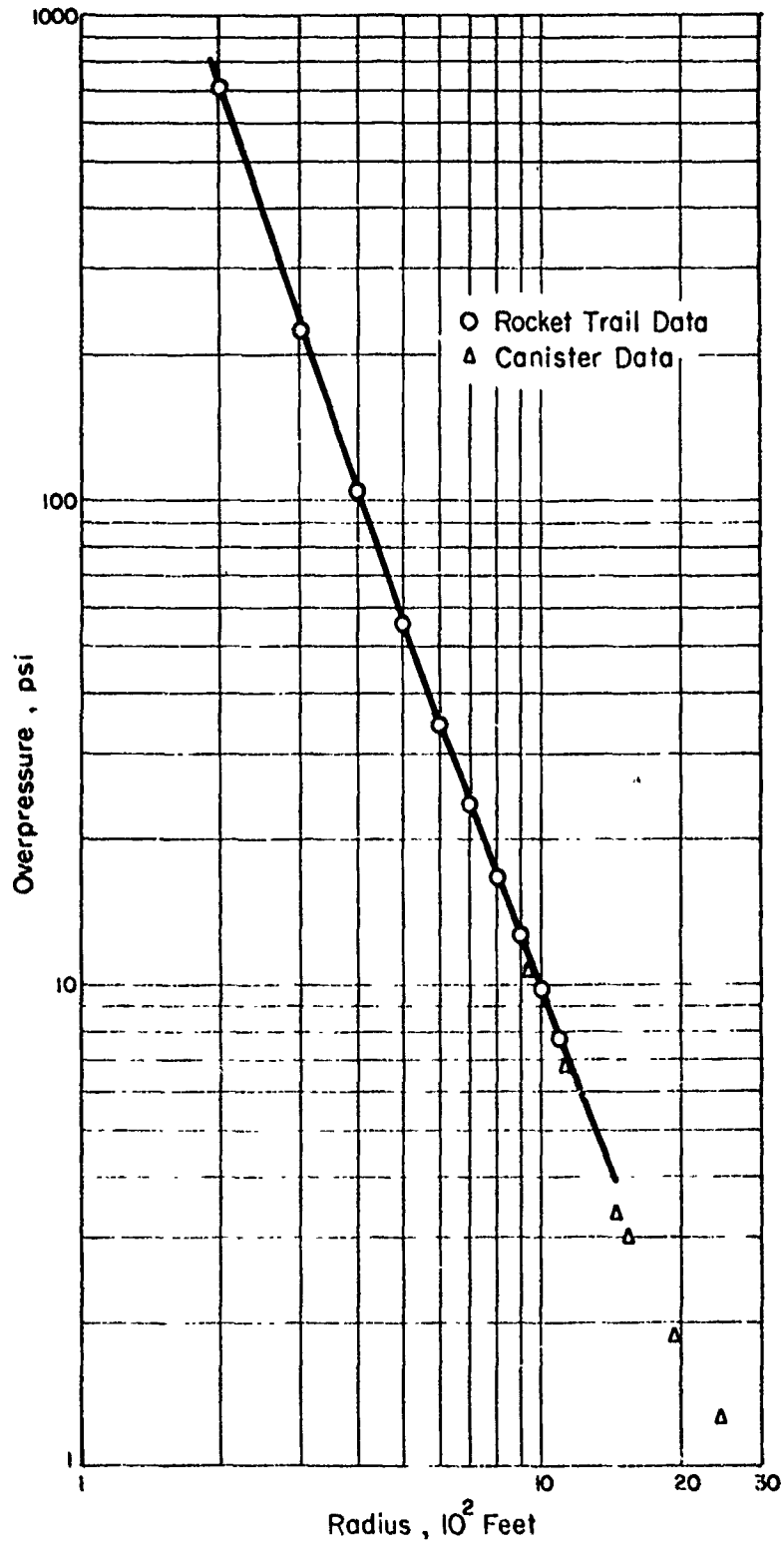

Figure 5.6 Smoke trail overpressure versus distance, Shot 10 (HA).

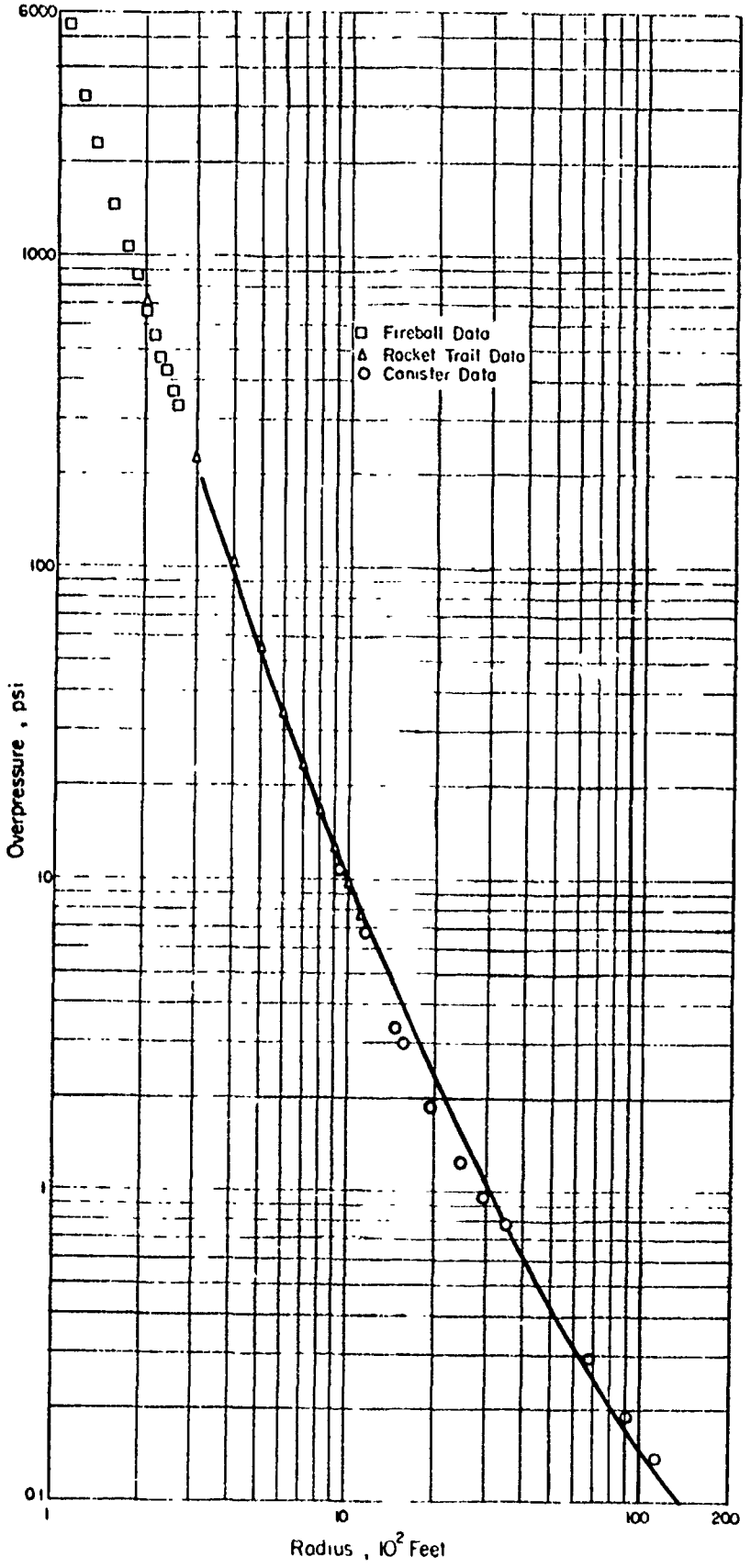

Figure 5.7 Overpressure versus distance, Shot 10 (HA).

5.3.8 Blast Summary for Shot 10. The shock overpressure versus distance values as obtained by various methods and projects are presented in Figure 5.7. The current 1 kt free-air pressure versus distance curve (Reference 22) has been Sachs scaled to Shot 10 burst conditions and 3.3 kt for comparison with the data points. The overpressures obtained by computa-

TABLE 5.10 SMOKE TRAIL PRESSURE, VELOCITY, DISTANCE DATA FOR SHOT 10

Radius	Shock Velocity	Peak Overpressure
ft	ft/sec	psi
200	13,098	712
300	7,478	225
400	5,124	104
500	3,884	55.7
600	3,137	34.5
700	2,647	23.5
800	2,306	16.8
900	2,056	12.7
1,000	1,867	9.8
1,100	1,720	7.7

TABLE 5.11 CANISTER DATA, SHOT 10

Canister Number	Radius	Overpressure	Arrival Time*	Duration*
	ft	psi	sec	sec
1	641	—	—	—
2	719	—	—	—
3	914	—	—	—
4	936	10.80	0.220	—
5	1,155	6.75	0.359	0.304
6	1,461	3.37	0.570	0.392
7	1,548	3.00	0.630	0.425
8	1,940	1.88	0.941	0.466
9	2,463	1.27	1.380	0.525
10	2,938	0.96	1.810	0.576
11	3,524	0.790	2.338	0.670
12	3,934	—	2.680	—
13	6,790	0.293	5.495	0.806
14	9,050	0.190	7.830	0.906
15	11,310	0.139	10.244	0.986

* The shock arrival time and duration were not modified Sachs scaled to burst altitude.

tion and measurement for the high-altitude Shot 10 were consistent with predicted values for a 3.3 kt detonation in the ambient atmosphere which prevailed. None of the blast measurements was of sufficient accuracy to warrant a conclusion of any variation of ordinary blast partition of energy on Shot 10. From Figure 5.7 it can be concluded that no large change in blast partition of energy occurred. The blast was certainly performing more nearly like a 3.3 kt detonation than a 2.5 kt or 4.0 kt detonation.

5.4 THERMAL RADIATION

5.4.1 Atmospheric Attenuation. Attenuation coefficients for both Shot 10 and Shot 9 were obtained by Project 18.2 (Reference 37). The attenuation coefficient β is defined by the relation

$$i = i_0 e^{-\beta d} \tag{5.7}$$

where i is the intensity of light transmitted by the atmosphere, i_0 is the intensity that would be observed without the atmosphere, and d is the length of the atmospheric path in statute miles. For a horizontal optical path, such as existed on Shot 9 to each of the thermal stations, d is the actual length of the path. The attenuation coefficient for Shot 9 was obtained from the visibility of Mount Charleston and reported (Reference 37) to be 0.078/mile.

The attenuation coefficient for a slant path through a varying ambient atmosphere to the thermal stations on Shot 10 was somewhat more complicated. The attenuation coefficient for scattering of visible light was determined (Reference 37) for the total-vertical atmosphere on the day of Shot 10. The scattering attenuation coefficient (β) was found to be 0.053/mile for the atmosphere reduced to normal temperature and pressure (NTP). Equivalent thicknesses of the atmosphere at NTP are given in Table 5.12 above pertinent elevations.

For thermal measurements obtained at a slant distance, the equivalent vertical thickness was increased by the cosecant of the angle between the horizontal and the burst position, and the attenuation coefficient (β) was a constant 0.053/mile. The optical path from Shot 10 to ground zero was 3.26 NTP miles; hence the fraction of visible light transmitted over this path was 0.84 using Equation 5.7. Similarly, the optical path between the drop aircraft (slant range 21,500 feet and burst point was 0.905 NTP mile giving a transmission of 0.954 for visible light over this path. The total vertical atmosphere, on the day Shot 10 was fired, would transmit 0.78 of the entering visible sunlight. The above data are found to be useful in the next section.

5.4.2 Thermal Yields for Shots 1, 9, and 10. Project 8.4 measured total radiant energy, using calorimeters (Reference 25). The results are summarized in Table 5.13. The total radiant energy Q measured at a distance R from a nuclear detonation can be expressed by

$$Q = \frac{(\lambda W)}{4\pi R^2} e^{-\beta d} \tag{5.8}$$

where λ is the fraction of the total yield W that is emitted as thermal energy. The attenuation coefficient β and optical path d were discussed in the previous section. The thermal yield (λ W) for Shot 9 was about 1.28 kt, or since the yield (W) was 3.16 kt, the fraction of energy (λ) emitted as thermal radiation was 0.40. The thermal yield (λ W) for Shot 10 was, however, only about 0.95 kt and the fraction emitted as thermal radiation was 0.29. This represents a major change in the thermal partition of energy. There is some uncertainty in the thermal measurements; however, this change is large and thought to be real. The maximum relative error between Shot 9 and Shot 10 values is estimated to be 10 percent, which is less than the observed 30 percent difference in the measured values.

Thermal energy emitted before the time of the minimum is given in Table 5.14. The data indicate an increase from Shot 9 to Shot 10 in the percentage of total thermal energy released before the thermal minimum. Although the percentage of total thermal energy released before the thermal minimum was larger for Shot 10 than for Shot 9, the actual amount of energy emitted was nearly the same, since the total thermal yield for Shot 10 was less than for Shot 9.

TABLE 5.12 AMOUNT OF ATMOSPHERE ABOVE SELECTED POINTS FOR SHOT 10

Altitude	Pressure	Fraction of Atmosphere Above	Equivalent Thickness At NTP
ft	mb		mile
Sea level	1,013	1.00	5.00
4,038, Ground Zero	883	0.872	4.36
4,125, Stations 400, 410	880	0.869	4.34
36,620, Burst point	222	0.219	1.10
46,000, Aircraft	143	0.141	0.705

TABLE 5.13 TOTAL RADIANT ENERGY VERSUS DISTANCE, SHOTS 1, 9 AND 10

Shot	Q Measured	Slant Range	Station	Transmission	Thermal Yield	Thermal Yield / Total Yield
	cal/cm^2	ft			kt	
1	6.83	2,428	—	—	0.52	0.45
9	17.3	2,397	—	—	1.29	0.41
9	6.66	3,808	—	—	1.27	0.40
10	0.17	21,500	B-36	0.95	0.96	0.29
10	0.0606	32,565	Ground Zero	0.84	0.89	0.27
10	0.0284	47,175	410	0.78	0.95	0.29

TABLE 5.14 PERCENT OF TOTAL THERMAL ENERGY RELEASED BEFORE MINIMUM

Project	Instrument	Shot 1	Shot 9	Shot 10
		pct	pct	pct
8.4f	Bolometer	0.47	0.63	1.2
18.2	Bolometer	—	0.7	0.9

5.4.3 Time to Thermal Minimum and Yield. The Mark V bhangmeter was the primary EG&G instrument used on Operation Teapot to record time to the light minimum. The time to the light minimum is a function of the wave length of light, hence, different types of instruments (bhangmeters, radiometers, and bolometers) give different times for the minimum for the same shot due to different spectral sensitivities. The time to light minimum obtained by the bhangmeter has been used to obtain an early value of yield. The present relationship (Reference 38) for yield W(kt) dependence on time to the light minimum t_{min}(msec) is

$$W = 0.09\, t^2_{min} \tag{5.9}$$

Shots 1 and 9 were identical weapons except for yield and Shots 9 and 10 were nearly the same except for different ambient atmospheres. The data for these three shots are given in Table 5.15. The yield obtained by time to thermal minimum for Shots 1 and 9 agreed well with the radiochemical yield. However, the yield obtained for Shot 10 by time to thermal minimum

TABLE 5.15 TIME TO THERMAL MINIMUM AND YIELD

Shot	t_{min}	Yield kt	Radiochemical Yield
	msec	$0.09t^2$	kt
1	3.5 ± 0.2	1.10	1.16 ± 0.03
9	6.0 ± 0.2	3.24	3.16 ± 0.16
10	5.4 ± 0.2	2.63	3.3 ± 0.4

was poor. It is concluded that Equation 5.9 should have a dependence on ambient air conditions to account for Shots 9 and 10 difference in time to thermal minimum for nearly the same yield. If ambient air density is assumed to be the correct quantity for such a dependence, Equation 5.9 becomes

$$W = 0.09\, (\rho_{\phi H})^{-0.22}\, t^2_{min} \tag{5.10}$$

where $\rho_{\phi H}$ is the ambient air density in grams per liter at the altitude H of the detonation.

5.4.4 Late Stage Fireball Diameter and Time of Second Thermal Peak. After the shock front expands and is not of sufficient strength to render the air luminous (Section 5.3.2) the shock front leaves the luminous air behind. The time at which this occurs is called breakaway. The luminous fireball diameter-time data (Reference 39) for Shots 1, 9, and 10 are given in Figure 5.8. Shots 1 and 9 were nearly identical devices detonated under similar ambient conditions, but having different yields. Shots 9 and 10 had nearly identical yields though detonated under different ambient conditions. It is observed that the difference in atmosphere (factor of three in density) caused about as much change in the sizes of the fireballs of Shots 9 and 10, as a factor of three in yield changed the sizes of the fireballs of Shots 1 and 9.

The time of the light minimum for each of the shots (data from Section 5.4.3) is plotted in Figure 5.8. Times for the second light peaks were obtained with blue sensitive (S-4 surface) photocells. The light recorder responds to total light output and not to surface brightness. The measured times to second peaks were:

Shot 1 ..... 57 msec ± 5 msec
Shot 9 ..... 68 msec ± 3 msec
Shot 10..... 41 msec ± 3 msec

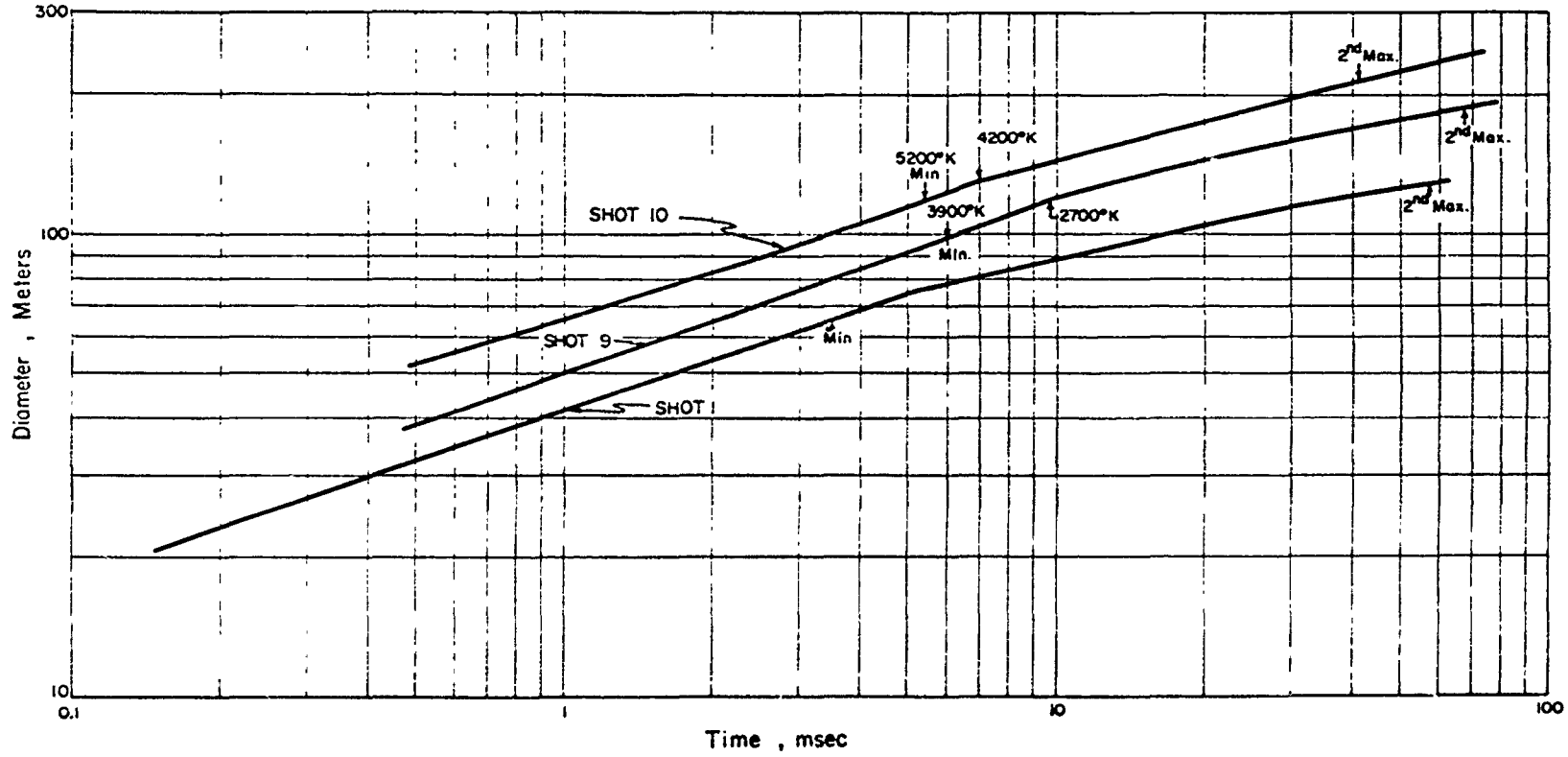

Figure 5.8 Fireball diameter time and thermal characteristics.

The fireball diameters at the time of the second light peak were:

Shot 1 ..... 128 meters ± 2 meters
Shot 9 ..... 186 meters ± 3 meters
Shot 10..... 207 meters ± 8 meters

The luminous fireball of Shot 10 was larger than Shot 9 at the time of the second peak principally because of the reduced atmosphere on Shot 10. Assuming that ambient density was the appropriate ambient condition, the scaling of the diameter of the fireball at time of second peak can be obtained from the foregoing data:

$$\frac{\text{Diameter Shot 9}}{\text{Diameter Shot 1}} = \left(\frac{\rho_1}{\rho_9}\right)^n \left(\frac{W_9}{W_1}\right)^m$$

and

$$\frac{\text{Diameter Shot 10}}{\text{Diameter Shot 9}} = \left(\frac{\rho_9}{\rho_{10}}\right)^n \left(\frac{W_{10}}{W_9}\right)^m$$

Substitution of the diameters at second peak, the ambient densities and the yields leads to a solution that n is about 0.10 and m is about 0.4. These data lead to the following equation for the radius of the fireball at the time of the second light peak:

$$\text{Radius (feet)} = 190\ \rho_0^{-0.1}\ W^{0.4} \qquad (5.11)$$

where the ambient density ρ_0 is in gram per liter and W is the yield in kilotons.

Shock-front temperatures at the surface of the fireball were calculated for Shots 9 and 10 (Section 5.3.3). Shock-front temperatures at the time of the minimum and breakaway are given in Figure 5.8.

5.4.5 Radiant Power Versus Time for Shots 9 and 10. Radiant power versus time plots obtained by Projects 8.4 and 18.2 for Shots 9 and 10 are given in Figures 4.1, 4.2, 4.3, and 4.4. Some pertinent time characteristics and ratios of radiant power are given (Reference 40) in Table 5.16. For comparison, the data for Shot 1 are also included in Table 5.16. These data were obtained with a high-time resolution bolometer instrument. Some of the time characteristics are different from the bhangmeter and photocell values (sections 5.4.3 and 5.4.4) because of different spectral sensitivities.

It is particularly important to note that the total thermal energy in Table 5.16 has been normalized to 10.3 miles in a vacuum for Shots 1, 9, and 10 using measured total thermal energies and attenuation factors. Due to loss of important bolometer data on Shots 1 and 9, the total thermal energies for these shots were the calorimetric data. The total thermal energy for Shot 10 was obtained by the bolometer. Contrasted with the results of Section 5.4.2 that Shot 10 had less thermal yield than Shot 9, from the bolometer data it would be concluded that Shot 10 had a slightly larger thermal yield than Shot 9.

5.4.6 Spectra for Shots 9 and 10. Low-resolution spectroscopy was reported (Reference 37) by Project 18.2 on Shots 9 and 10. The early first-maximum spectra obtained on Shot 9 show radiation absorption due to the following compounds: HNO_2, NO_2, O_3, and weak Schumann-Runge O_2. Corresponding spectra for Shot 10 show no absorption due to HNO_2, NO_2, or O_3 but only to Schumann-Runge O_2. This was the major difference spectrawise between Shots 9 and 10. The fact that HNO_2 was not present on Shot 10 was probably because of the low water-vapor content of the cold ambient air (−47.8 C). Most of the early NO_2 was formed beyond the fireball front, hence

NO_2 was all converted to N_2O_4 which has a continuous absorption spectrum. The reason for the absence of O_3 on Shot 10 is not definitely known, but may be due to the reduced probability of the formation of molecules involving multiple collisions at the reduced ambient air density (one-third of Shot 9) on Shot 10.

The second phase of the spectral history, which begins after the thermal minimum and persists until 5 to 15 msec after the second maximum (i.e., 70 to 80 msec), is nearly identical in both shots and consists of absorption due to CN, N_2, N_2^+, and Schumann-Runge O_2.

The third phase of the spectral history, which begins at about 80 msec after time zero and

TABLE 5.16 RADIANT POWER CHARACTERISTICS FOR SHOTS 1, 9, and 10

Quantity	Shot 1	Shot 9	Shot 10
Time 1st max, μ sec	210	140	225
Time min, msec	3.3	6.2	4.5
Time 2nd max, msec	44	69	42.5
Total energy, cal/cm^2 at 10.3 miles	0.0054	0.02	0.025
Power 1st max, cal/cm^2/sec	0.054	0.24	0.29
Power min, cal/cm^2/sec	0.0079	0.009	0.031
Power 2nd max, cal/cm^2/sec	0.052	0.13	0.26
Energy 1st pulse/total energy	0.0047	0.0063	0.012

persists through the end of the spectra, consists of the same gases present in the second phase except that now they are present in emission instead of absorption.

Unfortunately, the high-resolution spectra were lost on Shot 10, but this is not as serious as it would have been if new, unidentified structure had appeared in the low resolution films.

The significant difference between Shot 9 and Shot 10 spectra is the absence of HNO_2, NO_2, and O_3 in Shot 10 during the early spectra before the thermal minimum. Further, the amount of energy in the ultraviolet during second thermal pulse is significantly larger on Shot 10 when compared with Shot 9.

5.4.7 Rise of the Nuclear Cloud. The rise of the hot fireball is essentially a measure of the residual heat (thermal energy) at that time. The data (Reference 41) on rise of the nuclear clouds for Shot 9 and Shot 10 are given in Table 5.17. It is noted from Table 5.17 that the Shot 9 and Shot 10 nuclear clouds rose at about the same rate for the first 3 minutes; after the first 3 minutes, the Shot 9 cloud rose through larger distances than the Shot 10 cloud. Since the temperatures of the ambient atmospheres and the lapse rates of the atmospheres were different for Shot 9 and Shot 10, the rise of the nuclear clouds was only a rough index of the latent heat (unradiated energy). It is doubtful that an analysis could be made of the rise of the nuclear clouds with sufficient accuracy to conclude that Shot 10 carried off in the rising cloud the remaining thermal energy which would account for the difference in total thermal energy radiated during Shot 9 and Shot 10 (Section 5.4.2).

5.5 INITIAL NUCLEAR RADIATION (GAMMAS AND NEUTRONS)

5.5.1 Instrumentation. The nuclear devices for Shots 1 and 9 had the same ballistic cases, same size high-explosive spheres, and were detonated as air bursts in nearly the same ambient atmospheres. Shots 1 and 9 had different amounts of fissionable materials, hence different yields, in otherwise similar devices. Shots 9 and 10 were essentially identical nuclear devices (same high-explosive spheres, and amounts of nuclear material) in slightly different ballistic cases. Shot 9 was detonated at 4,933 feet MSL and Shot 10 was detonated at 36,620 ± 100 feet

MSL. The gamma-radiation instruments consisted of film dosimeters, ion chambers and chemical dosimeters. Neutron detectors consisted of gold, sulfur, and fission-threshold detectors for measuring both neutron exposures and neutron-energy spectra. On Shot 10, the nuclear-radiation instruments were placed, with the blast instruments, in the 15 parachute-borne canisters. The canisters were deployed on Shot 10 from the same aircraft that dropped the nuclear device. On Shots 1 and 9, canisters containing some of the nuclear-radiation instruments were placed on the ground at various distances from ground zero to account for the shielding effects of the canisters on the nuclear-radiation measurements.

5.5.2 Initial Gamma Radiation. The initial gamma radiation versus distance data for Shots 9 and 10 are given in Table 5.18. The Evans Signal Laboratory (ESL) film-badge data (Reference 13) have been corrected for the effect of neutrons measured at the same location. Gen-

TABLE 5.17 RISE OF THE NUCLEAR CLOUD

Time	Shot 9		Shot 10	
	Cloud Height	Rise	Cloud Height	Rise
minute	ft MSL	ft	ft MSL	ft
0	5,000	0	36,600	0
0.5	9,360	4,360	—	—
1.0	13,010	8,010	42,800	6,200
2.0	16,320	9,320	47,100	10,500
3.0	18,740	13,740	50,100	13,500
4.0	22,110	17,110*	52,100	15,500
5.0	24,140	19,140	53,200	16,600
6.0	26,120	21,120	54,200	17,600
7.0	27,950	22,950	54,800	18,200
8.0	29,370	24,370	—	—
Stable	31,740	26,740	57,000	20,400

erally, the corrected film-badge data have smaller exposure readings than the chemical-dosimeter data at the same distance. The canisters on Shot 10 were not at the same altitude as the burst, but were generally at a higher altitude depending upon the canister number. The distances of the canisters in Table 5.18 are their actual distance at time zero. The Shot 10 data were normalized (Reference 13) to an air density of 1 gm/liter using the mean density between the burst point and canister position at zero time. Shot 9 and Shot 10 gamma-exposure data (exposure times distance squared versus distance) normalized to air-density of 1 gm/liter are given in Figure 5.9. It must be concluded that when all corrections are made to the data, Shot 9 and Shot 10 gamma exposure versus distance data do not exactly scale. The basic cause for the difference is the modification of the Shot 9 data by the ground. Shot 1 and Shot 9 data were not free-air gamma exposures; rather they were gamma rays, measured at the ground-air interface, which were modified from the free-air values because of the reflection and energy spectra changes of the gamma rays, as well as neutron interactions with the ground (induced gamma activity in aluminum, manganese, and sodium).

The usual equation for gamma radiation is

$$r = Se^{-\frac{\bar{\mu}D}{D^2}} \qquad (5.12)$$

where: r = roentgens

S = source strength

$\bar{\mu}$ = apparent linear absorption coefficient for hetroenergetic radiation

D = slant distance between source and receiver (usually in yards)

The various values for the quantities in Equation 5.12 for Shots 1, 9, and 10 are given in Table 5.19. It is noted that the source strength (S) for Shot 10 is about twice as large as Shot 9 on a

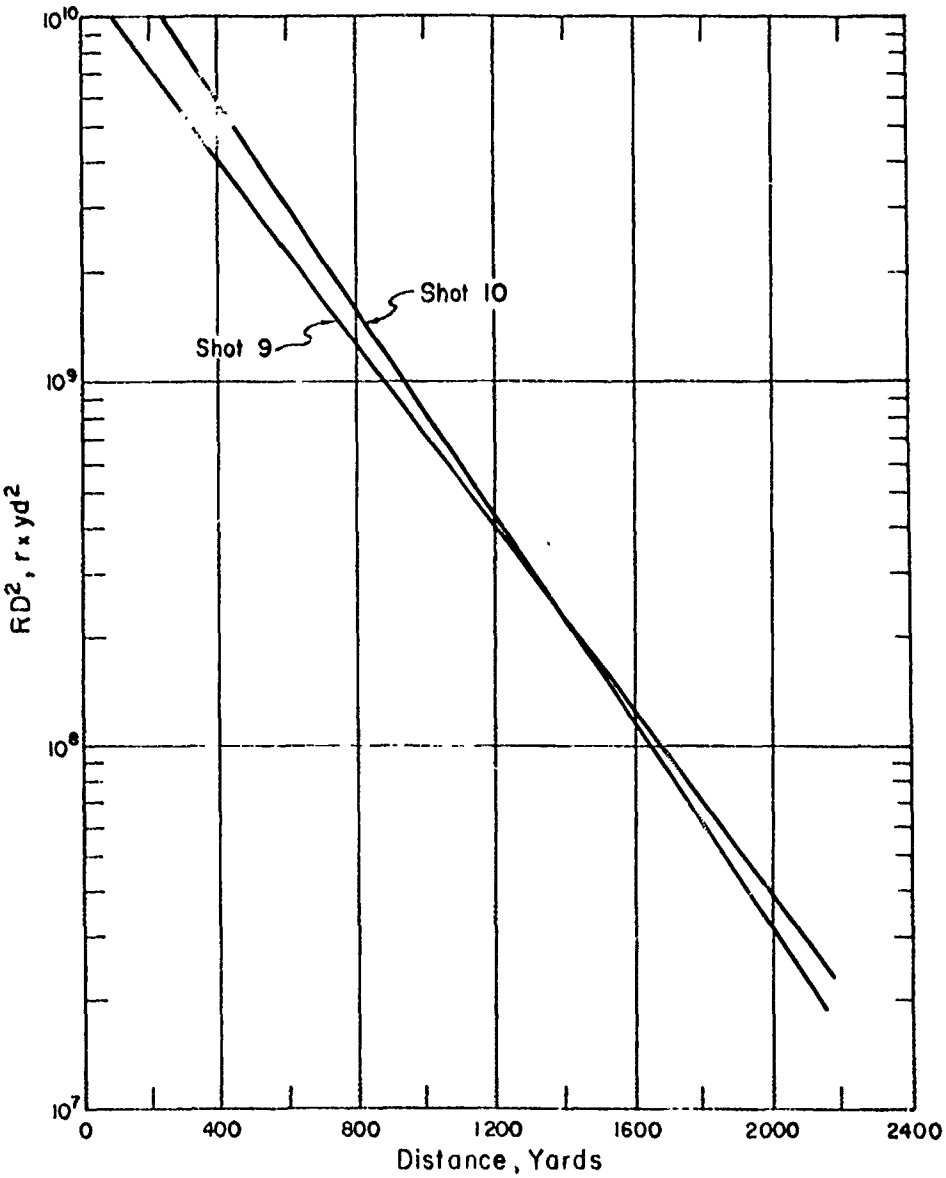

Figure 5.9 Normalized RD^2 versus D for comparison of Shots 9 and 10.

kiloton basis. The apparent mass-absorption coefficient (cm^2/ gm) would normally be a constant, if the energy spectrum of the gamma rays were similar.

TABLE 5.18 GAMMA-EXPOSURE VERSUS DISTANCE, SHOTS 9 AND 10

Shot 9			
Distance	Exposure	Distance	Exposure
yd	r	yd	r
280	70,000 *	1,154	242 *
380	28,500 *	1,161	300 *
461	16,000 *	1,225	225 *
522	10,000 *	1,252	161
603	6,300 *	1,333	140 *
709	3 200 *	1,349	106
837	1,500 *	1,449	69
943	800 *	1,546	46
997	660 *	1,646	29
1,044	580 *	1,744	19
1,098	410 *	1,844	14

Shot 10			
Canister	Distance	ESL †	Project 39.7 *
No.	yd	r	r
3	305	--	187,000
4	315	—	—
5	393	—	108,000
6	500	—	60,400
7	533	—	44,000
8	677	20,810	26,000
9	890	9,825	15,000
10	1,037	6,850	7,550
11	1,240	4,401	5,000
12	1,393	—	3,200
13	2,460	257	400
14	3,340	69	90
15	4,227	23	—

* Chemical dosimeter data (from Project 39.7 dosimeters provided by S. Sigoloff, School of Aviation Medicine, Randolph Field, Texas).

† Evans Signal Laboratory film badge data.

TABLE 5.19 GAMMA RADIATION SUMMARY

Shot	Yield	S Zero Intercept	S/kt	Apparent Mean Free Path	Air Density	Apparent Mass Absorption Coefficient
	kt	rD^2		yd	gm/liter	cm^2/gm
1	1.16	2.3×10^9	2.0×10^9	365	1.107	0.027
9	3.16	13.0×10^9	4.1×10^9	331	1.036	0.0318
10	3.3	24.0×10^9	7.3×10^9	934	0.3435	0.0341
A *	1	1.7×10^9	1.7×10^9	423	1.03	0.0250

* 1 kt values in TM 23-200, revised 1957.

5.5.3 Neutron Fluxes, Shots 9 and 10. Neutron flux measurements were obtained by Project 2.2 (Reference 14). Slow neutron-flux data obtained by activation of gold giving an integrated neutron flux below the cadmium cut-off at about 0.3 ev for Shots 9 and 10 are given in Figure 5.10. Data for Shot 10 has been corrected for air-density differences at canister altitudes and the burst point. Shot 10 slow-neutron values show wide fluctuation for all detectors at close range. Shot 9 slow-neutron data show the influence of the ground at small slant ranges in the form of

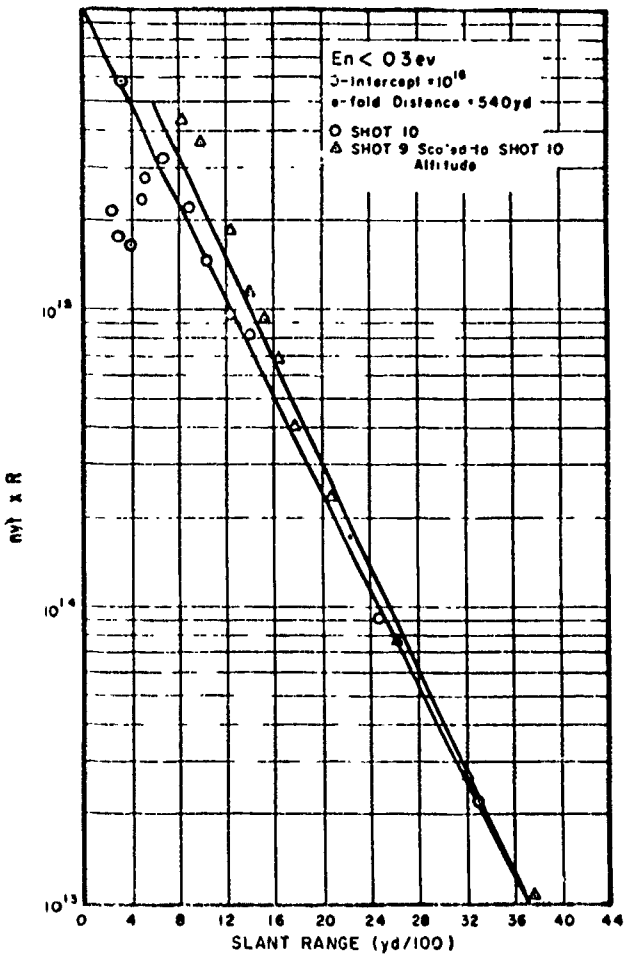

Figure 5.10 Shot 10, slow neutron data and Shot 9 scaled to Shot 10 altitude (nvt × R versus R).

more slow neutrons than would be expected by extrapolation of the data at large slant ranges to smaller distances. Generally, the scaling of the slow-neutron data is only fair even when the influence of the ground on Shot 9 is taken into account (Figure 5.10).

Fast neutron-flux data obtained by sulfur activation (threshold at about 3 Mev) are given in Figure 5.11.

Shot 9 data scaled to Shot 10 ambient conditions results in a fast-neutron curve having a different slope and different zero intercept. Differences in ambient density at the canisters and Shot 10 altitude have been taken into account. As in the case of slow neutrons, the fast-neutron data for Shots 9 and 10 scale only fairly well.

The use of threshold detectors in the intermediate-energy range makes possible the computa-

tion of a neutron spectrum at a given distance, as shown in Figure 5.12. Generally, the Shot 9 and Shot 10 data scale reasonably well and the neutron-energy spectra are similar. A Watt spectrum (normalized at 1 Mev) for neutrons from thermal fission does not fit the observed bomb-fission-neutron data. The neutron fluxes in the intermediate energy region are surprisingly high and are important in dose calculations.

A comparison of Shots 1, 9, and 10, as neutron sources, is given in Table 5.20. Since the zero intercepts (Figures 5.10 and 5.11) are not the same, Shots 9 and 10 appear to be different neutron sources for slow, intermediate, and fast neutrons. Generally, Shot 9 appears to have about twice as many neutrons as Shot 10. This is to be compared with the observation that Shot

TABLE 5.20 SHOTS 1, 9 AND 10 AS NEUTRON SOURCES

Shot	Yield	O-Intercept Fast Neutrons	Fast Neutrons Per kt	O-Intercept Slow Neutrons	Slow Neutrons Per kt
	kt				
1	1.16	1.1×10^{17}	9.5×10^{16}	1.1×10^{15}	9.5×10^{14}
9	3.16	1.5×10^{18}	4.7×10^{17}	2.0×10^{16}	6.3×10^{15}
10	3.3	9×10^{17}	2.7×10^{17}	1×10^{16}	3.0×10^{15}

9 was a weaker gamma source than Shot 10 (Section 5.5.2). The differences in the Shot 9 and Shot 10 zero-intercept values may be due in part to curve fitting of the data, and the differences may not be as large as indicated. The bombing error on Shot 1 was about 437 feet and corrections for the actual slant ranges were not made (Reference 14) for the Shot 1 neutron data. This, only in part, accounts for the fact that Shot 1 and Shot 9 do not scale on a yield basis. It must be concluded that neutrons do not scale in an exact way for devices which differ only in yield.

The number of neutrons at 1,000 yards, as obtained by the threshold detectors, is given in Table 5.21. In the case of plutonium and sulfur, the number of neutrons/cm^2 are all of those above the threshold energy. The gold (Au) value is for the number of neutrons less than the threshold energy. A sum of about 2×10^{13} n/cm^2 is obtained for the Project 2.2 data at 1,000 yards.

It is important to check the neutron results in Table 5.21 since they appear to be an order of magnitude larger than expected. The number of neutrons (n) emitted by a fission weapon of yield Y (kt) is

$$n = 1.45 \times 10^{23} (\nu - 1 - \beta) Y \qquad (5.13)$$

where ν is the average number of neutrons per fission, the (-1) accounts for the neutron producing the fission and β is the non-fission captures. Taking into account previous weapon information the term $(\nu - 1 - \beta)$ is about 1.25 for the Shot 10 type of device. Allowing for spherical divergence and atmospheric attenuation the maximum number of neutrons computed at 1,000 yards from Shot 10 was 2×10^{12} neutrons. It thus appeared that Project 2.2 measured more neutrons by a factor of 10 than would be computed. Perhaps the large number of measured neutrons was due to the flux becoming nearly isotropic. Similarly, the same relatively large number of measured neutrons was obtained for Shots 1 and 9.

5.6 SUMMARY OF HIGH ALTITUDE SHOT 10; BLAST, THERMAL, AND NUCLEAR RADIATION

The blast produced by high-altitude Shot 10 was consistent with a 3.3 kt detonation in the

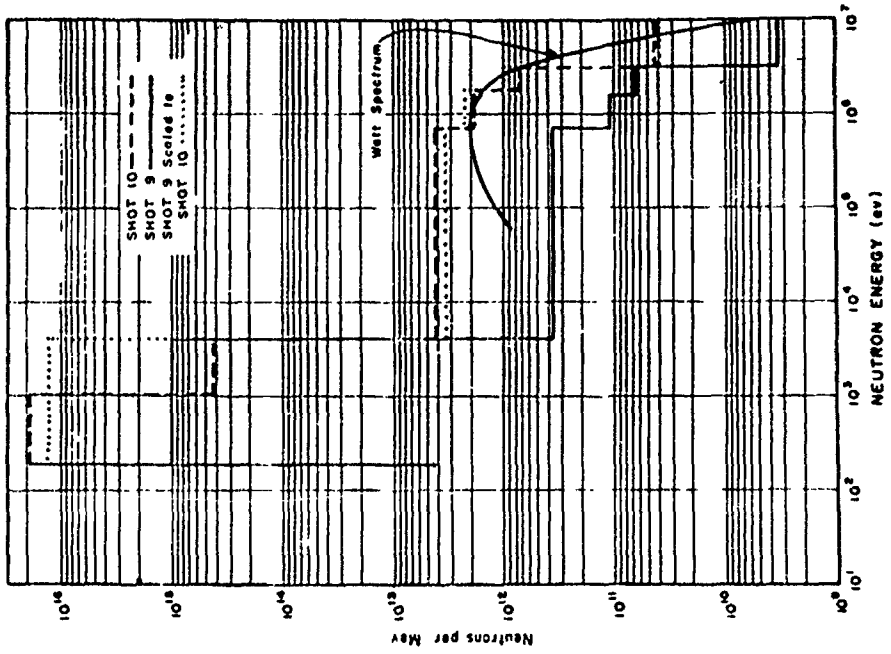

Figure 5.12 Neutron histogram at 1,000 yards.

ambient atmosphere which prevailed. The fireball yield was 3.2 kt using the EG&G method of computation. The pressure versus distance values obtained by computation and measurement, over the range of several thousand psi to tenths of a psi, were consistent with the values that would be obtained using current scaling methods (Sachs scaling) and the present free-air pressure versus distance curve.

The thermal radiation produced by high-altitude Shot 10 was different from a sea-level burst of the same yield. High-altitude Shot 10 had thermal- time characteristics similar to those of a smaller-yield weapon detonated at sea level. The Shot 10 spectra were different

TABLE 5.21 NEUTRONS AT 1,000 YARDS

Threshold Detector	Neutron/cm^2
Pu 1 cm B^{10}, 200 ev	9.5×10^{12}
Pu 1.5 cm B^{10}, 1 Kev	7.0×10^{12}
Pu 2 cm B^{10}, 4 Kev	5.3×10^{12}
S, 3 Mev	3×10^{11}
Au, less than 0.3 ev	1.5×10^{12}

from a sea level burst of the same yield. Generally, Shot 10 appeared to be a hotter device than Shot 9. Although the total-thermal radiation, as measured by the calorimeters (Project 8.4b, NRDL), was less for Shot 10 than Shot 9 by about 30 percent, which is a very significant change, it was found from bolometer data (Project 8.4f, NRDL) that Shot 10 total thermal may have exceeded Shot 9 by a small amount. It cannot be definitely concluded that there was a change in total thermal radiation for Shots 9 and 10.

The gamma-radiation-source strength of Shot 10 appeared to be about twice as large as Shot 9, due in part to different mean-free paths when scaled to the same atmosphere. Shot 9 gamma-radiation measurements were obtained at the ground-air interface and this influence may have resulted in values different from the free-air values obtained during Shot 10.

The neutron measurements indicate that Shot 9 had a neutron-source strength about twice as large as Shot 10, although their yields were nearly the same. It was concluded that the absolute magnitude of the number of neutrons per square centimeter as measured by the threshold detectors for Shots 1, 9, and 10 was larger by an order of magnitude (factor of 10 for Shot 10) than would be computed using only spherical divergence and atmospheric attenuation but neglecting scattering. Atmospheric scattering and hence an almost isotropic neutron flux would account for most of the increase in measured neutrons per square centimeter.

Chapter 6
UNDERGROUND SHOTS

6.1 INTRODUCTION AND BACKGROUND

6.1.1 Operation Buster-Jangle. During the Operation Buster-Jangle test series, two crater-producing 1.2-kt nuclear explosions and a series of four correlating high-explosive (TNT) shots were fired. The centers of the nuclear devices were 3.5 feet above the surface (Jangle S) and 17 feet below the surface (Jangle U). The TNT charges were fired at various depths to investigate the effect of charge depth (particularly on cratering and ground shock) and to investigate a possible high-explosive-nuclear scaling relationship. Three 2,560-pound TNT charges and one 40,000-pound TNT charge were fired. All test shots were detonated in the northern end of Yucca Flat at NTS (Jangle site, or Site 10) within an area where the gross subsurface characteristics were presumed to be uniform.

The Jangle site is dry and granular to the maximum depth of test borings (185 feet), and it is believed that it remains relatively unchanged to substantially greater depths. There is no apparent stratification, but the mass is a heterogeneous caliche composed of gravel and coarse grained and extremely find sand. The soil can be excavated with nearly vertical walls to a considerable depth, indicating that the particles are cemented together or that the grains interlock because of their shape. The direct-shear measurements of the angle of internal friction, ϕ, give a maximun of 58 degrees, a minimum of 37 degrees and a mean of 51 degrees. Typical densities at depths of 2, 3, 4, 10, and 15 feet were 85, 102, 94, 97, and 88 lb/ft^3, respectively.

6.1.2 Project Mole. Following Operation Buster-Jangle, Project Mole was conducted by SRI for the Office, Chief of Engineers (OCE) and AFSWP (AFSWP-291). This project used a fairly large number of 256-pound, center-detonated, spherical TNT charges at different burst positions, both above and below the ground surface. The principal observations were confined to cratering and earth-shock phenomena. Tests were conducted at four different test sites: dry clay, wet sand, wet clay, and the Jangle site. The different test sites permitted an examination of the effects of different soil characteristics, and the Jangle site tests were expected to provide a direct correlation to underground-nuclear-explosion effects. At each site a well-defined effect-of-charge-depth curve for cratering was obtained.

6.1.3 True and Apparent Craters. Throughout Operation Buster-Jangle and the early Mole program, only the apparent craters were reliably measured. Subsequent laboratory experiments by the BRL developed a reliable technique for true crater measurements which was later applied to additional Mole tests at the Jangle site and to the Operation Teapot underground shot. Consequently, the earlier tests permitted no conclusive discussion of true craters at the Jangle site. Due to restrictions imposed by radioactive contamination, the determination of the Operation Teapot true-crater profile by Project 1.6 was necessarily deferred until the fall of 1955. The unique operational characteristics associated with this experimental technique are described in detail in WT-1105 (Reference 42). For the measurements included in this chapter, the reference plane is the original ground level: depth, volume, and radius of the crater were measured at the original ground level.

6.1.4 Scaling and TNT Efficiency. Cube-root scaling has generally been used for the linear dimensions of underground-explosion phenomena. A comparison of the high-explosive and nuclear-crater dimensions and charge depths indicated that direct cube-root scaling in terms of pounds of TNT and kiloton of total-nuclear-energy release was not applicable, with two reasonable possible explanations: (1) the TNT efficiency of nuclear detonations in terms of crater dimensions is considerably less than 100 percent, and/or (2) the proper scaling relationship is greater than cube root: i.e., fourth root or greater.

The TNT efficiency of a nuclear detonation must be defined for the particular parameter being considered. If a nuclear detonation of known total yield, W_1 kilotons, at a depth, D, produces an apparent crater of radius, R, and if it is estimated that W_2 kilotons of TNT at this same depth, D, would produce the same crater radius, R, the TNT efficiency or equivalence of the nuclear detonation is defined as 100 W_2/W_1 in percent. Since extremely large TNT tests are not practical, some scaling relationship must be assumed to calculate the TNT efficiency or equivalence of nuclear test. For cratering, cube-root scaling for linear dimensions is assumed in this chapter.

There is little reason to suggest that the nuclear-TNT efficiency for cratering should be 100 percent. In fact, it is reasonable to assume that it would be substantially less than 100 percent. For instance, for the air blast in the region of principal interest from a free-air burst, the TNT efficiency of a nuclear explosion has been well documented at slightly below 50 percent. Hence, Item (1), noted previously, is not unreasonable. The TNT efficiency and scaling relationships are inextricably related; one cannot be determined without assuming a value for the other, unless absurdly large TNT tests are conducted.

The 40,000-pound high-explosive charge of Operation Buster-Jangle produced a smaller crater than would be estimated from the scaled, 2,560-pound high-explosive charge of Jangle. However, tests using still-larger TNT charges at Dugway did not show any systematic deviation from cube-root scaling, and extensive smaller tests clearly substantiated cube-root scaling. Although there are some analytical treatments to justify fourth-root scaling for some aspects of cratering for very-large explosions, the experimental results are inconclusive and within the known fluctuations of underground tests. Hence, Item (2), noted previously, may be justified but is not substantiated. Cube-root scaling is, therefore, used in this chapter. The principal conclusions following the Jangle and Teapot underground shots were not markedly influenced by the choice between cube-root and fourth-root scaling.

There remained the question of the effect of depth on the TNT efficiency of nuclear explosions, important in applying TNT test results to estimate the effects of nuclear weapons. Regardless of the scaling law chosen, the cratering TNT efficiency was much less for Jangle S than it was for Jangle U. Most studies indicated that still-greater TNT efficiencies would result from greater charge depths, although some studies suggested that depths greater than Jangle U would not result in a significant TNT efficiency increase. The differences between the hydrodynamic and thermodynamic properties for TNT and nuclear explosions suggest that the TNT efficiency will be a function of depth, approaching a constant value as the depth is increased. With the advent of atomic-demolition munition, it was considered necessary to fire an atomic weapon at a depth great enough to eliminate speculation on the amount of benefit, including TNT equivalence, which could be derived from deeper emplacement.

6.1.5 Operation Teapot. The Operation Teapot shot was originally specified to have a yield greater than 10 kilotons with great emphasis on the radioactive fallout as well as cratering, earth shock, and effects on underground targets. The larger yield would permit scaling studies needed to extend the results of Jangle U to larger nuclear weapons. Such scaling effects were particularly desirable in the study of radioactive fallout. However, because of offsite radioactive-fallout limitations, a ceiling of 1.2 kt was placed on underground detona-

tions at NTS. Consequently, the nuclear device chosen for the Operation Teapot underground shot (Shot 7) was a duplicate of those (1.2 kt) used for Jangle S and Jangle U.

Because of the reduced yield, the primary objective of the Operation Teapot underground shot was to determine the effect of charge depth on the crater, with a consequent determination of the effect of charge depth on cratering TNT efficiency. As outlined previously, such information would permit an evaluation of the benefits to be derived from deeper emplacements and would permit the more-general use of small-scale TNT results to estimate the effects of underground nuclear detonations in different locations at different depths. The principal Operation Teapot effort on the underground shot was devoted to measurements of both the true and apparent crater.

Secondary objectives of the Operation Teapot underground shot were to (1) obtain additional fallout and residual radioactive contamination data to give more reliable methods of estimating the nuclear-radiation characteristics of nuclear detonations of different sizes at different depths,[1] (2) obtain additional ground-shock and air-blast data to supplement and extend the Jangle results, and (3) obtain earth-shock loading and response on specialized structures and test devices.

To permit the most-dependable direct correlation with the Jangle U results, the shot point of the Operation Teapot underground shot was located adjacent to the Jangle U crater, at a distance where no interaction was assured. The precise location was chosen to properly utilize some of the underground target structures remaining from Jangle. A charge depth of 67 feet was chosen because it was appreciably greater than that for Jangle U, represented a depth estimated to include most of the TNT efficiency benefits which might accrue from greater depths, and represented a reasonably extreme emplacement depth for operational weapons regardless of the scaling method used.

The Operation Teapot underground shot was extremely well tamped. An elaborate emplacement technique, developed and executed in the field by the U.S. Army Corps of Engineers,[2] provided for essentially complete backfill of both the main emplacement shaft and the access shaft (Reference 42). After arming and insertion, the surrounding air space was filled with sandbags and dirt. There is little doubt that the Operation Teapot underground shot was far-better tamped than was the Operation Buster-Jangle underground shot. On the Jangle shot, substantial air spaces existed around the device, while on Operation Teapot such spaces were nearly nonexistent.

6.1.6 Yield. The yield of the Operation Teapot underground shot (Shot 7) was assumed to be 1.2 kt, although it was not measured by any independent hydrodynamic or radiochemical means. Identical nuclear assemblies were used for Jangle S and Jangle U, which were also assumed to be 1.2 kt each. Analytical considerations resulted in a high reliability for this particular nuclear assembly. Several identical devices have been fired as air bursts with the average measured yield being 1.2 kt, with little variation.

6.2 CRATERING

6.2.1 True Crater. The Engineer Research and Development Laboratories (ERDL) colored-sand-column method, implemented by ERDL on Project Mole in the fall of 1954, es-

[1] The nuclear-radiation results of the Operation Teapot underground shot are reported in Chapter 3.

[2] The field emplacement was accomplished by the 271st Engineer Battalion, U.S. Army, Corps of Engineers, under the overall supervision of representatives of the Engineer School, Ft. Belvoir, Va. Full details are included in WT-1105.

tablished an operational method for determining true crater profiles created by surface and underground explosions. A definition of the true crater as determined by this method is that zone from which material is completely disassociated from its previous position. The rupture zone is characterized, not by this extreme movement, but rather by extreme breaking up and fracture, together with much less mass motion or displacement. Probably a zone previously called true crater, and determined by probing methods, is the extent of the zone of complete rupture. The true crater results from Project Mole showed a trend in which there was less difference between apparent and true craters as the scaled depth of burial was decreased This general trend holds for the crater-radius, depth, and volume measurements.

In preparation for Operation Teapot Shot 7, twenty-one 8-inch-diameter vertical shafts were drilled along one diameter and through ground zero. These holes varied in depth from 50 to 200 feet and were backfilled with colored-sand mix. After the detonation of Shot 7, excavation work to uncover the colored-sand columns could not begin immediately because of the very-high residual-contamination hazard. During the summer of 1955, periodic contamination-level checks indicated that decontamination work would be necessary if the excavation were to proceed during the calendar year 1955. Since this was felt to be desirable, a program was established to use land-reclamation techniques to reduce the radiation hazard to reasonable levels.

The extreme slopes on the side of the crater from Shot 7 were not predicted from previous high-explosive work. This introduced some operational difficulties in excavation. A profile view of the Shot 7 crater (Figure 6.1) indicates the positions of the colored-sand columns after detonation. The top of the central column, when uncovered, was 128 feet below the original ground level, or 61 feet below the center of gravity of the charge. This point defined the depth of the true crater. While excavating for determination of the position of the central column, it was found that the residual-radiation activity dropped abruptly at a depth of about 110 feet below the original ground level. The dimensions of the true crater are included in Table 6.1.

6.2.2 Apparent Crater Results. The apparent crater was measured in considerable detail by aerial mapping techniques using previously placed aerial markers. The crater had steep walls, and occasional slides were observed subsequent to the shot. However, it is felt that these slides had no significant effect on the crater dimensions as reported herein. The crater was remarkably symmetrical, with little difference between several profiles drawn from the aerial contour maps (a slight asymmetry was noted in the southwesterly direction from ground zero). Figure 6.1 shows the general characteristics of the crater, while Figure 6.2 shows an average profile. The principal dimensions are given in Table 6.1; for purposes of comparison, the dimensions of the Jangle U and Jangle S craters are also included in this table. Figure 6.3 shows the Shot 7 crater profile; Figure 6.4 shows the Jangle U crater profile.

From Table 6.1, there is little difference in the radii of the true and apparent craters for Operation Teapot Shot 7 (150 feet versus 146 feet). There was little difference between the true and apparent center radii for Jangle U. In fact, examination of the Jangle U crater side walls has led some observers to conclude that the true and apparent crater radii at the original ground level were coincident. In order to use the Jangle U data for true-crater analysis, it would be reasonable to assume a value of about 133 feet for the true-crater radius at ground level.

6.2.3 Effect of Depth on Cratering. Jangle U and Operation Teapot Shot 7 used presumably identical nuclear devices in close proximity at a location where the gross subsurface characteristics were believed to be quite uniform. The two charge depths of 17 feet and 67 feet gave

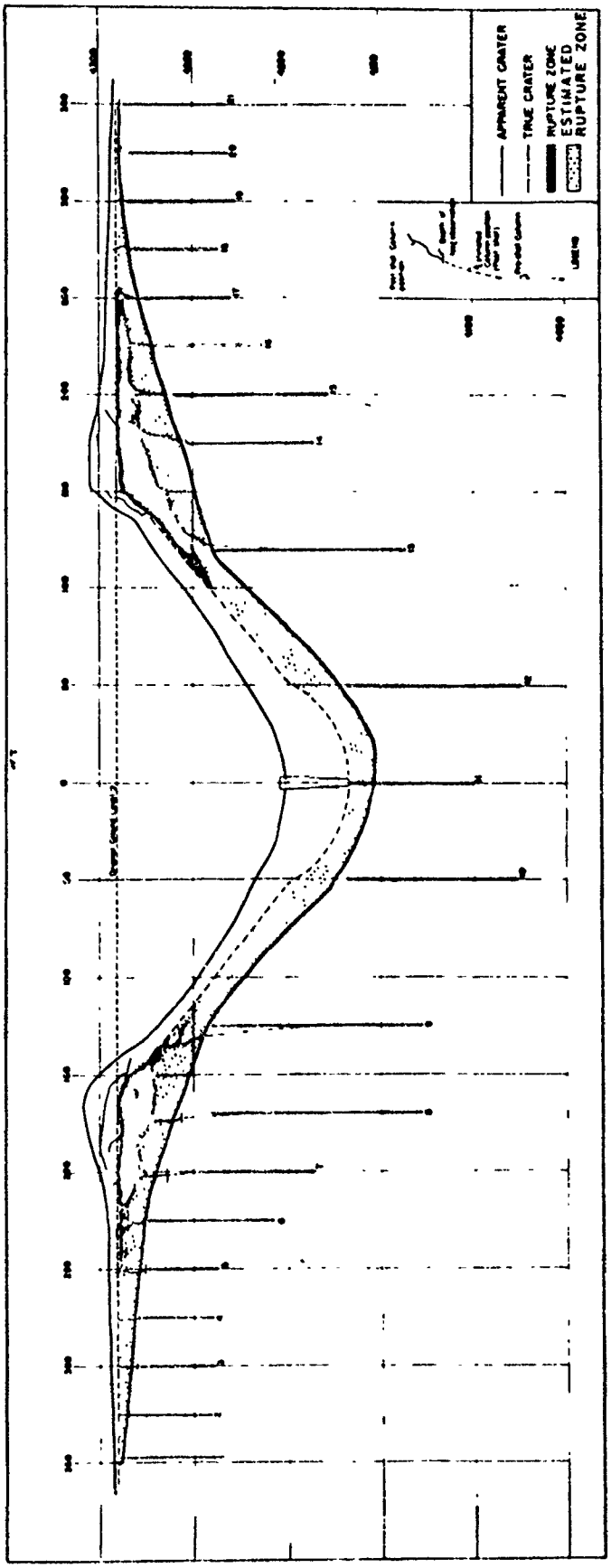

Figure 6.1 Profile of crater with postshot sand column positions, Shot 7.

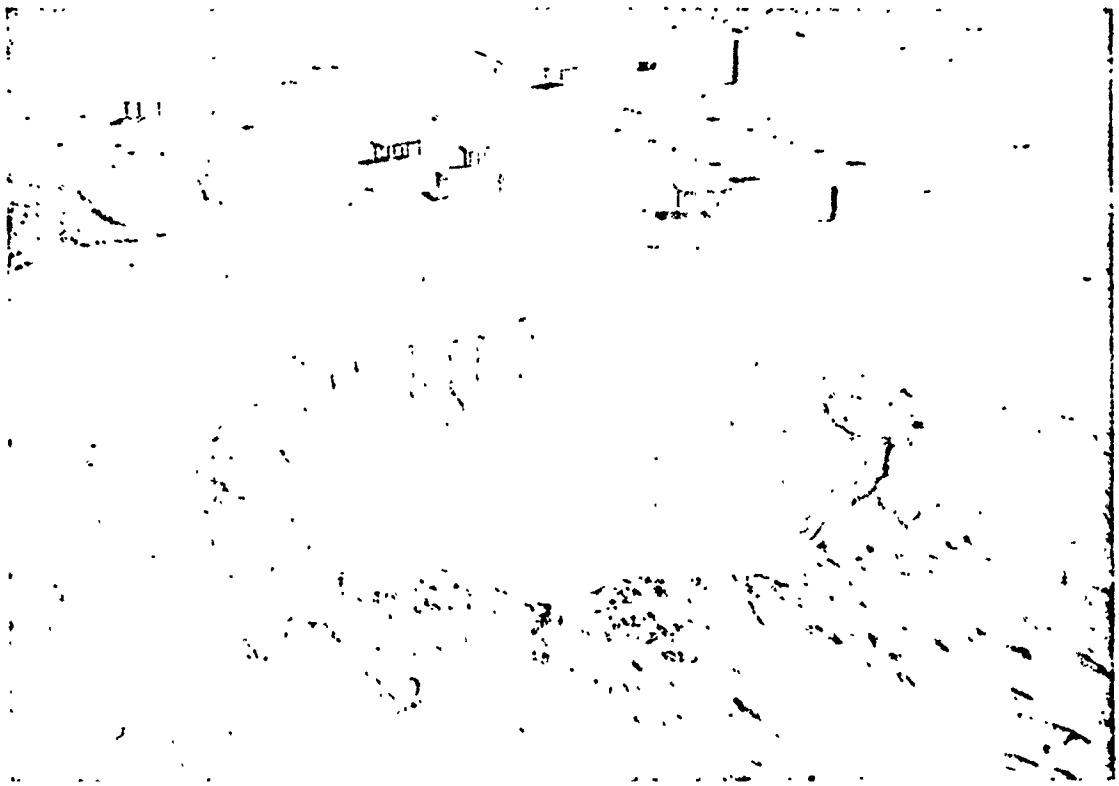

Figure 6.2 Aerial view of Shot 7 crater on D + 1 (Jangle U crater and structures in background).

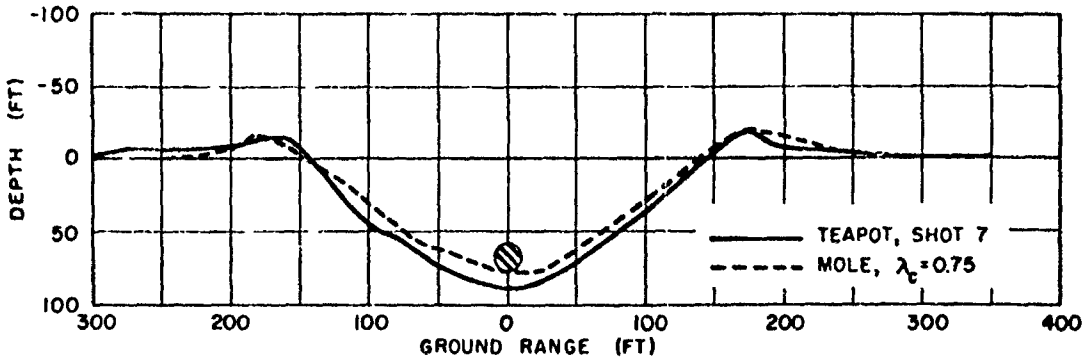

Figure 6.3 Apparent crater average profile compared to scaled Mole 256-pound TNT crater, Shot 7.

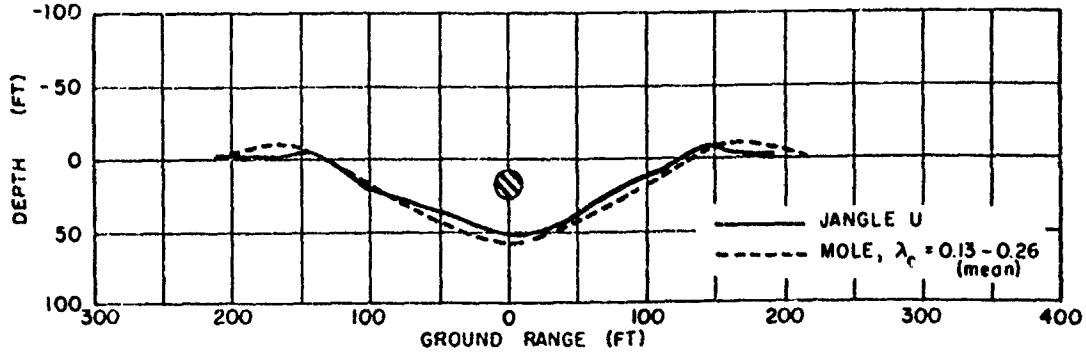

Figure 6.4 Apparent crater average profile compared to scaled Mole 256-pound TNT crater, Jangle U.

apparent crater radii of 130 feet and 146 feet, respectively, and true crater radii of 133 feet and 150 feet. Without regard to high-explosive tests or scaling techniques, since the two explosive devices were presumed to have been identical, it can be concluded that remarkably little effects benefit was derived from the much-greater depth of Operation Teapot Shot 7, insofar as crater radius is concerned. The crater depth, of course, and the volumn showed a greater effect of charge depth. Except for cases where crater volume is the parameter of greatest importance, it would appear that the depth effect for 1.2 kt from 17 feet to 67 feet is not of major importance.

The difference between the true and apparent radii at the original ground surface is small for scaled depths of burial down to 0.75 or 1.0, but below these scaled depths it is felt that the

TABLE 6.1 CRATER DIMENSIONS, NUCLEAR SHOTS

Shot	Shot Depth	Crater Radius	Crater Depth	Crater Volume
	feet	feet	feet	$feet^3$
Jangle Surface (apparent)	−3.5	45	21	4.5×10^5
Jangle Underground (apparent)	17	130	53	0.98×10^6
Teapot Shot 7 (apparent)	67	146	90	2.7×10^6
Teapot Shot 7 (true)	67	150	128	3.25×10^6

true crater radius remains a relatively constant value until camouflet depth is reached. No apparent craters will result for scaled depths of burial greater than about 2.0 to 2.5 for nuclear bursts which are fully tamped. Camouflet depth should be relatively independent of soil type except for differences in soil density, since the apparent crater, or lack of it, depends primarily on the capability of the available energy for throwout to heave clear the soil mass over the charge.

From the military-application point of view, the apparent crater can still be considered as a primary physical effect from underground explosions. Its size and shape can now be more reliably predicted, so that neither over destruction nor failure to accomplish a mission will result. However, it is the true crater, and particularly the true crater depth, that will be used for determination of the depth of burial required for destruction of underground installations.

6.2.4 Effect of Depth on Cratering TNT Efficiency. Figure 6.5 presents the Jangle high-explosive and Mole high explosive apparent-crater results as a function of charge depth. Cube-root scaling has been chosen for analysis and presentation. The curve of crater radius versus charge depth is split into two parts to include all but one Mole point and one Jangle high-explosive (high-explosive-2, 40,000 pounds) point, and reference is made to the upper and lower curves of this figure as an indication of the spread or uncertainty in underground explosion results.

If the charge depth and crater radius of a nuclear shot are known, the equivalent TNT charge can be considered unknown; the nuclear test data plot into a straight line on Figure 6.5 as the unknown TNT equivalent is varied. The intersection of the nuclear straight line with the high-explosive curves readily permits a calculation of the TNT efficiency, as defined in Section 6.1.4. The lines for Jangle U, Jangle S, and Operation Teapot Shot 7 are shown on Figure 6.5; the results are presented in Table 6.2.

Needless to say, these data show no TNT efficiency increase with charge depth from Jangle U (17 feet) to Operation Teapot Shot 7. In fact, a slight decrease is shown. Such a conclusion would perhaps be misleading because of the known erratic nature of underground effects. The efficiency calculation is extremely sensitive to small changes in crater radius. It is

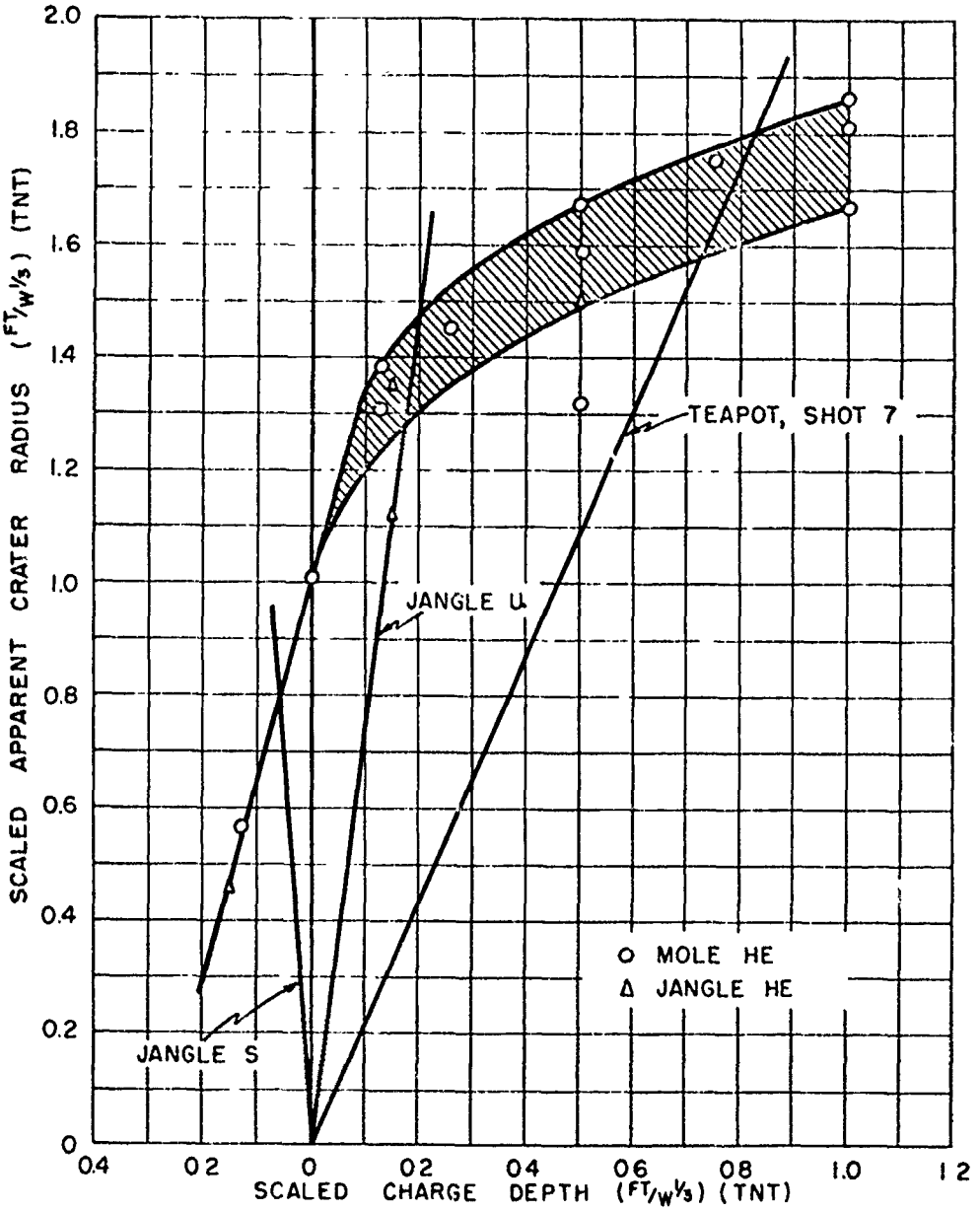

Figure 6.5 Apparent crater radius versus depth for high explosives at Jangle test site.

probably best to conclude that there is no significant change in the cratering TNT efficiency over the range of charge depths from 17 feet to 67 feet for 1.2 kt. Certainly, there is a marked change from 17 feet deep to the surface, which is not unexpected in view of the fundamental differences between high-explosive and nuclear explosions which would perhaps be most apparent near the ground surface for cratering effects.

A fourth-root scaling law would, of course, give higher TNT efficiencies. However, since all of the nuclear charges were of the same size, such a scaling law would not change the conclusion concerning the effect of depth on cratering. With charges of one size, it is not possible to resolve both the scaling-law and TNT-efficiency uncertainties. Likewise, TNT efficiencies have no meaning or use without the establishment or assumption of a scaling law.

This discussion of TNT efficiency has been based upon original-ground-level, apparent crater radii. A similar analysis can be made using the very-limited true-crater-radius data which were obtained by the same method (i.e., ERDL sand column technique). Since, for scaled charge depths covered here, the Jangle-site, Mole true craters had nearly the same radii at ground level as the apparent crater, and since the same was true for Teapot Shot 7, the general TNT efficiency pattern of Table 6.2 would result for an analysis based on ground-level true-crater radii.

Figure 6.6 presents apparent crater radius as a function of depth for nuclear charges at the Jangle site. The units are those conventionally used for the hydrodynamic or mechanical

TABLE 6.2 CRATERING TNT EFFICIENCY OR EQUIVALENCE, NUCLEAR SHOTS

Based on cube-root scaling; all 1.2 kt. Here and throughout this report cratering TNT efficiency refers to apparent crater radius. For TNT cratering efficiencies in terms of apparent volume and depth see the Project 1.6 report, WT-1105.

Shot	Depth	TNT Efficiency from Figure 6.5		Scaled Charge Depth (Feet/$W_{HE}^{1/3}$) = λ_c	
		Upper Curve	Lower Curve	Upper	Lower
	ft	pct	pct		
Jangle Surface	−3.5	8	—	−0.06	—
Jangle Underground	17	29	44	0.19	0.17
Teapot Shot 7	67	22	33	0.83	0.72

effects of nuclear explosions. No reference is made to high-explosive data, except to assist in determining the shape of the curve. Since only nuclear-explosion test data are used, and since all tests were the same size, no scaling law need be assumed to plot this curve. As presented, this curve can be applied to other size nuclear charges if cube-root scaling is used, while it may be readily applied to other scaling laws. It is important that the shape of the curve depends neither on TNT data nor on scaling laws. Figure 6.6 clearly demonstrates the relatively slight effect of charge depths greater than about 10 to 15 feet (A-scaled) and the great effect near the surface.

It may be suggested that the so-called small Teapot Shot 7 crater resulted from a low-yield detonation. Certainly the crater was smaller than expected by many observers who assumed that the greater charge depth would yield a substantial increase in TNT efficiency. The air-blast results and visual fireball observations indicate that the yield was not abnormal. Unless some conclusive and independent evidence of low yield is presented, the results, as discussed, must stand.

Figures 6.2 and 6.3 present the Jangle U and Teapot Shot 7 apparent craters as compared to the nearest scaled (on the basis of apparent crater cube-root scaling for equivalent TNT) Mole craters adjusted for equal radii. There appear to be no significant and systematic differences between the character of the high-explosive and nuclear craters. It is clear from Figure 6.2 that the deeper nuclear charge is slightly more effective than high explosive in producing volume as compared to radius, with an inverse conclusion from Figure 6.4 for the shallower charge. For crater volume, the TNT efficiency of the deeper charge would approach or exceed that for the shallower charge, as contrasted to the radius TNT efficiency being lower for the deeper charge.

6.3 TAMPING AND ENERGY DENSITY

Although the records are somewhat vague, it is the general consensus of opinion that the nuclear device for the Jangle U shot was placed in a fairly large underground room which was not subsequently filled with sandbags. For Operation Teapot, the emplacement was carefully backfilled, and there were no significant air spaces around the nuclear device. In other words, the Teapot underground device was well tamped, while the Jangle U device was not well tamped.

During the early stages of an underground nuclear explosion, the total energy released is

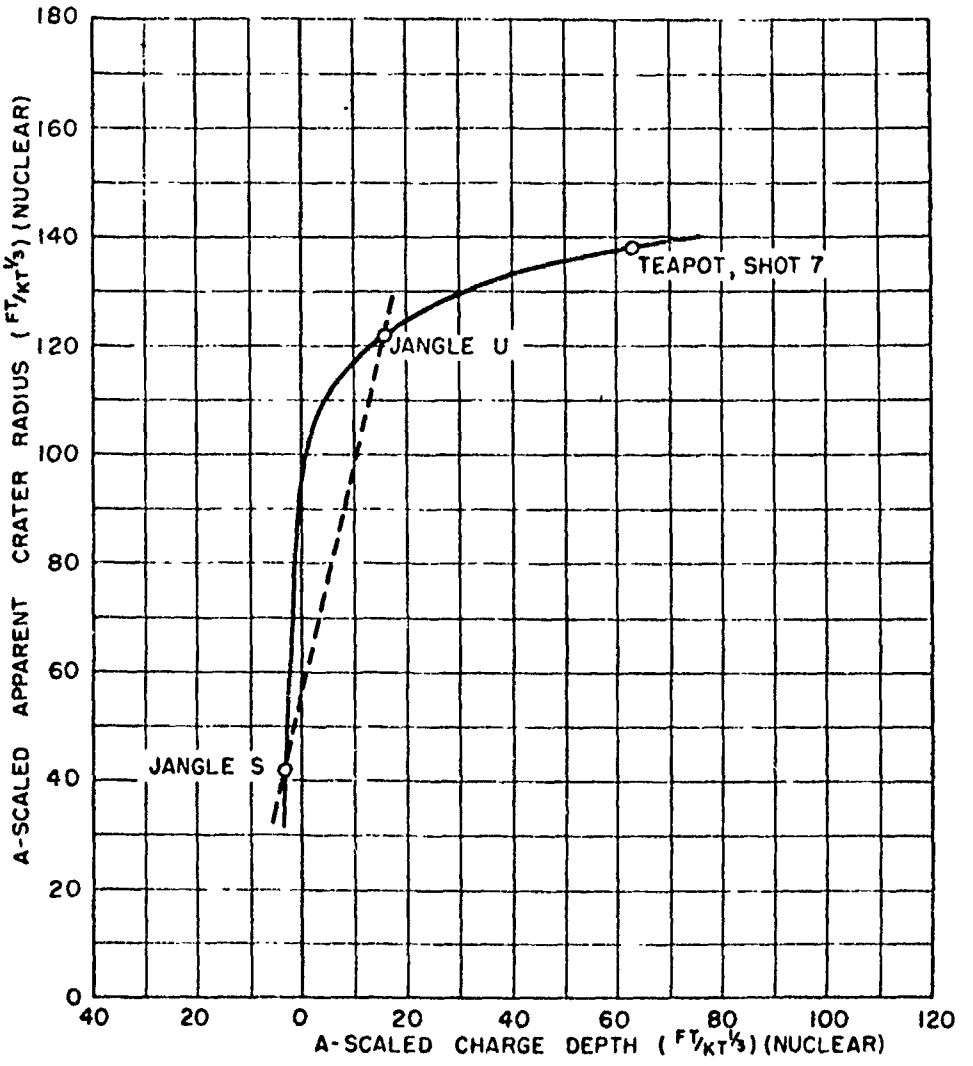

Figure 6.6 A-scaled apparent crater radius versus charge depth for nuclear charges at Jangle test site.

confined to a relatively small mass and volume of material. During this time, the expansion by radiative transport is more rapid than by hydrodynamic transport. At a later time, the mass and volume engulfed by the reaction have increased so that the hydrodynamic shock front breaks away from the heated material. This breakaway radius is sometimes called the effective-charge radius, since beyond this radius the mechanical or hydrodynamic effects of the nuclear explosion might be characterized by the similar effects from a high-explosive charge of the

same radius with the same shock strength at this radius, with proper consideration given to the thermodynamic differences between the materials contained within the breakaway sphere. For all practical purposes, the breakaway radius is determined by the mass of material enclosed. Because of the surrounding air space, the breakaway radius for Jangle U can be assumed to have been larger than that for the well-tamped Operation Teapot Shot 7. Hence, the energy per unit volume at breakaway was less for Jangle U than for Teapot Shot 7, while the energy per unit mass at breakaway was essentially the same for the two shots.

There have been attempts to explain the apparent reduced cratering effectiveness of Teapot Shot 7 by breakaway-energy-density considerations in relation to the cratering effects of so-called high-energy and low-energy high explosives. However, high-explosive energies are generally compared on a unit-mass basis; the breakaway energy densities on a mass basis for Teapot Shot 7 and for Jangle U were about equal. Conclusions based upon such comparisons may not be warranted, since there are not enough experimental data to identify nuclear-explosion effectiveness in terms of energy density.

It is possible that Jangle U was more effective than Teapot Shot 7 for cratering because of the air space around the nuclear device. However, the evidence is limited, and the associated reasoning and logic are tenuous. For this report, no attempt is made to explain the unexpected lack of increase of TNT efficiency with depth. The unexpected result is simply accepted as an experimental fact. The interested reader is referred to the Project 1.6 final report, WT-1105 (Reference 42) for an extensive treatment of cratering phenomena based on the assumption that the Teapot Shot 7 results can be explained by the excellent tamping or higher-energy density (defined as energy per unit volume at breakaway) achieved. However, the opinion herein is that the extensive conclusions presented in that report are not warranted by the limited available data.

6.4 PHOTOGRAPHY

The underground shot was photographed in considerable detail from ground stations and from the air. Some of the photography documented the time and space history of the base surge. Some examples of throwout and cloud growth are shown in Figure 6.7, and similar photographs of Jangle U are shown in Figure 6.8.

The photographic records show that the luminosity of the Shot 7 fireball, as it emerged from above the ground surface, persisted for nearly one second and that the smoke crown material mixed thoroughly with the fireball. The column attained a diameter (measured at the ground) of 925 feet at about H + 6 seconds. Maximum column height measured to the base of the smoke crown was about 400 feet. Radial throwout of crater material was symmetrical and had a maximum extent of approximately 2,000 feet. The maximum main-jet height was about 8,000 feet attained at H + 350 seconds.

By H + 35 seconds, the base surge had pushed through the throwout streamers and was clearly visible. Upwind extent of the base surge was about 2,900 feet, while the downwind extent was about 10,000 feet. The radial growth of the base surge versus time, using crosswind data from Teapot Shot 7, Jangle U, and high-explosive tests at the NTS, compared well on the basis of Froude (inertia-gravity) scaling; that is, results obtained from TNT tests at the same scaled depth as nuclear tests (nuclear-scaled depth computed on the basis of radiochemical yield) in similar soil, compared favorably.

The radiological data obtained by Program 2 projects support the belief that the radiation in the base surge can be a serious hazard to exposed personnel. Since the mechanism by which the surge becomes contaminated is not fully understood, the Operation Teapot results do not necessarily apply to base-surge formation by all underground bursts. The degree of contamination would be expected to vary with burst depth and soil type.

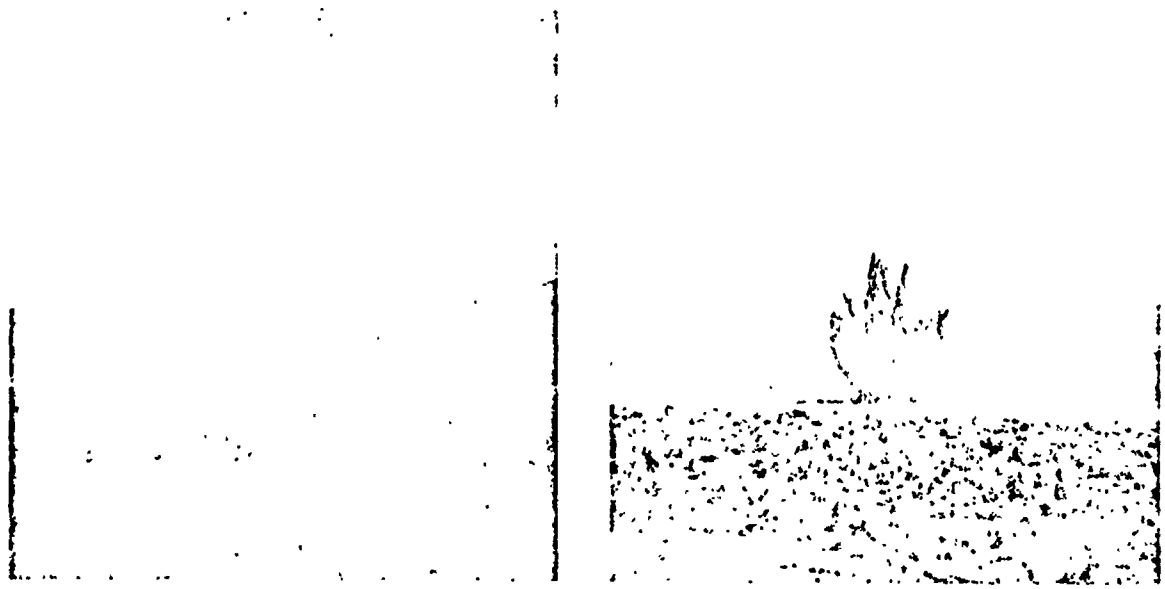

H plus 0.25 sec.

H plus 1.3 sec.

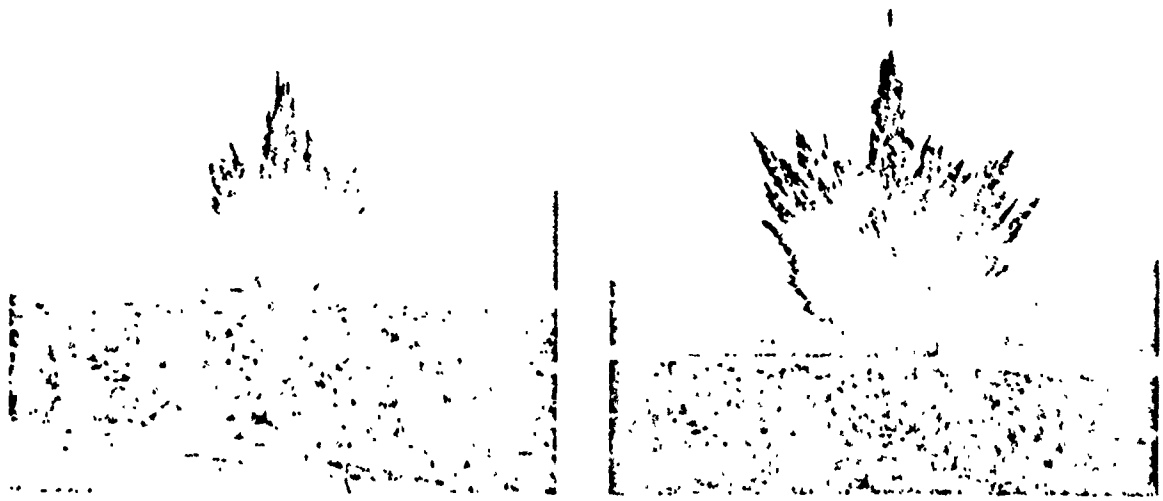

H plus 2.1 sec.

H plus 4.2 sec.

Figure 6.7 Photographic sequence, Shot 7.

H plus 8.4 sec.

H plus 33.6 sec.

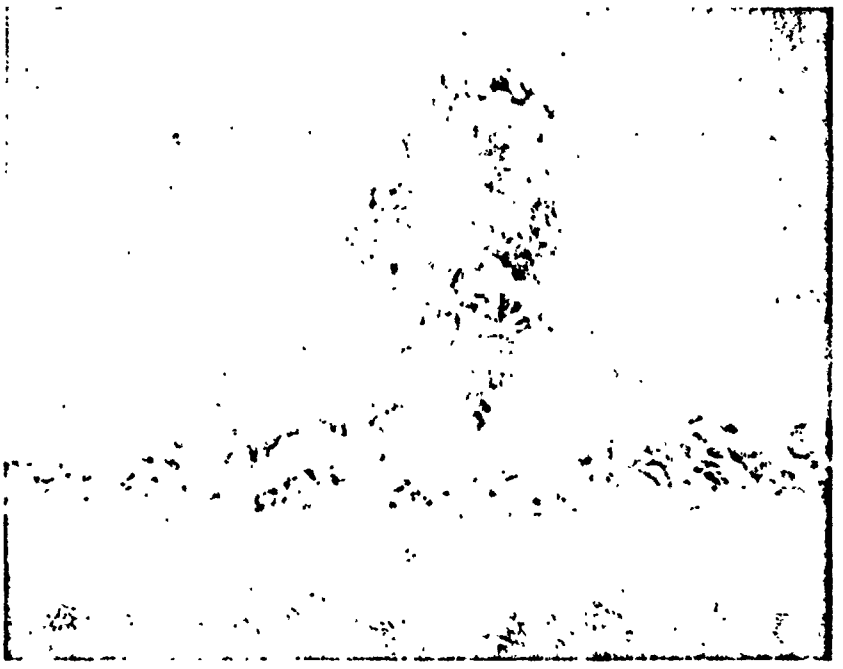

H plus 3 min.

Figure 6.7 Continued

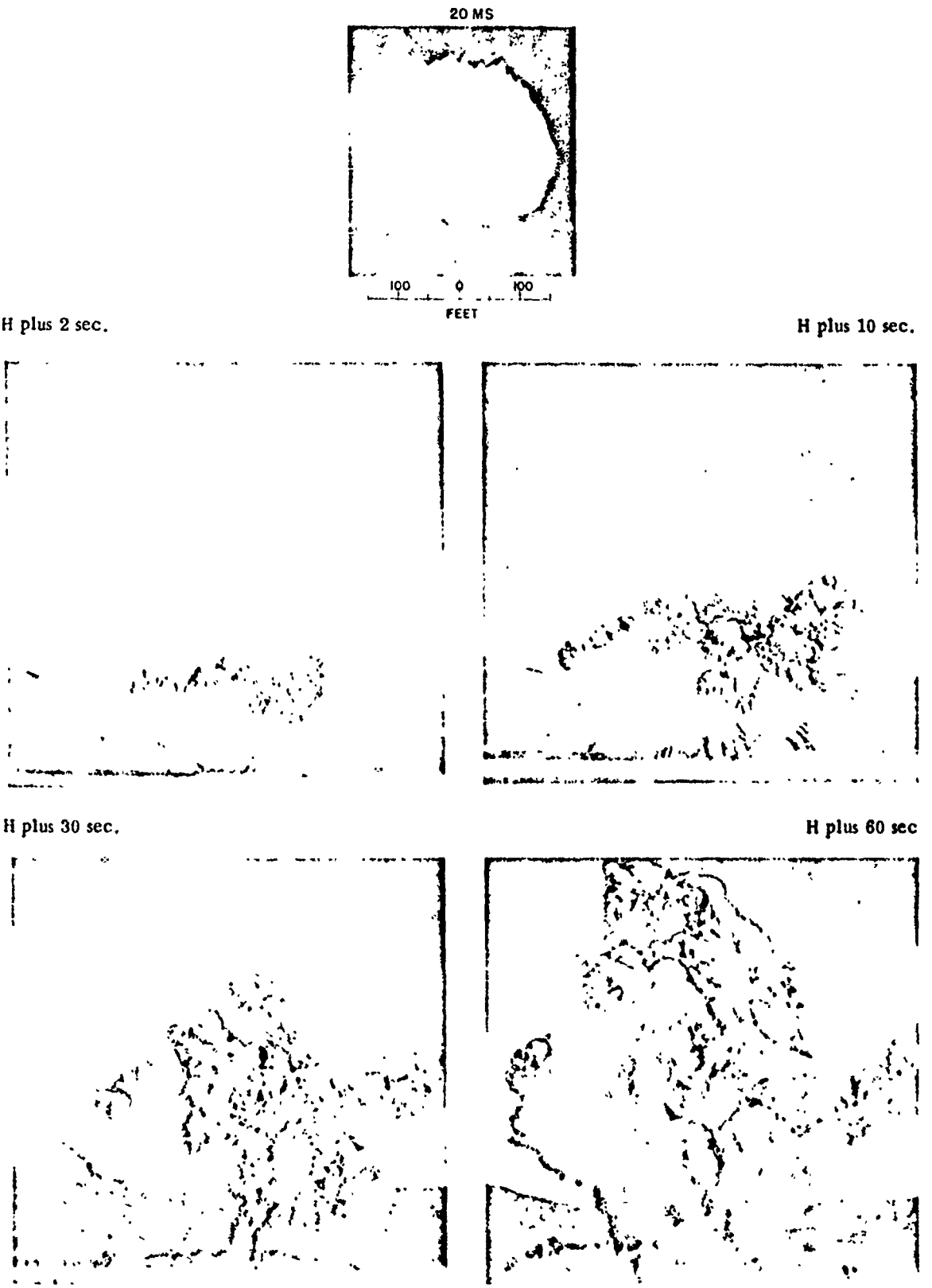

Figure 6.8 Photographic sequence, Jangle U.

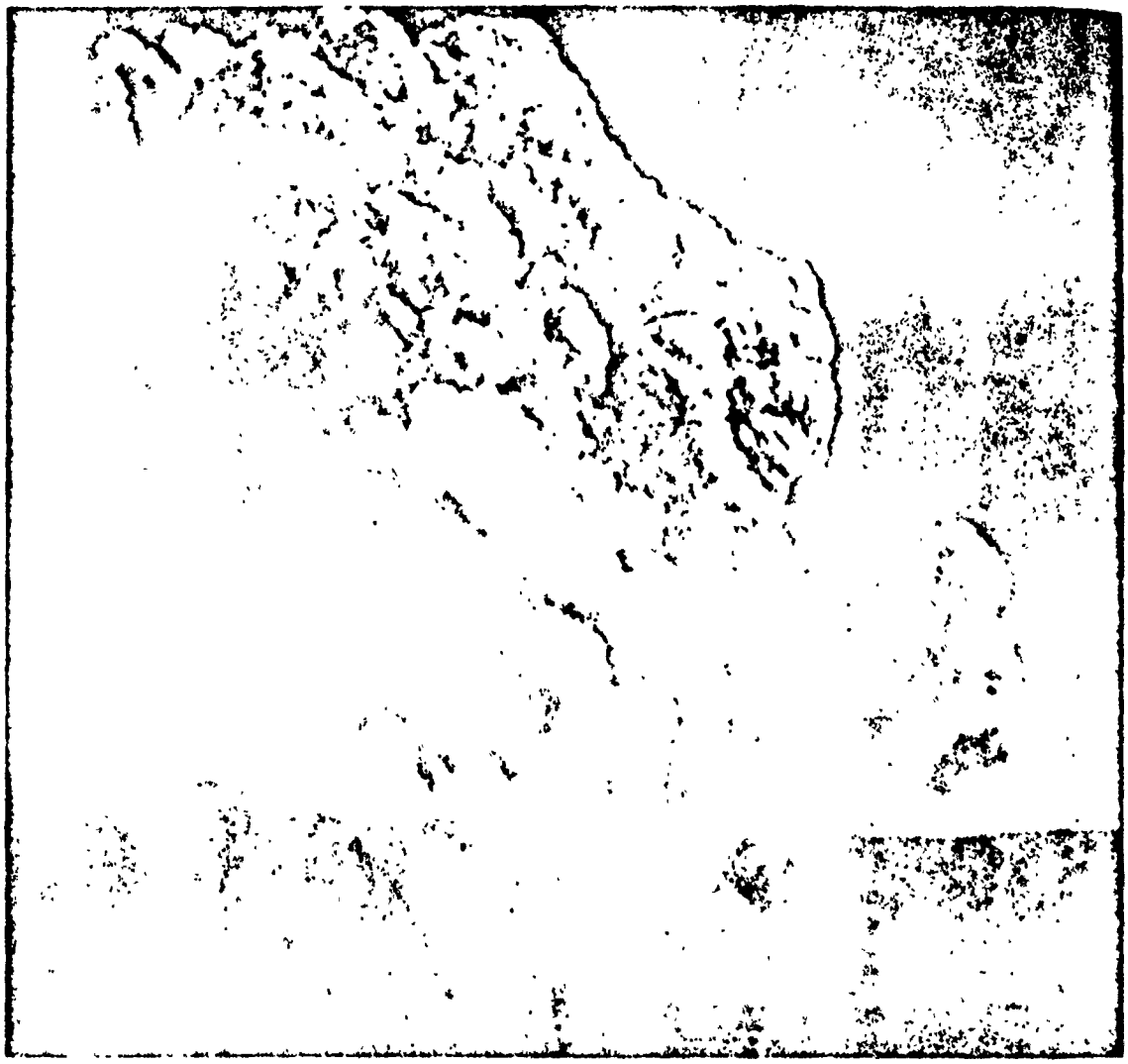

H plus 2 min.

Figure 6.8 Continued

6.5 EARTH SHOCK AND AIR BLAST

Transient surface and underground phenomena were measured by Project 1.7, WT-1106 (Reference 43). Measurements included surface-level air overpressure, underground earth acceleration, underground earth stress (pressure), and underground and surface earth strain, all as functions of time. Most of the underground measurements were made at a depth of 10 feet, although some additional measurements were included for direct free-field correlation with the modest program investigating the effects on targets and target elements. Surface-level monuments for the measurement of permanent displacement were installed.

The transient-phenomena measurements covered the range from 200 to 600 feet from ground zero. The preshot predictions of the free-field transient phenomena were based upon crater radius as a scaled parameter. Prior to the shot, it was the opinion of most observers that the greater burial depth of Teapot Shot 7 would yield a higher TNT efficiency than was obtained on Jangle U, and consequently the test programs were planned in anticipation of a larger crater than was ultimately obtained. Nevertheless, satisfactory transient measurements were obtained. Typical results are shown in Figures 6.9 and 6.10 for distances of 300 feet and 200 feet from ground zero.

In general, the wave forms of the various gage records of free-field earth measurements obtained on Teapot Shot 7 were quite uniform with respect to ground range and gage-burial depth. In addition, the induced effects which may be identified with air blast appeared to be small and of short duration. For this reason, unlike results from previous underground detonations, separation of air-blast effects from direct earth-transmitted effects seemed straightforward.

Comparing results of earth acceleration from the three pertinent nuclear detonations (Jangle U and Jangle S, and Teapot Shot 7), the basic difference between the Operation Buster-Jangle results and those from Operation Teapot was apparently caused by the air-blast induced slap. Specifically, for the Operation Buster-Jangle shots the air-blast arrival was almost simultaneous with the arrival of the earth disturbance, thereby introducing the high-frequency slap accelerations during the most significant portions of the time history. The horizontal, radial, earth-velocity results from the three nuclear detonations indicated a consistent charge-depth effect for this variable, the deeper the charge burial, the greater the peak-to-peak earth velocity at comparable ground ranges. The horizontal earth-stress measurements were little affected by air-blast-induced effects. Preshot predictions of peak earth stress, necessarily based upon small charge high-explosive data only, yielded values which were too low, particularly at close-in ground ranges. A significant observation is the relatively slow rise time of the earth stress, illustrated in Figures 6.9 and 6.10. Tangential strain measurements at the ground surface appeared to be consistent with the concept of a symmetrically-expanding soil medium, following the underground detonation.

The permanent-displacement measurements indicated that the vertical component was significantly smaller than the horizontal component. The contours of equal permanent displacement indicated an asymmetry in the southwest direction which was also noted on the aerial photographs. Maximum air-blast pressures observed on Shot 7 were two or three times greater than would be predicted using pertinent data from previous nuclear tests and underground high-explosive experiments. The Project 1.7 report (Reference 43) presents the results in considerable detail and discusses some tentative scaling conclusions as compared to high-explosive results.

6.6 EARTH SHOCK LOADING AND STRUCTURAL RESPONSE

A number of flexible measuring devices were installed at a depth of 15 feet at a ground range of 300 feet. These devices were designed to determine the effect of the structural response on the coupling obtained for earth shock. From these measurements, the loads acting on the facing and rear surfaces of the buried devices were believed to be caused, in considerable degree,

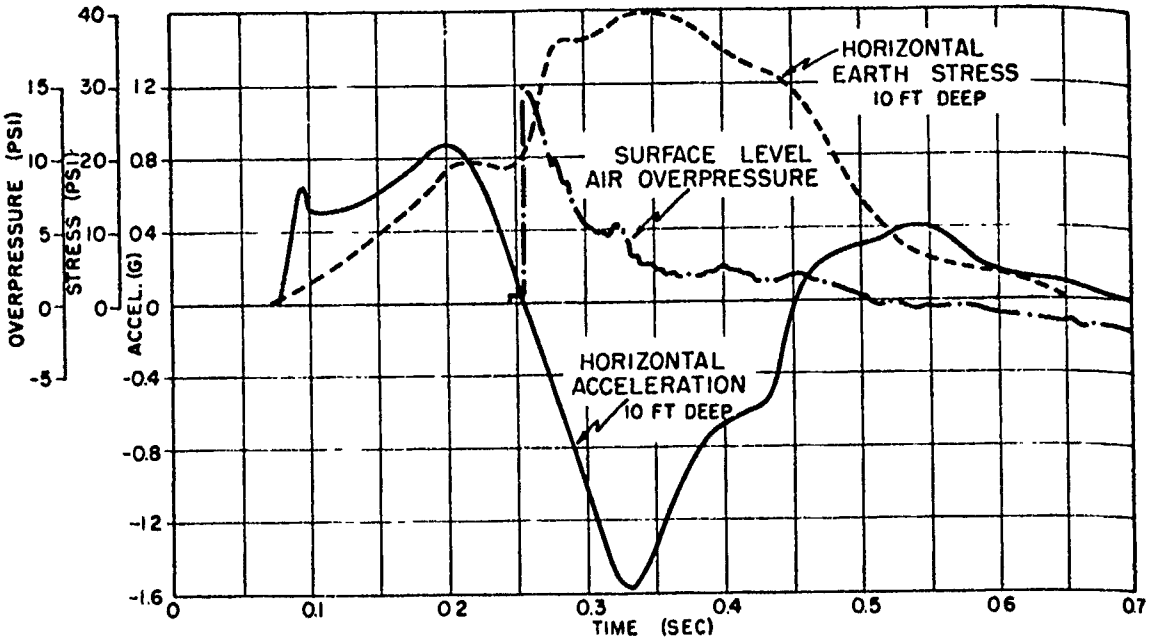

Figure 6.9 Transient measurements at 300-foot ground range, Shot 7.

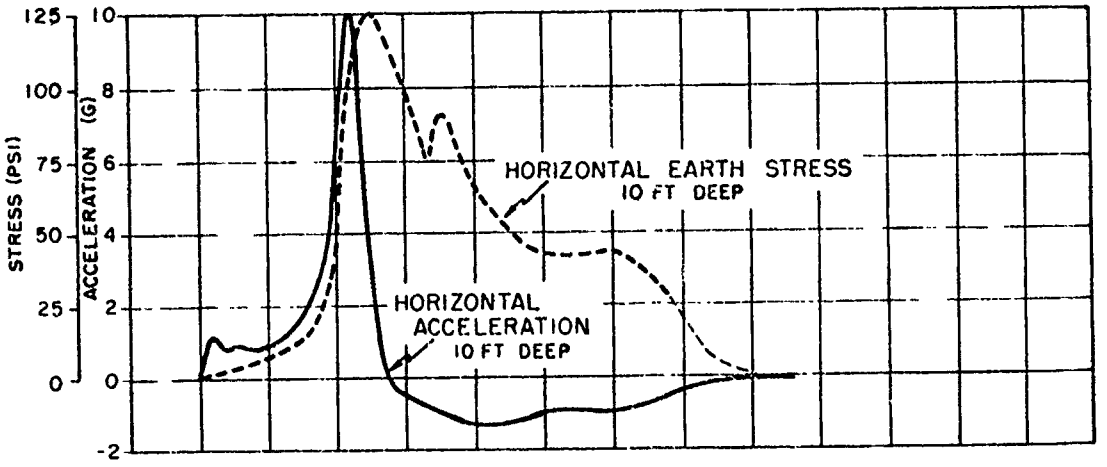

Figure 6.10 Transient measurements at 200-foot ground range, Shot 7.

by radial compression of the earth surrounding the structure. Two of the parameters considered, the mass of the loaded element and the mass of the rear supporting structure, appeared to have little effect on the loads acting on the devices. The change in static structural rigidity of the loaded element apparently did influence the total load. Also, a change in the length of the structure, in a direction normal to the wave front, evidently had a significant effect upon the magnitude of the loads generated by an earth pressure pulse. Of course, in this case the comparative length of the structure and the wave length of the pressure pulse were the important considerations. It appears that the response of a structural element can be approximately determined by static analysis, using the maximum loading applied by the blast pressure.

Two buried, open-ended, four-walled, concrete test structures were located at ranges of 200 and 250 feet from ground zero. Similar test devices were included on Jangle U test and on the extensive high-explosive test series at Dugway. The structures were instrumented to give transient loading and response data, along with permanent displacement and strain measurements. Aerial observation soon after the blast disclosed that the Project 3.3.2 boxes (Reference 44) were completely covered by throwout from the crater and could not be located. Primarily because of residual radiological contamination, posttest examination of the boxes was not conducted until October 1955.

The response of all of the walls of the 3.3.2 boxes was essentially elastic. Combined with the small response of the walls, there was a very large rigid-body motion of the boxes. Careful visual inspection indicated no sign of distress associated with the structures. The permanent displacements of the structures, the colored-sand columns at the depth of the structures, and the monuments at the ground surface all indicated that the permanent displacement of the soil near each structure corresponded closely to the permanent displacement of the structure. Regarding the measured pressures on the structure walls, the rise time of the measured-pressure inputs was generally about seven times the natural period of the walls of the boxes. Thus, the response of the walls was essentially static. The measured pressure on both the front and rear walls of the structure at 200 feet from ground zero was approximately 30 percent of the medium free-field stress, whereas the measured pressures on the walls of the more remote structure were close to the free-field pressure. This difference is not easily explained; however, it may be attributed to the more-severe motion experienced by the close-in structure. A structure with strength comparable to the Project 3.3.2 boxes will not be damaged structurally when located at distances equal to or greater than 1.3 crater radii (Reference 36).

In some respects, the behavior of the Project 3.3.1 devices (Reference 45) and the Project 3.3.2 boxes was quite similar. Primarily, the accelerations observed on the structures and in the free-field medium were comparable. Also, the response of both was essentially static. Finally, it is evident that the pressure measured over a relatively small portion of the area of the wall of the structure may not be an accurate measure of the average pressure acting on that wall.

Chapter 7
EFFECTS on STRUCTURES and EQUIPMENT

A total of ten projects were conducted under Program 3 to investigate blast effects from nuclear detonations on structures and equipment. Most of these projects participated only on the MET shot, which was discussed in Chapter 2. Two of them, however, Project 3.3.1, BuDocks (Reference 45), and Project 3.3.2, Office of the Chief of Engineers, U.S. Army (Reference 44), dealt with earth-shock loading and structural response from the underground shot discussed in Chapter 6 and are covered at length in Section 6.6. Individual projects in Program 3 were supported by Project 3.10, BRL (Reference 63), which provided a large amount of instrumentation to document nuclear blast effects on specific targets.

7.1 RESPONSE OF DRAG-TYPE EQUIPMENT TARGETS IN THE PRECURSOR ZONE

7.1.1 Background. As stated in Chapter 1, the military effects program of Operation Upshot-Knothole was concentrated on obtaining a knowledge of basic phenomena as well as general effects information on many critical items of military equipment, idealized structures, and other significant targets from two air bursts, Shots 9 and 10. The extensive structures and equipment program provided a wealth of data which clearly demonstrated the excessive damage effects on drag-sensitive targets within the dust laden precursor region.

Consequently, a comprehensive investigation of basic phenomena was planned for the MET shot of Operation Teapot to resolve some of the uncertainties concerning blast effects in the precursor region and to provide a basis for predicting damage to targets of military significance under environmental conditions different from the NTS. At the same time, measurements of blast, thermal and nuclear radiation would be made on a high-altitude shot and an underground shot. It was clear that actual effects on representative targets would have to be observed on the MET shot to determine the significance of the various blast parameters under investigation. As previously discussed, the yield and height of burst for the MET shot were chosen to meet experimental and operational requirements of the aircraft drone Project 5.1, WADC (Reference 4), which will be discussed in Chapter 8.

7.1.2 Overall Objectives. The overall objectives of Program 3 may be summarized generally as follows:

(1) To obtain loading and response data for structures, simple shapes, structural elements or components and military equipment over various test surfaces for a precursor-forming tower shot in the kiloton range, Projects 3.1, 3.2, 3.7, and 3.9 (References 12, 64, 65, and 66).

(2) To obtain a basic knowledge of the loading and response of buried and semi-buried structures from the effects of nuclear detonations, Projects 3.3, 3.4, and 3.6 (References 44, 45, 67, and 68).

Within this broad framework, a series of complex experiments was carried out which yielded extremely useful data. However, the overall scope of this effect was somewhat less than that fielded during Operation Upshot-Knothole. This was due in large part to the emphasis placed on obtaining a better understanding of the basic phenomena before going on to an elaborate structures program.

The results obtained by various projects are discussed in succeeding sections. Detailed summaries are presented in the Appendix. The reactivation of Area 10 for subsurface Shot 7 offered

an opportunity to observe additional blast effects on targets previously constructed in these areas. The results of these investigations in the Jangle area are presented in the Project 3.3 Summary in the Appendix. Certain existing structures in Frenchman Flat were also retested under Projects 3.2 and 3.4 (References 64 and 67).

7.2 RESPONSE OF DRAG-TYPE EQUIPMENT TARGETS IN THE PRECURSOR ZONE, (PROJECT 3.1)

7.2.1 Objectives. The primary objective of Project 3.1 was to investigate the response of drag-type equipment targets to blast waves propagated over three different surfaces: water, asphalt, and desert. Secondary objectives were to determine the effect on damage of variation in the positive phase duration or yield, to determine the damage from shock loading only, and to obtain data to improve knowledge of damage to equipment and damage criteria. In addition, an attempt was made to attain experimental design data for ordnance equipment and to determine the effectiveness of a roll-over safety bar placed on wheeled vehicles.

7.2.2 Background and Procedure. Results of previous tests indicated the need for additional data relating the magnitude of dynamic pressure to specific types of damage to drag-type equipment targets, particularly in the region of precursor formation. Ordnance equipment was included to determine weak components or discover modifications in design which would produce significant reductions in damage and repair times.

The ordnance equipment utilized included the following: fifty-six ¼-ton trucks (jeeps), twelve 2½-ton dump trucks, four 5-ton dump trucks, one M59 Armored Infantry Vehicle, one T97 self-propellor 155-mm gun, and three M48 tanks. Vehicles were exposed in different orientations and at different ranges on a total of nine shots during Operation Teapot. On Shots 6 and 12, equipment was exposed on both natural and artificial surfaces. On other shots, all equipment was exposed on the natural desert surface. Figure 7.1 shows a typical jeep installation.

Instrumentation involved the measurement of overpressure versus time and dynamic pressure versus time by self-recording gages at the particular equipment stations. Displacements of the vehicles were recorded, and the vehicles were inspected to determine and evaluate the degree of damage. A statistical analysis was conducted to determine the correlation coefficients between displacement and damage with blast wave parameters. Project 2.7 provided film badges and reduced data for the shielding studies conducted.

7.2.3 Results and Conclusions. Considerable damage data on various combat and transport vehicles were obtained. The data showed that damage was most extensive on the desert surface. An evaluation of the damage and displacement measurements showed that the drag forces were higher on the desert surface than either the water or asphalt surfaces. Displacement measurements of jeeps indicated that the shock wave was asymmetrical on Shot 12.

Statistical analysis revealed that a definite relation existed between peak dynamic impulse and displacement and peak dynamic pressures and damage for the ¼-ton truck in side-on orientation. Peak dynamic pressure seemed more closely related to damage to ¼-ton trucks side-on than the peak dynamic impulse.

A comparison of observed damage with predictions based on the curves presented in WT–733 (Reference 69) and TM 23-200, 1955 edition, (Reference 22) showed agreement to a fair degree of accuracy. Considering the effect of positive duration, the results showed that the scaling factor for damage radii was $W^{0.4}$ when the yield of the weapon was varied and the scaled height of burst range was between 80 and 500 feet.

Results indicated that an incident shock of about 25 psi overpressure in the regular reflection region was required to produce significant damage to jeeps from shock loading alone.

Protection against extensive damage to drag targets can be achieved by placing the targets behind a barricade of sufficient strength which, in itself, can withstand high drag forces. The placement of a roll-over safety bar serves to minimize damage to the cab and the vehicle controls.

At distances where tanks will withstand high drag forces, the personnel within will receive a lethal dose of nuclear radiation. The lethal radii from radiation will extend farther than blast damage radii. The average attenuation factors for gamma radiation of the tank M48, T97, and the M59 are 0.1, 0.6, and 0.7, respectively.

7.3 STUDY OF DRAG LOADING OF STRUCTURES IN THE PRECURSOR ZONE (PROJECT 3.2)

7.3.1 Objectives. The broad objective of this project was to determine the effects of ideal and nonideal shock waves from a nuclear detonation on drag loading of structures and structural components. Emphasis was concentrated on determining more accurately the transient drag effects associated with the three wave forms expected over the three controlled surfaces during Shot 12.

The specific objectives of the project were to: (1) establish a body of information to be used as a basis for model experiments; (2) investigate the drag-loading phenomena associated with precursor and nonprecursor shocks and to obtain quantitative data to be used as a basis for deriving methods for predicting drag loads on simple shapes; and (3) determine the feasibility of one meth. of measuring net forces under nuclear test conditions.

Figure 7.1 Typical arrangement of BRL jeeps, Shot 12 (Preshot) water line.

7.3.2 Background and Procedure. In Operation Upshot-Knothole, two well-instrumented structures, 3.1s and 3.1t, were placed so that they were well within the precursor region during Shot 10. The results obtained seemed to indicate that the forces on the structure could be given by multiplying the dynamic pressure in the blast wave by the drag coefficient for that shape times the frontal area of the structure. Superimposed upon these forces were large fluctuations of an apparently random nature due to large local variations in the flow conditions which caused large fluctuations in the dynamic pressure itself. In order to obtain an adequate description of the loading of structures within the precursor region, field tests under actual nuclear burst conditions were required.

Six structures were exposed on Shot 12 as indicated in Table 7.1. All structures were located with the front face normal to the blast wave.

The U-K 3.4e beam had the space between flanges filled with concrete grout to create a rectangular cross section. The four reinforced concrete cubicles, 3.2a-1 through 3.2a-4, were 3-by-3-feet in plan and 6 feet high. The U-K 3.1t structure was 6 feet by 12 feet in plan and 6 feet high. The targets were all loading structures, i.e., non-responding, except for the beam, which was a responding item.

The four small cubicles were placed on the three differing surfaces to obtain comparative information in clear and precursor type shock regions. The two cubicles on the desert had loosened soil in front of one and hard desert soil in front of the other, as shown in Figure 7.2. The remaining structures on the desert line were entirely in the precursor region.

Instrumentation of structures 3.2a-1 through a-4 was accomplished by Ballistic Research Laboratories (BRL). The Naval Ordnance Laboratory (NOL) reinstrumented U-K 3.1t. Measurements were made of point pressures on various faces of all structures and of strain measurements on the beam and beam supports. A total of fifty channels was employed. On the 3.2a

TABLE 7.1 STRUCTURES EXPOSED ON SHOT 12

Structure	Type	Distance to Ground Zero	Line
		ft	
3.2a-1	Cubicle	2,000	Desert
3.2a-2	Cubicle	2,000	Desert
U-K 3.4e	Rectangular Beam	2,000	Desert
U-K 3.1t	Structure	2,000	Desert
3.2a-3	Cubicle	2,000	Water
3.2a-4	Cubicle	2,000	Asphalt

type cubicles and U-K 3.4e beam, values of point pressure or strain were averaged for several gages at similar locations. Thus, the number of gage positions was considerably larger than the channels employed.

7.3.3 Results and Conclusions. A significant amount of information was obtained in the form of detailed pressure records for various positions on the structures and varying surrounding conditions. Records for all structures except the two cubicles on the asphalt and water lines gave satisfactory results. The records for those two cubicles were erratic because of electromagnetic signals at the time of bomb detonation and the loss of calibration values.

A difference in pressure between two identical structures on the loosened and compacted soil was noticed, with a considerably higher peak pressure and slightly higher net impulse for the structure on the loosened desert soil. The differences were probably due to different degrees of dust loading. The drag coefficients obtained for the test structures based on blast line q-gage measurements were about one-half to one-third those obtained from clean flow conditions.

The measured values of impulse on the test structures were high compared to ideal dynamic-pressure impulses. The difference was sufficiently great that the only possible way of accounting for it was a higher impulse in the precursor than that obtained from a blast wave over an ideal surface. Appreciably different shapes of pressure waves and lower impulses were obtained on the U-K 3.4t beam compared to the other cubicles at the same distance. A major part of this difference was probably due to the different dust flow conditions and effects on the two types of structures.

An appreciable variation of dynamic pressure with height was found on several of the test structures, probably because of boundary layer effects. A prediction scheme for the net load

on simple structures developed on the basis of Upshot-Knothole data was found to approximately predict the Operation Teapot results.

The net-force measuring system, as applied to a simple beam, i.e., U-K 3.4e, operated successfully. Such measurements may be expected to be successful in a fairly wide variety of conditions provided care is taken to separate the effects of the foundation and supporting structure vibrations.

7.4 AIR BLAST EFFECT ON UNDERGROUND STRUCTURES (PROJECT 3.4)

7.4.1 Objectives. The general purpose of the project was to obtain the necessary basic data from which to develop criteria for the economical design of efficient underground protection from

Figure 7.2 Soil conditions in front of Structure 3.2a-1.

air-blast forces. Specific objectives were: (1) to investigate the nature of the forces transmitted from an air burst of an atomic device through the earth to underground structures; (2) to determine the variation of these forces with the depth of the structure in the earth and with the flexibility of the structural elements; and (3) to study the response of simple structural elements of different stiffnesses and effective masses subjected to the transmitted dynamic forces.

7.4.2 Background and Procedure. In order to investigate the behavior associated with the above listed objectives, three buried structures were tested during Operation Upshot-Knothole. The structures were primarily reinforced-concrete boxes having a large number of simply supported steel beam strips as roofs. The three structures were buried so that the roofs of the structures were 1, 4, and 8 feet below level ground surface. Figure 7.3 shows the deepest structure, with the anchor bolts for attachment of the roof beam strips visible. The tops at the parapet walls are on a level with the tops of the beam strips.

The beam strips were arranged so that several strips of each of three different degrees of

flexibility formed the roof. All the beam strips had an 8-foot span. The three structures were located close together on an arc of 900-foot radius from ground zero.

During Operation Upshot-Knothole the beams sustained only small permanent deflections. The main reason was that one set of beam strips (the plastic beams intended to be considerably weaker than the others) were fabricated from a steel having a higher yield point. Therefore, only two different beam yield strengths existed instead of the planned range of three. For the current test, allowance was made for this by cutting material from the lower flanges of the plastic beam strips to weaken them.

From the results of Upshot-Knothole, it was concluded that for well-compacted, silty subsoil, of the type at the test site, there was little if any attenuation of a surface pressure by the soil

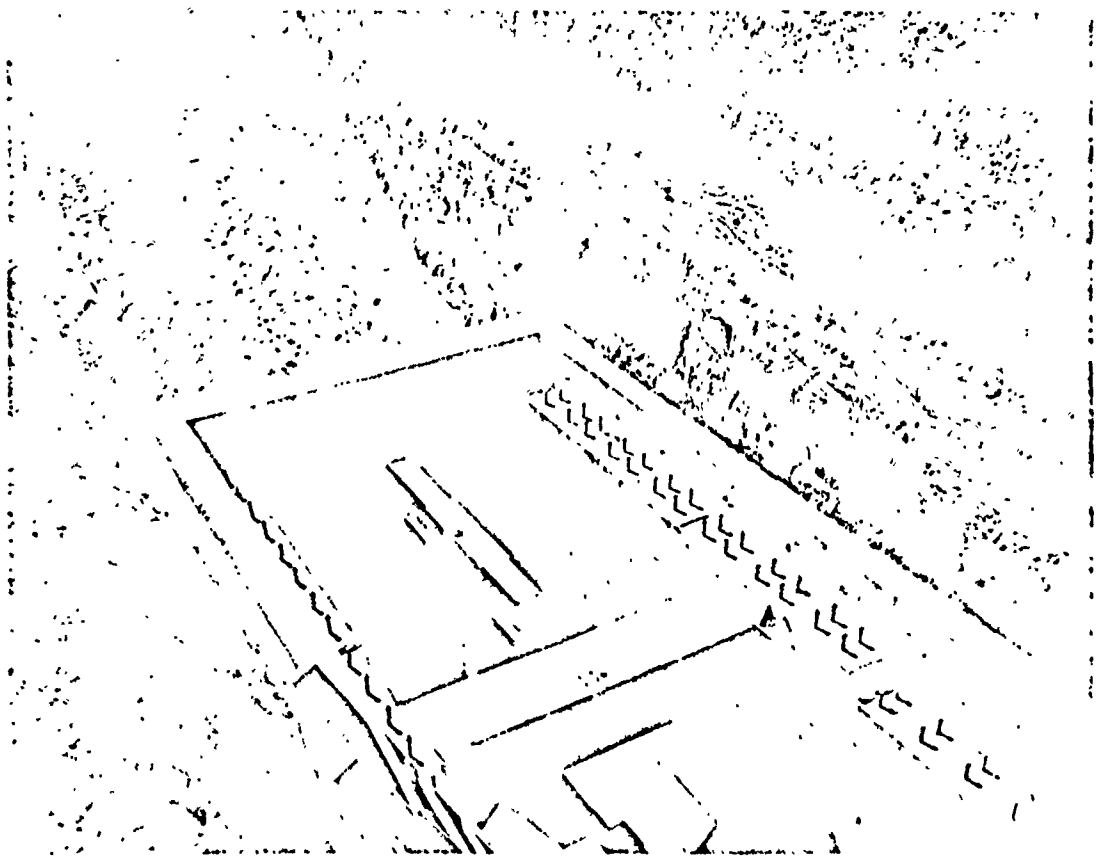

Figure 7.3 Structure 3.4c during construction.

above a structure. (Observations of the beams during Operation Plumbbob on a qualitative basis disclosed that there was significant attenuation of effective vertical earth pressures within the first few feet of depth.) Since the tests involved only small deflections under moderate degrees of loading compared with the maximum resistance of the structural elements, no definite conclusions could be reached as to the effect of the flexibility of the structures on the pressures transmitted to the structural elements.

Instrumentation during the Teapot test was limited to the measurement of: (1) transient air pressures, deflections, accelerations, and beam-strip reactions with electronic equipment; (2) permanent strains in the beam strips with mechanical strain gages; (3) peak transient strains at the center of selected beam strips; and (4) permanent deflections of the beam strips and relative vertical motions of the structures with a surveyor's level.

7.4.3 Results and Conclusions. The general level of pressures achieved in the Teapot MET shot was about 90 psi at the ground surface, compared with the two loadings of 15 and 63 psi during Operation Upshot-Knothole.

In the Teapot test, the response at the flexible P and M beam strips decreased as their depth of burial increased. The same decrease in response was not observed in the Upshot-Knothole tests. Thus, there appeared to be an important practical significance of arching of the soil over the structures, since the soil backfill had undergone additional consolidation during the 2-year interval between tests. The reason for the decrease in response with depth is believed to be due to the alteration of pressure pulse as it was transmitted through the soil. The time characteristics, particularly the rise time, were changed so that the load applied to the beam had the same effect as a static load. In contrast to this, the more rigid E beam strips, although they were buried at the same depth as the P and M beams, had an increased response. Therefore, it seems that the response was related to the modulus of the soil and the stiffness of the structure and might have been connected with a reflection phenomenon on the more rigid beam strips.

For the loads in these tests, the E beam strips had only small deflections, and therefore there was no reduction in load on them. However, for much higher loads, it is believed that the E beam strips would have yielded and experienced deflections of the same order of magnitude as the P and M beams. Once the deflections became large, there would have been a reduction in response for the E beams similar to that found for the P and M beams. It is possible to have a reduction in load on any roof beam if the backfill is deep and consolidated enough and the member is flexible.

7.5 EVALUATION OF EARTH COVER AS PROTECTION TO ABOVE GROUND STRUCTURES (PROJECT 3.6)

7.5.1 Objectives. The primary objectives of this project were to determine the degree of protection that earth cover offers to above ground structures and, particularly, to test the adequacy of an adaption of a standard Navy stock corrugated steel-arch ammunition magazine as a personnel shelter. Both the blast resistance and radiation resistance of such structures were objectives of the test.

7.5.2 Background and Procedure. Above ground earth-covered structures were tested on Operations Greenhouse and Upshot-Knothole. Past tests and studies indicated that the use of earth-covered prefabricated ammunition storage magazines was a relatively inexpensive and adequate method of providing personnel shelters. Figure 7.4 shows the basic 25-by-48-foot steel-arch ammunition shelter without the earth cover.

Analysis showed that a structure of this type (an arch) was sensitive to asymmetrical loading. Therefore, the earth berm was widened and flattened to reduce the differential air-blast force against the two sides of the building and to increase the strength beyond that of Upshot-Knothole Building 3.15. Figure 7.5 shows the plan and profile of the test configuration for the Teapot structure with its earth cover.

In addition to Building 3.6, the building constructed for Upshot-Knothole Project 3.15 was also tested on Shot 12. The building was similar to the Teapot structure but differed in the following respects:

(1) The arch shell was of a lighter gage (10-gage multiplate) instead of 8-gage shell for the new structure.

(2) The shape of the earth cover was different in that the top of the earth cover was tangent to the arch barrel at the crown.

(3) The endwalls were not reinforced with the tie-back to deadmen reinforcement shown in Figure 7.4.

Models were added to this experiment to determine the relationship between model and prototype performance. Six quarter-scale models were designed, three of steel to have the same

ultimate strength, and three of aluminum to have scaled deflections at yield. The models were located to cover the maximum range in response expected from a possible variation in yield of the device. See Table 7.2 for the location of the models and structures.

Instrumentation of the main Teapot structure consisted of the following: electronic deflection gages measuring the change in length of four chords in the central plane of the building, seven scratch gages placed around the inside of the arch, nine self-recording pressure gages on the earth berm, two dynamic pressure gages, and total dose of radiation at two locations inside the building. In addition, Building U-K 3.15 was instrumented with two scratch gages and two total

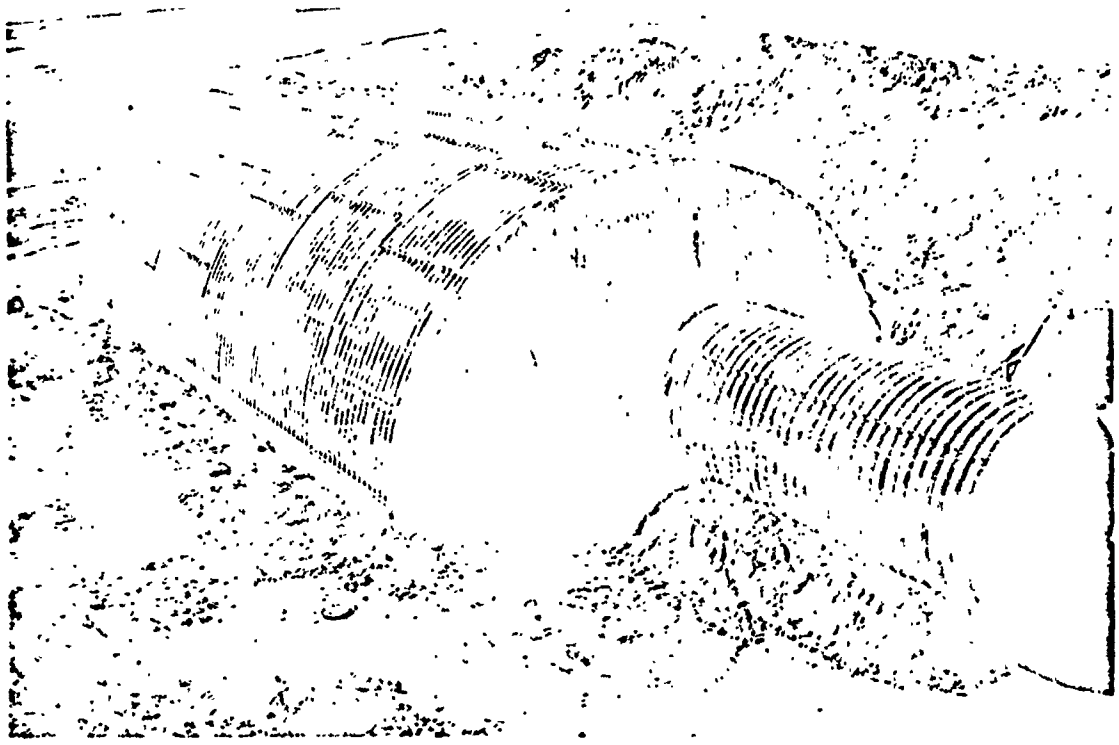

Figure 7.4 Building 3.6 without earth cover.

dose radiation measurements. Each of the models was instrumented to obtain both permanent and maximum deflection of the crown in the center plane.

7.5.3 Results and Conclusions. The main structure was collapsed by a peak dynamic pressure of 170 psi, associated with a peak side-on overpressure of 30 psi. Figure 7.6 shows the progressive distortion and final position of the ground zero side of the arch. Radiation measurements inside the building indicated that prompt radiation was attenuated by a factor of 100.

Building U-K 3.15 withstood forces of 15 percent of those applied to Building 3.6 with trivial deflections. Comparison of the radiation measurements inside the two buildings demonstrated the value of the 3 feet of earth cover above the crown of such a structure.

The performance of the models was in accord with predictions. Of the three steel models which were intended to collapse at the same values of applied external pressure as Building 3.6, the two at 1,400 feet and 1,500 feet, which received pressures similar to or larger than those applied to Building 3.6, collapsed. The one at 2,000 feet, which received roughly one-third the pressure applied to Building 3.6, remained standing. Of the three aluminum models which were expected to fail under pressures roughly one-quarter of those which would produce failure in the

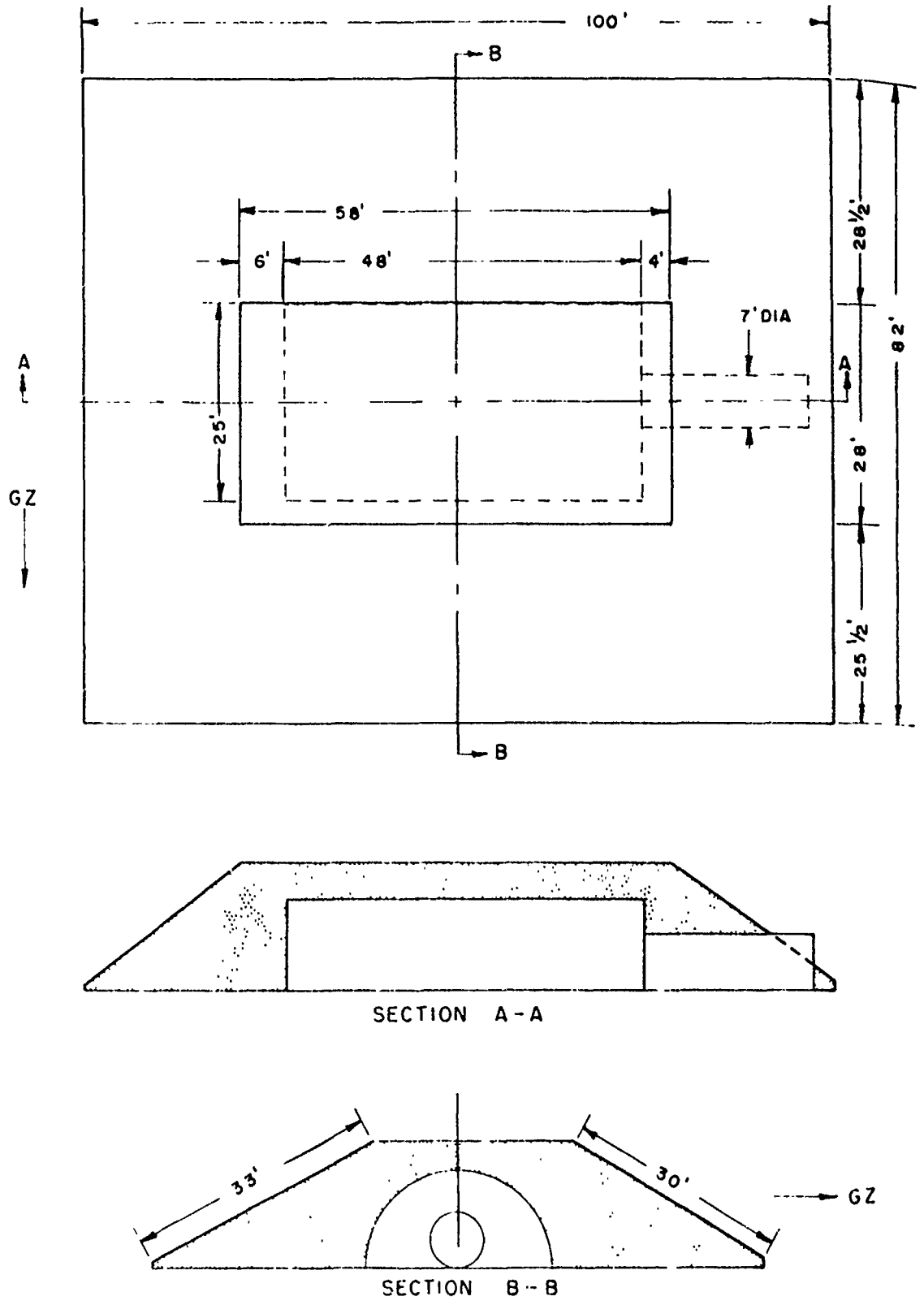

Figure 7.5 Profile of earth cover, Building 3.6.

main building, the one at 2,000 feet, where the pressure was on this basis roughly twice that expected to produce failure, did fail. Those at 2,500 feet and 3,000 feet, where the maximum pressures were less than one-quarter of those applied to Building 3.6, remained standing.

It was concluded that the structure in the configuration tested (Building 3.6) would serve as an adequate shelter under conditions in the open not exceeding any of the following conditions:

Average side-on overpressure	30 psi
Average dynamic pressure	80 psi
Total flux prompt radiation	10,000

Actually, the structure would probably withstand a still larger side-on overpressure if the accompanying dynamic pressures were significantly smaller. The models gave useful results and should be incorporated into any future testing program.

7.6 EFFECTS OF POSITIVE PHASE LENGTH OF BLAST ON DRAG AND SEMI-DRAG INDUSTRIAL BUILDINGS, PART I (PROJECT 3.7)

7.6.1 Objectives. The principal objective of this project was to investigate experimentally the effect of the length of the positive phase of blast forces. A secondary objective was the further study of the general problem of drag loading and response of structures to blast forces.

7.6.2 Background and Procedures. Theoretical analysis indicated that, for megaton weapons, the peak pressure required to cause a specific degree of damage to drag-type structures would

TABLE 7.2 LOCATIONS OF BUILDINGS AND MODELS

Unit	Material	Radius from Ground Zero
		ft
Building 3.6	Steel	1,500
Model No. 1	Steel	1,400
Model No. 2	Steel	1,500
Model No. 3	Steel	2,000
Model No. 4	Aluminum	2,000
Model No. 5	Aluminum	2,500
Model No. 6	Aluminum	3,000
Building U-K 3.15	Steel	2,300

be less than for the kiloton size because of the longer positive duration of blast-wave loading. In order to provide experimental evidence to support or refute this evidence, it was necessary that structures be exposed to two shots of widely differing yield. Exposure in the kiloton range was accomplished on Shot 12, Operation Teapot. Similar structures were also planned for exposure to a yield in the megaton range on Operation Redwing.

To satisfy the project requirements, four steel-frame structures of the single-story industrial type were tested. Two structures were of the drag type, the roofing and siding were frangible corrugated asbestos sheets which were expected to fail completely before transmitting any significant load to the supporting frame. The remaining two structures were of the semi-drag type with reinforced concrete side walls and corrugated asbestos roofing. A 7-foot high window opening, starting approximately 7 feet above grade, ran the full length of each wall giving a window opening of approximately 30 percent of the full wall area. All four structures had the same steel

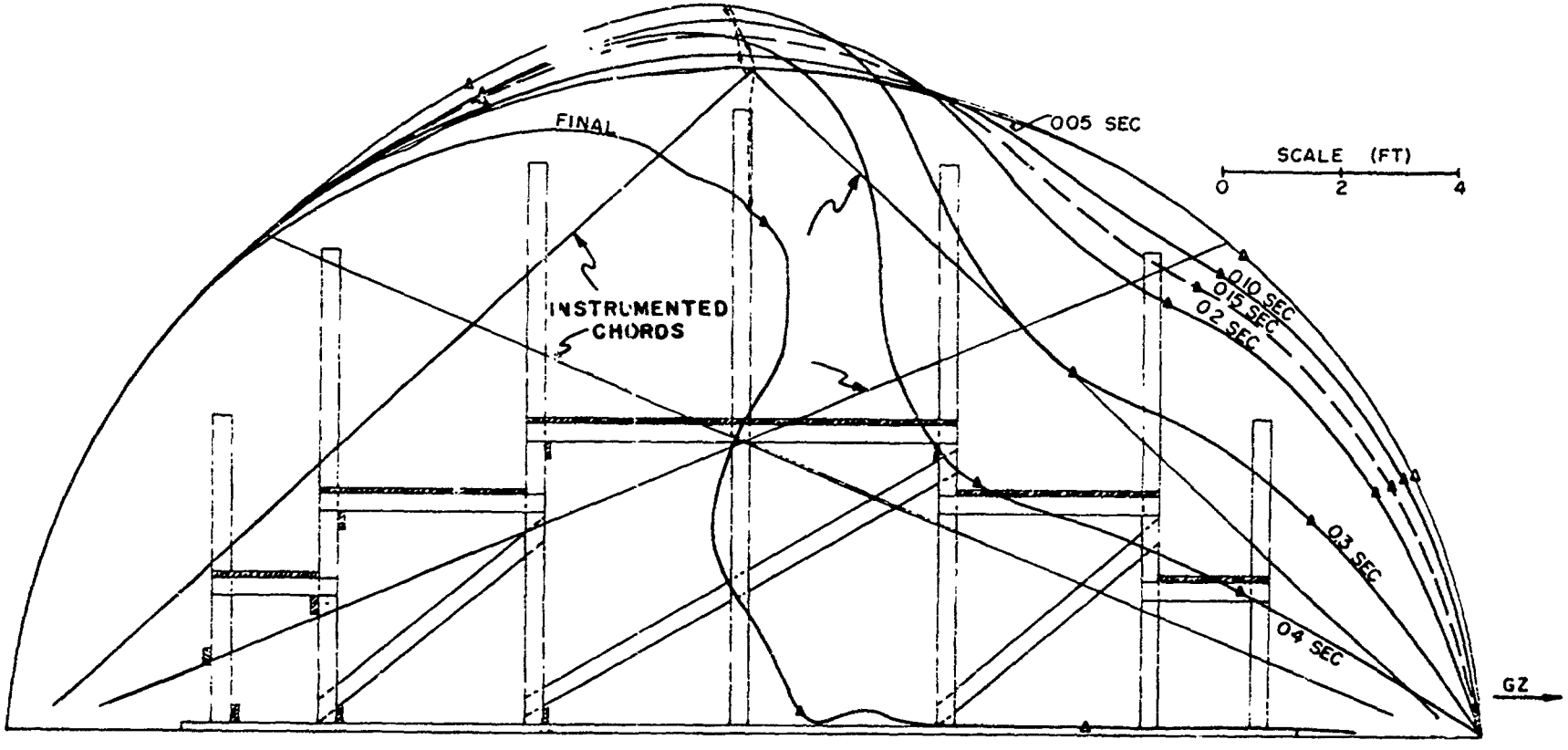

Figure 7.6 Profile at various times, Building 3.6.

frame, were approximately 30 feet in overhead height, and had spans of 40 feet. The drag structures had two 20-foot bays and the semi-drag structures had four 20-foot bays Figure 7.7 shows the drag type designated as 3.7-a, and Figure 7.8 shows the semi-drag type designated as 3.7-b. Each structure was so oriented that the blast wave impinged normally on the walls.

The two drag structures were located at distances of 3,600 feet and 4,350 feet from ground zero, and the semi-drag structures were located at ranges of 5,000 feet and 5,750 feet. It was expected that these ranges would result in damage close to collapse for the nearer structure of each type and only moderate damage for the more distant structure.

For each of the four test structures, measurements of the following quantities were taken: intensity of overpressure, intensity of dynamic pressure, deflections of center-windward and center-leeward columns, acceleration of the top of the columns (as a measure of the acceleration of the mass of the building) and shear strains near the base of the center-windward and center-leeward columns. These measurements were obtained by BRL and recorded on multichannel magnetic tape equipment for three of the buildings and with an oscillograph on the fourth building. Survey measurements of permanent deformations were also obtained, and photographic records of the behavior of the structures during the test were taken.

The resistance properties of the structures were measured both before and after the test. Before the test, the stiffness and natural period of vibration for each type of structure were determined by static tests below the yield load. After the test, complete load-deflection curves were determined by pull-down tests on each type.

7.6.3 Results and Conclusions. Studies of available pressure-time records indicate that the most probable peak intensities of overpressure were 6.5 psi and 4.7 psi for the two drag structures and 3.4 and 2.7 psi for the two semi-drag structures. The most probable peak intensities of dynamic pressure were 1.1 and 0.55 psi for the two drag structures and 0.31 and 0.20 psi for the two semi-drag structures. Conflicting records indicate that the overpressure value of 6.5 psi may have been as high as 8.0 and the dynamic pressure value of 1.1 psi may have been as high as 1.5 psi.

Good results, generally, were obtained from the deflection gages. The acceleration and strain records were poor because of extraneous high frequency vibrations and base line shifts at the instant of detonation.

The two drag structures experienced maximum transient deflections of 22 inches and 10.8 inches and were deflected permanently 14.6 and 2.4 inches, respectively. The roofing and siding were completely blown off as expected. All the columns in the close-in building suffered definite yielding in the region of the lower chord-to-column connection. The damage sustained by the columns of the other drag building was slight and amounted only to a slight yielding in the flanges of the lower chord-to-column connections. Figure 7.9 shows a general view of the close-in drag structure after the test.

The two semi-drag structures experienced maximum transient deflections of 13 inches and 6.8 inches and permanent deflections of 2.5 inches and 0.7 inch. The roofing of both semi-drag structures was blown off, and the concrete walls suffered only minor to negligible damage. All columns in both structures showed some yielding near the lower chord at the chord-to-column connections. Figure 7.10 shows a general view of the close-in semi-drag structure after the test.

The results obtained in Project 3.7 were such as to warrant the following intermediate and tentative conclusions pending analysis and comparison with results of Project 3.1 in Operation Redwing.

The maximum deflections observed for all four test structures were considerably smaller than would have been originally predicted even when account was taken of the fact that the weapon yield and consequently the peak pressures were slightly lower than had been expected.

The errors in the predicted maximum deflections were due primarily to incorrect original estimates of the drag coefficients of the test structures. Analytical studies indicated that instead

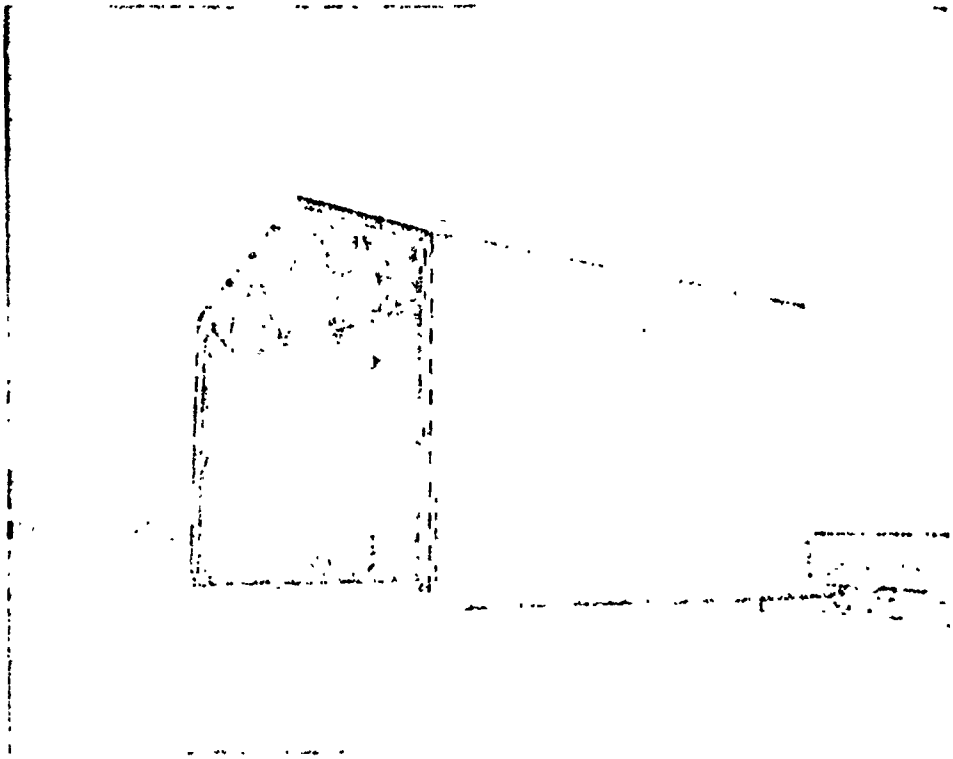

Figure 7.7 Structures 3.7-a as erected in the field.

Figure 7.8 Structures 3.7-b as erected in the field.

of being approximately 1.5 to 2.0 (assuming no shielding), the drag coefficients were about 0.6 for both types of structures. Though the validity of this latter value is difficult to accept, it leaves no doubt that the drag coefficients were much lower than originally estimated.

The analytical studies demonstrated that the impulse imparted to the drag structures by diffraction loading on the frangible siding before it broke was not negligible as was originally assumed. As a matter of fact, it appeared that this impulse was almost as significant as was the diffraction loading on the semi-drag structures. The impulse from the breaking siding can be crudely estimated if the dynamic breaking strength of the siding is known and the time required for it to break can be predicted.

The resistance curves used in the original predictions of response differed significantly from those determined by the pull-down tests in the field. The principal differences were two in num-

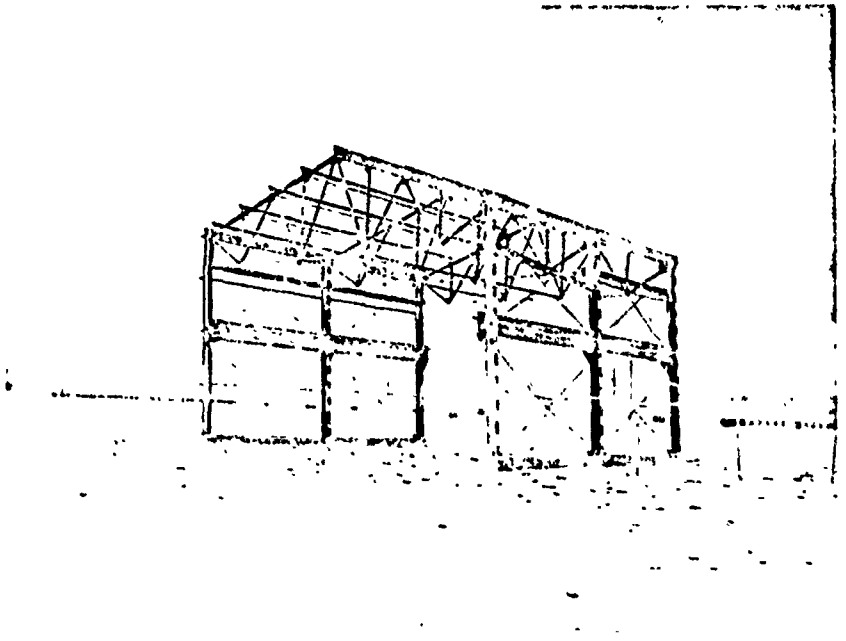

Figure 7.9 Overall view of Structure 3.7-a1 after weapon test.

ber. First, the measured decay rate beyond yield was much greater than had been predicted because of the failure of the windward lower-chord-to-column connections. This was especially evident in the case of the drag structure where an elasto-plastic resistance curve was originally assumed. Second, the predicted static yield resistances differed from the measured values. For the drag structures, the measured yield resistance was about 8 percent lower than the predicted value. For the semi-drag structure, the measured resistance was about 25 percent higher than the predicted value. The higher-than-expected static yield resistance of the semi-drag structures could probably be attributed to the participation of the concrete wall elements. However, for the original predictions, dynamic resistances 25 percent greater than the predicted static values were used. In the final analysis, due to the mode of failure in the column-to-truss connections, no dynamic increase in yield resistance was considered appropriate.

The success with which the measured deflection-time records were reproduced analytically indicated that the idealization of the structures as single-degree-of-freedom systems possessing bilinear resistance functions was reasonable, assuming that discretion was exercised in the choice of the resistance functions and the periods of vibration of the simplified replacement systems.

Results obtained from Project 3.7 of Operation Teapot were of themselves sufficient to contribute materially to the knowledge in the field of structural blast loading and response.

7.7 TEST OF CONCRETE PANELS (PROJECT 3.8)

7.7.1 Objectives. The objective of the project was to test fixed-end reinforced concrete panels under blast loading to obtain experimental data which would: (1) permit checking the accuracy of methods of analysis used by the Bureau of Yards and Docks; (2) provide a better understanding of time-variable parameters for beams and one-way panels; (3) provide a standard against which ease of application and accuracy of several existing methods of analysis could be compared; (4) aid in the determination of plastic range damping; and (5) permit verifying an analog solution response of a beam.

7.7.2 Background and Procedure. In the design of protective construction, it has become an economic necessity to permit plastic deformations in order to gain large energy absorbing capacity and to fully develop load resistance of a member. Little was known about the plastic action of

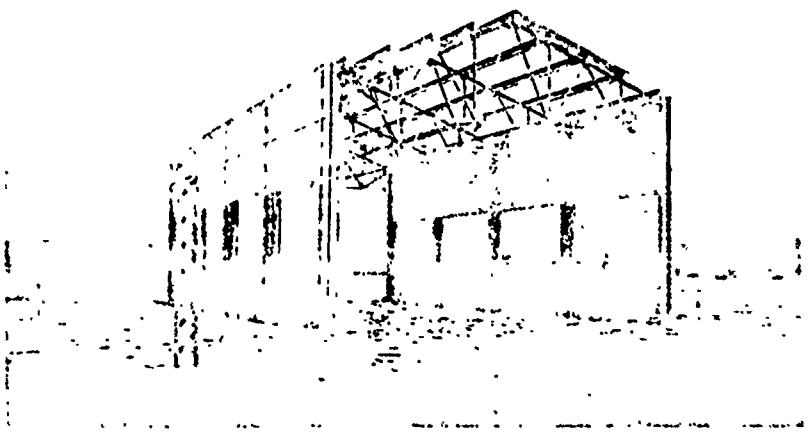

Figure 7.10 Structure 3.7-b1 after weapon test.

structures, particularly when subjected to blast loading. This project was an effort to extend the knowledge of plastic-dynamic behavior of structures and materials.

A ribbed and a solid panel were tested as fixed-ended members in Shot 12 at each of two locations, 3,500 and 4,850 feet from ground zero. The panels were 5 feet wide by 20 feet in length. The solid panels were 9¼ inches thick, and the ribbed panels were 2½ inches thick between ribs and 11¼ inches at the edges. Figure 7.11 shows the underside of a ribbed panel and Figure 7.12 shows the preshot appearance of the station nearest ground zero. The negative reinforcing steel was welded to plates anchored to the foundation steel in order to achieve fixity of the ends and develop the full yield moment of the panel.

The solid panel nearest ground zero was instrumented for strains, deflections, accelerations, and pressures (above and below the panel) versus time utilizing twenty channels of oscillographic equipment. In addition, rotating-drum type self-recording deflection gages and self-recording air overpressure gages were used for all panels. Pipe stake deflection gages were used to obtain maximum and permanent deflections, and crack surveys were made on all test panels.

To supplement field tests, two ribbed panels and fourteen 1-foot wide beams were tested

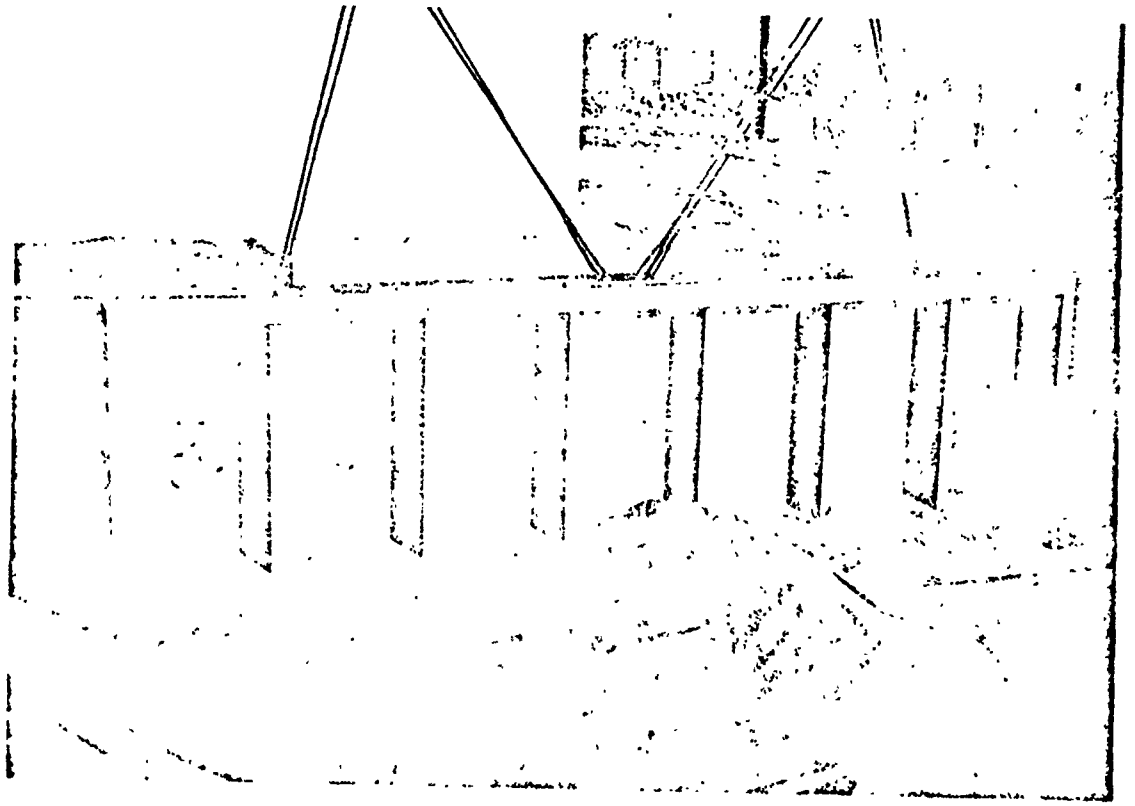

Figure 7.11 Under side of ribbed panel.

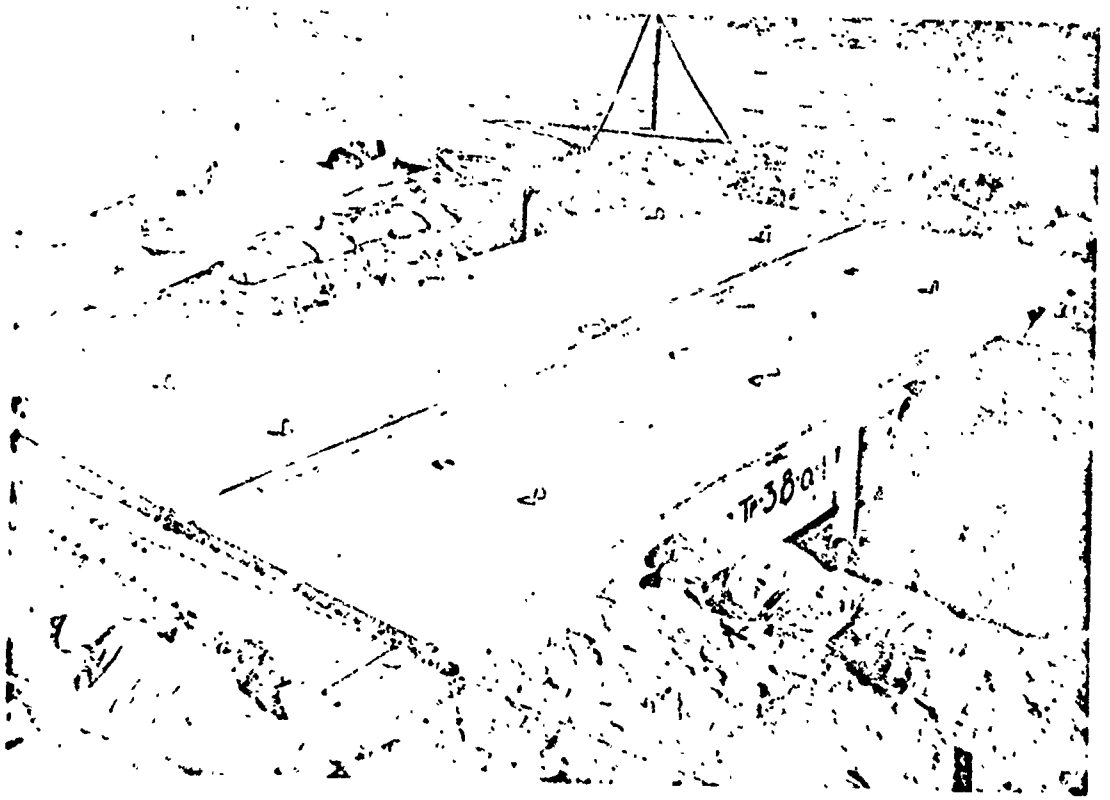

Figure 7.12 Preshot appearance of Structure 3.8-a-1.

statically in the laboratory. From these static tests the resistance curve was determined and the formation and spread of the yield hinge was studied.

7.7.3 Results and Conclusions. The peak overpressures at the two panel locations were approximately 6.6 and 4 psi. Only minor damage was incurred by the panels; hence the results did not permit optimum demonstration of the influence of controlling parameters.

Data from the field and static tests were correlated with theory, and the following conclusions were deduced from the analysis:

(1) The spring-mass-dashpot system provides a satisfactory analogy to the symmetrically restrained and loaded beam of uniform section; however, care must be exercised in the application of this analogy, since violation of any of the conditions of symmetry can invalidate the analogy.

(2) It is possible to predict the rate of strain in the reinforcing steel with sufficient accuracy by combining the maximum velocity and strain measurements.

(3) The percent of fixity of a beam may be determined from steel strain measurements.

(4) Yielding occurs over a large portion of the beam even at relatively small plastic range deflections.

(5) A modification to the Bureau of Yards and Docks method which accounts for damping was determined to provide better accuracy than the approach previously used.

7.8 RESPONSE OF SMALL PETROLEUM PRODUCTS STORAGE TANKS (PROJECT 3.9)

7.8.1 Objectives. The objective of this project was to obtain data on the modes of failure of small cylindrical storage tanks remaining from Operation Upshot-Knothole. The more specific investigations included: (1) obtaining data on the extent of failure of filled, small petroleum-products storage tanks of the types tested, in pressure regions where damage was sufficient to satisfy offensive planning; (2) determining in what pressure regions the tanks would fail by shell rupture, sliding or overturning; and (3) correlating observed results with analytical procedures for predictions of damage to tanks of all sizes, if and when such procedures are developed.

7.8.2 Background and Procedure. Four small petroleum storage tanks which had remained substantially undamaged during Project 3.26.1, Operation Upshot-Knothole, were used for this test. One tank was a standard Army storage tank of bolted construction, 15.5 feet in diameter and 8 feet high, as shown in Figure 7.13. Three tanks were 15 feet in diameter by 10 feet high constructed of $\frac{1}{4}$-inch welded steel plate with all joints butt-welded. A preshot photograph of a typical welded tank is shown in Figure 7.14.

No special foundations were used; the sites were graded smooth and the tanks were placed on the desert surface with no restraints. The bolted tank had its original roof intact and was filled with water up to a height of 8 feet. The welded tanks did not have roofs and were filled up to a height of approximately $6\frac{1}{2}$ feet.

No instrumentation was used on the tanks themselves. Measurements of overpressure and dynamic pressure were available from Program 1 basic blast measurements. Photography was limited to still photographs before and after the tests.

7.8.3 Results and Conclusions. All four tanks received extensive damage. Table 7.3 lists the locations and dynamic pressures for the four tanks.

Although damage was heavy at all ranges, useful information relating to the mode of failure for small filled storage tanks was obtained. The tanks at the two closer ranges (1,200 and 1,350 feet) demonstrated the type of damage one would expect in large tanks, i.e., rupture of the shell directly by blast rather than by rigid-body motion. The welded tank at 1,500 feet provided a pattern of response for that region in which rigid-body motion of small tanks, with associated rup-

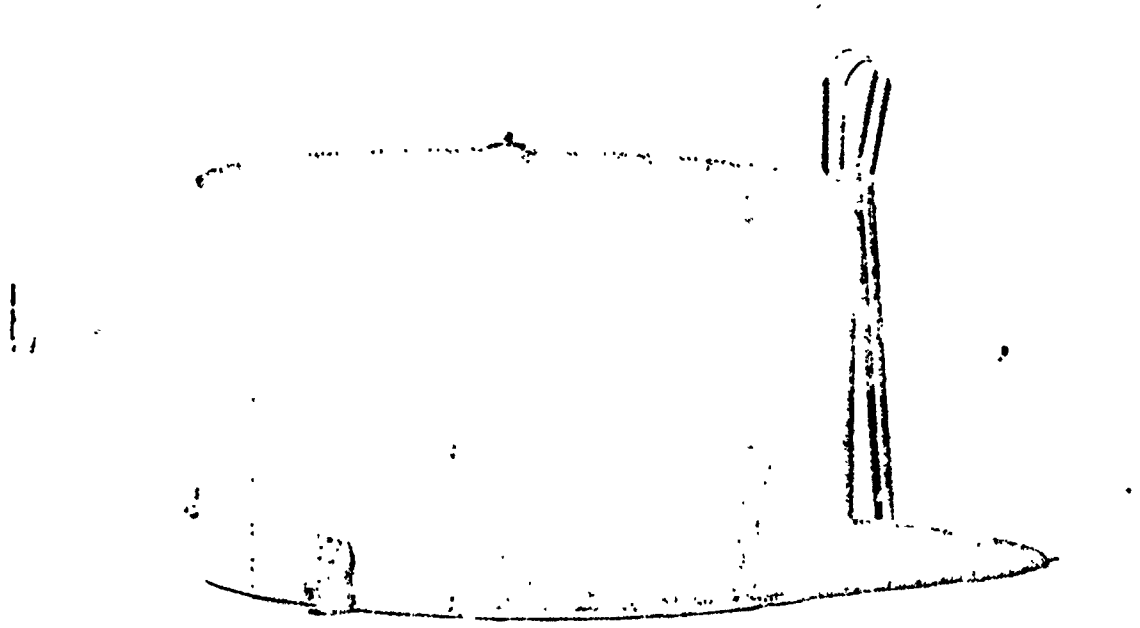

Figure 7.13 Typical view of 3.9a-1 tank, preshot.

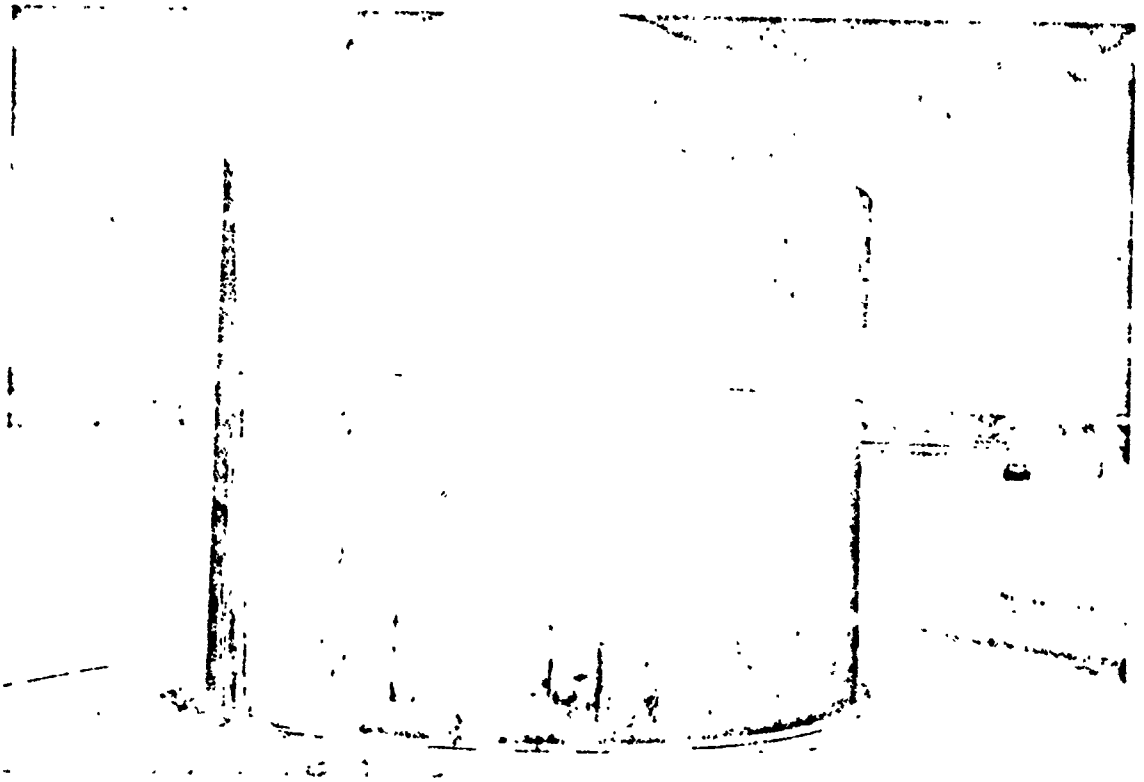

Figure 7.14 Typical view of 3.9b tank, preshot.

turing, could be expected to occur. The response of the welded tank at 2,100 feet indicated that it was a little closer to ground zero than the region in which simple sliding, without overturning or rupturing, would have occurred.

Consequently, a limited amount of empirical data on damage to small filled storage tanks is now available. For a precursor-forming tower shot in the kiloton range at the NTS, the following are known: (1) a combination of overpressure and drag pressure which will rupture filled tanks of this size and shell thickness, without rigid-body motion (40 psi overpressure and 125 psi dynamic pressure); (2) a combination of overpressure and drag pressure which will cause sliding, overturning, and rupturing of such tanks (35 psi overpressure and 90 psi dynamic pressure); and (3) the region in which such tanks would slide without overturning or rupturing but with sufficient force to break pipe connections and cause loss of contents (10 psi overpressure and 10 psi dynamic pressure). It should be possible to correlate the observed damage and basic field data with such theories of plastic response as may be developed in the future.

TABLE 7.3 SUMMARY OF TANK LOCATIONS AND DYNAMIC PRESSURES

Item	Identification	Ground Range	Overpressure	Dynamic Pressure
		ft	psi	psi
3.9a-1	Bolted Steel Tank	1,200	45	200
3.9b.1	Welded Steel Tank	1,350	40	125
3.9b.2	Welded Steel Tank	1,500	35	90
3.9b.3	Welded Steel Tank	2,100	14	30

Chapter 8
EFFECTS on AIRCRAFT

8.1 INTRODUCTION

Recently the utilization of atomic warheads for continental air-defense purposes has been given intensive study. One of the more important aspects of this matter concerns the determination of the nuclear-energy yield of the warhead necessary to give reasonable assurance of destroying an enemy aircraft or missile. Rational approaches concerned with establishing the optimum warhead yield for unguided air-defense weapons require a knowledge of the distance from the weapon burst point at which the enemy aircraft or missile will be destroyed. This distance is usually termed the lethal range. Most of the aircraft weapon-effects-test work in Operation Teapot was devoted to this topic. A general discussion of the information obtained in this test series concerning the effect of nuclear weapons on aircraft and missile materials, as well as on complete aircraft, is given in this chapter.

8.2 DESTRUCTIVE LOADS ON AIRCRAFT

Methods for computing the lethal range associated with a specific weapon yield contain certain assumptions regarding the nature of the blast loading of an aircraft and the structural response of the aircraft to this loading. Analytical techniques for determining structural response in the elastic region are founded on principles known to be correct. If conditions corresponding to aircraft destruction are to be investigated, response accompanied by plasticity and buckling must be dealt with. The analytical determination of response in a plastic or post-buckling era involves assumptions regarding the physical properties of aircraft components during these eras. Since assumptions regarding plastic and post-buckling physical properties under actual dynamic loading conditions require experimental confirmation, it was considered advisable to expose aircraft to a full-scale atomic detonation and to instrument them to obtain response history to complete failure. Project 5.1 for Operation Teapot was devised for this purpose and to yield experimental data for comparison with analytical computations (Reference 4).

It was required that the drone aircraft employed by the project be subjected to a single shock, since a second shock arriving shortly after the first would complicate the blast loading and corresponding response and would not simulate the free-air characteristics of an antiaircraft detonation.

In early planning for this project the use of large bombers participating in the high-altitude shot was contemplated since specific information was needed regarding the lethality of relatively small antiaircraft nuclear weapons utilized to attack large bomber-type aircraft. This was not considered operationally feasible in view of precise timing and positioning requirements and the lack of droned bomber-type aircraft capable of such participation. The decision was then made to simulate the free-air shock characteristics as nearly as possible by using a surface burst that would give a single shock. A surface burst having a yield of approximately 10 kt was needed in order to provide a lethal range sufficiently large to be compatible with the physical limitations imposed by accuracy with which the drone aircraft could be positioned. The Atomic Energy Commission would not approve a surface burst of this size, and the actual test was conducted with a 22-kt device fired on a 400-foot tower. This was designated Shot 12. Under these shot conditions it was predicted that the incident- and reflected-shock waves would merge in a region directly

above the shot tower, as discussed in Section 2.7. In two earlier shots, pressures were measured in an attempt to verify that the incident and reflected shocks would merge above the burst and properly positioned drones would be subjected to a single shock. Results of these experiments were not conclusive, but they did indicate that single-shock conditions would prevail. During Shot 12, the drone aircraft apparently received one shock. There was, however, a small pressure rise approximately 1.7 seconds after the arrival of the incident shock.

Because of the expected variation in yield and the uncertainties involved in calculating blast and thermal inputs and the resulting response, it was decided that three aircraft positioned at different altitudes would be required. This was intended to insure that the minimum requirement of having at least one drone within the lethal range would be satisfied. In addition to actual

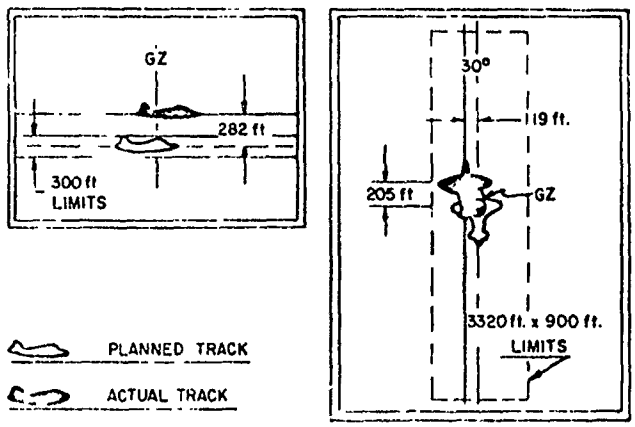

	Planned	Actual
Indicated Airspeed, mph	250	257
True Airspeed, mph	NA	294
Ground Speed, mph	NA	310
Altitude, MSL, ft	8,577	8,859
Slant Range (From Air Zero), ft	5,100	5,386
Overpressure, psi	2.8	2.18
Thermal Radiation, cal/cm^2		44 ± 15 pct

Figure 8.1 Actual and planned conditions for the top drone.

and planned aircraft positions, overpressure and thermal radiation values at each drone are given in Figures 8.1, 8.2, and 8.3. The thermal energies listed for the low and middle drones are not maximum values since the thermal energy received was increasing when the record was interrupted at shock arrival. The positions were selected to produce a blast loading at each drone of 75, 100, and 140 percent of the loading expected to produce failure in the horizontal stabilizer. On the day of the test, one drone aircraft crashed immediately after takeoff because of loss of elevator control. The remaining three F-80 instrumented-drone aircraft were flown by radar control directly over the shot. The low drone sustained extensive damage to the horizontal stabilizer. Drone control by the director aircraft was intermittent and although the drone continued to fly for approximately 8 minutes it crashed into a mountain during the approach to landing. The middle drone was flown to an emergency landing field on a dry lake where it crashed when the landing was attempted. The top drone remained under complete control and was landed at Indian Springs Air Force Base. While landing, the nose wheel of the top drone

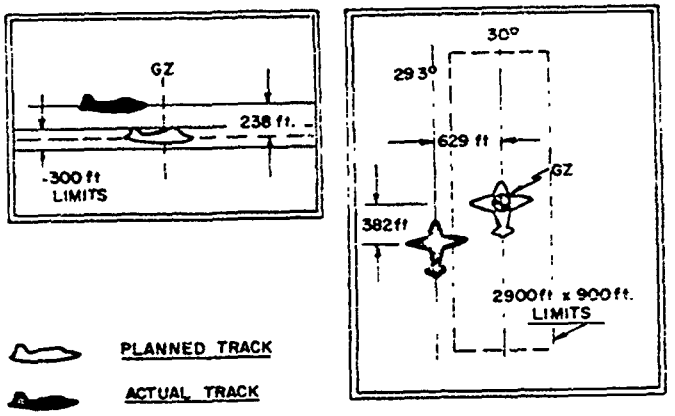

	Planned	Actual
Indicated Airspeed, mph	250	254
True Airspeed, mph	NA	286
Ground Speed, mph	NA	305
Altitude, MSL, ft	7,777	8,015
Slant Range (From Air Zero), ft	4,300	4,596
Overpressure, psi	3.8	3.07
Thermal Radiation, cal/cm^2		51 ± 15 pct

Figure 8.2 Actual and planned conditions for the middle drone.

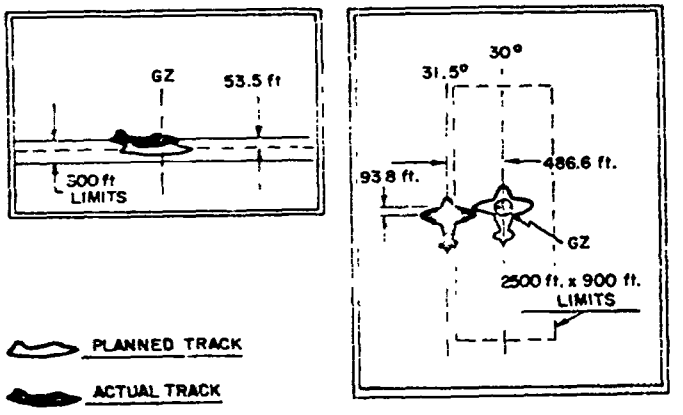

	Planned	Actual
Indicated Airspeed, mph	250	258
True Airspeed, mph	NA	289
Ground Speed, mph	NA	300
Altitude, MSL, ft	7,277	7,331
Slant Range (From Air Zero), ft	3,800	3,885
Overpressure, psi	4.8	4.19
Thermal Radiation, cal/cm^2		99 ± 15 pct

Figure 8.3 Actual and planned conditions for the low drone.

collapsed and the right tire blew out, causing the aircraft to veer sharply and leave the runway before stopping. No damage to the horizontal stabilizer, wings, or fuselage resulted from the landing accident.

As a result of the telemetering failure at shock-arrival time and fogging of the oscillograph records, little strain data was obtained. Furthermore, the overpressure records were not complete, and the overpressure data given in Figures 8.1, 8.2, and 8.3 were obtained by extrapolating the early portion of the records and contain some inaccuracy. Good time-deflection records of the wing and stabilizer response could, however, be constructed from photographs taken by cameras mounted on the test aircraft. Individual frames from the film describing the motion of the horizontal stabilizer of the low drone are displayed in Figure 8.4. The time-deflection record for the right-horizontal stabilizer of this drone appears in Figure 8.5.

In general, the drone damage was not as severe as anticipated. Elastic conditions were exceeded and permanent deformation resulted between Stations 40 and 50 on the horizontal stabilizers of both the low and middle drones. All wing response was apparently elastic. The top drone suffered only slight damage in the form of skin buckles between Stations 40 and 50. Thermal damage was primarily confined to areas not having clean white paint. It is unlikely that thermal damage increased the amount of deformation resulting from the blast loading, since no severe thermal damage occurred near the failure station.

Although incomplete strain data was obtained, the excellent photographic coverage of the structural response will provide experimental information that can be used to demonstrate the applicability of the procedure formulated to compute structural response.

This experiment clearly indicated that destruction of airborne aircraft would not necessarily result from permanent deformation of the horizontal stabilizer.

8.3 EFFECTS OF NUCLEAR EXPLOSIONS ON FIGHTER AIRCRAFT COMPONENTS

In order to supplement the in-flight response information arising from the drone experiment, six F-80 and three F-86D horizontal-stabilizer assemblies (Project 5.5a) were exposed on the ground during Shot 12 (Reference 46). Response data obtained from test conditions simpler than those prevailing in the drone experiment were desired in order to provide experimental confirmation of an analytical technique less complex than the one required for the drones. In this way the possibility of establishing a satisfactory technique for determining the nonlinear structural response for aircraft in flight would be much improved. The F-86D components were employed in order to secure experimental-response data on a different and more modern type structure, which could also be compared with analytically determined response.

Each stabilizer was mounted vertically and was oriented at an angle of attack slightly less than the stall angle. The ranges were chosen so that the stabilizer farthest from ground zero would be essentially undamaged and the one nearest to ground zero would fail completely. Time history of weapon phenomena and response information was obtained. Input instrumentation for each station consisted of the measurement of dynamic pressure, yaw of air flow, and overpressure. Instrumentation for measuring response in the stabilizer at the position where failure was anticipated and bending-moment measurements at various span-wise locations was included. Motion-picture photography was utilized to describe bending-mode deflections and nature of the failure for three F-80 stabilizers. Instrumentation of the ground-mounted F-80 stabilizers was similar to that on the F-80 drones. This made it possible to compare the data obtained on the ground with that obtained in the air.

Postshot examinations indicated that the F-80 stabilizers at the first two ranges were completely severed near the foot, as was expected. On the other hand, the damage received by the F-80 stabilizers at the two farthest ranges was about 50 percent greater than predicted. Inasmuch as damage varied from a small amount of permanent deformation to complete demolition,

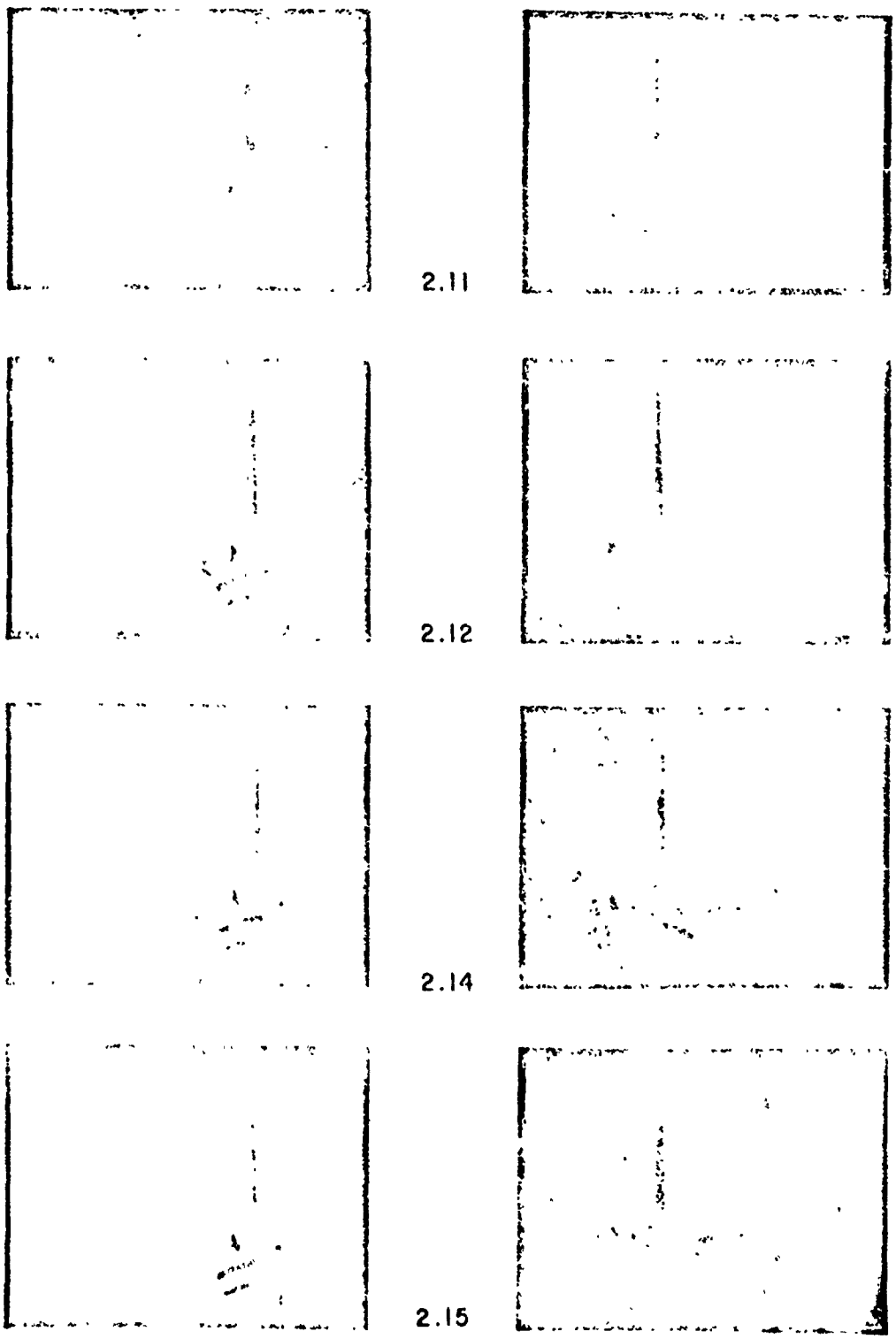

Figure 8.4 Horizontal stabilizer deflection at shock arrival, Drone 3.

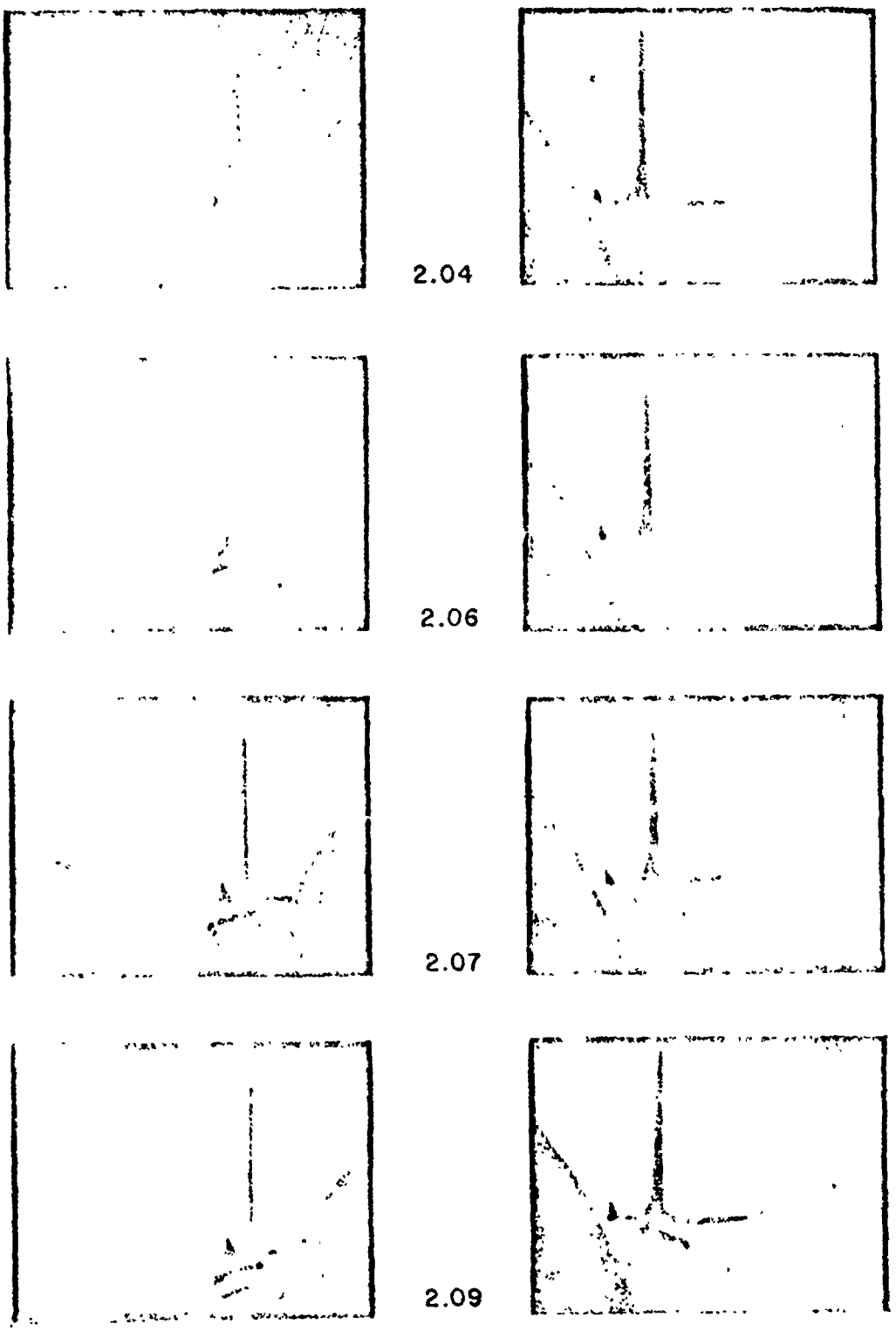

Figure 8.4 Continued.

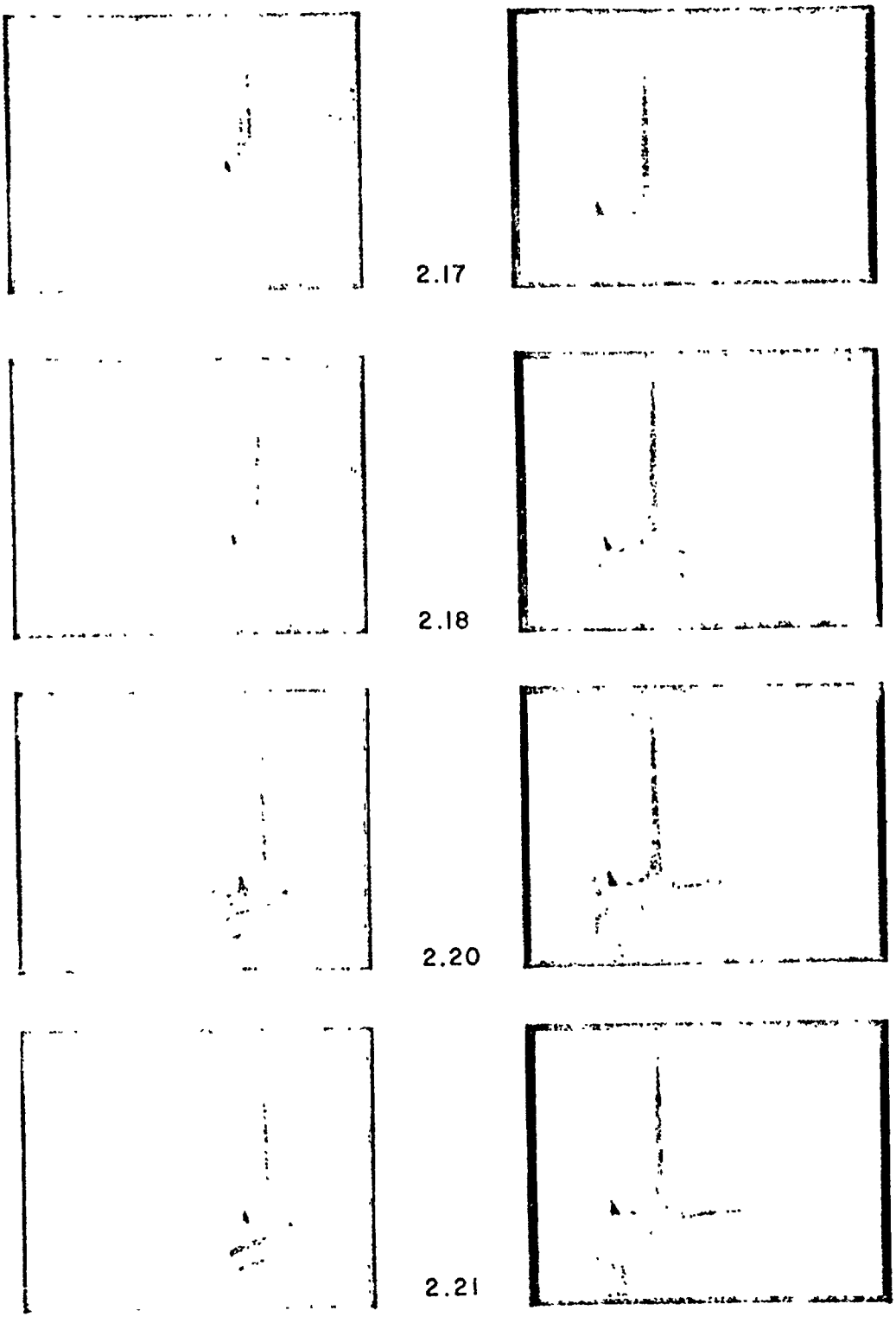

Figure 8.4 Continued.

a sufficient range of F-80 stabilizer loading and response data was obtained. None of the three F-86D stabilizers was subjected to failure loads, and the only structural damage consisted of rib buckling near the section where failure was expected to occur. Good data regarding large elastic response of the F-86D stabilizers were obtained. Pure overpressure-type damage to both stabilizer types was slight, even at overpressure levels of approximately 12 psi. Thermal damage was adequately prevented by the aluminum-foil thermal shield on the irradiated side of the stabilizer. Except for small perturbations, the shock wave was essentially ideal at all ranges. Measured angle of horizontal-air flow (yaw) was obtained only at the ranges farthest from ground

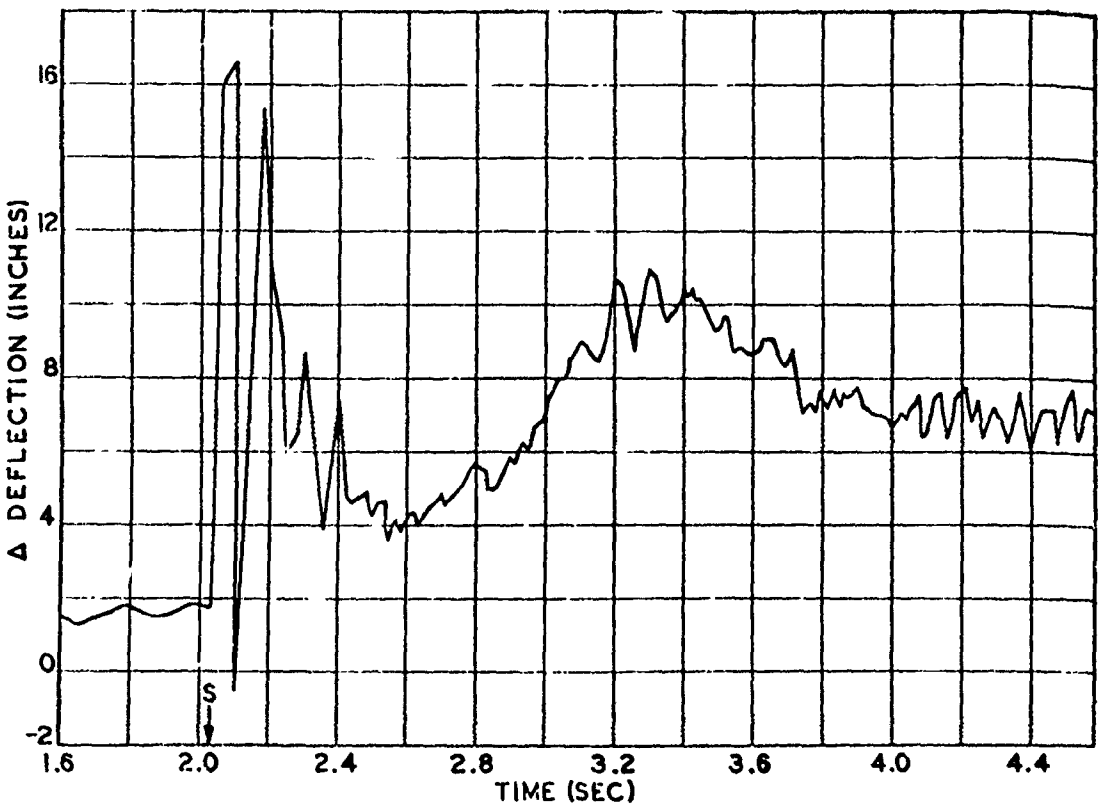

Figure 8.5 Right horizontal stabilizer tip deflection, low drone.

zero. Computations have been made which indicate a very small yaw angle existed at the other ranges. Bending moment and strain-time-history data were obtained for all exposed stabilizers. Only the F-80 stabilizer data will be useful in determining structural response to destructive loads, since the F-86D stabilizers remained elastic. Radiation fogging of the film and water vapor and dust obscuration rendered the motion-picture film useless in evaluating the F-80 stabilizer response.

8.4 THERMOELASTIC RESPONSE OF AN ALUMINUM-BOX BEAM

Since it was established that empirical data to assist in the study of thermoelastic response of aircraft components were needed, an aluminum-box beam instrumented for temperature and strain was exposed during Shot 12, Project 5.5b, (Reference 47). A shield was used to eliminate all blast effects. High-thermal absorptivity was desired; therefore, the front face of the box beam was blackened by means of anodization. Response data consisted of temperature and strain

measurements. Total thermal energy and thermal-energy intensity were measured behind a glass panel inside the blast shield to permit correlation of box-beam response with thermal input. The exposure site was chosen so that a thermal input between 30 and 40 cal/cm^2 would be obtained. The two total-thermal-energy measurements made produced values of 29.1 and 30.0 cal/cm^2 and integration of the thermal-energy-intensity data yielded values of total thermal energy of 30.2 and 31.1 cal/cm^2.

The maximum temperature rise in the front face of the box beam was 188 F which was slightly lower than would have been computed from the thermal energy received by the beam. It has been concluded that either the absorptivity calculation was in error or the absorptivity was modified by a slight amount of dust which had settled on the surface. All temperature rises were normal, and no peculiarities were observed.

A theoretical stress analysis was performed on the box beam using the measured instantaneous-temperature distribution at several times. Comparison between measured and theoretically-determined strain is shown in Figure 8.6.

This experiment was primarily concerned with collecting empirical data, and it can be concluded that the data are of sufficient accuracy and completeness to satisfy requirements.

8.5 THERMAL EFFECTS ON MISSILE MATERIALS

Since one of the most promising methods of accomplishing destruction of a missile appears to be engulfing it in the fireball of a nuclear weapon, Project 5.4 (Reference 48) was devised to obtain quantitative experimental evidence of the effect of the fireball on certain missile-type materials. Steel and aluminum spheres and hollow-steel cylinders 5 inches in diameter and 10 inches long were exposed to the nuclear fireball on Shot 12. The specimens were mounted in the shot cab and on light towers located at horizontal distances of 60, 120, 180, 240, and 300 feet from the shot tower. A radial line drawn through the specimen position and the shot-tower cab made an angle of 41 degrees with the horizontal.

All test specimens, except those in the shot cab, were recovered. The maximum change in radius of the steel spheres was 0.4 inch, of the aluminum spheres 1.3 inches, and of the steel cylinders 0.26 inch. Several types of ceramics were inserted in some of the aluminum spheres. Because of heavy blast damage, the data on the vulnerability of the ceramics were only qualitative, indicating that the ceramics were somewhat less vulnerable to material loss than aluminum.

The thermal-shock resistant characteristics of various materials designed for use as protective surfaces for intercontinental ballistic missiles under conditions of rapid heating, such as would be expected during re-entry of the missile into the atmosphere, were investigated by exposing small samples of aluminum graphite and two ceramic materials at ranges greater than the fireball radius. A parabolic reflector was used at the farthest range to concentrate the thermal energy on the specimens at this location. The ceramics at the parabolic reflector were extensively glazed, but no thermal-shock damage was observed. The materials directly exposed at closer ranges sustained sufficient blast damage to obscure any thermal damage that may have been inflicted on the specimen.

8.6 INVESTIGATION OF PROTECTIVE PAINTS AND RADOME MATERIALS

One of the problems involved in the protection of aircraft against excessive thermal stressing of the aluminum and magnesium skins concerns the development of a protective paint possessing high resistance to thermal radiation. Among the paints currently used are MIL-E-7729 high altitude camouflage enamel and a flat white paint, PV-100, developed by Vita-Var Corporation and specifically formulated for its high thermal-resistance properties.

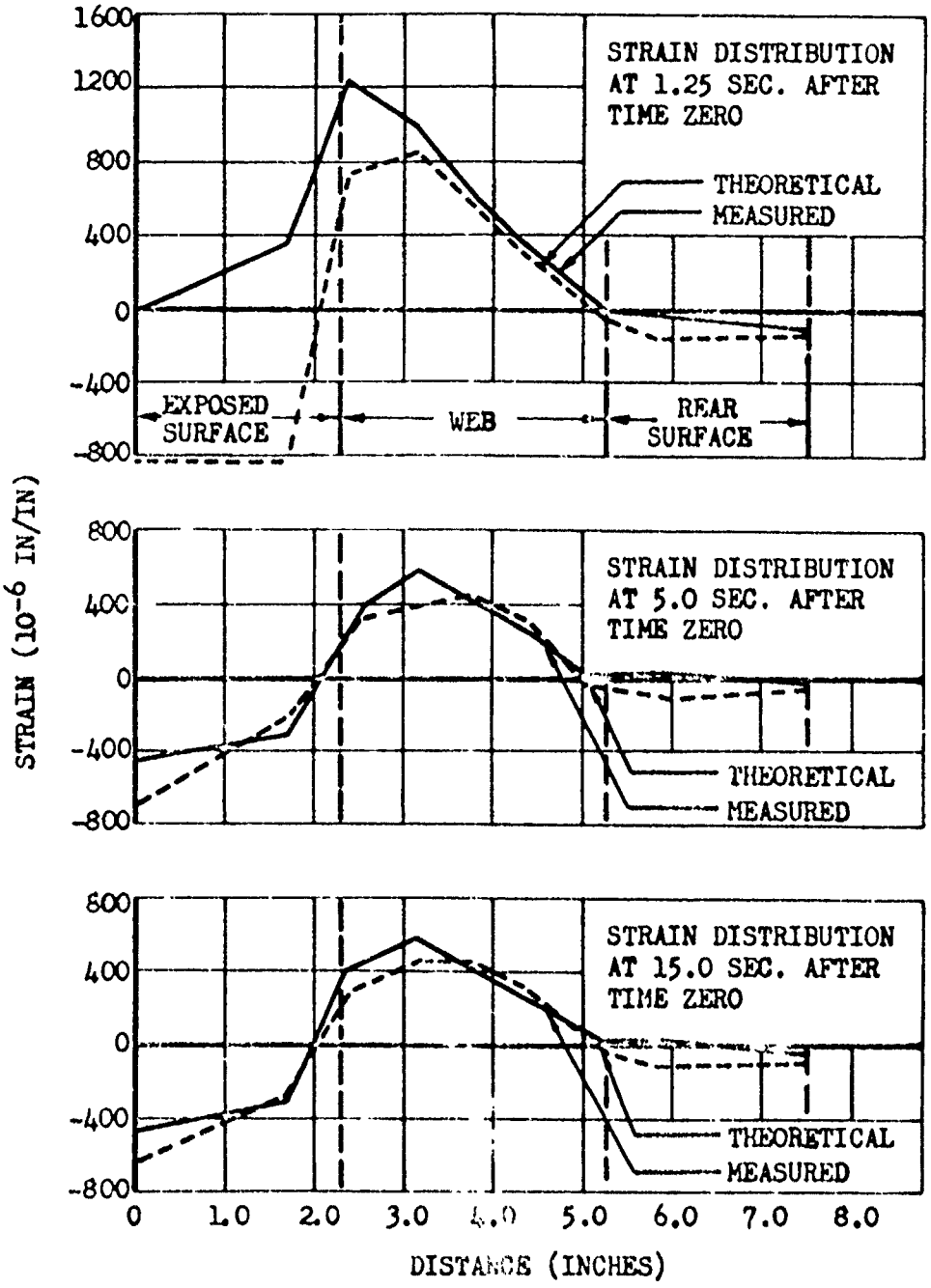

Figure 8.6 Comparison of the theoretical strain distribution with the measured strain distribution at Station C approximately mid-span at 1.25, 5.0, and 15.0 seconds after time zero.

In order to determine the critical energy level for each paint and to compare the field performance of both paints with the results of laboratory tests, as well as to evaluate both paints under field conditions when applied to clad aluminum and magnesium alloy at various thermal-energy levels, it was decided to expose several aluminum and magnesium panels coated with various thicknesses of the two paints.

TABLE 8.1 RANGES AND THERMAL INPUTS FOR PAINT PANEL SPECIMENS

Station	Range	Radiant Exposure
	feet	cal./cm^2
1	2,900	69.9
2	3,400	53.5
3	4,000	39.5
4	4,700	29.2
5	5,500	21.9
6	6,400	16.7

One clad aluminum and one magnesium-alloy panel, each 0.064-inch thick, were exposed at six ranges. The distances from ground zero, along with the thermal inputs for each specimen site, are presented in Table 8.1.

All conclusions are based on results obtained at the station closest to the burst, the only station at which any significant damage was observed. Results at this station indicate that the PV-100 paint had thermal-resistance properties superior to those of the MIL-E-7729 enamel.

TABLE 8.2 RADOME MATERIALS

Panel No.	Resin	Reinforcement	Plies
1560	S-5016	Nylon Cloth	27
1548-1552	S-5016	181-RS 49 Fiberglass Cloth	31-32
1592	S-5016 (25%) L-4232 (75%) Agent #120 (5.25 phr)	181 Fiberglass Cloth	20
M 8	S-5016	Glass Fiber Mat Preform	—
1515	DC-2106	181-112 Fiberglass Cloth	35
1591	L-4232	181-RS 49 Fiberglass Cloth	33
1590	V-135	181-RS 49 Fiberglass Cloth	33

S-5016 - Selectron 5016, Pittsburgh Plate Glass Co.
L-4232 - Laminac 4232, American Cyanamid Co.
DC-2106 - Dow-Corning Corp.
V-135 - Vibrin 135, Nangatuck Chemical Co.

Furthermore, the effective thermal resistance of either paint was better when applied to aluminum and magnesium in a two-mil coat than when applied in a four-mil coat and was better when applied to aluminum than when applied to magnesium.

In addition to the thermal testing of paints, seven radome materials and one B-58 aft radome were exposed to various amounts of thermal radiation. Table 8.2 presents the basic components

TABLE 8.3 COMPARISON OF MEASURED AND CALCULATED TEMPERATURE RISES AS A FUNCTION OF THE COSINE OF THE INCIDENCE ANGLE

Incidence Angle	Cosine of Incidence Angle	Measured Temperature	Calculated Temperature	Difference
degrees		°F	°F	°F
33.6	0.833	46	46	0
41.5	0.749	40	41.4	1.4
41.6	0.748	38	41.4	3.4
59.7	0.505	22	27.9	5.9
82.5	0.131	4	7.2	3.2

TABLE 8.4 PERCENTAGE OF 80-PERCENT LIMIT LOAD ACHIEVED

Reference axis for measured values is waterline 8.8, and for 80-percent-limit values is waterline zero.

Location	Measured Load	80-Percent Limit Load	Percentage Achieved
	10^3 in-lb	10^3 in-lb	
Shot 13			
Wing			
B.M. Station 90	800	3,260	24.5
B.M. Station 150	367	1,220	20.0
Stabilizer			
B.M. Station 12	46	132	25.6
B.M. Station 35.5	24	52	46.1
Fuselage			
Vertical B.M. Station 365	310	880	35.2
Shot 5			
Fuselage			
Lateral B.M. Station 365	207	468	44.2
Torque, Station 365	136	437	31.1
Vertical Stabilizer			
B.M. Station 20	105	256	41.0
B.M. Station 53	28	83	33.8

of each of the seven different materials. Four resins and two reinforcement materials were used in various combinations to make the seven materials. The DC 2106 was the only high-temperature resin tested. Panel M-8 was the only material which was of mat-preform construction. The other six were made by ordinary lamination techniques. The radome was constructed by lamination, using high-temperature resin with fiberglass-cloth reinforcement. Approximately one half of the sample materials were given a coat of white camouflage enamel.

The air blast removed most of the sample radome materials from their mounts and scattered them over the ground. Only 4 of the 70 panels were not recovered. All of the samples at the closest range, where the thermal radiation was 90 cal/cm^2, were charred and in some cases partial delamination occurred. The delamination was probably caused by the combination of the thermal and blast effects. Most of the specimens at the 2,900-foot range, which received 69.9 cal/cm^2, showed slight thermal damage and little blast damage. With the exception of those which were painted, no other samples at ranges greater than 2,900 feet were visibly affected. All the painted samples were blistered. The B-58 radome, which received 28.1 cal/cm^2, displayed no observable damage. No changes in electrical characteristics were detected in any of the test articles, including the most severely charred specimens.

The mat-preform samples were the most susceptible to thermal damage, and those samples using the Vibrin-135 resin suffered the greatest blast damage. Selectron 5016 resin, with 181 fiberglass cloth, displayed the best overall characteristics of the low-temperature material.

8.7 RESPONSE OF F-84F AIRCRAFT IN FLIGHT

The determination of optimum maneuvers for an F-84F aircraft delivering a nuclear weapon required that experimental information be obtained regarding stress produced by thermal radiation and the effect of asymmetrical blast loading. In order to secure this information, Project 5.2 (Reference 27) was established. The project used two F-84F aircraft. One aircraft was instrumented to record thermal response and thermal radiation received only, and the other aircraft was instrumented to record blast overpressure and structural response as well as thermal radiation. Both thermal and blast measurements were obtained at various aircraft orientations with respect to ground zero.

The highest temperature rise recorded during the operation was 81 F on the left wing flap. Measured-temperature rise and calculated-temperature rise based on measured thermal radiation were in fairly good agreement. On the average, the calculated temperatures were 11 percent higher than the measured temperatures. A comparison between measured and calculated temperatures for various incidence angles is given in Table 8.3. Aerodynamic cooling appeared to reduce the skin temperature rise by 5 to 10 percent. This cooling effect may be more significant when higher temperature rises prevail. A summary of the data for the structural-response portion of the experiment is given in Table 8.4. The percent limit load listed in the table is the maximum measured during the operation.

The wide spread between predicted and maximum yields of development shots and the conservative positioning criteria applied caused the test aircraft to be positioned at low-input levels with a resultant loss of much significant data.

Chapter 9
TEST of SERVICE EQUIPMENT and OPERATIONS

Program 6 included those general projects which did not fall into one of the primary effect or response programs. The program had two primary fields of study: operational and technical evaluations of instruments designed to assess the lethality of nuclear radiation in the field, and tests of systems which provide an indirect estimate of the damage caused by nuclear detonations.

Nearly every operation since Operation Crossroads has contained a formal program of nuclear radiation dose or dose-rate instrumentation evaluation. By the time of Operation Teapot, the implementation of such projects was well standardized. Project 6.1.1a (Reference 49) was, then, a continuation of similar experimentation performed on earlier tests.

A developmental radiac meter (TM-108) was subjected to a user test in fairly large quantities by personnel from the Army training exercise conducted in conjunction with Operation Teapot. The readings obtained were compared with indications of older assumed-standard radiacs. These comparisons, together with user comments and ruggedness tests, provided the basis for the evaluation.

Several types of dosimeters were tested under more controlled conditions, both to initial and residual radiation. The test involved placing the dosimeters in groups in the field and comparing their indicated-dose values with those obtained either by the National Bureau of Standards (NBS) film pack (initial radiation) or Victoreen chamber (residual radiation).

Of the dosimeters tested, the quartz-fiber electroscope model (IM-93) was found most satisfactory. A self-developing film badge (DT-65) and a chemical color-change step dosimeter (E1R3) were labeled unsatisfactory by the project, though considerable controversy over the validity of the evaluation of the E1R3 still exists. Detailed results of this project may be found in the appendix.

A so-called radiological calculator developed by the Signal Corps Engineering Laboratories (SCEL) was subjected to a limited field test. The calculator was essentially a simple analog computer designed to permit rapid mathematical manipulation of the radioactive decay equation. Given two values of radiation intensity at a given field location, the calculator provided the dose rate at any other time and an estimate of the dose during any selected interval. The device had indexes for several decay slopes in the vicinity of the empirical $t^{-1.2}$ value commonly accepted for mixed-fission fallout fields.

Evaluation by comparison of predicted to actual dose rates demonstrated a basic fallacy in the assumption of uniform decay in the field radiological situation. Local areas in the field were subjected to natural disturbances (e.g., wind, precipitation) so that the radex at any time showed little relationship to the status at earlier times.

A more subtle approach to the problem of radiac evaluation was undertaken by Project 6.1.2 (Reference 50). The available types of high-range ratemeters were exposed and their readings compared to a laboratory standard under highly controlled experimental conditions in the field.

An additional effort involved investigation of the directional properties of several typical field-source situations and determination of the response of various radiacs (mounted on a human phantom) at various orientations to these fields.

It was found that the internal configuration of the various instruments had a pronounced effect on their field response, primarily because of calibration errors. Further, various units of the same type, though they received care and maintenance far superior to the combat situation,

showed dispersion in readings as high as 50 percent in identical radex situations. On the basis of this finding, it was noted that standard radiac readings were not sound foundations for casualty prediction in operational situations.

Based upon the field results, revised calibration procedures for each instrument type were formulated. These procedures were successful in removing the systematic errors induced by normal calibration.

Laboratory work in conjunction with this project resulted in development of an improved gamma-radiation standard for radiac calibration. This standard compensates for the reduced lethality of effective radiation energies below about 100 kev.

As a result of an Army Corps of Engineers requirement, a simple detonation-warning device was designed and tested by Project 6.1.1b (Reference 51). The device consisted of blast, thermal, and nuclear-radiation detection devices connected to operate a secondary warning or protective-device closure circuit. The system operated satisfactorily under all three perturbing influences with more than adequate sensitivity.

A study of the isolated effects of intense gamma radiation, as distinct from the usual blast thermal gamma radiation combination, was undertaken using selected electronic components. Exposed in blast-thermal shields to fluxes of greater than 10^4- r initial radiation were several types of electron tubes, a complete radar transponder, and a variety of frequency-control crystals. The only measurable effects were observed in the crystals, which showed varying degrees of frequency shift and resistance increase. Even in the aluminum shields the mechanical effects were often more severe than the sought-after radiation effect.

Several possibilities have presented themselves during past operations for rapid intelligence-gathering systems for damage assessment on either friendly or enemy atomic strikes. Ideally, such a system would provide information on ground zero, height of burst, and yield, a short time after the detonation. Two general classes of detection systems were proposed: a line-of-shight (or radar) system for use in drop aircraft (IBDA) and a ground-based detection system operating at ranges in excess of fifty miles. Project 6.3 (Reference 52) was concerned with evaluation of a bread-board model of the ground-based, long-range system.

The three pieces of information for complete indirect bomb-damage assessment were independently sought by three instrumentation efforts. The electromagnetic pulse emanating from atomic detonations at zero time provided an excellent means of ground-zero determination. Preliminary studies directed toward increasing the range of time to thermal minimum yield measurement were made using essentially a narrow-band bhangmeter. And an attempt was made to measure height of burst by seismic means.

The electromagnetic ground-zero measurement made use of an inverse loran principle; i.e., the reception time of the weapon pulse at two or more stations was compared to provide one or more lines of position. The pulse receivers used were designed for response to the broad-frequency band which contained the majority of the radio-frequency energy in the weapon pulse. Interstation timing comparisons were made by microwave link, while the time interval was measured by a crystal clock. The network contained two stations on each of two baselines, one at 60 miles and the other at approximately 200 miles from the test site.

Of the 13 shots on which the equipment was operated, only the underground event was not detected. Nearly 50 percent of the possible positive indications of detonation were achieved, though the percentage of full-system function to provide a line of position was somewhat less. This experiment proved the feasibility of using the electromagnetic pulse for burst location. (The Signal Corps Engineering Laboratories continued the development of a tactical-range, up to 500 miles, location system, and participated in both Operation Redwing at Eniwetok, 1956, and Operation Plumbbob in Nevada, 1957.)

As a result of the lack of success in attempts to correlate electromagnetic wave-form parameters to yield, preliminary studies toward extending the range of light-pulse (bhangmeter) meas-

urements were undertaken. It was known that time-to minimum varied with wave length in the thermal pulse, though the empirical equation relating yield to time to minimum had been developed on the basis of the results for a specific broad-band receiver. Because of the increased transmissivity of the atmosphere for the infrared wave lengths, it was felt that a narrow-band bhangmeter sensitive only to these wave lengths would be capable of reliable yield measurement at greater ranges than normally attempted. The preliminary investigation involved gathering band spectra versus time in the 0.5 to 2.5 μ region. Since the investigation was exploratory in nature, no attempt was made to extend the measurements to very long ranges.

The results demonstrated a definite shift in time to minimum with wave length, though insufficient data were obtained to provide yield-time relationships for all the spectral bands investigated. It was observed that time to minimum decreased with increasing wave length, which in effect would tend to negate the other advantages associated with the use of the longer wave lengths. (More-sophisticated spectrometer measurements from an airborne station on Operation Redwing indicated that time to minimum was a complicated double-valued function of wave length. See the report for Project 8.5, Operation Redwing, ITR-1342, Reference 53). The project results did not justify a recommendation that the narrow-band technique be used as the yield-measuring portion of the tactical-range bomb-damage-assessment system.

The third parameter to be ideally furnished by the tactical-range locator system was height of burst. Attempts to correlate electromagnetic wave-form parameters with burst height were not successful. The possibility of determining burst height by measuring the difference between time of arrival for a hypothesized thermal-induced seismic shock and that for the blast-induced seismic shock was investigated. Equipment difficulties and the large electrical transient induced in transmission lines at zero time precluded detection of the thermal seismic, if such a signal existed, and the technique was abandoned.

Although not officially a part of the Weapons Effects Programs, Project 40.5 (Air Force Cambridge Research Center, AFCRC) was of some interest. This project fielded a more complex system for burst location using the inverse-loran technique. Ground-zero fixes with an average error of one nautical mile were obtained on all above-surface events from stations more than 200 miles distant. (Successful fixes were obtained at ranges in excess of 4,000 miles on Operation Redwing; References 54 and 55). Since the observation during Operation Crossroads that nuclear detonations produced a significant return on operational radar screens, the U.S. Air Force has been studying the possibility of using this phenomenon for IBDA. Basically, the burst presentation on a plan-position-indicator screen appears first as an expanding bright return at the location of ground zero, and later develops an area of no return (not even normal ground clutter) in the center of the bright area. The no-return area often eclipses the bright return on the side away from the observing station, giving rise to a horseshoe-shaped presentation.

Early attempts were made to extract all three IBDA parameters from radar alone, by time comparison and simple geometrical calculations, assuming the no-return area corresponded to the visible fireball and cloud. When these methods failed, the radar observations were used for ground-zero location only, and as in Operation Teapot Project 6.4, cameras and bhangmeters were added to provide at least clear-weather IBDA capability. (Recent experience, Operation Redwing, with electromagnetic radio-frequency measurements has again raised the possibility of yield measurement by this means; References 56 and 57.)

By the time of Operation Teapot, a complete IBDA system had been developed, and Project 6.4 was designed as an engineering evaluation of the various components. The bhangmeter technique for yield measurement was evaluated for ground-to-air ranges over 140 miles, as an additional objective. The complete IBDA system consisted of a standard radar set, a K-17 aerial camera, a recording set and photosensitive receiver for time to minimum measurements, and an associated programming and power-supply installation.

Results comparable to those obtained by ground stations were obtained by the airborne bhangmeter at ranges over 100 miles. Both the radar set and K-17 camera provided good ground-zero location, and the height-of-burst measurements under Nevada weather conditions were successful. The Air Force thus established an IBDA capabil ty for operational drop aircraft.

Project 6.5 (Reference 58) was the first attempt by Naval Air Forces to delineate their capability for IBDA by radar methods. The Navy project was limited in scope and used unmodified operational equipment. No means of determining height of burst or yield were included in the instrumentation.

Operational difficulties limited the project to a total of eight runs on five shots, and of these, only two positive records of the burst were obtained. Radar interpreters were unable to determine the ground-zero parameter from either of the recorded bursts, thus leaving the project without any successful participations.

Based upon these sparse observations, it was concluded that the equipment tested might provide the Navy with an interim IBDA capability, though standard radar-set operating procedures need to be developed for this purpose.

Appendix
PROJECT SUMMARIES

Brief summaries of the specific activities of each Operation Teapot project are presented herein as a complement to the more-general discussion of the test programs contained in Chapters 2 through 9.

A few of the final project reports were as yet unpublished at the time this final summary report was prepared. In general, the draft manuscripts of such reports were available and were consulted in order to make these project summaries as complete as possible. In any case, the published versions of the final (WT) project reports should be referred to for complete, final information. The report title and short title (WT number) are indicated herein for each project; information on the availability of these reports may be obtained from the Chief, Defense Atomic Support Agency, Washington, D.C.

PROGRAM 1: BLAST AND SHOCK MEASUREMENTS

Project 1.1: "Measurement of Free Air Atomic Blast Pressures" (WT-1101); Air Force Cambridge Research Center, Bedford, Massachusetts; Richard Brubaker, Major, USAF, Project Officer.

This project had a twofold objective. First, it was desired to obtain peak free air overpressure versus time measurements in the 10- to 2-psi range as a function of distance directly over a nuclear burst at a low scaled height. These data were expected to establish the points in space where the reflected wave merged with the direct wave to form a coalesced shock and to determine the overpressure as a function of distance of the merged wave. The data were required in direct support of Project 5.1 (Shot 12) to position the drone aircraft of that project. Second, free air peak overpressure versus distance measurements were to be made at ranges from a burst at a high altitude (40,000 feet).

The project participated in three shots, Shots 4, 8, and 10. Parachute-borne canisters were deployed from an aircraft at a predetermined time so that they would be at various slant ranges from the burst point at H hour. Each canister contained two differential-pressure transducers, a pressure-altimeter transducer, and a radiotelemetry transmitting unit.

On Shots 4 and 8, ten canisters were deployed from a B-29 aircraft. The positions attained by the canisters at shock-arrival time were such that information on overpressure distribution directly applicable to the drone positioning problem could not be provided. A merged shock wave was not recorded. Reflected waves were recorded; however, they showed a small amplitude in each case, and this suggests that, if the reflected wave does overtake the direct wave above the shot, it will result in only a small increase in peak overpressure.

On Shot 10, 15 canisters were deployed from the B-36 strike aircraft. Peak overpressure data were obtained over the range from 7.6 to 0.13 psi, along a curved array (increasing altitude outward), and extending upwind from air zero for approximately 12,000 feet. Reducing these pressures and slant ranges to equivalent values at shot altitude with modified Sachs scaling, it was found that fairly close correlation was obtained with a 2 kt curve by scaling (also modified Sachs) up to shot altitude a normalized, composite, free-air curve. Inasmuch as the yield for this shot was close to 3.1 kt, this result would seem to indicate that the application of Sachs scaling from sea-level conditions to this altitude may not be appropriate and/or the blast efficiency is not as high at this altitude as previously had been supposed.

Project 1.2: "Shock Wave Photography" (WT-1102); Naval Ordnance Laboratory, Silver Spring, Maryland; J. F. Moulton, Jr., Project Officer.

High speed, high-resolution photography was employed by this project to obtain: (1) pressure-distance data in the free-air region; (2) information on the closure of the direct- and reflected-shock waves; (3) records of precursor phenomena and precursor-shock interactions; and (4) arrival-time data for the base surge.

The project participated in 10 of the 14 shots, including the underground, the military-effects tower, and the high-altitude detonations. On four shots (Shots 4, 8, 10, and 12), a smoke grid was established behind the burst, with respect to the camera, to facilitate detection of the shock waves.

Results may be summarized as:

1. Coalescence of the direct and reflected waves was observed to occur on Shots 4 and 12. Pressure-distance data were obtained from analysis of shock-wave-velocity measurements for the merged wave on both tests. The observations on Shots 4 and 12 were

not consistent; however, the deviation has not as yet been explained.

2. The smoke grid, produced by jet aircraft for Shot 10, was of little use to detect the shock wave, and lack of contrast on the films taken by direct-shock photography made it difficult to see the shock front. However, some time of arrival data were obtained from the Fastax camera film. In addition, shock-wave refraction of the smoke puffs, Project 1.9, was observed; these data, with time of arrival data from Project 1.1 canisters, were used to establish the pressure-distance curve.

3. On Shot 12 a most extensive precursor was observed over the asphalt area and, to a lesser extent, over the desert area. The dust which followed closely behind this wave obstructed the view of the blast wave near the water surface. Precursors were also observed on some of the other shots. Measurements of these precursors led to a more complete understanding of the nature and effect of this phenomenon.

4. On Shot 7, a well-formed base surge was observed. The photographic records documented the radial growth of the base surge versus time, and gave data which may be used in comparisons with high-explosive results. It is concluded that nuclear radiation in the base surge can be a serious hazard to exposed personnel.

Project 1.3: "Microbarographic Pressure Measurements at Ground Level from High-Altitude Shot" (WT-1103); Sandia Corporation, Albuquerque, New Mexico; Ron Millican, Project Officer.

The objective of this project was to measure peak overpressure (both incident free-air and reflected) near the ground resulting from Shot 10. Results obtained were used to examine free-air-pressure scaling techniques, surface reflection of shocks, the effect of atmospheric structure; and to obtain tentative indications of the blast efficiency at high altitudes.

This was accomplished with millibarographs and microbarographs located at an array of ground stations in a line to the south extending to the Mercury camp (140,000 feet). Ballistic Research Laboratories (BRL) provided self-recording microbarographs at approximately 40,000 feet from ground zero in north, east, and west directions.

The data as recorded indicated that shock overpressures at the ground surface from high-altitude bursts may be more accurately predicted with modified Sachs scaling than with ordinary Sachs scaling. Modified Sachs-scaled observations showed about 20 percent lower overpressures than those expected from the free-air-pressure distance curve, while ordinary Sachs-scaled observations measured about twice the expected overpressures. Similarly, predictions made by modified Sachs scaling of the extended overpressure curve gave results slightly higher than observed.

Positive- and negative-phase durations and the difference between acoustic and shock-arrival times were found to be best predicted by ordinary Sachs scaling. Therefore, time parameters for small-yield weapons depend upon ambient conditions at burst altitude and the strong-shock region and not upon conditions at or near the observing point. Measurement of the surface-pressure-reflection coefficient gave average values of 0.92. No correlation with surface texture or incident angle was possible. Atmospheric-accoustic effects on the overpressure distribution were too small to be measured in this experiment.

Project 1.5: "Preshock Sound Velocities Near the Ground in the Vicinity of an Atomic Explosion" (WT-1104); Navy Electronics Laboratory, San Diego California; R. C. McLoughlin, Project Officer.

The primary objective of this project was to determine preshock air-sound velocities at elevations up to 6 feet over different types of surfaces in the region where the precursor shock existed.

The measurements were accomplished by transmitting acoustic waves across air paths of fixed lengths and observing the times of transit. The project made a preliminary test of its equipment on Shot 8. Its main effort was concentrated on Shot 12. Instruments were placed at 1½-, 3-, and 6-foot elevations over special surfaces and at ranges from ground zero as follows:

1. Frenchman Flat desert soil, 1,000 and 2,000 feet.
2. Asphalt, 1,000 and 2,000 feet.
3. Water, 1,000 feet.
4. Fir boughs, a special plot at 2,000 feet on the desert line.
5. Broad leaf cover (ivy), a special plot at 2,000 feet on the desert line.
6. Concrete, a special plot at 2,000 feet on the desert line.

Results may be summarized by the following statements:

1. The preshock velocities of sound over water, asphalt, desert, and the concrete slab were similar. Magnitudes varied, in general, from 1,150 to 1,400 ft/sec.
2. Velocities did not vary appreciably with height, irrespective of the surfaces.
3. Over the fir bough and ivy plots there were marked evidences of turbulence, and velocities appeared as high as 1,700 ft/sec.
4. The pressure amplitudes of the acoustic signals dropped to about one tenth their ambient values at all 1,000-foot range locations within 70 msec and, in general, remained there until shock arrival some 70 to 100 msec later. At 2,000-foot ranges the amplitudes dropped to about one tenth ambient within 150 msec and

generally remained small until shock arrival some 350 msec later. Postshot experimentation on the instrumentation revealed that the signal loss was due to changes in the physio-chemical characteristics of the direct-air path.

Project 1.6: "Crater Measurements" (WT-1105); Engineer Research and Development Laboratories, Fort Belvoir, Virginia, and Ballistic Research Laboratories, Aberdeen, Maryland; J.G. Lewis, Project Officer.

It was desired that this project determine the physical characteristics of the crater and lip formed by the underground explosion of an atomic weapon. A further objective was to define the terms apparent crater and true crater in the light of their meaning based on the movement of the soil.

In preparation for Shot 7, 21 vertical shafts of colored sand were placed along one diameter through ground zero. After detonation of Shot 7 and when the residual contamination had decreased to a safe level excavation work to uncover the colored-sand columns was begun. The top of the central column, when uncovered, was 128 feet below the original ground level, or 61 feet below the center of gravity of the charge. This point defined the depth of the true crater. The radius of the true crater was determined at 150 feet, and the true-crater volume at approximately 3.25×10^6 ft^3.

The apparent crater was measured in considerable detail by aerial-mapping techniques using previously placed aerial markers. The crater had steep walls and was remarkable symmetrical. From the profiles, the dimensions of the apparent crater were determined to be 146-foot radius at original ground level, 90-foot depth below original ground level, and apparent volume of 2.7×10^6 ft^3.

Also presented in the project final report are methods of determining energy density and the energy partitioning of the explosion, as well as what effect these parameters have upon crater formation. In addition, using data from Project Mole (Stanford Research Institute), predictions of crater dimensions in various soil types are presented.

Project 1.7: "Underground Explosion Effects" (WT-1106); Stanford Research Institute, Menlo Park, California, and Office of Naval Research, Washington, D.C.; L.M. Swift, Project Officer.

One objective of Project 1.7 was to obtain data on the free-field effects of the underground test, Shot 7. It was hoped to establish a correlation between these effects and similar measurements made on small charge high-explosive tests and the results of the Operation Buster-Jangle underground shot at a different depth of burial. A second objective of the project was to furnish instrumentation for Projects 3.3.1 and 3.3.2, concerned with measurement of blast loading of structur l devices by an underground nuclear explosion. Ana vsis and reporting of these data were a responsibility of these projects.

Seventy-six channels of instrumentation were installed; 75 usable records were obtained. The free-field parameters which were measured included air-blast pressure, earth acceleration, earth stress and strain, and permanent-earth displacement.

In general, the wave forms of the various gage records of free-field-earth measurements obtained on Shot 7 were quite uniform with respect to ground range and gage-burial depth. In addition, the induced effects which may be identified with air blast appeared to be small and of short duration. When the results of the Jangle U and S shots were compared with those of Operation Teapot Shot 7 it was found that the horizontal-radial component of the velocity parameter presented the most consistent picture. In most cases, the predictions of peak-transient surface and underground phenomena, which were based upon crater dimensions, were higher than the measured values. Maximum air-blast pressures observed on Shot 7 were two or three times greater than would be predicted using pertinent data from previous nuclear tests and underground high-explosive experiments. The Project 1.7 report presents the results in considerable detail and discusses some tentative scaling conclusions.

Project 1.9: "Material Velocity Measurements of High Altitude Shot" (WT-1108); Sandia Corporation, Albuquerque, New Mexico; Ron Millican, Project Officer.

The objective of this project was to use smoke puffs as a means of obtaining particle position (hence, particle velocity and shock pressure) as a function of time on Shot 10. The data were to be obtained in the high-pressure region interior to that normally feasible for airborne canisters and were to fill in some pressure-time information over this region where only peak pressures were being obtained by the smoke-trail technique.

By photographically following the motion of smoke puffs two types of information were to be obtained: a time of shock arrival curve, and the displacement time history of the smoke puffs after they were engulfed by the shock front. The proper smoke-puff pattern was obtained; however, the plane of this pattern was about 900 feet above the burst point. This error removed the smoke puffs from the region of interest and introduced complications in the data reduction.

The desired particle-position history in the region of interest, 400 to 1,200 feet from burst point, was not obtained. It is apparent that the results have little value. First, data scatter was doubled by projecting the apparent motion upward and compounding the computational inaccuracies. Secondly, data reduction was hampered

by the original misplacement of the array above the air zero point.

The only conclusion that could be reached on the material-velocity behavior was that there were no indications that the predicted displacements did not occur. Although the smoke puff data had some shortcomings regarding absolute magnitudes, the smoke-puff-displacement times were smooth and indicated nothing abnormal, such as secondary shocks, in the positive phase. Further, the shortcomings of the smoke-puff data were not as serious as they would have been if drastic changes had occurred in the blast partition of energy on the high-altitude Shot 10.

Project 1.10: "Overpressure and Dynamic Pressure versus Time and Distance" (WT-1109), Stanford Research Institute, Menlo Park, California, and Office of Naval Research, Washington, D. C.; L. M. Swift, Project Officer.

The objective of Project 1.10 was to obtain data on the variation with range of side-on and dynamic pressures from a nuclear explosion over three types of surfaces: namely, a dust-free reflecting surface (water), a dust-free absorbing surface (asphalt), and a desert surface. A relationship was sought between side-on and dynamic pressure in regions of perturbed wave forms, to be used for modification and reinforcement of theory as to precursor formation. Specific data were also to be furnished to Programs 1 and 5 for use in calculating structural effects.

The project participated on two shots (Shots 6 and 12) installing 24 and 123 channels of instrumentation, respectively. Usable records were obtained on 141 of the 147 channels. This excellent performance was due, to a large extent, to well-designed instrument towers which withstood the blast effects on both shots.

Measurements of side-on and dynamic pressure were taken using a Pitot-tube gage at 3- and 10-foot elevations above the surface. Side-on pressure was also measured at ground level and at 10 feet, using a baffle mount. On Shot 12, at one radius on each line, investigation was made of the variation of dynamic pressure with height up to 40 feet. Also, at two radii on the water line, measurements were made of variation of dynamic pressure across the water surface. Channels consisted essentially of Wiancko balanced variable-reluctance transducers connected through modified Wiancko station equipment to William Miller Corporation oscillograph recorders.

The data from both shots showed pronounced differences in measurements over the different surfaces. In both cases, the asphalt surfaces caused higher-propagation velocities, lower-peak overpressures, and disturbed wave forms out to greater ground ranges than did the desert surfaces. The water surfaces of Shot 12 produced lower-propagation velocities, higher overpressures, and a lesser extent of disturbed wave forms than did desert or asphalt surfaces. In general, the measured maximum-dynamic pressures varied between the ideal value and twice that value, being generally highest on the desert lines and lowest on the water line.

With a few exceptions, it was possible to group the pressure-time results into two sets of wave form classification; one system for overpressure, and another for Pitot-tube dynamic-pressure measurements. As expected, wave-form behavior as a function of ground range was sensitive to the characteristics of the blast-line surface. Analysis was made of preshock near-surface temperatures as computed from measured-blast parameters. There was evidence from the offset gages on the water line that led to the conclusion that a precursor formed over the water for Shot 12.

The limited effort expended to measure forces acting on two H-beam devices yielded only tentative conclusions. It is believed that the presence of particulate matter in the blast wave had a profound effect upon the drag force experienced by such structural elements.

Project 1.11: "Special Measurements of Dynamic Pressure versus Time and Distance" (WT-1110); Sandia Corporation, Albuquerque, New Mexico; Ron Millican, Project Officer.

On Shot 12, Project 1.11 undertook to examine the parameters that determine dynamic pressure and to measure the effect of air and suspended dust on dynamic pressure in the precursor region. In addition, wind-direction gages were used to study pitch and yaw of the flow as a function of time.

For simplicity, the following table is presented to show the instrumentation, the parameters each measured, and the interrelation of some of the instruments.

These instruments were mounted on twin 3-foot towers placed at 2,000- and 2,500-foot ranges on each of the three blast lines of Shot 12. The wind-direction gages were not included in this array; however, one was placed (to measure pitch) at each location where a Pitot-static tube was mounted for dynamic pressure measurement by Project 1.10. Two each, to measure yaw, were also located at offset distances at ranges of 1,500 and 2,500 feet on the water line.

The pitch of flow was found to be considerable over all three blast lines out to 2,500-foot ground range. Little yaw was recorded on the water line. Over the desert and asphalt, pitch-time records showed initial upward flow followed by horizontal, or, when beyond 2,500 feet, downward flow. The upward-flow component was found to be larger at the 10-foot elevation than at 3 feet. Records taken over the water line were complex and erratic.

The appeal to the Bernoulli principle is not substantiated, since the sum of overpressure and air-dynamic

Quantity	Symbol	Instruments
Overpressure	ΔP	Snob Back Transducer, Transducer in Centripetal Density Gage Baffle
Air density	ρ_2	Centripetal Density Gage
Air velocity	u_2	Wind Velocity Gage
Air dynamic pressure	q_a or $\frac{1}{2} \rho_a u_a^2$	Snob Forward Transducer
Dust density	ρ_d	Medium-Density Gage
Dust velocity	u_d	About the same as air velocity if particles small
Dust dynamic pressure	q_d or $\rho_d u_d^2$	Dynamic pressure of Greg Dynamic pressure of Snob
Head-on pressure	$(p_t)_f$	Force Plate
Head-on pressure	p_t or $\Delta P + q_a q_d$	Greg Gage
Pitch	θ	Wind Direction Gage
Yaw	ϕ	Wind Direction Gage

pressure was not constant at the same ground distances over the three surfaces; if the dust dynamic pressure is added, the difference is even more pronounced. The contribution of dust to dynamic pressures is well established, since the dust-dynamic pressure exceeded that of air on the desert line. Even disregarding the dust, air-dynamic pressures were much higher than would be expected from measured overpressure and Rankine-Hugoniot relations. Density measurements show that the increased air-dynamic pressures are caused by high velocities, rather than increased air densities.

Project 1.12: "Drag Force Measurements" (WT-1111); Naval Ordnance Laboratory, Silver Spring, Maryland; J. F. Moulton, Project Officer.

The objectives of this project were to measure drag forces on simple geometric shapes and to determine drag coefficients as a function of time and distance. It was desired to obtain data in a clean-shock region, a dusty-precursor region, and a nondusty-precursor region, to provide a basis for prediction of drag forces on full-scale structures in similar shock regions.

The shapes took the form of 3- and 10-inch spheres, each containing a gage capable of responding to the applied force in three orthogonal directions. A cylindrical model, responding in two right-angle components, was also used. These models were mounted 3 feet above the ground surface. The project also instrumented a structure for Project 3.2. The drag-force instrumentation was new and not yet field tested so it was planned to first place it on Shot 8 prior to the intended participation on Shot 12. However, because of schedule delays, this was abandoned so that full effort could be expended for the more important Shot 12.

The following general results were obtained:

1. In general, only the horizontal axial component measured by the spheres proved to be of significance; the vertical and transverse components were small by comparison. These results were consistent with the pitch measurements made by Project 1.11.

2. It was found that the degree of reproducibility for measurements obtained on the same size spheres at the same station increased as the ground range increased. The data-evaluation picture was clouded by the ambiguity associated with corrections due to air leakage at the seal between the sting and the sphere; in most cases it was not possible to determine how much leakage occurred during the actual test.

3. A compilation of the peak drag-force measurements obtained on Shot 12 indicated that the peak axial-

drag force decreased with ground range over the three test surfaces. For the clean-air case it would be expected that the drag force measurements on the 3- and 10-inch spheres would be in the ratio of their projected areas, or approximately 11 : 1. This ratio appeared to hold quite well in most cases.

4. In general, the drag forces developed on the desert line were substantially greater than the asphalt or water lines at corresponding distances. In some cases the drag pressures on the asphalt line were greater than on the water line, and in other cases the results were the opposite. Comparisons of this nature are limited and relatively inconclusive.

5. With respect to pitch and yaw effects, scouring and denting of the force spheres were distributed symmetrically about the horizontal axis.

6. Because the drag force versus time and the dynamic pressure versus time records at a specific station exhibited radically different wave forms, the calculated drag coefficients fluctuated wildly as a function of time. However, the fluctuations appeared to decrease at larger ground ranges. In any case, it was virtually impossible to make quantitative comparisons of drag coefficients computed for the three different blast-line surfaces.

7. Subsequent to the Operation Teapot field operations, a program of laboratory investigations was undertaken in an effort to correlate these results with those obtained in the field. Few definitive conclusions could be drawn from this effort; however, it had value as the first well-organized attempt to understand the fundamental phenomena associated with drag forces on simple shapes.

Project 1.13: "Dust Density versus Time and Distance in the Shock Wave" (WT–1113); U.S. Army Chemical Warfare Laboratories, Army Chemical Center, Maryland; E. H. Bouton, Project Officer.

The objectives of Project 1.13 were to characterize the dust present at 3- and 10-foot levels on the desert- and asphalt-blast lines of Shot 12. Measurements were to be made during the passage of the precursor so as to give data on total-air density as a function of time, to determine the ratio of ρ dust/ρ total, and to obtain a measure of the particle-size distribution in the shock wave.

For the purposes of this project the dust density, ρ dust, was defined as the weight of dust per unit volume of air; and total air density, ρ total, was defined as the weight of dust plus air per unit volume of air.

It was hoped that data obtained on total air density within the precursor would supplement available data in determining the role of dust in damaging targets and in understanding the precursor-shock formation, development, and decay.

Total air density as a function of time and distance was to be measured with the beta densitometer. These units were located at 2,500 and 3,000 feet on the desert and asphalt lines. They operated satisfactorily, and camera records were obtained; however, data on total air density could not be determined, since the detectors in each unit were exposed to an excessive amount of radiation.

Dust samplers, located 2,000, 2,500, and 3,000 feet on the desert and at 2,000 and 2,500 feet on the asphalt, obtained air samples during four consecutive 0.050-second intervals followed by one 0.100-second interval of the first 300 msec of the shock wave. Opening of a valve at the desired sampling time permitted a vacuum tank to draw a volume of air through filter. The dust collected was weighed and examined for particle-size distribution. The higher-than-expected shock-front velocity and material velocity hampered the sampling techniques.

Results on ρ dust/ρ total, accurate to ±50 percent, were based on sample volumes calculated from overpressure data and estimated shock-wave air temperatures. Three feet above ground level on the desert line, the ratio ranged from 0.12 to 0.75 at 2,000 feet from ground zero, 0.05 to 0.19 at 2,500 feet from ground zero, and 0.04 to 0.05 at 3,000 feet from ground zero during the 40- to 350-msec period after shock arrival; and an increase in dust concentration, ρ dust, was noted progressing with the sampling interval. Ten feet above ground level on the desert line, ρ dust/ρ total was about 0.43 at 2,000 feet from ground zero, ranged from 0.06 to 0.11 at 2,500 feet from ground zero, and was approximately zero 3,000 feet from ground zero during the 40- to 340-msec period after shock arrival. The mean particle-size distribution of the dust collected on the desert line was an NMD of 1.21μ, and MMD of 15μ, and a σg of 2.87. The dust sampled over the asphalt line at distances of 2,000 and 2,500 feet from ground zero consisted of a hot-asphalt aerosol which destroyed the filter used for collection; the sample being collected on the filter backing cloth. The best estimate of ρ dust/ρ total was less than 0.33.

Project 1.14a: "Transient Drag Characteristics on Spherical Models" (WT–1114); Ballistic Research Laboratories, Aberdeen, Maryland; J. J. Meszaros, Project Officer.

This project had as its objective the investigation of the aerodynamic-drag characteristics of simple shapes when exposed to the transient-blast loading conditions resulting from the detonation of a nuclear weapon.

To accomplish this objective, the project planned participation on Shots 8 and 12. Shot 8 participation was to be in the nature of an instrumentation check out of the drag gages; however, shot-schedule delays forced abandonment of this plan.

Drag forces were measured as a function of time at various pressure ranges along the three blast lines of Shot 12. A developmental three-component-force balance system, consisting of 3- and 10-inch spheres as model shapes mounted 3 feet above the surface, was used.

Higher drag pressures were obtained in the dust-loaded precursor type wave of the desert line than were found on either the asphalt or water lines. On the desert line, drag pressures at the 2,000- and 2,500-foot stations were found to be much higher for the 10-inch gage than for the 3-inch gage. At the 2,750-foot station, however, the pressures were nearly the same, and, on this basis, it appeared that the drag coefficients for the 10-inch spheres increased at the higher pressures in a dust loaded atmosphere.

Because of the disturbed blast-wave conditions existing on Shot 12 and the fact that parameters such as Mach number and medium density were not determined directly, it was not possible to make a direct comparison between Operation Teapot drag coefficients and those documented in wind-tunnel investigations. The drag coefficient data are presented as a function of measured dynamic pressure, and some trends are noted and discussed. It is quite likely that the Pitot-static gage (q') responds differently to dust or particulate matter loading than does a force gage sphere, and consequently the fact that the computed drag coefficient appears to change with time is understandable.

Project 1.14b: "Measurements of Air-Blast Phenomena with Self-Recording Gauges" (WT 1155), Ballistic Research Laboratories, Aberdeen, Maryland; J J Meszaros, Project Officer.

This agency furnished basic blast instrumentation for two projects of its own (Projects 1.14 and 3.1) and for projects of other agencies. The results of this instrumentation are presented in WT-1155.

Further objectives of Project 1.14a (Reference A.1.12, above) were: (1) to check for blast asymmetries at one ground range along an arc of approximately 220 degrees, using mechanical pressure-time gages; (2) to establish the existence and determine the magnitude of any pressure variations existing between the boundaries of the surfaced blast line areas; and (3) to obtain pressure time information at or near the ground surface at great distances from a high-altitude detonation.

To accomplish the first two of these objectives, the project participated in Shot 12. Self-recording, or mechanical, pressure-time gages were installed on a 220 degree arc at a 2,500-foot range. This arc encompassed all three blast lines. The data obtained showed the blast wave to be asymmetrical at the 2,500-foot range. Pressure time records showed the blast wave in many shapes and varying pressures. Gages located not more than 100 feet apart showed marked differences in wave character and arrival time. The data further seemed to indicate that transverse-flow effects existed, emanating from the strong precursor region on the desert. A similar gage-ring layout used on Shot 14 produced no unusual deviations from blast symmetry; however, the instrumentation on Shot 14 was located at a shorter scaled ground range than was the case for Shot 12, and therefore the measurements were taken in a region of strong precursor effects. This result suggests that the anomalous behavior observed on Shot 12 may be characteristic of the so-called clean-up region of the disturbed blast-wave evolution.

Pressure-time information at the ground at great distances from a high-altitude detonation was obtained on Shot 10. Data were obtained with very-low-pressure gages located approximately 40,000 feet from ground zero. These gages were placed at the request of Project 1.3. Project 1.14b collected data including peak overpressure, positive-phase duration, and peak-dynamic pressure, on a wide range of yields for a variety of surface conditions. In addition, comparisons were made between gage results under a smoke layer and on clear desert for Shot 5.

Project: Instrumentation Towers; Directorate, Weapons Effects Tests, Field Command, Sandia Base, Albuquerque, New Mexico; W. M. McLellon, CDR, USN, Project Officer.

In planning for Operation Teapot, it was necessary to establish criteria and obtain designs for the various towers to be used for instrumentation support. Towers of various types were required by several projects to mount such instrumentation as q gages, force plates, density gages, dust samplers, drag spheres, etc. In the previous effects test in Nevada, tower designs supporting blast instrumentation had proved to be unsatisfactory out to 2,500 feet. These towers were of the guyed type and were leveled in the strong precursor region. Evidence indicated that the cable clamps or guy wires were suspect and that many failures occurred because of guy failures. It was desired in the early Operation Teapot planning to obtain designs for towers that would stand under severe shock loadings. The majority of tower designs were processed through Programs 1 and 3, DWET. The only exception was a tower type used by BRL, which is described later.

For the initial design of instrumentation towers, estimated pressures and durations were chosen for typical instrument locations and steel-tower sections computed (Reference 59). These sections were preliminary and were compared with designs prepared by the contractor. Close liaison was maintained with aerodynamics personnel of Sandia Corporation to secure the best possible design considering the factors of drag and vibration troubles, availability of material, and ease of fabrication. For the heavier towers, a two-pipe section was selected, since pipe and plate were

readily available and easily assembled and the aerodynamic properties were satisfactory under certain restrictive conditions.

Therefore, steel designs for common-use-instrumentation towers (3 feet and 10 feet) were picked, using the two-pipe sections close in and single-pipe sections at the farther distances. One of the basic uncertainties in the design was the value of dynamic pressure to be used, since little information was available in the higher pressure regions. Accordingly, designs used were conservative, since it was estimated that the dynamic pressure might be three to four times ideal. For the most part, the predicted dynamic pressures were twice the ideal value.

Designs were also selected for specific use by other projects, such as to support the Projects 1.12 and 1.14 drag spheres. The design of the 40-foot common-use towers was prepared by the contractor, based on criteria submitted by DWET. It is to be noted that guys were omitted from all design considerations except for the 40-foot towers. DWET personnel selected the sizes of foundations for the 3- and 10-foot-high towers. Foundation steel was designed by the contractor, and this steel and the tower anchorage in the foundation were checked by DWET.

The Ballistic Research Laboratories prepared one tower design for the support of the BRL self-recording gage. This tower was constructed in two heights, 3 and 10 feet. The towers consisted of two 3-inch extra-heavy pipe sections separated 13 inches and trussed with welded 3- by $\frac{3}{8}$-inch strap. The gages were mounted on top of the pipes with unions. The foundation consisted of a 3- to 4-foot deep, irregular mass of grout. The 10-foot towers were guyed in three directions with $\frac{3}{8}$-inch wire leading to metal anchors. The 10-foot tower was a two-pipe section of 8-inch double-extra-heavy pipe and 1-inch-thick side plates welded in solidly. The 3-foot towers were single pipe 8-inch sections. A 3-foot BRL pipe tower appeared at the far end of the row.

All of the tower designs processed by DWET were successful. Both sizes, 3 and 10 feet, were used for instrumentation on two shots, with no failures occurring, although dynamic pressures in some cases were 50 percent higher than predicted (twice ideal predicted). The 40-foot tower design was successfully used on one shot. The designs have now been proved and are available for future use in test series. Furthermore, all towers constructed on Operation Teapot will be available for reuse.

The BRL trussed towers were somewhat experimental, and some failures occurred early in the series. These, in general, were in very-high-pressure regions (60 to 80 psi dynamic) and consisted of the mount shifting because of inadequate anchorage. The mount was improved as the test series progressed. The highest successful use was 43-psi dynamic for the 3-foot mount and 14 psi dynamic for the 10-foot mount. This mount, designed for a specific use, was an economical and successful solution.

PROGRAM 2: NUCLEAR MEASUREMENTS AND EFFECTS

Project 2.1: "Gamma Exposure Versus Distance" (WT-1115); U. S. Army Signal Engineering Laboratories, Fort Monmouth, New Jersey; J. B. Graham, Capt, USA, Project Officer.

The objectives of this project were to determine the initial gamma exposure as a function of distance from various Operation Teapot detonations and to compare data obtained with methods for predicting the initial-gamma exposure for various devices detonated under similar circumstances. The main effort was placed on Shot 10 and the two low-altitude correlation shots, Shots 1 and 9. In addition, dosimetry service was provided to other projects to support their effects studies.

The dosimeters consisted of photographic films of five sensitivity ranges placed in NBS-type film holders. The films were calibrated in the NBS holder by means of a 72.5 curie Co^{60} source located at NTS.

On Shot 10 a circular array of film dosimeters was mounted internally in the instrument canisters. They were placed at 60-degree intervals, where possible, with at least five dosimeters per canister. On the correlation shots, film holders were placed in suitably modified canisters and positioned in the field at the desired distances from Shots 1 and 9 to allow comparison between the events.

The results obtained indicated that $r D^2$ versus D was linear in the region from which data were gathered. Preliminary analysis showed that variations from a straight line function due to one point source consideration and the rise of the fireball were negligible in the region beyond 1,000 yards. Also the irregular distribution of air, due to passage of the blast wave, did not affect the data. Corrections for film darkening due to neutron flux giving a higher gamma exposure have been made.

On Shots 2, 3, 4, 5, 6, 8, 11, and 12, dosimeter lines were instrumented. The apparent mean-free path for these events varied over a range of 20 percent. The shots for which these deviations were noted were the thin-skinned high-neutron-flux devices from which a different gamma output was expected.

Project 2.2: "Neutron Flux Measurements" (WT-1116); Naval Research Laboratory, Washington, D. C.; T. D. Hanscome, Project Officer.

The purposes of this project were to determine the neutron-energy spectrum as a function of distance and to compare the data obtained with the predictions of

neutron flux based upon similar devices detonated under similar conditions. Primary emphasis was placed on measurements on Shots 9 and 10 and on weapons of essentially new design.

Detectors employing gold, sulfur, plutonium, neptunium, and uranium-238 were employed. These detectors were exposed to the neutron fluxes from selected shots and were recovered by removing the cable to which they were attached or by removing them from the canisters in the case of Shot 10.

The gold and sulfur data for Shots 1, 9, and 10 showed irregular points. Shots 9 and 10 appeared to be nearly alike as neutron sources, but the data for Shot 10 showed wide fluctuations for all detectors at close range. Further analyses will be required before this inconsistency can be explained.

The results from Shots 3 and 11 showed the expected asymmetry, but both weapons gave higher fluxes than expected.

Shot 12 gave results approximately as expected.

Project 2.3: "Neutron-Induced Radioactive Isotopes in Soils" (WT-1117); Naval Radiological Defense Laboratory, San Francisco, California; C.S. Cook, Project Officer.

The scintillation-spectrometer measurement technique was applied to the problem of evaluating the spectral characteristics of the gamma-energy distribution in the residual-radiation fields resulting from contaminating types of atomic detonations. Since the available types of gamma-radiation dosimeters and survey meters were energy dependent in their response to low-energy radiation, it was essential to determine the gamma-energy distribution in order to assess the biological significance of the low-energy fraction and to provide data to aid in evaluating the adequacy of currently available gamma dosimeters and radiac instruments.

A large, essentially totally-absorbing thallium-activated sodium-iodide crystal and DuMont 6364 photomultiplier-tube combination was employed to measure the gamma-ray spectral-pulse-height distribution. Using either a single channel or 20-channel analyzer, spectra of selected sources whose activities resulted from three Operation Teapot detonations were measured.

The residual gamma-ray spectra observed by this project fell into two general categories; fallout material originating in the device, and activities induced by neutrons in the earth or material in the vicinity of the device at the time of detonation. The fallout material contained fission-product activities and, in most cases, activities induced by neutrons or device material. Following the air bursts, Shots 1 and 9, the residual radiation at the earth's surface appeared to consist entirely of neutron-induced activities, Na^{24} and Mn^{56}. No significant quantities of either of these activities were found following Shot 7. The spectral characteristics following Shot 7 were qualitatively those of the fallout material as defined above. Most of the tower shots appeared to have produced residual radiation of both types, with relatively large quantities of induced activities in the regions closer to ground zero.

Work is still in progress to convert pulse-height data into gamma-ray distributions. Only preliminary data is available.

Project 2.4: "Gamma Dose Rate Versus Time and Distance" (WT-1118); U.S. Army Signal Engineering Laboratories, Fort Monmouth, New Jersey; J.B. Graham, Capt, USA, Project Officer.

The objective of this project was the documentation of the gamma-radiation dosage as a function of time and distance from early times after detonation. Three different types of instruments were used: a scintillation detector for measuring high gamma-radiation rates, an ionization-chamber detector for measuring both high- and low-gamma-radiation rates, and a cadmium-sulfide photo-conductivity detector. This instrument, however, was used as a field suitability study. The instruments were constructed to have a range from 10 to 10^4 r/hr, or from 10^2 to 10^6 r/hr.

On Shot 7 two main instrument lines were arranged to cover the main axis of the fallout pattern, based upon a predicted wind from 280 ± 20 degrees at low altitudes, 4,000 to 11,000 feet MSL. In addition, several stations were located crosswind and upwind, in order that contribution from the base surge could be separated from those effects due to fallout alone. In an attempt to obtain further data concerning Shot 7, total dose and dose rate devices were dropped into the crater on D day and D day plus 2.

For these events, Shots 1, 2, 3, and 9, where the decay rates of the neutron-induced activity in the vicinity of ground zero were of interest, stations were located at the vertices of an equilateral triangle centered on the expected ground zero. The distance from zero to the station was determined by the expected survival capability of the instrument.

Results obtained appeared in the report in the form of curves. Analysis of the data from Shot 7 indicated that the decay rate of the residual contamination, in general, obeyed the decay law $R = R_u t^{-x}$ where x is close to 1.2. There was also clear evidence of redistribution of the activity by wind action. The total dose and dose rate devices dropped into the crater could not be recovered.

The data from Shots 1, 2, 3, and 9 showed that the main contributions to the neutron induced activity in the vicinity of the ground zeros were apparently due to Na^{24} with a 14.9-hour half life and to Mn^{56} with a 2.59-hour half life. On the air bursts (Shots 1 and 9) the

intensities recorded at H + 1 hour supported the values predicted in the revised edition of TM 23-200, Capabilities of Atomic Weapons. In addition, the decay rates obtained clearly illustrated that only the induced effects are important and that the contribution afforded by fission products is small.

Project 2.5.1: "Fallout Studies" (WT-1119); Chemical and Radiological Laboratories, Army Chemical Center, Edgewood, Maryland; E. H. Bouton, Project Officer.

This project thoroughly documented the radioactivity associated with the base surge, fallout, and crater-lip areas of Shot 7. In particular, data were desired which (1) would allow the closing of the 1 r/hr at H + 1 hour dose rate contour line, (2) would give radiation intensities in areas contaminated by fallout, base surge, and the crater-lip region, (3) would give time of arrival of activity at locations within 2 to 5 miles of ground zero, (4) would give depth of burial of activity in the crater and on the lip, and (5) would give air to ground correlation factors developed during aerial surveys of contaminated areas.

The instrumentation employed consisted of intermittent fallout collectors, aerosol samplers, aerial survey instrument, land survey instrument, core samplers, and normal radiac equipment. In addition, data were received from the Rad-Safe group and other nuclear effects studies projects for correlation.

The data recorded by the ground and aerial intensity measurements allowed the closing of the 100 mr/hr contour line at H + 1 hour and to nearly close the 10 mr/hr isodose line at H + 1 hour contour. These contours showed the area inside the 3,000 r/hr at H + 1 hour contour to be roughly three times that predicted by existing scaling methods and the area within the 100 r/hr contour to be less than one half that predicted.

Preliminary analysis of time of arrival data and photography indicated that the base surge carried the fallout and its associated activity in the upwind and crosswind directions. About 90 percent of the activity on the crater lip was contained in the first 12 inches of depth. Time of arrival data were secured at seven locations, 300 to 4,500 yards from ground zero. The fallout appeared to have traveled downwind at ground speed of approximately 2 miles per hour. The gamma intensity measurements made in the fallout area showed that the dose rate from H + 2 hours to D + 4 days followed the $t^{-1.2}$ decay. Data were also obtained which furnished information concerning the effect of scaled depth upon such properties as specific activity, activity particle size distribution, and total activity associated with fallout.

Project 2.5.2: "Distribution and Intensity of Fallout from the Underground Shot" (WT-1154); Naval Radiological Defense Laboratory, San Francisco, California; R. S. Stetson, Project Officer.

This project's effort was directed at securing data to define the magnitude and extent of the entire fallout event from the subsurface atomic detonation, Shot 7, in terms of quantity of material dispersed and deposited. The preliminary report was limited to reporting the results of the on-site work in terms of success or failure of the sampling effort and gave gamma field data at the sampling points as recorded by standard radiac equipment.

The principal sampling device employed consisted of polyethylene-lined buckets mounted on poles 6 feet above ground level and located at stations on radial lines extending outward from ground zero. These buckets, or total collectors, had a sampling area of approximately $\frac{1}{2}$ ft^2. Where fallout was moderate to light, gummed papers of the same sampling area were mounted to obtain samples for particle studies. In addition, at three locations incremental collectors were employed to sample the fallout in timed increments to determine time and rate of arrival and cessation and information on the particulate nature as a function of time. Gamma time-intensity records, film badge data, and radiac readings were also obtained.

Sufficient samples were obtained to meet the objectives of the project.

Project 2.6: "Radiation Energy Absorbed by Human Phantoms in a Fission Fallout Field" (WT-1120); Naval Medical Research Institute, Bethesda, Maryland; G. W. Imirie and R. Sharp, LT, USN, Project Officers.

Phantoms resembling humans and made of tissue-equivalent materials were placed in prone and upright positions in fallout fields to measure the surface and depth dosages received. Measurements of the dose received were taken over the surface and at several internal locations corresponding to the positions of vital organs.

The principal radiation detector used consisted of a miniature ionization chamber featuring tissue-equivalent material walls. The phantoms were so constructed as to accommodate a system of blocks and plugs in which the detectors were mounted. In addition, absorption studies were made with polyethylene and gold up to thicknesses of 500 and 3,000 mg/cm^2, respectively. Phantoms were exposed to the radiation fields resulting from Shots 4, 7, and 8.

The presence of a soft component, strongly indicative of beta radiation, was found which gave a surface dose in many cases 20 times the average internal dose for a man lying prone. This factor can be reduced by 50 percent by brushing the ground, but this apparently has little effect upon the internal dose received. The upright man received doses differing by a factor of 8 between feet and head. Although the internal doses agreed favorably with standard radiac equipment, sur-

face dose was found to be significantly greater. It can be concluded that a fallout field delivers a large dose of absorbed energy to the body which is not usually measured and that further study is required to determine the biological hazard of the unmeasured components.

Project 2.7: "Shielding Studies" (WT-1121); Chemical Warfare Laboratories, Edgewood, Maryland, and U.S. Army Signal Engineering Laboratories, Fort Monmouth, New Jersey; E. Engquist, Project Officer.

Nuclear shielding studies were conducted on a variety of surface and underground structures, shelters, field fortifications, foxholes, vehicles, and vehicle trenches. These studies were conducted on three types of atomic detonations: a tower burst of 24 kt yield, an underground detonation of 1.2 kt yield, and two tower bursts of linear assembly devices of 7.0 ± 0.2 kt yield and 1.53 kt yield, respectively. Total gamma dose was obtained using the ESL-NBS film packet in a standard holder. Two types of chemical dosimeters were also used, one the Chemical Corps E-1 and the other the University of Texas Laboratory Model. Total neutron dose was obtained using gold, sulfur and fission threshold detectors. The studies on foxholes were directed to the determination of the effect of film badge orientation upon the results of shielding studies conducted at previous atomic weapons tests. On the underground shot, emphasis was placed on determination of the shielding against the residual as well as the initial gamma radiation.

In most instances gamma ray and neutron measurements were made at more than one height above a shelter floor and at entranceways as well as the interiors of many shelters in order to determine interior dose contours.

The average attenuation factors for armored vehicles against initial gamma radiation was determined to be 0.1, 0.6, and 0.7 for the M48 tank, the T97 self-propelled gun, and the AIV-M59 personnel carrier, respectively. Greater protection was afforded when the T97 and M59 were oriented rear on to the burst. The average attenuation factors of the same vehicles against residual gamma radiation were 0.1, 0.4, and 0.6, respectively.

Gamma shielding data were determined on 38 field fortifications, and neutron data on 29 field fortifications. The covered bunker type of fortification, with a 12- to 25 foot line-of-sight earth cover afforded greatest protection. The gamma attenuation factors were 10^{-3} to $\frac{1}{4} \times 10^{-3}$ for these structures. The neutron attenuation factor was 10^{-6} for fast neutrons and 10^{-4} for slow neutrons. The remaining field fortifications offered less protection. The gamma attenuation factors varied from 0.01 to 0.1; the fast neutron attenuation factors varied from 10^{-6} to 10^{-1}. The principal ground ranges of the field fortifications from Shot 12 were 1,000, 1,150, and 1,400 feet. Vehicle trenches at 1,500-, 2,100-, and 2,700-foot ground ranges offered some protection against radiation exposure. The gamma radiation attenuation factor was 0.6, and the neutron attenuation factors were 0.25 and 0.7 for fast and slow neutrons, respectively, at 2,100 feet.

The studies showed that on devices where a high neutron to gamma ratio exists, such as thin high-explosive tactical weapons, a neutron exposure results inside shelters, emplacements, etc., when only line-of-sight shielding is present, because of scattering of thermal neutrons. In underground shelters and field fortifications where sufficient line-of-sight thickness of shielding material is present to shield out all the direct rays from a conventional air-burst atomic weapon, the main hazard is from air scattered neutrons and gamma rays which proper and adequate baffling of entranceways reduces to a minimum.

The neutron measurements made at the bottom of foxholes showed that the protection was high, 96 to 98 percent, against fast neutrons and lower, 40 to 75 percent, against thermal neutrons.

The underground structures afforded the greatest amount of protection against neutrons and gamma radiation; the OCE concrete shelter, Upshot-Knothole 3.8c, with 8 feet of earth cover offered the greatest protection. The attenuation factors were 10^{-4} to 10^{-5} against neutrons and gamma radiation.

The value of providing minimum earth cover for all structures to increase gamma and neutron protection was demonstrated, $2\frac{1}{2}$ feet of earth cover reducing the gamma dose by a factor of 1,000 at close-in ground ranges.

Project 2.8a: "Contact Radiation Hazard Associated with Contaminated Aircraft" (WT-1122); Air Force Special Weapons Center, Albuquerque, New Mexico; P. L. Crumley, Capt, USAF, Project Officer.

During recent years concern has grown over the potentially serious contact radiation hazard maintenance personnel might encounter when working on aircraft recently contaminated by flight through an atomic cloud. The objective of this project was to determine whether there was a correlation between the contact radiation hazard associated with aircraft which have recently flown through an atomic cloud and the radiation intensities indicated by standard gamma survey meters held near the contaminated components of the aircraft.

After each shot of the test series, with the exception of the underground burst, aircraft which flew through the atomic cloud at times varying from 18 to 150 minutes after detonation were surveyed at predetermined points. The measurements made employed T1B's, JUNO's, AN/PDR-27C's, a specially constructed thin-window ion chamber, a thin-crystal scintillation rate meter, and special film badges employed in radiantographic studies.

Analyses of the data indicated that multiplication factors of 90 for the impingement surfaces and 40 for other surfaces applied to surface T1B gamma readings would give practical effective surface intensities of total radiation on the areas of interest. A study of the contamination on the jet engine of a T-33 aircraft showed (on T1B) intensities two to three times higher than that found on outer surfaces of the airplane.

PROGRAM 3: EFFECTS ON STRUCTURES AND EQUIPMENT

Project 3.1: "Response of Drag Type Equipment Targets in the Precursor Zone" (WT-1123), Ballistic Research Laboratories, Aberdeen, Maryland; E. J. Bryant, Project Officer.

As a practical compromise between the purely abstract approach to blast measurements (by means of gages) and the outright empirical approach of exposing every conceivable target type to full-scale blast effects, small standard items of ordnance equipment, particularly jeeps, were chosen as response gages for correlation with pressure values.

Project 3.1 had as its primary objective the extension of previously obtained results on equipment response to controlled situations involving nonideal blast waves. Shot 10 of Upshot-Knothole had clearly demonstrated the fallacy of correlation of peak side-on pressures with damage to drag-sensitive targets; thus, arrays of ordnance equipment were placed on the water, asphalt, and desert surfaces of Shot 12 for direct comparison of damage. Shots 6 and 9 provided additional information on surface effects and non-precursor blast waves, respectively.

Additional objectives included the study of the effect of positive phase duration on damage, determination of design parameters for future ordnance equipment (including a roll-over-safety bar for wheeled vehicles), and in conjunction with Project 2.7, measurement of the shielding effect of tank armor against gamma radiation.

In all, vehicles were exposed on nine shots at ranges selected to provide interesting damage gradation. All these shots were instrumented with self-recording overpressure and dynamic-pressure gages for correlation. An evaluation of damage and displacement was made on each item after exposure and the results subjected to a statistical analysis to relate them with blast-wave parameters.

It was found that damage was most severe on the desert surface, indicating that higher drag forces were present in this region of the dust-loaded precursor blast wave than over either the asphalt or water surfaces. Contrary to expectations, the water-line jeeps were more severely damaged than those on the asphalt line, indicating possible water (and mud) loading of the blast wave. A fair degree of agreement with damage predictions from TM 23-200 was demonstrated.

Increasing positive-phase duration with increasing yield enhanced the damaging effects of blast beyond normal cube-root scaling. The scaling factor for damage radii was determined to vary as $W^{0.44}$ for the equipment types exposed. The investigation of positive-phase duration was continued with similar targets in conjunction with Project 1.5 of Operation Redwing (Reference 60).

The statistical analysis demonstrated a definite relation between dynamic impulse and displacement, as well as peak dynamic pressure and damage for those ¼-ton trucks which were oriented side on to the blast. It was concluded that the addition of a roll-over safety bar to wheeled vehicles served to minimize the damage to cab and vehicle controls. Additional conclusions regarding possible design features are presented in the project report.

Results of the gamma-radiation attenuation study indicated attenuation coefficients between 0.1 and 0.7 for conventional tanks. These values were not sufficient to bring the lethal radius for gamma radiation inside the significant blast-damage area for the yield ranges involved.

Project 3.2: "Study of Drag Loading of Structures in the Precursor Zone" (WT-1124); Wright Air Development Center, Dayton, Ohio; B. J. O'Brien, Project Officer.

The general objective of this project was to obtain information on the drag loading of simple shapes and structural components in precursor and non-precursor regions. In addition, a further test of a method of measuring net forces on a structural element was planned.

Measurements were made of net pressures acting on identical concrete structures exposed at equal ranges on four controlled surfaces on Shot 12: a compacted desert surface, a desert surface in a loosened state, a water surface, and an asphalt surface. The average pressure on the front and rear face of each structure was obtained by averaging pressure measurements at several points. The feasibility of net-force measurement by means of strain measurement in beam-supporting sensor bars was investigated. Measurements of pressure on Operation Upshot-Knothole Structure 3.1t were made for comparison with the results of that earlier operation. All test items were designed to be non-responsive and, in fact, remained rigid during the test.

Because of instrumentation complications, two structures on the artificial surfaces yielded no useful information. For the identical structures on loosened and compacted desert surface a considerable difference in pressures was noticed. The structure on the loos-

ened soil received a markedly higher peak pressure and somewhat higher net impulse than the one on compacted desert soil.

The impulse on these structures, when compared to the impulse obtained from blast-line instrumentation, gave a net drag coefficient of approximately two-thirds for these rectangular structures. This value was about half the value that was predicted from free-air measurements; however, the measured values of impulse on the test structures were high compared to ideal dynamic-pressure impulse. The prediction scheme developed as a result of Operation Upshot-Knothole, which involved a peak value of ideal dynamic pressure, gave reasonably good agreement with measured results.

The net-force measuring system, as applied to a simple beam, was successful in this application.

Project 3.3.1: "Flexible Measuring Devices and Inspection of Operation Jangle Structures" (WT-1125); Bureau of Yards and Docks, U.S. Navy, Washington, D.C.; L.D. Mills, LT(jg), USN, Project Officer.

The objective of this project was to obtain basic earth loading data to enable the prediction of the loading on underground structures and development of criteria for the most economical and efficient design of underground protection from unground blast forces. To be more specific, it was desired to obtain data on the nature of forces transmitted through the earth to buried structures from an underground atomic explosion and to determine the response of simple structural elements of different stiffnesses, lengths, and masses to these forces. Additionally, it was planned to make pretest and posttest inspections of Jangle structures within 1,000 feet of Shot 7 ground zero to document damages.

Pretest analysis indicated that four variables would enter into the experiment design, assuming constant range and depth of burial. These were the mass of the loaded element, stiffness of the device, mass of the supporting structure, and length. Accordingly, 15 steel and concrete structures were constructed and installed on an arc around Shot 7 ground zero at a range of 300 feet. Burial depth at the front face was approximately 15 feet, and all devices were aimed at the weapon point below ground zero. Three of these devices were standard comparison units to check the symmetry of effects along the arc. The other 12 units were divided into groups to investigate the effect of varying each of the parameters mentioned above. Details are as given in the project report.

The array was instrumented with 32 channels of instrumentation to measure strains, accelerations, and earth pressures on the various devices. Included were two channels to measure the free-field earth pressure incident on the array. All channels, except one, strain, functioned satisfactorily and usable records were obtained although some deflections were so small as to reduce reading accuracy.

From these measurements it was concluded that the loads acting on the facing and rear surfaces of the buried devices were believed to be caused, in considerable degree, by radial compression of the earth surrounding the structure. Two of the parameters considered, the mass of the loaded element and the mass of the rear supporting structure, appeared to have little effect on the loads acting on the devices. The change in static structural rigidity of the loaded element apparently did influence the total load. Also, a change in the length of the structure, in a direction normal to the wave front, evidently had a significant effect upon the magnitude of the loads generated by an earth pressure pulse. Of course, in this case the comparative length of the structure and the wave length of the pressure pulse were the important considerations. The results seemed to indicate that the response of a structural element could be approximately determined by static analysis, using the maximum loading applied by the blast pressure.

The conclusions resulting from a damage inspection of the existing Jangle structures may be summarized as follows:

1. For light construction, shallow depth-of-burial structures suffered little damage at greater than 2.5 crater radii, severe to light damage from about 1.5 to 2.5 crater radii, and total destruction at less than about 1.5 crater radii.
2. The drag forces on a structure from which portions of the brick curtain walls had been knocked out and on which there was evidence of cracking, were not quite sufficient at about 2.3 crater radii (from Teapot Shot 7) to destroy the structure.
3. Damage to the concrete runway was minor at about 2.6 crater radii.
4. The drag type steel frames at about 3.5 crater radii were deflected without failure.
5. Ground pressures were not sufficient to cause damage to buried concrete instrument shelters at approximately 2.0 crater radii.

Project 3.3.2: "Behavior of Underground Structures Subjected to an Underground Explosion" (WT-1126); Office, Chief of Engineers, Department of the Army, Washington, D.C.; T.O. Stark, Project Officer.

The objectives of this project were to obtain data on effects of a large scale underground explosion on buried structures and to correlate the results with previous test results from small scale high-explosive charges, primarily at Dugway, Utah, and with results obtained from the Jangle underground shot.

Two reinforced concrete structures were constructed for this project. These structures were identical and were located at 200 and 250 feet from Shot 7 ground zero. The structures consisted of modified Dugway boxes, open top and bottom. Both were 12 feet 6 inches square and 8 feet 10 inches high, outside dimensions. The front and rear walls were 24 inches thick, and side walls were 12½ inches thick. Walls were reinforced with both tension and compression steel. Both structures were buried so that the bottom of the walls was 12 feet 7 inches below the ground surface.

Both structures were located adjacent to the blast line of Project 1.7 and were instrumented by Stanford Research Institute. Measurements were made of earth pressure, acceleration, and deflection versus time at various points on the structures. Sixteen channels were installed. In addition, pretest and posttest meas urements were planned to determine the permanent strain in the reinforcing bars of the front and rear walls.

All electronic channels functioned and gave useful records, although many of the deflections were so small as to reduce the reading accuracy. Aerial observation soon after the blast disclosed that the Project 3.3.2 boxes were completely covered by throwout from the craters and could not be located. Primarily because of residual radiological contamination, posttest examination of the boxes was not conducted until October 1955.

It was concluded that the response of all of the walls of the 3.3.2 boxes was essentially elastic. Combined with the small response of the walls, there was a large rigid body motion of the boxes. Careful visual inspection indicated no sign of distress associated with the structures. The permanent displacements of the structures, the colored sand columns (Project 1.6) at the depth of the structures, and the monuments (Project 1.7) at the ground surface, all indicated that the permanent displacement of the soil near each structure corresponded closely to the permanent displacement of the structure.

Regarding the measured pressures on the structure walls, the rise time of the measured pressure inputs was generally about seven times the natural period of the walls of the boxes. Thus, the response of the walls was essentially static. The measured pressure on both the front and rear walls of the structure at 200 feet from ground zero was approximately 30 percent of the medium free field stress, while the measured pressures on the walls of the more remote structure were close to the free field pressure. This difference is not easily explained. However, it may be attributed to the more severe motion experienced by the close-in structure. It was concluded that a structure with strengh comparable to the Project 3.3.2 boxes would not be damaged structurally when located at distances equal to or greater than 1.3 crater radii.

Project 3.4: "Air Blast Effects on Underground Structures" (WT-1127); Office, Chief of Engineers, Department of the Army, Washington, D.C.; T.O. Stark, Project Officer.

This project was to obtain the necessary basic data from which to develop criteria for the economical and efficient design of underground protection from air-blast forces. These efforts were a continuation of studies to determine the nature of forces transmitted through the earth to buried structures from the explo sion in air of a nuclear weapon. Previous work on Operation Upshot-Knothole involved the exposure of the same structures to different conditions of loading.

The structures used were fundamentally reinforced-concrete boxes with a number of simply supported beams for roofs. Depth of burial varied from 1 to 8 feet, and each structure had roof beams of several degrees of stiffness. All roof beams had 8-foot spans All structures were exposed at the same range from the burst.

The air-blast pressure above the structures was approximately 90 psi, considerably higher than on the Operation Upshot-Knothole tests. As a result, the plastic beam strips in the shallowest structure deflected as much as 2 inches, and the deflections in the beam strips of intermediate stiffness were greater than in the previous test.

Analysis of the test data showed that the beams could be divided into two groups with respect to their behavior. The response of all of the beams tested in Operation Upshot-Knothole and the shallowest beams and all of the plastic beams on Teapot indicated that there was no attenuation of pressure with depth The other group included those flexible and intermediate beams tested on Teapot which were buried at a depth greater than one-half span. The response of this latter set of beams was close to that corresponding to static deflection under the peak overpressure experienced.

Based on the results of both operations, it was concluded that the design of the roof of box-type underground structures for air-blast effects should be made for the pressure experienced at the ground surface with no attenuation of pressure, at least for depths of burial less than the roof-beam span.

Project 3.6: "Evaluation of Earth Cover as Protection to Aboveground Structures" (WT-1128), Bureau of Yards and Docks, U.S. Navy, Washington, D.C., L.D. Mills, LT(jg), USN, Project Officer.

The primary objective was to determine the degree of protection that earth cover affords to aboveground structures and, particularly, to determine the adequacy of an adaptation of a steel ammunition magazine, such as Upshot-Knothole Structure 3.15, as a personnel shelter. A further supplementary objective was to compare performance of scale models with that of full-

scale test structures in order to permit more economical conduct of future tests.

Earth-covered corrugated-steel structures, both full-size and quarter-scale models, were tested on Shot 12 in order to provide a measure of the blast and radiation resistance for personnel shelter applications.

One full-scale structure successfully withstood pressure of 13-psi side on and 33-psi dynamic, while another structure failed under the loads produced by 30-psi side on and 150-psi dynamic pressures. Prompt radiation was attenuated by a factor of 100; this figure might be improved by the addition of more earth cover over the crown. The performance of the models was roughly consistent with expectations. The results of the model study suggest that static model tests prior to any further full-scale blast tests will enhance the value of the results and will reduce the cost of such full-scale test operations.

Conclusions regarding the relationships between blast and radiation protection in personnel shelters must be viewed within the framework of the non-simple variation of these parameters with yield, height of burst, and other criteria.

Project 3.7: "Effect of Positive Phase Length of Blast on Drag Type Structural Buildings" (WT-1129); Wright Air Development Center, Dayton, Ohio, B. J. O'Brien, Project Officer.

The objective of this project was to obtain information on the effect of positive-phase duration on damage to drag-sensitive targets. Theoretical analyses have indicated that the peak pressure required to produce a given degree of damage would be less for a kiloton-range than for a megaton-range detonation as a result of the longer positive phase of the latter blast wave. Project 3.7 was implemented to perform the first of a two-part study by exposing certain industrial structures to the relatively short positive-phase blast of Shot 12. The study was completed under Project 3.1 of Operation Redwing, (despite a gross bombing error on Operation Redwing Shot Cherokee used for the second part of this study, it was conclusively demonstrated that one of the building types failed at an overpressure which was less than the overpressure which the same type building withstood with only minor permanent deflection on Teapot, Reference 61) where the locations of the similar structures were chosen on the basis of the Teapot results.

Four structures were exposed on Shot 12 at ranges from 3,000 to 5,750 feet. Two structures were typical industrial frames with transite siding and roofs. These structures were thus pure-drag targets, since the transite failed at the onset of the blast wave before any significant loading could be transferred to the frame. The other two buildings were semi-drag targets, as their front and rear walls were reinforced concrete panels with about 30-percent window opening at mid height.

Pretest and posttest static pull tests were made on each structure type; the pull tests after exposure were to destruction. Surveys were made for permanent deflections and high-speed photography employed to give time histories of the deflections.

In general, all structures suffered less permanent deflection than had been predicted, possibly because of the slightly lower-than-planned yield of the device. The results of these tests were used to evaluate analytical procedures for the prediction of structural response to blast loading.

Project 3.8: "Test of Concrete Panels," (WT-1130); Bureau of Yards and Docks, U. S. Navy, Washington, D.C.; L. D. Mills, LT(jg), USN, Project Officer.

This project was planned to permit study of the actual behavior, as compared with the theoretically determined response, of reinforced-concrete panels loaded into the plastic range. One ribbed and one solid panel were tested with high end fixity under peak overpressures of 6.5 and 4 psi.

Twenty channels of information were recorded, including pressure, deflection, acceleration, and strain These measurements were successful and permitted accurate delineation of the response. Analogous specimens of both ribbed and flat panels were tested statically for determination of the resistance curve and for studies of the formation of the yield hinge.

Limited damage was incurred on the full-scale tests, and thus the results did not permit optimum demonstration of the influence of the damage-related parameters. The results did demonstrate that symetrically restrained members of the type tested could be studied by analogy with the spring-mass-dashpot system.

Project 3.9: "Response of Petroleum Products Storage Tanks" (WT-1131), Wright Air Development Center, Dayton, Ohio; B. J. O'Brien, Project Officer.

Four small, steel petroleum-products storage tanks remaining from Upshot-Knothole Project 3.26 were emplaced on the desert line of Shot 12 to investigate the mode of failure for filled tanks in the small size range. No additional test equipment was required and no time-histories of blast and response information were taken.

The exposure items consisted of one bolted tank with cover and three welded tanks without covers. All tanks were filled to 80-percent capacity. Preshot and postshot inspections and still photographs were made to determine the modes of failure.

The first three tanks (at ranges of 1,200, 1,350, and 1,500 feet) suffered gradations of severe damage, the most remote tank (2,100 feet) was overturned but

not ruptured. The two close-in tanks suffered the type of damage expected of larger tanks: rupture of the shell directly by blast rather than rigid-body motion. The tank at 1,500 feet suffered perhaps the most interesting damage from the standpoint of small tanks as targets, destruction of the tank and contents from rigid-body motion.

Thus, information formerly lacking on the response of small filled storage tanks was obtained, although no knowledge was added in the field of damage prediction for large tanks. Information on the radii of effect for the following parameters was obtained: combination of overpressure and drag pressure which will rupture filled tanks of this size and shell thickness without rigid body motion, combination of overpressure and drag pressure which will cause sliding, overturning, and rupturing of such tanks, and the region in which such tanks will slide without overturning or rupturing, but with sufficient force to break pipe connections and cause loss of contents

Project 3.10: "Structures Instrumentation" (WT-1107); Ballistic Research Laboratories, Aberdeen, Maryland; P. Lorrain, Project Officer.

The objective of this project was to provide instrumentation support to Projects 3.2, 3.4, and 3.7. Measurements included shock pressures, acceleration, displacement, and strain measurements on several structures. A total of 94 electronic channels with both magnetic tape and sensitive paper recording were employed on the various structures. A majority of records were obtained from the channels installed, of the failures, the strain gages predominated, where difficulties were encountered at zero time.

PROGRAM 6

Project 6.1.1a: "Evaluation of Military Radiac Equipment" (WT-1137), U.S. Army Signal Engineering Laboratories, Fort Monmouth, New Jersey, J. B. Graham, Capt., USA, Project Officer.

This project had as its objective the evaluation of untested and developmental models of various radiac equipment. The project followed the precedent of testing the instruments under full-scale field test conditions, as had been done on most previous operations.

The models tested were self-developing (polaroid) film dosimeter, DT 65, chemical (color-change) dosimeter, E1R3, quartz-fiber electroscope dosimeter, IM-93( ) UD; radiac ratemeter, TM-108 (XE-1, XE-2)/PD; and a radiological calculator

The dosimeters were evaluated in both initial- and residual-radiation situations to determine their rate and energy dependence. The standards used were the NBS film pack for the initial situation and a Victoreen r-meter for residual fields. The two mechanically different models of the TM-108 radiac were subjected to field use by personnel from Camp Desert Rock, their accuracy was assessed by comparison with readings of the assumed standard AN/PDR-39 and AN/PDR-T1 B radiacs.

The radiological calculator was essentially a simple slide rule to facilitate integration of the decay curve for various values of average decay curve slope It was tested by comparing dose rates predicted from two field readings at a given position to the actual dose rate measured at that position at a later time.

The results indicated that the IM 93 dosimeter would be the most desirable individual instrument for military use, though considerable controversy still exists over the qualifications of the E1R3 chemical dosimeter for this use. Both models of the IM 108 were found to be satisfactory, though the user-preference was for the XE-2, L-shaped model.

The radiological calculator proved unsatisfactory for predictions of intensities and doses in the distributed fallout field. The failure was the result of the non-ideal behavior of the fallout contaminant (e.g., due to wind or other naturally occurring disturbances), rather than any inadequacy in the calculator itself

Project 6.1.1b: "Evaluation of a Radiological Defense Warning System (Project Cloudburst)" (WT-1112); U.S. Army Signal Engineering Laboratories, Fort Monmouth, New Jersey, J. B Graham, Capt USA, Project Officer.

A radiological defense warning system, developed by the Signal Corps for the Corps of Engineers, was evaluated during six shots.

The detection system was designed to operate in the region of 1-psi overpressure It consisted of thermal-radiation, initial-gamma radiation, and blast-overpressure detectors housed in a weatherproof, aluminum, cylindrical container. The photosensitive thermal-radiation detector responded selectively to the rapid rise of the initial thermal pulse from a detonation. The gamma-radiation detector consisted of an ion chamber and associated circuitry. The blast-sensitive portion of the device utilized a low-range aneroid transducer.

The device was so designed that activation of any or all detector sections could be utilized to trigger a secondary alarm circuit. The device was thus usable to control protective devices which would be activated automatically in case of atomic attack.

All parts of the detector system operated satisfactorily within the 1-psi region on the shots tested. Positive results were obtained for the thermal and gamma radiation parts of the detector at a distance of 17.8 miles.

Project 6.1.2: "Accuracy of Military Radiacs" (WT-1138); U.S. Naval Radiological Defense Labora

tory, San Francisco, California; George A. Work, Project Officer.

Originally scheduled as an evaluation of Navy Radiac instruments along the lines of Project 6.1.1a, this project was modified to include the first realistic evaluation of radiac performance under field conditions in terms of actual dose rates. The principal objective was to measure the errors of standard military radiacs by comparing them with laboratory gamma-ray standards in the field situation. As a secondary objective, the directional properties of typical radiation fallout fields were investigated in order to more accurately assess gomiometric effects on instrument accuracy.

The accuracy of several types of radiac equipment was measured. The five types of ratemeters chosen for the project represented the entire complement of high-range radiac instruments available to military and civil defense forces at the time of the field work. Instrument response, relative to a gamma-ray standard and an initial Co^{60} calibration, was determined in several different radiological situations and as a function of time after fission.

All instrument types were found to read low relative to the standards because of deficiencies in the present calibration procedures. Changes in the calibration methods for each type were formulated and are specified in the project report.

The directional properties of the residual-radiation fluxes were investigated and a number of source configurations were determined. For the close-in situation, radiation reaching the detector resembled that from a point source, while at greater distances from ground zero, the radiation appeared to emanate from a ring or distributed source.

Wide variations were found in the indications of instruments of the same type in identical field situations, indicating the fallacy of using these field radiacs for close estimates of percentage radiation casualties.

Project 6.2: "Effects on Selected Components and Systems" (WT 1139), U. S. Army Signal Engineering Laboratories, Fort Monmouth, New Jersey; J. B. Graham, Capt., USA, Project Officer.

This project was implemented to study the performance of Signal Corps equipment subjected to the intense radiation of an atomic detonation, either while in use or in storage.

The equipment exposed included several types of electron tubes, a complete radar beacon (AN/DPN-19) in operating and stored configuration, and frequency-control crystal units of various nominal frequencies. The test items were exposed in an aluminum shield for protection against thermal and blast effects and in every case received initial gamma radiation doses of at least 4×10^4 r. Performance of all items was determined by laboratory studies before exposure; the same tests were run again after exposure.

The results indicated no effects on the normal functioning of the electron tubes, based upon dynamic tube characteristics. The radar beacon was not affected by exposure to 47,000 r. The effects of the exposure on the five types of crystal units exposed were varied. In some cases (excluding mechanical damage) the radiation had little effect, while in others virtually all of the crystals tested were rendered unfit for military usage.

It was concluded that the electron tubes and the radar beacon were far more susceptible to blast and thermal damage in any normal storage or operating condition than to ionizing radiation. Even in the case of the crystal units, malfunction may be more related to mechanical misuse and radiation effect on bonding materials than it is to direct radiation effect on the crystals themselves.

Project 6.3: "Missile Detonation Location" (WT-1140); U. S. Army Signal Engineering Laboratories, Fort Monmouth, New Jersey; J. B. Graham, Capt., USA, Project Officer.

The objective of Project 6.3 was to test the feasibility of a tactical range detonation-locator system. The system was designed to locate ground zero by detection and analysis of the electromagnetic radiation emitted by the burst. Ideally, such a system would provide yield and height-of-burst information as well. The project thus evaluated, in three separate experiments, instrumentation for the measurement of the three detonation parameters.

The detonation locator consisted of broad-band receivers set up on baselines at 60 and 200 miles from the test site. Radio links between the stations provided the time comparisons necessary to determine relative electromagnetic-pulse time of arrival at each station. The experimental setup was not designed to provide fixes, in that angular resolution between lines of position for the two sets of stations was poor. Crystal clocks were used for accurate time-of arrival analysis.

Seventeen lines of position were obtained from the locator stations. The average line-of-position error was 1.2 miles, with the 200-mile stations no less accurate than those at 60 miles. The wave forms recorded as broad-band oscillograms were generally similar for all shots, with the exception of the high-altitude shot.

From a study of the oscillograms, it was concluded that electric field strength correlated in a direct manner with yield and that some correlation existed between yield and peak observed frequency and pulse duration though these observations were based upon the narrow range of yields presented in the Operation Teapot series. The signal strength recorded for all successful events indicated the feasibility of locator measurements at much greater ranges than those used.

Information was gathered on site relative to the determination of yield of nuclear devices by a modified bhangmeter technique. The measurement of yield by time to minimum using only a narrow band width offered the possibility of increased accuracy and greater range capability.

Lead sulfide cells were used to detect the various portions of the thermal energy from the detonations after refraction by a lithium fluoride prism. Plots were made of the yield versus time to minimum for the various bandpasses employed. The results indicated that for the same yield, time to minimum decreases with increasing wave length. The information gathered was insufficient to establish a new empirical relationship between yield, time to minimum, and wave length. Yield measurement was not accomplished by the narrow-band technique at ranges comparable to the detonation-locator portion of this project.

The height-of-burst measuring phase of the system was studied by investigating the possible existence of a heat-induced seismic signal from air bursts. Such a signal might be used to determine the height of burst by comparison with the shock induced seismic, if yield is known.

The experimental procedure was to install seismic detectors (geophones) at distances of from 2 to 10 miles from ground zero and record the detected signals.

No positive results were obtained, primarily because of noise in the transmission lines to the recorder station and the large transient induced in these lines at zero time. This did not rule out the possibility of a thermally induced seismic signal, but the difficulties involved in detecting such a signal were large enough to nullify the questionable advantages of this method of determining height of burst.

Project 6.4: "Test of IBDA Equipment" (WT-1141); Wright Air Development Center, Dayton, Ohio; Thomas J. Deegan, Capt., USAF, Project Officer.

The primary objective of Project 6.4 was to gather engineering evaluation data for a complete Indirect Bomb Damage Assessment (IBDA) system installed in a B-50D aircraft. The secondary objective was to determine the maximum operating range of the yield-measuring component of the system.

The B-50D IBDA system consisted of the standard radar set AN/APQ-24, a bomb-damage evaluation group AN/APA-106 (XA-1); a recording set, light and time, AN/ASH-4(XA-1); and a K-17 aerial camera. To accomplish the secondary objective, two F-94 aircraft were each instrumented with one ASH-4 recording set and one A-4 bomb-spotting camera.

The B-50D was positioned by radar navigation, simulating a drop aircraft, and at zero time was located from 3 to 7 nautical miles from ground zero. The F-94's were positioned by radio navigational aids at ranges of 35 to 153 nautical miles from ground zero.

The ASH-4 recording set on the B-50D obtained a yield measurement on all shots except the underground event. The K-17 camera obtained good results on 10 of the 12 shots on which the project participated, and radar-scope photos good enough for analysis were obtained on 8 of 12 shots.

A review of the results obtained by the F-94's indicated that for daylight operation the range of the ASH-4 was between 90 and 110 nautical miles and for night operations between 110 and 140 nautical miles. The observed ranges apply to yields between 10 and 40 kt, and for the normally clear weather encountered at NTS.

The average error in yield determination by the ASH-4's for all shots was 16 percent. On shots of 7-kt yield or above, the average error was reduced to 6 percent. This was comparable to the short-range bhangmeters commonly in use at ground stations.

In locating ground zero by radar-scope photo assessment, the average error was 550 feet. The average error in locating ground zero and determining height of burst by K-17 photoanalysis was 630 feet and 180 feet, respectively.

The system as tested was technically and operationally suitable. With the minor modifications indicated by the Teapot results it should be suitable for installation in SAC aircraft.

Project 6.5: "Test of Airborne Naval Radars for IBDA" (WT-1142); Bureau of Aeronautics, Department of the Navy, Washington, D. C., R. Zirkind, Project Officer.

The objective of this project was to test the suitability of unmodified operational Navy radars for Indirect Bomb Damage Assessment (IBDA) and to provide fleet personnel with experience in the analysis of IBDA data.

Two aircraft, an AJ-2 equipped with ASB 1 radar bombing system and a R4D-5Q with APS-31 radar set, were flown in simulated attack configuration on five shots. At zero time, the aircraft were on inbound headings approximately 7 miles from ground zero. Standard radarscope photography was used to record the presentations from zero time until about $t_0 + 10$ seconds. A total of eight hot runs were made on the five shots.

Essentially negative results were achieved on all but Shots 8 and 13. The ASB-1 systems did not provide acceptable results on any event. Mechanical difficulties with aircraft and radar sets severely limited the participation. Difficulties with gain settings and power outputs further reduced successful participation.

The conflicting requirements of high scan rate to define the short-lived phenomena and wide sweep angle for mapping purposes prevented successful ground-

zero location on any of the shots. Difficulty in balancing excessive ground clutter with high-enough gain setting for burst recording was experienced.

It is possible that with proper crew indoctrination and correct operating procedure, an interim capability for IBDA exists for the tested equipment.

PROGRAM 8: SUMMARY

Project 8.1. "Measurement of Direct and Ground-Reflected Thermal Radiation at Altitude" (WT-1143); Bureau of Aeronautics, Department of the Navy, Washington, D.C., J.E. Tefft, CDR, USN, Project Officer.

This project had as its purpose the study of the contribution of thermal energy reflected from the earth's surface to the total thermal radiation received by aircraft in the vicinity of nuclear detonations. The measurements were to be correlated with an analytical treatment of the subject. This analytical treatment assumed a point source of radiation above the reflecting surface and an absorbing but non-scattering atmosphere. Calculations were made from the analytical treatment for the case of a plane (2π steradian) receiver oriented parallel to the reflecting surface, and these calculations were used as the basis for delivery doctrine presently employed by the Naval air arm.

Three Navy AD aircraft were instrumented with USNRDL MK6F calorimeters and radiometers having 90-degree fields of view. Two of the AD aircraft were positioned at various slant ranges and altitudes on Shots 4, 6, 8, 12, and 13 by means of MSQ-1 radars. The third Navy AD aircraft was used as standby but flew in formation on Shots 8, 12, and 13 with one of the two radar positioned aircraft on two shots. For each aircraft one set of instruments, two calorimeters, and one radiometer were oriented on the fireball. A second identical set of instruments was oriented with radiation sensing surfaces parallel to the reflecting plane so as to receive a portion of the reflected thermal energy. In all cases the calorimeters measured both the total radiant energy (cal/cm^2) and the radiant energy in broad spectral bands using Corning filters. Radiometers were employed to obtain total thermal irradiance as a function of time in each case. GSAP cameras were also installed with each set of instruments to determine the orientation of the thermal instruments during the recording periods so that orientation corrections could be made to the observed data.

Data were available for total radiant energy received by the calorimeters and the radiant energy in broad spectral bands in WT 1146 (Reference 25) for all shots on which the project participated.

Additional calculations were performed by the Douglas Aircraft Company for the particular conditions of this experiment, i.e., 90 degree field of view instrument oriented toward fireball and 90-degree field of view instrument with sensing element surface parallel to ground. These calculations would appear consistent with experimental values if the assumptions on atmospheric scattering reported in WT 1143 (Reference 26) could be substantiated.

An auxiliary phase of this project was the determination of the temperature rise in selected aircraft skin specimens exposed to, and shielded against, aerodynamic cooling. Data on this phase are also presented in Reference 26.

Project 8.2: "Spectral and Radiometric Comparison of Wasp and HA" (LASL Project 18.2, NRL Report 4555 RD 538); Harold Stewart Project Officer.

This project's objectives were established jointly by the Los Alamos Scientific Laboratory and the Armed Forces Special Weapons Project and it was conducted as Project 18.2 of the Los Alamos diagnostic programs. The purpose of the project was the measurement of thermal radiant power as a function of time with high time resolution and extensive spectral measurements on Shot 10 and the correlation shot, Shot 9. Specifically, the following measurements were required:

1. Measurement of the radiant power as a function of time in the wave length interval 0.2 to 10μ and with a time resolution of 5 μsec. Two identical sets of equipment were used.

2. Measurement of radiant power in selected wave length intervals as a function of time using filtered selective receivers. Time resolution in these experiments was approximated using filtered selective receivers. Time resolution in these experiments was approximately 50 μsec. Three wave length bands were used; one in the visible which would be detected using a filtered photocell, one the vicinity of 1 μ using a filtered lead sulfide cell, and one in the vicinity of 3 μ which would be detected using a filtered lead selenide cell.

3. Measurement of the spectrum of the first maximum in the wave length interval 2,200 to 7,800 Å using a spectrograph having resolution of approximately 11 Å/mm.

4. Measurement of the spectrum as a function of time in the wave length interval 2,800 to 5,300 Å with a spectrograph having a resolution of 5 Å mm, a time resolution of 100 μsec, and a running time of approximately 100 msec.

5. Measurement of the spectrum of the explosion in a manner identical to No. 4 above, except that the instrument would have a time resolution of 2 msec and a running time of 2 seconds.

6. Measurement of the spectrum of the explosion with low resolution equipment had time resolution of approximately 2μsec and a running time of approximately 1 second.

7. Measurement of the spectrum of the explosion as a function of time using a cine spectrograph which would take 500 low resolution spectra per second and had a running time of approximately 1 second.

Additional experiments of fundamental interest, although not stated requirements for the project included:

1. Measurement as a function of time of the optical thickness of the ozone layer about the fireball.

2 Fireball diameter as a function of time with 1-μsec time resolution and a running time of 100 μsec. This was done with a Bowen camera.

3. Limb darkening of the fireball as a function of time with 1-μsec time resolution, running time of 100 μsec, and measurements made in two narrow wave length intervals. This was done with a Bowen camera.

All the required measurements were successfully completed on Shot 9. On Shot 10, all the required measurements were successful except 3, 4, and 5 above. The additional experiments listed above were at best only moderately successful.

Data are available in Chapters 4 and 6 of this report and in NRL Report 4555 RD 538 (Reference 37). As of the preparation of this report a final report of this project is not available.

Project 8.3: "Protection Afforded by Operational Smoke Screens Against Thermal Radiation" (WT-1144); Chemical and Radiological Laboratory, Army Chemical Center, Maryland, E. Engquist, Project Officer.

The purpose of this project was the evaluation of the effectiveness of an oil fog smoke screen in scattering thermal radiation from nuclear detonation. By interposing such a screen between a detonation and thermally sensitive objects, the net result should be a decrease in the amount of thermal radiation incident upon the object. The data to be obtained were required for the determination of operational doctrine for the use of such smoke screens and to provide experimental data for comparison with theoretical studies and other laboratory experiments. An auxiliary objective was the determination of the effects of the smoke screen, if any, on the blast phenomena.

The particular fog oil used had a low absorption cross section and a high scattering cross section for thermal radiation.

The smoke screen was established east of ground zero on Shot 5 which was detonated from a 300-foot tower and gave a total yield of 3.6 ± 0.1 kt. Thermal instrumentation was positioned inside the smoke screen at 1,000, 1,400, 1,900, and 2,400 feet. The basic instrumentation was composed of USNRDL MK6F calorimeters with 90- and 180-degrees fields of view and CRI thermistor calorimeters with 180-degrees fields of view. The 90-degree field of view instruments were used to measure the radiant energy in broad spectral bands and were made with 180-degree field of view instruments. Photography was employed to determine the physical extent of the smoke screen USNRDL MK6F calorimeters and radiometers were used outside the smoke screen BRL self-recording pressure-time gages were installed to document the blast phenomena both under and outside the smoke screen.

The maximum height of the smoke screen was estimated from photography to be 55 feet The average height appeared to have been between 30 and 40 feet. The average area concentration of fog oil smoke was approximately 300 to 425 gallons per square mile. Attenuation factors were documented from measurements using 180-degree field of view instruments with detecting surfaces normal to air zero direction at 1,000, 1,900, and 2,400 feet to vary from 78 to 90 percent and with identical instruments with detecting surfaces normal to the vertical. The angular distribution of radiation was measured at 1,000, 1,400, and 1,900 feet. These measurements revealed maximum radiant energy was delivered on a vertical surface facing ground zero. A horizontal surface received less radiant energies. Under the latter conditions, the radiation was attenuated by 77 to 96 percent at ranges of 1,000 and 2,400 feet, respectively. The smoke screen had no significant effect on the blast wave in the precursor of Mach front region except to reduce the range to which the precursor extended.

Evaluation of the experimental data indicated that adequate information was obtained for the establishment of a speculative doctrine for thermal-radiation-attenuating smoke screens and correlation of experimental work with theoretical studies performed by the Chemical Corps.

Further details of this experiment are to be found in WT-1144 (Reference 28) and WT-1146 (Reference 25).

Project 8.4: "Thermal Measurements from Aircraft in Flight" (WT-1145),
"Basic Thermal Radiation Measurements" (WT-1146);
"Radiant Energy Delivered Prior to the First Minimum" (WT-1147);
"Spectrometer Measurements" (WT-1148),
"Air Temperature Measurements Over Several Surfaces" (WT-1149),
"Thermal Radiant Power Measurements with High Time Resolution" (WT-1150);
U. S. Naval Radiological Defense Laboratory San Francisco, California; W. B. Plum, Project Officer.

The purpose of this project was to document a number of the thermal radiation characteristics of nuclear detonations. Specifically, these were:

1. On Shot 10, and the correlation event, Shot 9: measurement of the total radiant energy and radiant

energy in broad spectral bands at the delivery aircraft on Shot 10, measurement of the total radiant energy and radiant energy in broad spectral bands at ground station, measurement of the total radiant energy and energy in broad spectral bands prior to the minimum of the thermal pulse, measurement of total radiant power as a function of time with high time resolution (50 r/sec), and measurement of the spectral distribution of radiant power as a function of time with relatively high time resolution (100 to 200 r/sec).

2. For the Military Effects Tower shot this project was to perform preshock arrival air temperature measurements above special surfaces in support of shock precursor studies. In addition, the project undertook the measurement of the thermal inputs (radiant energy and irradiance as a function of time) at the air temperature instrumentation stations.

3. As support to other projects, instrumentation to measure the thermal energy received at aircraft positioned in the vicinity of nuclear detonations was to be provided projects who had as objectives such measurements.

4. As support to projects studying the structural characteristics of aircraft components and missile structural studies, instrumentation to measure thermal inputs was to be provided these projects.

5. Instrumentation to document the thermal radiation penetrating thermal radiation attenuating smoke screens was to be provided the project performing this experiment.

6. For detonation of devices of small yield and, in particular, those with mass to yield ratios of 5,000 lb/kt or less, basic thermal characteristics were to be documented for use in the study of scaling relationships.

Because of the extensive measurements effort undertaken by this project, the project was divided into six subprojects. This was done to expedite the conduct of the project in the field and the publication of the necessary reports. Subprojects were as follows: Projects 8.4a, 8.4b, 8.4c, 8.4d, 8.4e, and 8.4f.

Project 8.4a performed radiant energy measurements from the delivery aircraft employing USNRDL MK7F calorimeters, Minneapolis-Honeywell thermopiles, and USNRDL thin foil calorimeters. Measurements of total radiant energy and radiant energy in broad spectral bands were obtained. Photocells to obtain the time to the second maximum of the thermal pulse were also installed in the delivery aircraft, as well as GSAP cameras to determine the orientation of the instruments with respect to the line of site to the fireball. In addition, this project provided NRDL MK6F calorimeters and radiometers to Projects 5.1, 5.2, and 8.1.

Project 8.4d measured the total radiant energy and radiant energy in broad spectral bands and the time to the second maximum of the thermal pulse from the vicinity of ground zero on Shot 10. USNRDL MK7F calorimeters, Minneapolis-Honeywell thermopiles, and photronic cells were used. Radiant energy and function of the field of view of the calorimeter radiant energy in broad spectral bands and thermal irradiance as a function of time were made on the correlation event, Shot, 9, and, in addition, on Shots 1, 2, 3, 5, 6, and 8. These measurements were performed with NRDL MK6F calorimeters and radiometers. The thermal inputs to the various surfaces on Shot 12 were measured with limited success with MK8F calorimeters and MK6F radiometers because of electromagnetic pickup and recorder failures. This subproject provided instrumentation support to Project 8.4 on Shot 5 for thermal measurements beneath the thermal radiation attenuating smoke screen and to Projects 5.1, 5.4, and 5.5 on Shot 12.

Project 8.4c attempted to measure the energy received prior to the minimum of the thermal pulse on Shots 9 and 10, using a thin foil calorimeter. Unfortunately the instrument operated unsuccessfully.

Project 8.4d measured spectral distribution of radiant power as a function of time with a time resolution of 100 to 200 r/sec on Shots 1, 2, 3, 5, 6, 8, 9, 10, and 11. Data on Shots 9 and 10 are available in WT-1148 (Reference 62). The spectrometer used in this experiment measured the radiant power in 22 narrow spectral regions from 0.25 to 2.7 μ with a time resolution of 100 or 200 r/sec depending on the particular detector; i.e., photocells and lead sulfide cells. A Hilger medium quartz spectrometer and Bair interference filters were used to separate the spectral regions. Results were only partially successful and further instrument development is indicated.

Project 8.4e attempted to measure the preshock air temperature as a function of time on Shots 4 and 12. Measurements were attempted at levels from $\frac{1}{2}$ to 10 $\frac{1}{4}$ feet above the surface. On Shot 12 stations were located at 1,000 and 2,000 feet from ground zero on the desert and asphalt surfaces and at 1,000 feet on the water area. At 2,000 feet on the desert line, additional measurements were to be made over 20- by 20-foot plots consisting of soil, ivy, painted wood, concrete, and fir boughs. This phase of Project 8.4 was conducted jointly with the California Fire Research Experimental Station of the U.S. Forestry Service. Electromagnetic pickup and record failures limited the amount of data collected. Attention is invited to WT--1149 (Reference 29) and Chapter 2 of this report for additional details.

Project 8.4f measured the total radiant power versus time with high time resolution (50 r/sec) on Shots 1, 2, 4, 5, 6, 9, 10, and 11. Primary emphasis was placed on Shot 10, and the associated relatively low height of burst air drops, Shots 1 and 9. The bolom-

eters used were of the NRL design with engineering improvements. These measurements were, in general, quite successful.

In addition to the above referenced WT's pertaining to each phase of Project 8.4, data are summarized in Chapter 4 of this report with further discussion of the high altitude thermal phenomena in Chapter 6 of this report.

REFERENCES

5. J. R. Banister and R. J. Emrich; "Preliminary Investigation of Dust Raised by Blast Waves (Operation Greasy Stake)"; SC-3610 (TR), January 1955; Sandia Corporation, Albuquerque, New Mexico; Unclassified.

38. "Technical Photography of Fireball Growth and Light Intensity"; EG&G, Inc., Report No. 1434, Operation Teapot; Edgerton, Germeshausen & Grier, Inc., Boston, Massachusetts, and Las Vegas, Nevada.

39. "Late Stage Fireball Diameter and Times of Second Peaks"; EG&G, Inc., Report No. LV-188, Operation Teapot; Edgerton, Germeshausen & Grier, Inc., Boston, Massachusetts, and Las Vegas, Nevada.

Pg 227 Deleted.

49. A.E. Cohen, M.H. Jachter and H.M. Murphy, Jr.; "Evaluation of Military Radiac Equipment"; Project 6.1.1a, Operation Teapot, WT-1137, February 1958; U.S. Army Signal Engineering Laboratories, Fort Monmouth, New Jersey; ~~Official Use Only~~.

50. George A. Work; "Accuracy of Military Radiacs"; Project 6.1.2, Operation Teapot, WT-1138, November 1957; U.S. Naval Radiological Defense Laboratory, San Francisco 24, California; ~~Official Use Only~~.

59. W.J. Francy; "An Instrument-Tower Design for a Nuclear Test"; SC Tech Memo 268-54-51, December 1954; Sandia Corporation, Albuquerque, New Mexico; Unclassified.

63. Paul H. Lorrian and E.G. Schwartz; "Structures Instrumentation"; Project 3.10, Operation Teapot, WT-1107, May 1958; Explosion Kinetics Branch, Terminal Ballistics Laboratory, Ballistic Research Laboratories, Aberdeen Proving Ground, Maryland; Unclassified.